Aus der Klinik für Innere Medizin – Kardiologie
des Deutschen Herzzentrums Berlin

Direktor: Professor Dr. med. Eckart Fleck

Habilitationsschrift

Gefäßgeometrie und Blutströmung als koronarer Risikofaktor – Modell und Simulation in der kardialen Bildgebung

zur Erlangung der Lehrbefähigung

für das Fach Innere Medizin

vorgelegt dem Fakultätsrat der Medizinischen Fakultät

Charité – Universitätsmedizin Berlin

von

Dr. med. Ernst Wellnhofer

geb. am 5.8.1952 in Schwandorf

Eingereicht: Januar 2010

Dekanin : **Professor Dr. med. Annette Grüters- Kieslich**

1. Gutachter: Professor Dr. med. Jürgen Schrader, Düsseldorf

2. Gutachter: Professor Dr. med. Christian W. Hamm, Bad Nauheim

Inhaltsverzeichnis

Abkürzungen

WSS	Wandschubspannung
WSSG	Wandschubspannungsgradient
OSI	Oszillatorischer WSS Index
(3 D-)QCA	(dreidimensionale) quantitative Koronaranalyse
3 D- Rekonstruktion	Dreidimensionale Rekonstruktion
IVUS	Intravaskulärer Ultraschall
VRML	virtual reality modelling language
HDRI	high dynamic range image
KHE	Koronare Herzerkrankung
MRI	magnetic resonance imaging
CT	Computertomographie
(ox)LDL	(oxididiertes) low-density lipoprotein
ROS	reactive oxygen species (Oxidantien)
MMP	Metalloproteinase
NADPH	reduziertes Nicotinsäureamid-Adenin-Dinukleotid-Phosphat
NO	Nitroxid
eNOS	endotheliale Nitrogensynthetase
t-PA	tissue-Plasminogen Aktivator
VSMC	vascular smooth muscle cell
ATP	Adenosintriphosphat
EDHF	endothelial hyperpoloarizing factor
RNA	Ribonucleinsäure
MAPK	mitogen activating protein kinase
SREBP	Shear reponsive elements
PECAM-1	platelet endothelial cell adhesion molecole 1
NF-κB	nuclear factor 'kappa-light-chain-enhancer'
TGF-β	transforming growth factor β
BMP-4	bone morphogenetic protein 4
VCAM-1	vascular cell adhesion molecule-1
TF	tissue factor
ICAM-1	intercellular adhesion molecule 1
E-Selectin	endothelial adhesion molecule 1
MCP-1	monocyte chemotactic protein-1
TNF-α	Tumornekrosefaktor α
IFN-γ	Interferon γ
IL-1	Interleukin 1

1. Einleitung

ΤΑ ΠΑΝΤΑ ῥΕΙ

(Heraklit 600 BC)

Die koronare Herzerkrankung (KHE) führt über eine zunächst belastungsabhängige Durchblutungsstörung zu Leistungseinschränkungen bzw. langfristig zu Herzinsuffizienz, Rhythmusstörungen und Tod. Häufig führt der atherothrombotische Gefäßumbau zu lokalen Verengungen an größeren epikardialen Gefäßen (Leitungsgefäße) (1-4) und kann deshalb mit lokalen Revaskularisationsmaßnahmen (Wiederherstellung der Durchblutung), z. B. Bypass Operation oder perkutaner Angioplastie interventionell behandelt werden. Die selektive Koronarangiographie ist das Standarddiagnoseverfahren für solche kritischen lokalen Engstellen, da sie hochauflösende Darstellungen liefert und ggf. die Durchführung lokaler Interventionen unmittelbar im Anschluss an die Diagnostik erlaubt. Die klinische Diagnose der koronaren Herzerkrankung ist deshalb auf diese lokalen Engstellen fokussiert, obwohl es sich hierbei nur um lokale, funktional schlechte Ergebnisse der Gefäßumbauvorgänge handelt.

1.1. Koronarien – ein exklusiver Teilkreislauf

Der Koronarkreislauf ist durch viele Besonderheiten charakterisiert. Ca. 5-10% des Herzzeitvolumens fließen in die Koronargefäße (5). Durch die Anatomie der Klappen und der Abgänge am Boden der Taschen ist ein gleichmäßiger Einstrom des Blutes vor allem in der Diastole gewährleistet. Im Gegensatz zu allen anderen Teilkreisläufen ist die Hauptströmungsphase die Diastole, wohingegen die Kompression intramuraler Arterien in der Systole zu einer deutlichen phasischen Widerstandserhöhung führt. Das System drainiert überwiegend über das Koronarvenensystem direkt in den rechten Vorhof. Im Gegensatz zu anderen Teilkreisläufen ist das System laufend relativ großen zyklischen Translations,- Dreh- und Scherbewegungen ausgesetzt. Dies stellt eine Herausforderung an die Bildgebung und die Strömungsmechanik dar.

Tabelle 1: Eigene Messungen zur Bewegung der Herzkranzarterien

	N	Mittelwert Gesamtweg in mm	Mittelwert Geschwindigkeit in mm/s	Mittelwert max. Abstand vom Ursprung in mm
LCA* proximal	31	**30,0** (14,7 – 51,03)	**53,0** (30,6 – 79,9)	**8,2** (3,3- 13,5)
RCA* proximal	26	**41,8** (26,2 – 84,4)	**69,3** (35,4 – 112,9)	**10,9** (6,3-22,5)
LCA* distal	39	**39,8** (16,7 – 91,2)	**64,9** (33,2 – 125,0)	**11,0** (3,6-27,8)
RCA* distal	48	**59,7** (30,86 - 128,2)	**102,4** (45,4 – 320,7)	**16,8** (7,7-47,2)

*LCA linke Koronararterie, RCA rechte Koronararterie

Eine weitere Besonderheit ist die große Kapillaroberfläche- und - Dichte. Mit ca. 500-575 cm²/g Feuchtgewicht ist die Kapillaroberfläche des Herzens zwar deutlich kleiner als die der Lunge aber doch sehr eindrucksvoll (ca. 12,5 m² bei 250 g Herzgewicht) (6). Die kapilläre Dichte im Herzen beim Menschen wird in der Literatur mit ca. 3200 pro mm² Schnittfläche angegeben (7).

1.2. Prozesse und Regelmechanismen

In der medizinischen Bildgebung des Koronarsystems werden Momentaufnahmen eines fließenden biologischen Prozesses erfasst, die das Ergebnis einer Entwicklung festhalten. Das Endothel ist nicht nur die Grenze der Gefäßwand zum Blut, sondern auch ein Bindeorgan (link), das strömungsmechanische, chemische, humorale und zelluläre biologische Signale des fließenden Bluts über komplexe Regulationsmechanismen in adaptive biologische Antworten der Gefäßwand umsetzt. Physiologische Umbauprozesse und atherosklerotische Entzündungsprozesse überlagern sich mit physiologischen Stimulationsprozessen und pathologischen Aktivierungsprozessen durch strömendes Blut in höchst komplexer Weise mit unterschiedlicher Gewichtung in Abhängigkeit von der Zeit (8).
Ein zentraler Regelprozess ist die Anpassung der Gefäßweite an Veränderungen der Strömung, die letztendlich durch den metabolischen Bedarf der versorgten Gewebemasse definiert ist (9-11). Es kann zwischen einer Kurzzeitregulation (Vasodilatation, Vasokonstriktion) und einer Langzeitregulation (Gefäßumbau) unterschieden werden. Für beide Prozesse ist die Wandschubspannung (WSS) die zentrale strömungsmechanische Regelgröße (12-17), der somit die entscheidende Rolle in der gesamten Gefäßregulation zukommt. Die Wandschubspannung ist die Kraft, die in Strömungsrichtung pro Flächeneinheit auf die Gefäßwand wirkt (Einheit: N/m² = Pascal [Pa] oder dyne/cm²; 1 Pa = 10 dyne/cm²). Bei der Beurteilung des Sollwerts dieser Regelgröße sind zwei wesentliche Aspekte zu berücksichtigen:

- Eine direkte Messung der Wandschubspannung in sehr kleinen Gefäßen, wie den Koronarien, ist unter klinischen Bedingungen nicht möglich. Selbst unter experimentellen Bedingungen wird die Wandschubspannung in der Regel aus der Strömung unter Annahme eines Strömungsprofils berechnet. Das häufig angenommene parabolische Strömungsprofil ist zumindest im Koronargefäßsystem aufgrund der vielen Krümmungen, Verzweigungen und kurzen Einlaufstrecken fast nirgends vorhanden. Numerische Strömungssimulationen umgehen dieses Problem weitgehend (18).
- Gemessene Stellwerte dieser Regelgrößen variieren erheblich zwischen Spezies und verschiedenen Teilkreisläufen. Wahrscheinlich ist auch, dass diese Sollwerte unter pathologischen Bedingungen Übergänge aufweisen („change of balance“) (19).

Physiologisch ist die Wandschubspannung ein eindeutig gerichtetes, mehr oder weniger pulsierendes aber nicht oszillierendes mechanisches Signal. Physiologische WSS ist ein Bewegungstraining, der das

Endothel in einem differenzierten und funktionalen Zustand erhält. Unter pathologischen Bedingungen treten mehrdeutige um Null oszillierende oder niedrige Signale in Rezirkulations- und Stagnationszonen oder Ablöseströmungen auf. Niedrige WSS ist definiert als durchschnittliche WSS <10-12 dyne/cm² (8;20-22). Oszillatorische WSS ist definiert durch bidirektionale Richtungsänderung und zyklische Amplitudenschwankungen mit einem Durchschnittswert nahe Null (23). Voll ausgebildete turbulente Strömungen sind in den Koronarien aufgrund der durch die kleinen Gefäßdiameter bedingten niedrigen Reynoldszahlen[1] und Womersley - Zahlen[2] selten zu erwarten. Bei eigenen Untersuchungen an Koronarstenosen fanden wir mittels quantitativer Koronaranalyse (QCA), Viskositätsbestimmungen aus Hämatokrit und Gesamtprotein und Dopplerflussgeschwindigkeits-messungen Reynoldszahlen von 617 ± 464 <<2000. Die Womersley- Zahlen lagen im Median bei 3 (range 1.3 -7).

Das Endothel verfügt über Sinnesorgane für die Wandschubspannung, die sogenannten Mechanorezeptoren (24;25):

- Hyperpolarisationsmechanismen über Ionen Kanäle (endothelial hyperpolarizing factor EDHF, inward rectifying currents, ATP-abhängige Kaliumkanäle) ermöglichen schnelle Antworten und eine komplexe Decodierung des strömungsmechanischen Signals (25).
- Die Glycocalix präsentiert sich der Strömung mit einer Vielfalt von membrangebundenen Makromolekülen, die insbesondere Glycoproteine besetzt mit sauren Oligosacchariden und terminalen Sialsäuren als auch Proteoglycane mit Glycosaminoglycanseitenketten umfassen. Unter physiologischen Bedingungen entsteht durch die Reaktion von Blutmolekülen mit dieser negativ geladenen polyanionischen Zelloberfläche eine biologisch aktive Kopplungsschicht an der endothelialen Oberfläche. Die WSS aktiviert wahrscheinlich spezifische Signalkaskaden in der Zelle (z.B. NO- Produktion) über durch Kernproteine der Glycocalix vermittelte spezifische Verbindungen mit dem Zytoskelett und der Plasmamembran. Basale Adhäsionsplaques (z.B. Integrine) und interzelluläre Verbindungen (z.B. PECAM-1) reagieren unabhängig vom Zustand der Glycocalix auf die WSS (26-32) und führen auch bei geschädigter Glycocalix z.B. zu WSS – abhängiger Prostazyklin-Produktion (33).

---

[1] dimensionslose strömungsmechanische Kennzahl: Verhältnis der trägen Kräfte zu den viskösen Kräften $Re=\rho vd/\mu$ mit ρ Dichte, v Geschwindigkeit und μdynamische Viskosität des Fluids und d Durchmesser des Gefäßes.

[2] dimensionslose strömungsmechanische Kennzahl: Verhältnis der pulsatilen Strömungsfrequenz zu den viskösen Effekten $\alpha = r\sqrt{\frac{\omega\rho}{\mu}}$ mit ρ Dichte, ω Winkelgeschwindigkeit und μ dynamische Viskosität des Fluids und r Radius des Gefäßes.

- Die experimentell belegte Mechanotransduktion der WSS über das Zytoskelett unterstreicht die Bedeutung einer eindeutig gerichteten Strömung (25;34;35).
- Ein Teil der Kommunikation der WSS mit dem Endothel läuft über Rezeptoren an der Zelloberfläche, z.B. G- Proteine, NADPH- Oxidase, und Tyrosinkinase (36-38).
- Die WSS wirkt zudem indirekt über Rezeptoren für (inflammatorische) Zellen und gelöste Blutbestandteile, deren Kontaktzeit über die Strömung reguliert wird (33;39;40).

1.3. Der Risikofaktor lokale Wandschubspannung

Die lokale WSS hängt wesentlich von der dynamischen Gefäßgeometrie ab. Andererseits steuert sie ihrerseits Umbauprozesse, die zu Veränderungen der Geometrie führen. Die zentrale Bedeutung der lokalen Geometrie und Strömungsmechanik in pathologischen Prozessen besteht darin, dass sie mit Ausnahme struktureller und funktioneller Unterschiede verschiedener Gefäßabschnitte der einzige atherosklerotische Risikofaktor ist, der lokale Verteilungsmuster von frühen und kritischen atheroskleotischen Läsionen bestimmt (21;41-56). Die Bereitstellung dieses Risikofaktors (lokale Geometrie und Strömungsmechanik) für die individuelle klinische Diagnostik ist das zentrale Anliegen dieser Arbeit.

Die Wandschubspannung aktiviert Mechanorezeptoren, die ihrerseits komplexe und vernetzte intrazelluläre Prozesse auslösen (Mechanotransduktion) (24;57). Ein großer Teil dieser Prozesse führt zu einer kaskadenartigen Aktivierung von mitogen-aktivierten Proteinkinasen (MAPKs) auf verschiedenen Ebenen, denen eine Schlüsselrolle zugeschrieben wird (37). Das Zytoskelett gilt als weiterer zentraler Mediator in der Mechanotransduktion, da es ein Gerüst für die Entstehung und Translokation verschiedener Signalmoleküle bildet und die der WSS ausgesetzte Oberfläche mit verschiedenden luminalen, basalen und junktionalen Strukturen verknüpft, die ihrerseits Signalkaskaden auslösen (24;57). Diese Kaskaden führen zur Phosphorylierung verschiedener Transskriptionsfaktoren, die ihrerseits an positive oder negative „shear responsive elements“ an Promotoren mechanosensitiver Gene binden. Dadurch wird die Expression dieser Gene und schließlich auch zelluläre Funktion und Struktur moduliert (20;58-61). Unter physiologischer Beströmung exprimiert das Endothel verschiedene atheroprotektive Gene und unterdrückt verschiedene atherogene Gene (60;62). In Regionen mit niedriger oder oszillatorischer WSS werden unter Einfluss der mehrdeutigen Strömungssignale atherogene Gene hoch reguliert und atheroprotektive Gene supprimiert (60;62).

- Niedrige WSS schwächt die physiologische NO (nitric oxide)- abhängige atheroprotektive Schutzwirkung. NO besitzt anti-inflammatorische, anti-apoptotische, anti-mitogene und anti-thrombotische Eigenschaften (63). Physiologische pulsatile Strömung ist ein zentraler Stimulus der NO- Produktion. Die endotheliale NO- Synthase (eNOS) wird über Gen Expression (64) und post-transkriptionell über Phosphorylierung und Aktivierung moduliert (65). Niedrige WSS in Gefäßregionen mit gestörter Strömung führt zu einer Verminderung der Messenger RNA für und der Proteinexpression von eNOS (63;66-69). Darüberhinaus wird durch niedrige WSS Prostazyklin herab reguliert und Endothelin- 1 hoch reguliert (20;68).

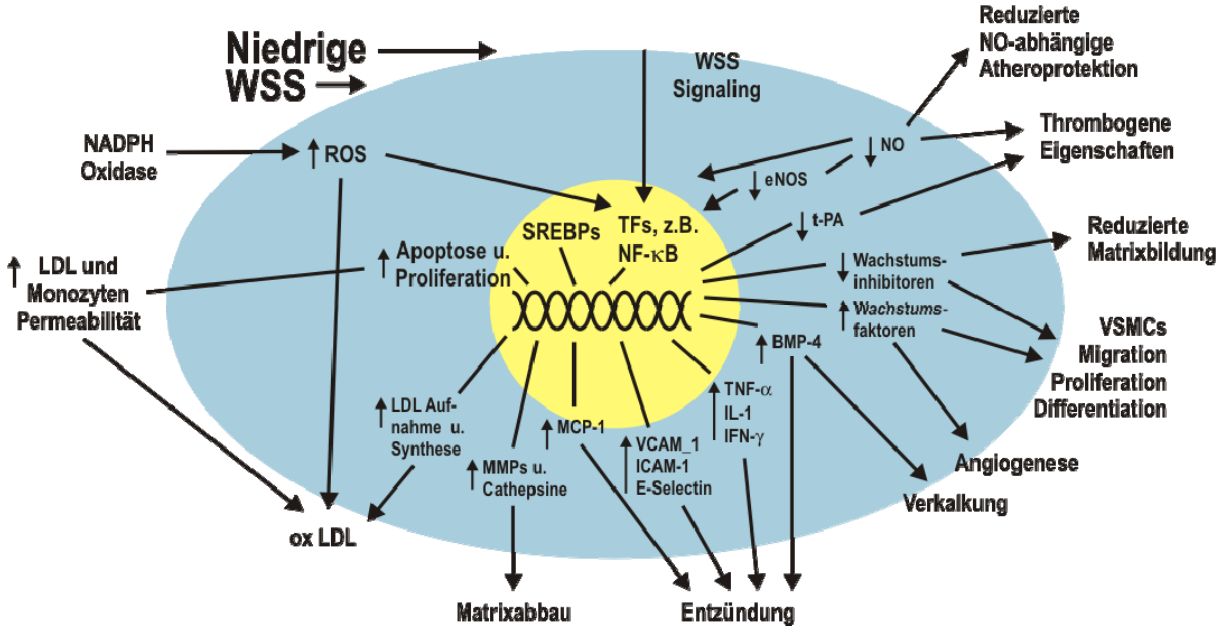

Abbildung 1: Rolle der niedrigen Wandschubspannung im Prozess der atherosklerotischen Entzündung (modifiziert nach (8), graphisch überarbeitet von Herrn Haselbach)

BMP =bone morphogenetic protein, ICAM = intercellular adhesion molecule, eNOS= endothelial nitric oxide synthase, IFN= interferon, IL = Interleukin, LDL = Low Density Lipoprotein Cholesterol, MCP = monocyte chemoattractant protein, MMP = Matrixmetalloproteinase, NADPH = reduziertes Nicotinsäureamid- Adenin-Dinukleotid- Phosphat, NF- κB = Transskriptionsfaktor nuclear factor kappa B, NO = nitric oxide, ROS = Oxidantien (reactive oxygen species), SREBP = sterol regulatory elements binding protein, TF = Transskriptionsfaktor, t- PA = Tissue Plasminogen Aktivator, TNF= Tumornekrosefaktor, VCAM = vascular cell adesion molecule, VSMC = glatte Gefäßmuskelzelle (vascular smooth muscle cell).

- Niedrige WSS fördert die Aufnahme, Synthese und Permeabilität für low-density Lipoprotein Cholesterol (LDL). Die Erhöhung der Aufnahme und Synthese erfolgt über die Aktivierung von sterol regulatory elements binding proteins (SREBPs) (26;70;71). Zusätzlich ist die Permeabilität der Endothel Oberfläche für LDL in Regionen verlangsamter oder gestörter Strömung erhöht (72-74). Das Endothel ändert seinen Phänotyp und in den Zellverbindungen entstehen Lücken (20;70;75-77). Außerdem ist in fluidmechanischen Stagnationszonen das Endothel länger den LDL-Konzentrationen im Blut ausgesetzt (60;78).

- Niedrige WSS erhöht den oxidativen Stress. Die oxidativen Enzyme, insbesondere NADPH Oxidase werden hoch reguliert und aktiviert. Dadurch kommt es zu einer vermehrten Bildung von „reactive oxygen species“ (ROS) (63;79-81). Darüberhinaus inaktiviert niedriger WSS Schutzmechanismen (scavengers) (58;82). NO wird zu Superoxiden und Peroxinitriten abgebaut (63).

- Niedrige WSS befördert Entzündungsprozesse über die lokale Steuerung von Adhäsion und Infiltration von Immunzellen. Hierbei spielt die Aktivierung bestimmter Transskriptionsfaktoren, z.B. NF- κB, Gene von Adhäsionsmolekülen, Chemokinen und Zytokinen, eine zentrale Rolle (45;58;59;83-87). Die träge oder stagnierende Strömung erleichtert die lokale Infiltration von Immunzellen auch unter physikalisch-mechanischen Gesichtspunkten (->Schaumzellen) (24;60;78;84).

- Niedrige WSS fördert die Migration, Differentiation und Proliferation glatter Muskelzellen (VSMC). Im Endothel wird durch niedrige WSS die Gen- und Proteinexpression potenter VSMC Mitogene gesteigert (20;45;68;69;88;89). Die vermehrte Bildung von ROS und inflammatorischen Zytokinen trägt indirekt zu diesem Prozess bei (90). Inhibitoren und Suppressoren von Zellwachstum- und- Migration werden durch niedrige WSS herabreguliert (28;91). Die vermehrte Expression von Mitogenen kombiniert mit der verminderten Expression von Wachstums Inhibitoren stimuliert die Migration glatter Muskelzellen durch Lücken der Lamina elastica interna (92;93).

- Niedrige WSS führt zum Abbau der extrazellulären Matrix in Geäßwand und fibröser Plaquekapsel. Niedriger WSS regelt die Expression von Matrix Metalloproteinasen im Endothel hoch (45;91;94;95). Diese Proteasen bauen die extrazelluläre Matrix ab (45;96-99). Außerdem fördert niedrige WSS die Akkumulation von Macrophagen und VSMC im Plaque (20;28;45;68;69;88;89;91-93). Macrophagen und VSMC werden durch pro-inflammatorische Zytokine zur Sekretion von Metalloproteinasen angeregt. ROS verstärken Expression und Aktivität der Metalloproteinasen (98;100).

- Niedrige WSS bremst die Neubildung extrazellulärer Matrix. Interferon- γ aus durch niedrigen WSS aktivierten T- Lymphozyten inhibiert die Kollagensynthese durch VSMC (101;102) und verstärkt die Fas- related Apoptose von VSMC (103). Letztere wird auch durch erhöhte ROS Konzentrationen gefördert (104). Die Herabregulation von TGF- ß und NO, Induktoren der Kollagensynthese, durch niedrigen WSS trägt zu diesem Prozess bei (105).

- Niedrige WSS spielt möglicherweise eine Rolle bei der Entwicklung von Verkalkungen über eine Hochregulation von „bone morphogenic protein“ (BMP-4) (44;46;106-108).

- Niedrige WSS erhöht die Thrombogenität durch Herabregulierung protektiver Faktoren (eNOS, Prostazyklin und „tissue plasminogen activator“ (t-PA)) (68;69;74) und die Akkumulation gerinnungsaktiver Faktoren und Blutplättchen in der stagnierenden Strömung (78).
- Das lokale Strömungsfeld spielt eine wesentliche Rolle beim Remodeling (51;78;98). Dilatierendes bzw. kompensatorisches Remodeling wird auch als Glagov Effekt bezeichnet nach der Erstbeschreibung beim Menschen (109). Jüngere Studien zeigen, dass es im Bereich koronarer Plaques mit leichter Stenose zwar in der Mehrzahl der Fälle zu einem kompensatorischen Remodeling kommt aber in immerhin 20% überschießende Umbauvorgänge mit aneurysmatischer Dilatation auftreten (51;110;111). Während in normalen Blutgefäßen eine Erniedrigung der WSS zu einem Negativremodeling führt, weist dieser Regulationsmechanismus in atherosklerotischen Arterien komplexe Störungen auf (21;45;51;112). Aktuelle Untersuchungen weisen darauf hin, dass sehr niedrige WSS mit Zerstörung Lamina interna elastica und exzessivem dilatierendem Gefäßumbau verbunden sind (44). „High risk plaques“ sind typischerweise Fibroatherome häufig mit nekrotischem Kern und dünner fibröser Abdeckung (113). In einer aktuellen Studie in einem diabetischen Schweinemodell für Atherosklerose konnte gezeigt werden, dass niedrige WSS ein unabhängiger Prädiktor für Lokalisation, Progression und Entwicklung zum High risk plaque mit exzessiv dilatierendem Gefäßumbau ist. Der Schweregrad der Veränderungen korreliert mit der WSS Minderung (44).
- Die pathophysiologische Bedeutung des abnorm überhöhten WSS ist demgegenüber schlechter belegt. Es wird vermutet, dass er zu mechanisch bedingten Erosionen in hochgradigen Stenosen beitragen könnte (114;115). Außerdem kann er über mechanische Beanspruchung zur Ulceration vulnerabler Plaques beitragen (116).

Um WSS-Analysen durchzuführen, ist zunächst eine 3-dimensionale Rekonstruktion des Gefäß-Lumens im Euklidischen Raum notwendig. Hiermit befasst sich der erste Abschnitt der Arbeit. Außerdem ist bei der Auswahl entsprechender Untersuchungsdaten zu berücksichtigen, dass das aufwändige Verfahren nur eine kleine Stichprobe erlaubt, die deshalb stratifiziert sein sollte. Notwendig ist auch eine Entscheidung zur Ordnungsstruktur des Baums.

1.4. Stichprobe

Während die meisten Arbeiten zur WSS-Simulation sich auf fokale Verlaufskontrollen konzentrieren, richtet sich in dieser Arbeit die Betrachtung auf den gesamten Gefäßbaum. Für die Modellbildung wird neben einer Kontrollgruppe (Patienten mit Ausschluss einer koronaren Herzerkrankung) auf das Konzept der dilatierten und der obstruktiven Atherosklerose zurückgegriffen (117), wobei das Konzept von Schoenhagen, das sich auf lokale Veränderungen

bezieht, in der Interpretation auf Gefäßbäume erweitert wird. Der Gruppe der aneurysmatischen Koronarerkrankung (118;119) wird die klassische koronare Herzerkrankung mit ausgeprägtem Negativ- Remodeling und Stenosierungen gegenübergestellt.

Ziel unserer Untersuchungen war unabhängig von lokalen Stenosierungen Messparameter für die frühzeitige Erkennung und Graduierung der Schwere obstruktiver und die dilatierender Verlaufsformen zu entwickeln (54;120-122). Gleichzeitig diente dieses Konzept als Grundlage für stratifizierte Stichprobenerhebung für unsere Simulationsansätze (54;123).

Im Rahmen dieses Ansatzes untersuchte der Autor die Hypothese, dass die Gefäßbaumstruktur der Koronarien eine fraktale Ordnung (120;124) aufweist und atherosklerotisches Remodeling diese fraktale Ordnung zerstört. Diese Daten wurden nur als Poster auf dem American Congress of Cardiology (120) und stark verkürzt in Wahle et al. 1995 (125) veröffentlicht.

Neben dem Modell der Stichprobe (dilatierende KHE, Kontrollen, stenosierenden KHE) ist für die Untersuchungen auch ein Gefäßbaummodell zugrunde zu legen.

Kontrollgruppe

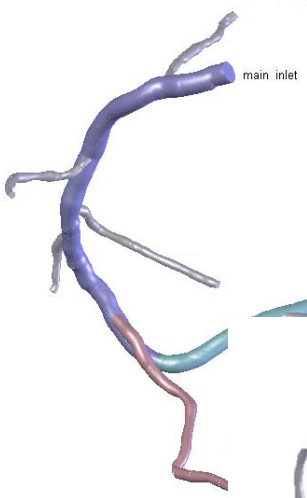

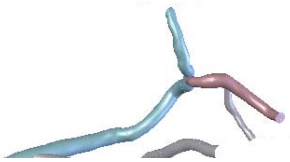

Aneurysmatische KHE

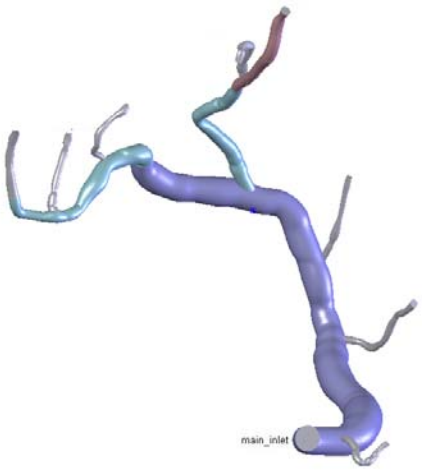

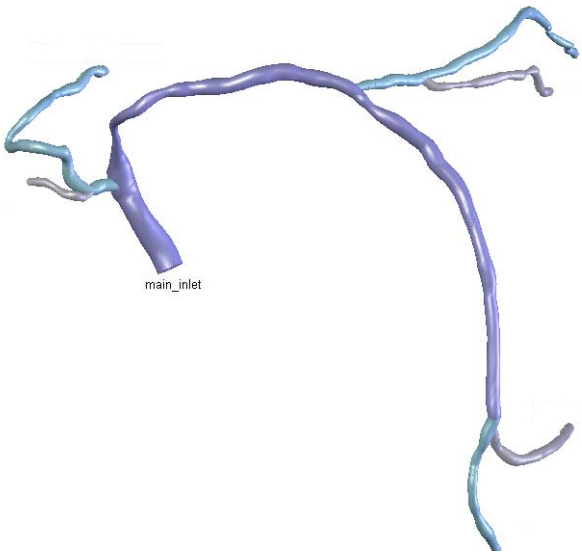

Stenosierende KHE

Abbildung 2: Repräsentative Gefäßbäume für die untersuchten Modellgruppen

1.5. Gefäßbaumstrukturmodell

Bäume und ihre Verzweigungen können grundsätzlich ausgehend vom Stamm (Weibel Modell (126)) oder von den Endverzweigungen (Strahler Modell (127)) geordnet werden.

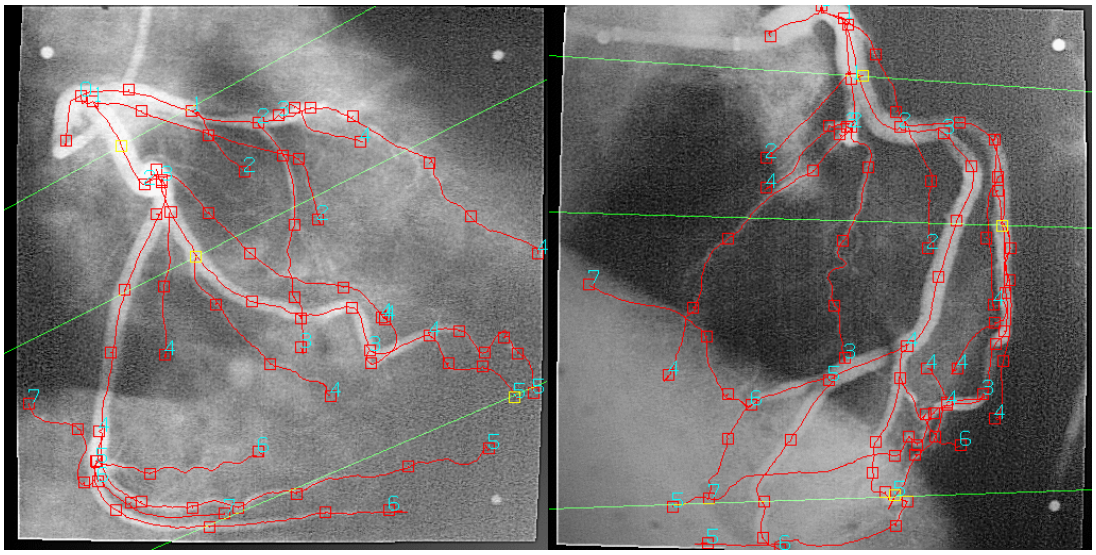

Abbildung 3: Repräsentatives Angiographiebeispiel

Beim Versuch dem Baum in Abb. 3 eine Diameter-definierte Strahler Ordnung (128) aufzuerlegen, ergäben sich folgende Probleme (siehe auch Diskussion) :

- Die Ordnung der Äste an den Gefäß-Enden wäre nicht definiert. Insbesondere ist nicht bekannt wie viele Ordnungen zwischen den sichtbaren Gefäß-Enden und den Kapillaren fehlen.
- Es gäbe nur ca. 3 Diameterklassen, also maximal 3 Ordnungen mit einer sehr asymmetrischen Aufteilung des Baums.
- Das Ende des Baums, der Abgang des Hauptstamms ist der einzige wohl definierte Punkt.

Für unsere Analysen benutzten wir deshalb ein modifiziertes Weibel Modell (126). Die Modifikation besteht darin, dass für jede Ordnung die distale Verzweigung auch bei kleinen asymmetrischen Abzweigen als Ganzes dem Stamm zugeordnet wird. Das modifizierte Weibel Modell liefert eine funktionsgerechte Interpretation (129). Der distale Unterbaum reflektiert die Größe des Perfusionsgebiets proportional auch dann (9-11;130), wenn die Gefäße angiographisch nur begrenzt in die Peripherie verfolgt werden können. Der zugehörige Stamm stellt die Zuleitung zu diesem Perfusionsgebiet dar. Da auch kleine asymmetrische Gefäße Perfusionsgebiete versorgen, ist die Erhöhung der Ordnung bei jeder Verzweigung gerechtfertigt. Dieses vom Autor entwickelte Modell wurde von Kassab in „Scaling Laws of Vascular Trees: Of Form and Function“ der Strukturanalyse des koronaren Gefäßbaums zugrunde gelegt bzw. übernommen (131).
Nachdem die Kontextmodelle für Stichprobe und Baumstruktur festgelegt sind, ist der nächste Schritt die Entwicklung eines dreidimensionalen (3D) Modells spezifischer Koronarbäume aus angiographischen Projektionsabbildungen. Die Struktur dieses Modells wird im Weiteren für alle Nicht-Mathematiker verständlich als Geometrie des Baums bezeichnet. Im mathematischen Sinne handelt es sich um keine

Geometrie, vielmehr um ein in einer euklidischen Geometrie aus projektiven Abbildungen rekonstruiertes dreidimensionales Objekt.

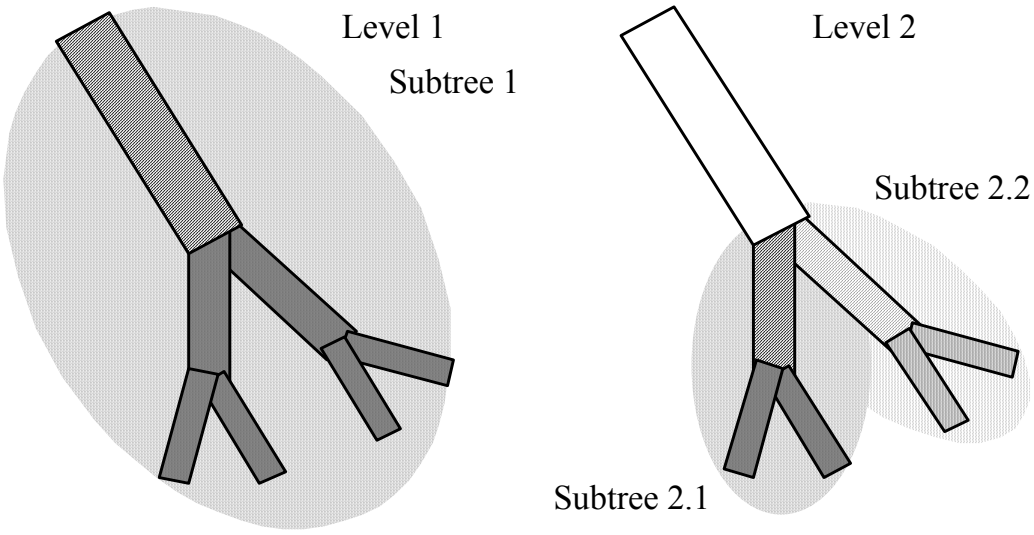

Abbildung 4: Modifiziertes Weibel Modell (129)

1.6. Dreidimensionale Rekonstruktion der Gefäßbäume aus angiographischen Projektionen

Die selektive Koronarangiographie ist immer noch das Standarddiagnoseverfahren bei der koronaren Herzerkrankung, da sie allein das lokale Verteilungsmuster der Veränderungen des Gefäßinneren mit ausreichender Auflösung für die Planung und ggf. Durchführung lokaler Interventionen liefert. Frühzeitig wurden quantitative zweidimensionale Auswerteverfahren zur Beurteilung lokaler Gefäßverengungen entwickelt und validiert (132-136). Diese zweidimensionalen Verfahren eignen sich nur bedingt zur Beurteilung der Querschnitte längerer Gefäßsegmente und erlauben keine Analyse der Längen, der intravaskulären Volumina und der Geometrie des Gefäßbaums (137). Nur bei absolut identischen Bildaufnahmebedingungen sind Verlaufsuntersuchungen mit diesem zweidimensionalen Verfahren durchführbar (138). Insbesondere sind 2-dimensionale Projektionen für numerische Strömungssimulationen (flow- profiling) ungeeignet. Aus den aus unterschiedlichen, - bevorzugterweise orthogonalen - Richtungen aufgenommenen Angiographieprojektionen ist es jedoch möglich, den Gefäßbaum dreidimensional zu rekonstruieren.

Die dreidimensionale Rekonstruktion (Abb. 5) und quantitative Vermessung von Koronargefäßbäumen erlaubt eine exakte Beurteilung von Längen, Krümmungen, Verzweigungen und Volumina und führt unabhängig von den Projektionsbedingungen zum selben dreidimensionalen Objekt (137;139). Sie besitzt das Potential einer hochgenauen Methode zur Analyse der Geometrie der Herzkranzgefäße und ihrer Veränderung bei Atherosklerose und konstituiert einen Raum, in den andere lokal hoch auflösende Bildmodalitäten, wie intravaskulärer Ultraschall, integriert werden können (47;140-143).

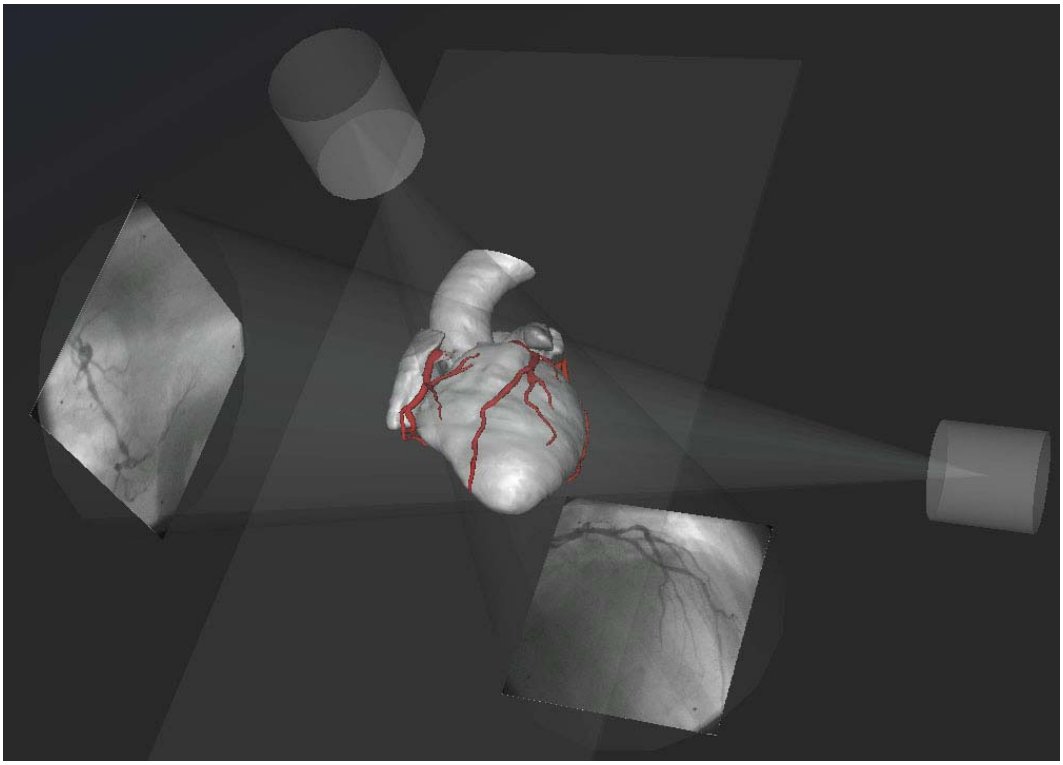

Abbildung 5: Aus einer virtual reality modelling language (VRML)- Simulation der biplanen Angiographie (freundlicherweise zur Verfügung gestellt von Herrn Zeiler, TU- Berlin, Elektronics and Medical Signal Processing (EN3))

Zudem können in entsprechenden Rekonstruktionen Strömungssimulationen durchgeführt werden (8;21;47;51;54;123;144-154). Wesentliche Vorzüge der 3 D- Rekonstruktion aus Routineangiogrammen ohne Fusion mit anderen Bildmodalitäten sind die Möglichkeit retrospektive Analysen durchzuführen, die fehlende Notwendigkeit Zusatzinterventionen durchzuführen und die Bereitstellung des gesamten Koronarbaums mit allen Seitenästen bis in den Submillimeterbereich. Eine ungenauere Rekonstruktion bei irregulären, konkaven oder stark exzentrischen Lumina im Vergleich zu Fusionstechniken mit IVUS kann in Kauf genommen werden. Die 3 D-Rekonstruktion mit Fusion anderer Bildmodalitäten ist keine Alternative sondern eine Ergänzung und Erweiterung der 3 D- Rekonstruktion ohne Fusion, die Zusatzinformation, z. B. Plaquedicke, in ausgewählten Gefäßsegmenten zur Verfügung stellt. Ausgehend von Vorarbeiten auf dem Gebiet der 3 D- Rekonstruktion von koronaren Gefäßbäumen wurden in den letzten Jahren Methoden entwickelt, die in der Lage sind auf sehr allgemeiner Ebene dreidimensionale Gefäßverläufe zu bestimmen. Sowohl die Methoden für die Gefäßsegmentierung als auch die Rekonstruktionsalgorithmen können gleichermaßen auf 2 D-Bilddaten und 3 D-Volumendaten angewendet werden (155). Auch eine zeitabhängige Analyse, z.B. zur Bestimmung von Bewegungsvektorfeldern für die Bewegungsschätzung, ist damit möglich (156).
Kommerzielle Systeme (z. B. CAAS 3D QCA (157), CardioOp- B (158)) haben sich auf dem Markt etabliert und wurden validiert (159-162). Neue Entwicklungen in der nicht invasiven (MRI, CT) (163-166)

und invasiven koronaren Bildgebung (Rotationsangiographie) (163-172) eröffnen neue Perspektiven. Der erhebliche Zuwachs der Rechen- und Speicherleistung der Hardware und die Entwicklung standardisierter Softwaretools eröffnen ein Zeitalter der virtuellen Endoskopie in Echtzeit (154).

Der erste Abschnitt dieser Arbeit (1992-2002) befasst sich mit eigenen Beiträgen zur Entwicklung und Validierung einer 3 D-Rekonstruktion (DFG Anträge [Fl 165/3-1 und Fl 165/3-2]). Der Autor war beteiligt an der Entwicklung der Verfahren durch Herrn Wahle (125;173), hat das Gefäßbaummodell entwickelt (120;129), die klinischen Fragestellungen konzipiert sowie die Validierung des Verfahrens und klinische retrospektive Verlaufsuntersuchungen zum Stellenwert der 3 D-QCA durchgeführt (122;137).

1.7. **Flow – Profiling und dimensionslose Modellierung**

Die in vivo (an Patienten) geeigneten aktuellen Methoden der Messung des Geschwindigkeitsfeldes mittels Magnetresonanztomographie und Ultraschall- Dopplerverfahren sind wegen noch unbefriedigender räumlicher und/oder zeitlicher Auflösung bei weitem zu grob, um im Koronarbereich die WSS aus wandnahen Messungen zu ermitteln (18). Experimentelle Methoden der Strömungsmechanik zur flächenhaften Messung der WSS in komplexen, anatomisch realen Koronargefäßgeometrien sind in vivo nicht möglich oder sehr aufwändig (18). Deshalb kann die Einbeziehung der WSS als Risikofaktor in die Beurteilung dieser Prozesse und Muster derzeit nur über Simulationsstudien in dreidimensionalen Rekonstruktionen erfolgen (18;150;152).

Die Weiterentwicklung von modernen Methoden der medizinischen Bildgebung, 3D- Rekonstruktion und Programme zur numerischen Modellierung der Strömung ermöglicht jetzt auch die Untersuchungen an anatomisch realistischen Geometrien von Patientengruppen (54;137;141;145;148;149;172;174-182).

Die Einzelaspekte der numerischen Modelle, z.B. elastische oder feste Wände (183), Newton‘sche oder nicht- Newton‘sche Fluid-Eigenschaften (184-186), Einfluss der Pulsatilität (185;187) und Geometrieveränderung bzw. Gefäßbewegungen durch das schlagende Herz wurden in mehreren Studien untersucht (188-191). Basierend auf diesen Untersuchungen lässt sich sagen, dass die Annahme einer starren Wand unproblematisch und eine Vernachlässigung der nicht- Newton‘schen Fluid-Eigenschaften als Annäherung vertretbar ist. Für über den Zyklus gemittelte Messgrößen ist eine stationäre Simulation ausreichend. Unter den Gefäßbewegungen hat die Torsion den größten Einfluss auf die WSS. Eine Simulation in der stabilen bewegungsarmen end-diastolischen Phase ist eine repräsentative Momentaufnahme für die meisten Fragestellungen (18).

Für die allgemeine Theorie der Bewegung zäher Flüssigkeiten gelten die aus den Prinzipien der Erhaltung der Massen und Momente abgeleiteten Navier-Stokes- Gleichungen:

$$\rho\frac{du}{dt} = \rho X - \frac{\partial p}{\partial x} + \mu\Delta u$$

$$\rho\frac{dv}{dt} = \rho Y - \frac{\partial p}{\partial y} + \mu\Delta v$$

$$\rho\frac{dw}{dt} = \rho Z - \frac{\partial p}{\partial z} + \mu\Delta w$$

Mit $\Delta = \partial^2/\partial x^2 + \partial^2/\partial y^2 + \partial^2/\partial z^2$ und $du/dt = \partial u/\partial t + u\,\partial u/\partial x + v\,\partial u/\partial y + w\,\partial u/\partial z$ etc.

(∂ partieller Differentialoperator) (192)

Die Differentialgleichungen wurden unter Annahme entsprechender Randbedingungen (s. u.) numerisch in einem Finite-Elemente-Modell mit einer Standardsoftware gelöst (FLUENT 6™ , ANSYS- Fluent Inc., Lebanon, USA). Die lokale WSS wird dabei über partielle Differentiation der wandnahen lokalen Geschwindigkeit (V) normal (senkrecht) zum lokalen Fächenelement (F) ermittelt:
WSS= μ*(∂(V)/∂($\downarrow$ F)) mit μ = Viskosität.
Die Transformation des rekonstruierten Gefäßmodells in das Finite Elemente Gitter erfolgte mit einer hierfür entwickelten Software (Gambit™, ANSYS- Fluent Inc., Lebanon, USA). Für die Triangulation der Oberfläche wurden die Knotenabstände auf 5% des mittleren Gefäßdurchmessers festgelegt. Ausgehend von diesem Gefäßwandgitter wurde das gesamte Volumen in Tetraeder und Prismen aufgerastert (durchschnittlich 350 Elemente pro Querschnitt). Aktuelle Studien zur notwendigen Gitterauflösung für Wandschubspannungsberechnungen zeigten, dass im Wandbereich eine Verfeinerung der Gitter erforderlich ist (193;194). Eigene Untersuchungen im Herzkranzgefäßmodell mit vier verschiedenen Gitterauflösungen mit und ohne Grenzschichtgitter (460.000 bis 1.300.000 Zellen) bestätigten, dass für eine genaue Berechnung der WSS sehr hohe Gitterauflösungen im wandnahen Bereich erforderlich sind. Deshalb wurde eine Grenzschicht aus 3 Reihen von Prismen mit einem Zoomfaktor von 1.2 in das Finite Elemente Modell integriert (Verfeinerungsverhältnis zwischen 2 aufeinander folgenden Schichten). Die Stärke der ersten Schicht ist dann 0,02 mm. Bei einer solchen Schichtdicke ist der Fehler für Geschwindigkeitsberechnungen kleiner als 3,5 % und für die WSS kleiner als 5,1 %. Die resultierende Anzahl der Volumenelemente des Gitters lag zwischen 1.250.000 and 3.400.000. Die Anzahl der Knoten lag zwischen 425.000 and 1.350.000.
Weitere Randbedingungen für die Strömungssimulation waren die Annahme eines stationären laminaren Flusses. Diese Annahme ist vertretbar, weil die kleinen Gefäßdiameter nur niedrige Reynoldszahlen und Womersley- Zahlen zulassen (siehe auch eigene Messungen Abschnitt 1.2. und Literatur (18;187)). Weiter wurde näherungsweise eine starre Wand angenommen, was insbesondere bei Atherosklerose vertretbar ist (183). Im Wandbereich wurde, wie üblich, eine “no-slip condition” unterstellt. Es wurden keine Annahmen zu Drücken am Gefäßausgang (Widerstandsmodell) getroffen. Blut wurde als Newton’sche Flüssigkeit mit

einer kinematischen Viskosität von $3,5*10^{-6}$ m²/s modelliert. Die Kopplung zwischen Druck und Fluss wurde über ein Diskretisierungsschema zweiter Ordnung mit einem SIMPLEC–Modell realisiert. Die Konvergenzgrenze für relative Fehlerkomponenten von Geschwindigkeit und Druck wurde bei $2* 10^{-5}$ gesetzt. Für die Einlaufströmung wurde ein flaches Geschwindigkeitsprofil angenommen, da die Herzkranzgefäße aus einem größeren Kompartment abgehen (Sinus Valsalvae der Aortenwurzel). Die mittleren Einlaufgeschwindigkeiten wurden mit 0,17 m/sec für Kontrollen, 0,27 m/sec für Patienten mit obstruktiver KHE und 0,09 m/sec für Patienten mit aneuysmatischer KHE angesetzt. Hierbei handelt es sich um Mittelwerte aus entsprechenden eigenen Messungen. Die Massenflüsse wurden aus dem Produkt der mittleren Einlaufgeschwindigkeit mit den rekonstruierten Eingangsquerschnitten berechnet (108±47 ml/sec in Kontrollen, 139±48 ml/sec obstruktive KHE, 75±36 ml/sec aneurysmatische KHE). Die entsprechenden Reynoldszahlen waren 175±39 (Kontrollen), 252±48 (obstruktive KHE), and 105±28 (aneurysmatische KHE).

Die absolute WSS hängt aber stark von der Größe der Flüsse ab, die ihrerseits eine Funktion des absoluten Gefäßquerschnitts und der absoluten Geschwindigkeit sind. Dies verbietet einen direkten Vergleich der WSS bei unterschiedlichen Patienten, wo große Unterschiede dieser Parameter erwartet werden müssen. Aufgrund der Variabilität der Koronaranatomie ist eine lokale Zuordnung der WSS im Patientenvergleich nur äußerst grob, z. B. bezogen auf ganze Segmente der Herzkranzgefäße möglich. Es gab deshalb bisher nur einige sehr aufwändige serielle Studien zum „coronary flow profiling“ bei Patienten und im Tiermodell im Verlauf (21;44;51;195).

Die dimensionslose Charakterisierung hat sich in der Strömungslehre (z. B. Reynoldszahl) und in der Medizin (z. B. Auswurffraktion) als sehr effektive und effiziente Methode zur Lösung solcher Skalierungsprobleme erwiesen. Jedenfalls muss ein Ansatz gewählt werden, bei dem mehrere Parameter so in Beziehung gesetzt werden, dass eine reine Größenänderung per se zu keiner Änderung der Bewertung führt. Dies wird auch zum Teil durch statistische Verfahren (z. B. standardisierte Diskriminanzanalyse) erreicht (54).

2. Ergebnisse

2.1. 3-D Rekonstruktion und Geometrieanalyse

2.1.1. Assessment of Diffuse Coronary Artery Disease by Quantitative Analysis of Coronary Morphology Based upon 3-D Reconstruction from Biplane Angiograms

Diese Arbeit (125) stellt das am DHZB entwickelte Verfahren zur 3 D-Rekonstruktion und 3 D-QCA, d.h. die Definition von 3 D Maßen, und erste klinische Anwendungen dar.

In Abschnitt 2 A wird die 3-D Rekonstruktionsmethode aus biplanen entzerrten und rektifizierten Aufnahmen beschrieben. Durch Kombination interaktiver Markierung von Topologiemerkmalen, wie Gefäßverzweigungen oder Ursprung und automatischer Gefäßerkennung werden 2-D Projektionsbaummodelle generiert, und das aus geometrischen Protokolldaten generierte initiale euklidische Raummodell iterativ verfeinert. Da das Isozentrum (siehe Messungen Abschnitt II D) sich als instabil erwies, d. h. die beiden Projektionsachsen der Anlage windschief im Raum lagen und nicht notwendigerweise einen Schnittpunkt aufwiesen, wurde durch den minimalen Abstand in einer zu beiden Projektionsachsen orthogonale Raumdimension eine Isoachse definiert und als Referenz benutzt. Als Ursprung des Koordinatensystems wurde ein gewichtetes Mittel der Schnitte der 2 Projektionsachsen mit der Isoachse definiert. Zur genauen Größen-Kalibration erwies sich eine Hüllkugel um eine Pigtail-Katheterschlaufe besser als nicht symmetrische Messgrößen wie Markerabstände auf Kathetern. Die Geometrieapproximation erfordert weitere Gewichts- und Kostenfunktionen zur globalen Fehlerminimierung. Die entsprechenden Validierungen am Phantom sind in Abschnitt II D dargestellt.

Der Zweitautor hat methodische Beiträge zur Entwicklung der Verfahrens durch Herrn Wahle, z.B. für Geometrieapproximation und 3-D QCA geliefert (125;173). Insbesondere geht das Gefäßbaummodell auf den Zweitautor zurück (120;129).

Die 3-D-Diameter-, Längen- und Volumenmaße (Abschnitt II B) waren damals eine besondere Funktionalität bzw. ein Alleinstellungsmerkmal des Algorithmus (196). Es konnte gezeigt werden, dass die 3-D QCA hohe Genauigkeit bei Phantomvermessungen aufwies (siehe Abschnitt II D). Das Verfahren beruht auf einer virtuellen Metrik mit dreidmensionalen Messvolumina. Auch nach Rekonstruktion eines elliptischen Gefäßlumens sind die Radien streng genommen nur bei dreifacher Orthogonalität repräsentativ für die Querschnitte. Zur Bestimmung des lokalen Radius werden deshalb die elliptischen Querschnitte projektionsabhängig ausgerichtet (siehe Fig. 8). Zur Volumenmessung wurden entsprechende verallgemeinerte elliptische Kegelschnittvolumen-elemente ins Gefäß eingepasst. Zur Längenbestimmung wird eine virtuelle Kugel mit adaptiver Größe durch das 3-D-Lumen gerollt (siehe Fig. 10).

Ein besonderes Anliegen des Zweitautors war das Potential der 3-D QCA in der klinischen Anwendung auf diffuse generalisierte Atherosklerose und der Blick auf den gesamten Gefäßbaum. Abschnitt III, IV und die Diskussion basieren auf Konzepten und Analysen des Zweitautors und wurden von diesem entwickelt und weitgehend geschrieben.

Wir untersuchten die Hypothese, dass die Gefäßbaumstruktur der Koronarien eine fraktale Ordnung aufweist und atherosklerotisches Remodeling diese fraktale Ordnung zerstört. Diese Daten wurden ausführlich als Poster auf dem American Congress of Cardiology veröffentlicht (120).
Eine negative Kontrollgruppe bestand aus 6 RCAs und 3 LCAs von Patienten ohne erkennbare koronare Veränderungen (n=10). Eine weitere Gruppe wurde basierend auf diffusen aneurysmatischen koronaren Veränderungen (2 RCAs, 5 LCAs) definiert. In einer dritten Gruppe wurden Koronarbäume von Patienten mit stenosierenden koronaren Veränderungen eingeschlossen (3 RCAs, 6 LCAs). Alternativ wurde der Schweregrad der koronaren Veränderungen als 1- bis 2- (3 RCAs, 4 LCAs) oder 3- Gefäßerkrankung graduiert (2 RCAs, 7 LCAs).
Da im Mittel 13 Unterbäume pro Koronargefäßbaum analysiert werden konnten, war es möglich Korrelationen der Ordnung und proximaler Diameter mit Längen, mittleren Durchmessern und Volumina stratifiziert nach Untergruppen und für einzelne Gefäßbäume durchzuführen.
Mittels Diskriminanzanalyse konnten durch die Korrelationen 80 % der Gefäßbäume bzgl. der angiographisch morphologischen Klassifikation korrekt charakterisiert werden. Bei Stratifikation nach Anzahl der betroffenen Gefäße wurden sogar 96% der Bäume korrekt charakterisiert. Wir schlussfolgerten, dass die Korrelationsanalyse auf 3-dimensional rekonstruierten Koronargefäßbäumen bei individuellen Patienten Normalbefunde von aneurysmatischer KHE und stenosierender KHE unterscheiden lässt und möglicherweise geeignet ist, das Fortschreiten der Erkrankung auch bei diffusen Verlaufsformen ohne lokale Stenosen zu quantifizieren.

Assessment of Diffuse Coronary Artery Disease by Quantitative Analysis of Coronary Morphology Based upon 3-D Reconstruction from Biplane Angiograms

Andreas Wahle, Ernst Wellnhofer, Ignace Mugaragu, Hans U. Sauer, Helmut Oswald, and Eckart Fleck

Abstract—**Quantitative evaluations on coronary vessel systems are of increasing importance in cardiovascular diagnosis, therapy planning, and surgical verification. Whereas local evaluations, such as stenosis analysis, are already available with sufficient accuracy, global evaluations of vessel segments or vessel subsystems are not yet common. Especially for the diagnosis of diffuse coronary artery diseases, we combined a 3-D reconstruction system operating on biplane angiograms with a length/volume calculation. The 3-D reconstruction results in a 3-D model of the coronary vessel system, consisting of the vessel skeleton and a discrete number of contours. To obtain an utmost accurate model, we focussed on exact geometry determination. Several algorithms for calculating missing geometric parameters and correcting remaining geometry errors were implemented and verified. The length/volume evaluation can be performed either on single vessel segments, on a set of segments, or on subtrees. A volume model based on generalized elliptical conic sections is created for the selected segments. Volumes and lengths (measured along the vessel course) of those elements are summed up. In this way, the morphological parameters of a vessel subsystem can be set in relation to the parameters of the proximal segment supplying it. These relations allow objective assessments of diffuse coronary artery diseases.**

I. Introduction

ATHEROSCLEROTIC coronary artery disease is a major epidemiological problem associated with functional impairment, expensive treatment, and fatal outcome in many patients. Whereas the diagnosis of local stenosis is well-established and often amenable to invasive therapy, diffuse disease is a domain of conservative therapy. A quantitative assessment of progression of the latter is desirable in order to judge the effects of different modalities of medical treatment and epidemiologic interventions decreasing risk factors. This remains true, even if stress tests and other clinical information supply additional data for evaluating disease and help in decision making.

Angiographic images of the coronary tree convey the impression that diffuse disease might be associated with remodeling of the coronary vascular branches. This may be seen in Fig. 1, where the angiographic images of a "normal" left coronary artery and a left coronary artery with diffuse dilating atherosclerotic disease are compared. Absolute measurements of diameters, lengths, or volumes of the segments of the artery afford 3-D reconstruction of the tree. Since these absolute dimensional values are of limited use due to large physiological variation in the size of coronary arteries, we aimed to construct a set of nondimensional measures. This set needs to be independent of size and functional state of the coronary vessel, while allowing quantification of morphological changes in the 3-D tree. To do this, the spatially reconstructed vessel trees were decomposed hierarchically, analyzing stems and crowns of the thus derived subtrees. Based upon these analyses, a nondimensional measure assessing loss of order defined on sets of subtrees was selected and tested clinically.

Manuscript received November 26, 1993; revised January 10, 1995. This work was supported by the Deutsche Forschungsgemeinschaft, Bonn, Germany, by Grant Fl 165/3-2 and the DeTeBerkom GmbH, Berlin, Germany, Project BERMED. The Editor responsible for coordinating the review of this paper and recommending its publication was M. W. Vannier.

The authors are with the Department of Internal Medicine–Cardiology, Free University of Berlin and German Heart Institute, Berlin, D-13353 Berlin, Germany; e-mail: andreas@pmi.dhzb.de.

IEEE Log Number 9411371.

II. Modeling and Evaluation

Within the last decade, much work has been performed in the field of vessel detection and 3-D reconstruction of the coronary system of the heart. Thus, in this section, we primarily figure out differences and enhancements in relation to earlier works of other authors. A rather theoretical presentation of the model generation and evaluation process is followed by a validation in several phantom studies and the verification of the entire system. The medical application will be the main topic of Section III.

A. 3-D Reconstruction

1) The Reconstruction Pipeline: In Fig. 2, the reconstruction process is shown. It starts with the image acquisition, where biplane images are obtained. The problem of handling distortions such as pincushion and sigmoidal effects is already solved. In this section, we assume that the biplane angiograms are rectified, centered (i.e., the central beam is located in the center of each image), and free of axial rotations. The sizes of the image intensifier entrance fields are assumed to be known.

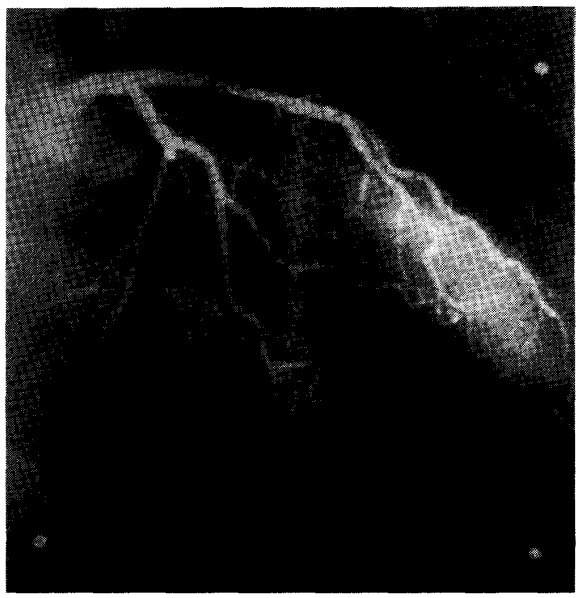

(a)

(b)

Fig. 1. Right anterior oblique views of left coronary arteries without (a) and with (b) diffuse dilating atherosclerotic disease.

By a combination of interactive topology marking and automatic vessel detection, for each projection, a 2-D model is generated. A complex imaging geometry analysis and approximation system was developed to reconstruct a 3-D model as accurately as possible. This model can then either be visualized to obtain a realistic impression of the vessel morphology, or quantitative analyses can be performed with high accuracy. Especially in those evaluations that cannot be performed by simple manual measurements on angiograms, 3-D evaluations are indispensible to obtain important morphological parameters. Thus, we focused on imaging geometry analysis and on finding an optimum model for volume representation.

2) Imaging Geometry: Standard biplane angiographic equipment consists of two X-ray systems having a common coordinate system. The geometries of biplane imaging devices were analyzed by Wollschläger *et al.* [1]. They assumed a fixed rotational origin of both systems, the isocenter: The projection axes intersect at this isocenter. The geometry is derived from the known angulation parameters and the distances of the X-ray sources and image intensifiers to the origin. Several evaluation systems are based upon these and other idealized assumptions, e.g., performing an isocentric calibration for diameter analyses on local stenoses [2]–[4].

For volume measurements, we need a very high reconstruction accuracy because linear reconstruction errors raise to the third power. The classic isocentric model could not satisfy this requirement due to various mechanical influences: First, a significant amount of gantry sag during rotation causes the projection axes to not intersect, thus the isocenter becomes blurred. Second, there is no adequate way to measure the required distances manually in medical routine, distances assumed to be fixed also vary due to gantry sagging [5]. In Section II-D, we list the results of our phantom studies regarding instabilities of the isocenter.

In our imaging geometry model, we use a variable isoaxis instead of a fixed isocenter to consider the real mechanical properties. The distance of the projection axes creates a unique isoaxis orthogonal to both of them (Fig. 3). The locations of X-ray sources and image intensifiers are determined in terms of distances to this isoaxis. The origin of the world coordinate system is defined as the weighted middle of the intersections of both projection axes with the isoaxis. The angulation is obtained conventionally as a sequence of rotations, considering the shift. Since the orientation of the isoaxis depends on the angulation, the isoaxis may vary between different acquisitions. Since the distance of the projection axes is not a constant—even in acquisitions with the same angulations—the location of the origin may slightly vary between acquisitions as well. This fact is not relevant for our purposes.

The transformation of a point from metric world (WC) via X-ray system (XC) to the dimensionless image (IC) coordinates of projection p is

$$[x_{\mathrm{xc}}, y_{\mathrm{xc}}, z_{\mathrm{xc}}] = \left([x_{\mathrm{wc}}, y_{\mathrm{wc}}, z_{\mathrm{wc}}] + \vec{I}_p\right) \cdot \mathbf{R}_p \tag{1a}$$

$$[u_{\mathrm{ic}}, v_{\mathrm{ic}}] = [x_{\mathrm{xc}}, y_{\mathrm{xc}}] \cdot \frac{D_{S_p} + D_{I_p}}{s_p(D_{S_p} + z_{\mathrm{xc}})} \tag{1b}$$

$\vec{I}$ is a 3-D translation vector (iso-axis portion);
$\mathbf{R}$ is a 3× 3 rotation matrix (angulation);
D_S is the distance between X-ray source and isoaxis;
D_I distance image intensifier input surface to isoaxis;
s is the scaling factor of the image intensifier.

3) Point Reconstruction: While the imaging process results in unique projections of a point, the reverse is ambiguous. Due to the loss of one dimension, only one ray per projection can

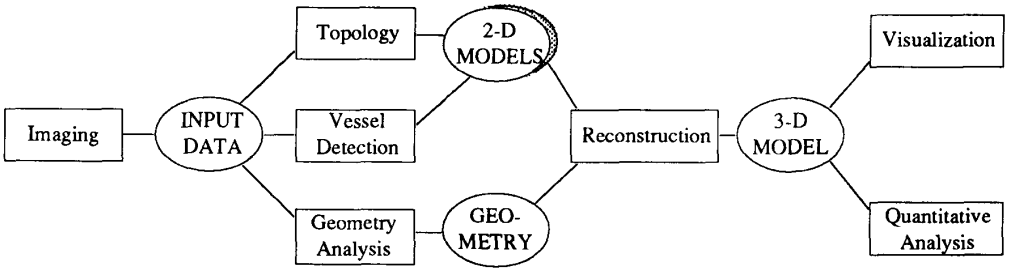

Fig. 2. The reconstruction pipeline.

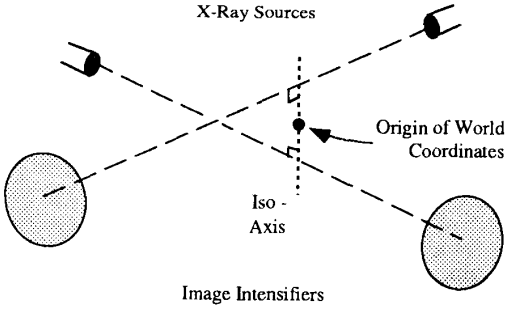

Fig. 3. Isoaxis imaging geometry model.

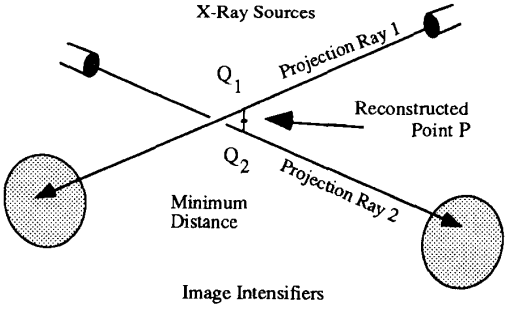

Fig. 4. Point reconstruction.

be reconstructed that pierced the object point during imaging. The ray $q(t)$ with $0 \leq t \leq 1$ of a projected point $[u, v]$ is then

$$q_{\mathrm{xc}}(t) = [0, 0, -D_{S_p}] + t \cdot [s_p u_{\mathrm{ic}}, s_p v_{\mathrm{ic}}, D_{S_p} + D_{I_p}] \quad (2a)$$

$$q_{\mathrm{wc}}(t) = q_{\mathrm{xc}}(t) \cdot \mathbf{R}_p^{-1} - \vec{I}_p. \quad (2b)$$

In theory, two rays of an object point coming from different views intersect at the location of this point. In practice, they miss due to several possible error sources. The definition of a generalized intersection point is used to solve this problem [6], [7]. For both projections, a point Q_p on ray q_p is searched where their distance is minimum. The weighted middle of these points is the desired object point P (Fig. 4).

In the next section, we show how to use this reconstruction error for a global error detection and correction; nevertheless, the generalized intersection point has to be used for local error considerations because a global correction can only minimize the mean errors.

4) Analysis and Approximation of the Imaging Geometry: Fencil and Metz [8] have developed algorithms to determine the imaging geometry from eight points, including angulation, distances, and isocentric shifts (i.e., the deviation of the projection axes from the rotational origin). Again, this method is rarely applicable in clinical routine, thus we have to make some obvious assumptions and restrict ourselves to points or objects visible in the angiograms without additional phantom measurements.

Some parameters are mainly a matter of adjustment. Once fixed, they are either constant (e.g., image intensifier size), or they can be easily determined by rulers, etc. (angulation). The spatial locations of X-ray sources and image intensifiers must be calculated as accurately as possible, but they cannot be determined by rulers or manual measurements. Unavoidable inaccuracies of the given parameters must be detected and corrected. Our method uses both known imaging parameters and at least two to five interactively marked reference points of known correspondence in the angiograms. From the known geometric parameters, an initial imaging geometry is calculated. In an iterative process, this initial geometry is improved by a mean-value based statistical approach, analyzing the errors from reconstructing the reference points [5].

The total error $y_i = f(x_i, t_i)$ in projection p of the i-th reference point is a function of the distance x_i of the reconstructed point to the projection axis in the direction of the isoaxis and the relative location t_i of the point in direction of the projection axis. The total error is

$$y_{i_p} = \sum_{j=0}^{m-1} y_{ij_p} = \sum_{j=0}^{m-1} f_j(x_{i_p}, t_{i_p}) \quad (3)$$

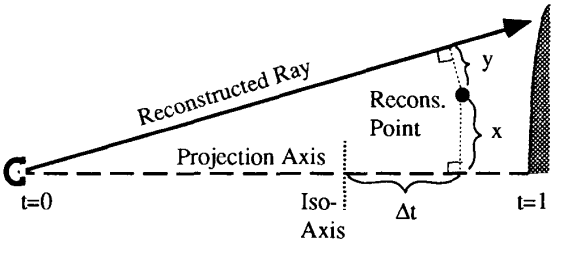

The extraction of a component delivers one correction coefficient to apply to the actual geometry. Afterwards, this component Δy_j is subtracted from the original error. The next error component is extracted, and so on. The dimensionless correction coefficients k_0 for the isoaxis portion, k_1 for the magnification and k_2 for the perspective distortion, are determined as follows:

$$k_{0_p} = \frac{\sum_{i=1}^{n} y_{i_p}^{\langle 0 \rangle}}{\sum_{i=1}^{n} 1[\mathrm{m}]}; \tag{4a}$$

$$k_{1_p} = \frac{\sum_{i=1}^{n} \left(y_{i_p}^{\langle 1 \rangle} \cdot \mu_{x_p}(x_{i_p}) \right)}{\sum_{i=1}^{n} \left(t_{i_p} \cdot x_{i_p} \cdot \mu_{x_p}(x_{i_p}) \right)} \tag{4b}$$

$$k_{2_p} = \frac{\sum_{i=1}^{n} \left(y_{i_p}^{\langle 2 \rangle} \cdot \mu_{\Delta t_p}(\Delta t_{i_p}) \cdot \mu_{x_p}(x_{i_p}) \right)}{\sum_{i=1}^{n} \left(\Delta t_{i_p} \cdot x_{i_p} \cdot \mu_{\Delta t_p}(\Delta t_{i_p}) \cdot \mu_{x_p}(x_{i_p}) \right)} \tag{4c}$$

where

$$y_{i_p}^{\langle j \rangle} = y_{i_p} - \sum_{j^*=0}^{j-1} \Delta y_{j_p^*};\ \Delta t_p = t_p - t_{I_p};\ t_{I_p} = \frac{D_{S_p}}{D_{S_p} + D_{I_p}}$$

$\mu(\ )$ weighting functions; [m]: length dimension.

The functions $\mu(\ )$: are required to ensure that points near the projection axes (x) and the isoaxis (Δt) are weighted less than those of higher informational value. Without this weighting, the algorithm may not properly approximate if many of the reference points are of less significance. The applied functions preserve the sign and are continuous

$$\mu(v, r_1, r_2, r_3) =$$

$$\begin{cases} \left\{ \begin{array}{ll} 1 - \frac{1}{2\left(1 + \frac{v - r_1}{r_2}\right)} & \text{if } v > r_1 \\ \frac{1}{2} & \text{if } v = r_1 \\ \frac{1}{2\left(1 - \frac{v - r_1}{r_2}\right)} & \text{if } v < r_1 \end{array} \right\} \cdot \left(1 - \frac{1}{1 + \frac{v}{r_3}} \right) & \text{if } v > 0 \\ 0 & \text{if } v = 0 \\ \left\{ \begin{array}{ll} -1 + \frac{1}{2\left(1 - \frac{v + r_1}{r_2}\right)} & \text{if } v < -r_1 \\ -\frac{1}{2} & \text{if } v = -r_1 \\ -\frac{1}{2\left(1 + \frac{v + r_1}{r_2}\right)} & \text{if } v > -r_1 \end{array} \right\} \cdot \left(1 - \frac{1}{1 - \frac{v}{r_3}} \right) & \text{if } v < 0 \end{cases} \tag{4d}$$

v is the input value to weight;
r_1 is a fixed parameter for $\mu(v) = \pm 0.5$ threshold;
r_2 is a fixed parameter for the steepness at $\mu(v) = \pm 0.5$;
r_3 is a fixed parameter for overall curve steepness.

After extracting all components, the actual geometry is corrected by application of the coefficients and the reference points are reconstructed again. If the mean reconstruction error is less than a self-adjusting threshold, the iteration stops and the actual geometry is used as the final approximation.

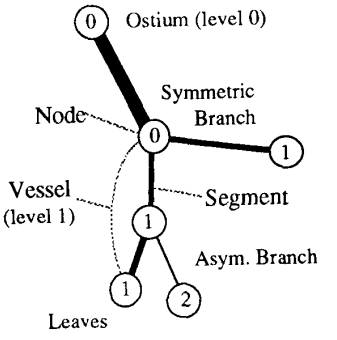

Fig. 5. Vessel hierarchy.

While the approximation algorithm is able to correct errors relatively between projections, there is no absolute measure for magnification. Thus, at least one object of known size within the images has to be known. Conventional methods use the projected radius of a catheter in one projection for calibration, which leads to gross errors in later quantitative evaluations.

To get a reliable reference size, we either use markers on a catheter with known distances (cardiomarkers) or the outer diameter of the pigtail catheter loop. During the geometry approximation process, the object is reconstructed with the actual geometry. The relation between the calculated and the real spatial sizes of the calibration object results in an additional correction coefficient for the geometry approximation [5]. Refer to Section II-D concerning the achieved accuracy of the imaging geometry.

5) 2-D Hierarchical Model Generation: To obtain a 3-D model, for each projection a 2-D model has to be generated. This is done by interactive marking of the vessel topology. The operator selects corresponding points in both projections, called nodes: the vessel ostii, branches, leaves (where to stop reconstruction), or other striking points (Fig. 5). The biplane correspondence is defined during this step, assigning for each vessel in one projection the corresponding vessel in the other projection.

A structural attribute of a node is its level, indicating the membership to a vessel and the tree hierarchy. A vessel is defined as a set of connected nodes of the same level. From each node, other vessels of a lower level may branch. The nodes split the vessels up into different segments. While the nodes are set interactively, the vessel course and edges are determined automatically by using the nodes as guide points for a vessel detection algorithm [9]. As a result, each segment consists of a discrete number of elements, containing the 2-D image coordinates of centerline and both edge points.

For details of the tree representation refer to [10].

6) Segment Reconstruction: After geometry and vessel topology have been determined and the nodes of the vessel system have been reconstructed, the vessel segments found during the vessel detection algorithm have to be reconstructed. Segments are always enclosed by two nodes. While node points create only one ray per projection, segments create ray bundles where the corresponding ray pairs have to be found. A cost matrix is generated, which contains the distances of

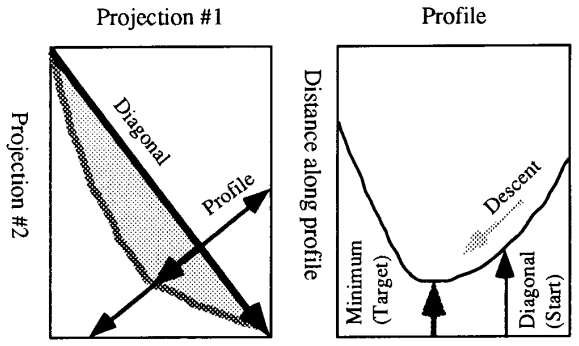

Fig. 6. Optimum correspondence path.

the rays for each pair of segment elements (Fig. 6). This is done by calculating the points of the minimum distance. The correspondence is defined by the path of lowest distances from matrix elements (0, 0) to $(n-1, m-1)$.

Parker *et al.* developed a method where the elements are discretely assigned and reconstructed [11]. We created a new algorithm with additional interpolation of missing elements to any desired segment length. The resulting 3-D segment contains at least the number of elements of the longer 2-D segment. The diagonal represents the simplest case of linear assignment. Bilinearly interpolated profiles of the cost matrix are obtained orthogonally to the diagonal, then descent and minima on the profile are evaluated, resulting in an element of the optimum path.

Difficult shapes of the vessel segment (e.g., S-curvatures) may cause local ambiguities in the matrix. In extreme cases, a plateau of same values is created when several projection rays are in the same level. As a fallback solution, linear assignment with additional smoothing is performed then. Thus, the cost minima are not necessarily zero for all matches.

The global geometry approximation algorithm can minimize only the global mean error, local errors may remain. Without considering the remaining geometric errors, the determined path may be incorrect. These errors need to be corrected before performing the element matching. The geometric error vectors derived from the nodes enclosing the segment are interpolated along the error direction. The error direction in a node P is orthogonal to both projection rays. It consists of a constant portion orthogonal to the projection axes and a variable portion dependent on the distortion due to perspective. Thus, error directions of nodes that are close to each other are nearly collinear. The mean error direction of two or more neighboring nodes is defined as the intermediate of their local error directions

$$\vec{e}_{\mathrm{MEAN}} = \begin{cases} \vec{e}_A + \vec{e}_B & \text{if } \vec{e}_A \cdot \vec{e}_B \geq 0 \\ \vec{e}_A - \vec{e}_B & \text{else} \end{cases}$$
$$\vec{e}_A = P_A Q_{A_p} \text{ and } \vec{e}_B = P_B Q_{B_p}. \tag{5}$$

For each projection p, the error vectors $\vec{e}$ from the reconstructed node P to the nearest points Q_p on their rays are extracted for both surrounding nodes A and B of a segment. Along the mean error direction $\vec{e}_{\mathrm{MEAN}}$, for each element an individual error vector $\vec{e}_{\mathrm{ELEM}}$ is interpolated (Fig. 7). This is performed by obtaining the scalar products of the reconstructed world coordinates of both nodes and the desired element with the mean error direction vector. Weighted by the element's distances to A and B, their local error vectors are interpolated

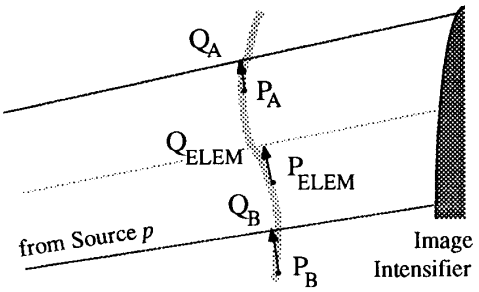

Fig. 7. Local error correction.

$$\vec{e}_{\mathrm{ELEM}} = (1-t)\cdot\vec{e}_A + t\cdot\vec{e}_B;$$
$$t = \frac{\vec{e}_{\mathrm{MEAN}}\cdot(\vec{q}_A - \vec{q}_{\mathrm{ELEM}})}{\vec{e}_{\mathrm{MEAN}}\cdot(\vec{q}_A - \vec{q}_B)}. \tag{6}$$

The points Q_p of an element are then moved by their negative error vectors, thus the minimum distance between the two ray candidates is now correct according to the surrounding nodes [7].

B. 3-D Volume Determination

1) Modeling of Vessel Cross-Sections: The vessel detection algorithm delivers both centerline and edges in 2-D images. They can be reconstructed to a radius vector for each projection, i.e., for biplane views there are two vectors available. Thus, there is no need to restrict ourselves to circular contours (e.g., as done in [4]). However, it is necessary to consider some ambiguities when calculating elliptical cross-sections.

For each element of a vessel, the 3-D centerline points are calculated. For each projected centerline point P, two edge point pairs E exist with symmetrical distance from P. Their image points can be used to reconstruct the radius vectors.

The distance $B_{\mathrm{Edge}} - B_{\mathrm{Point}}$ in world coordinates multiplied by the factor t for object point P yields the radius r. Due to an oblique entering of the ray by angle α, this radius is radially lengthened by $1/\cos\alpha$. More significant are errors due to point-spreading for small vessels. These have to be corrected empirically by phantom measurements [9].

As already described in Section II-A, the 2-D coordinates of the segment elements are interpolated. This requires the additional interpolation of the edge information. Although we can achieve a high correspondence of the selected radius vectors, small errors in the correspondence remain due to tolerances in setting of the nodes, etc.

After establishing both radius vectors, they can be used to form the elliptic contour. Only in the case of triple orthogonality [12], [13] can the radius vectors be used directly as the axes, otherwise the form of the ellipse is ambiguous due to a systematic loss of spatial information. To compensate for

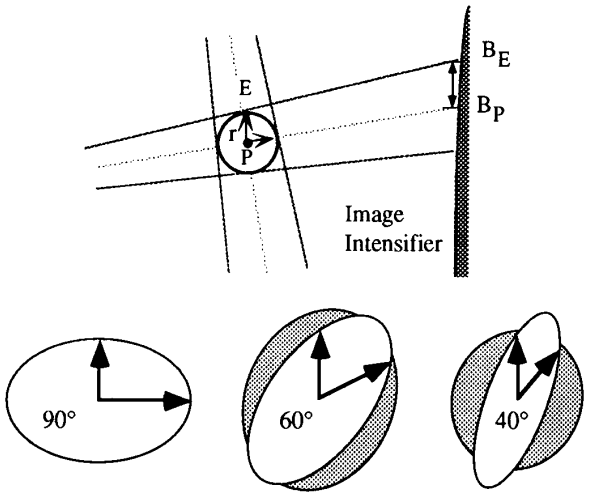

Fig. 8. Radius reconstruction and ellipse deformation.

this effect, we continuously change the shape of the contour from elliptic to circular depending on the amount of spatial information for each element (Fig. 8).

2) Generalized Elliptical Conic Sections: The cross-section reconstruction results in discrete contours. They are defined by their center points and tupels $(\vec{a}, \vec{b})$ of axes. Neither the planes of the contours nor the vector pairs $(\vec{a}_1, \vec{a}_2)$ and $(\vec{b}_1, \vec{b}_2)$ are necessarily parallel (Fig. 9). The volume of a vessel is calculated by integration of the cross-sections in relation to its length, where between two adjacent contours the volume has to be interpolated. The total volume is thus the sum of the volumes between adjacent pairs of contours

$$\sum_{i=1}^{n-1} v(\vec{a}_i, \vec{a}_{i+1}, \vec{b}_i, \vec{b}_{i+1}, \vec{d}_i). \tag{7}$$

The volume determination is based on the mathematical definition of a truncated cone

$$V = h\frac{G_1 + \sqrt{G_1 G_2} + G_2}{3} \tag{8}$$

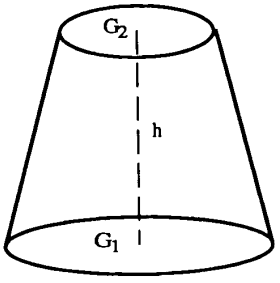

The elliptical base results from the elliptic axes to

$$G_i = \pi |\vec{a}_i||\vec{b}_i|. \tag{9}$$

The axis $\vec{d}_i$ between the contour centers may not be related orthogonally to the bases, thus

$$h_i = \cos\phi_i \cdot |\vec{d}_i|. \tag{10}$$

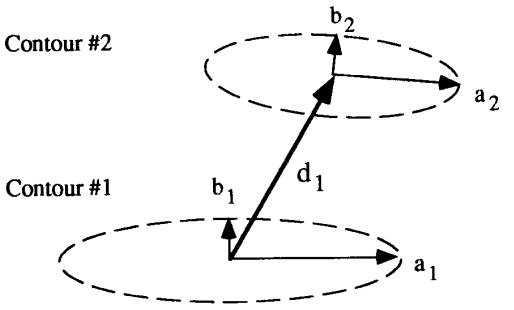

Fig. 9. Relations between adjacent contours.

Twisting, i.e., (G_1, G_2) are parallel, but $(\vec{a}_1, \vec{a}_2)$ and $(\vec{b}_1, \vec{b}_2)$ are not, does not influence these equations. A more complex problem is caused by oblique bases, i.e., (G_1, G_2) are not parallel. This problem is partially solved by volume balancing for small angles μ

$$|\vec{a'}| = |\vec{a}| \cos\mu \tag{11}$$

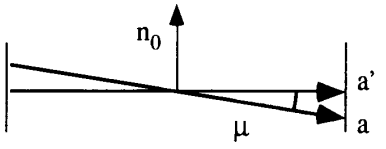

where $\vec{a'}$ is orthogonal to $\vec{n}_0$. The base areas are now

$$G_i = \pi |\vec{a}_i||\vec{b}_i| \cos\mu \tag{12}$$

assuming nearly cylindrical volume elements. The normal $\vec{n}_0$ must be selected in a way that minimizes the approximation error for conic elements. Thus, it is calculated as the area weighted middle of the adjacent contour normals $\vec{n}_1$ and $\vec{n}_2$

$$\vec{n}_1 = \vec{a}_1 \times \vec{b}_1; \quad \vec{n}_2 = \vec{a}_2 \times \vec{b}_2; \quad \vec{n}_0 = \vec{n}_1 + \vec{n}_2 \tag{13}$$

which results in the equations for angles ϕ and μ

$$|\cos\phi_i| = \frac{|\vec{n}_0 \cdot \vec{d}_i|}{|\vec{n}_0||\vec{d}_i|}; \quad |\cos\mu_i| = \frac{|\vec{n}_0 \cdot \vec{n}_i|}{|\vec{n}_0||\vec{n}_i|}. \tag{14}$$

By inserting (13) and (14) into (10) and (12), respectively, and those using (8) into (7), the desired volume equation is found.

3) Vessel Length Calculation: The total length of a vessel is the sum of the distances between adjacent contours. The lengths of the $\vec{d}_i$ vectors cannot be taken since these are not parallel to the vessel course. Thus, small deviations in the vessel centerline sum up to significant errors. The volume heights h_i cannot be used either, because, due to the reconstruction process, the contours are not necessarily orthogonal to the vessel. In fact, the determination of the vessel course is a main problem of length measurement.

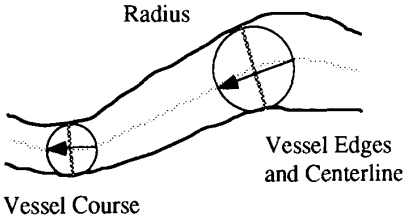

Fig. 10. Vessel length in relation to its course.

We developed a new method for calculating the distance of adjacent contours that considers the local radius to suppress tolerances in the detected vessel shape. The radius at a specific vessel element is used to form a sphere within the vessel. The points where the centerline enters and leaves this sphere mark the environment (Fig. 10). The mean direction within this environment is used for the determination of the length. Thus, the total length of a vessel is a sum of local distances depending on tupels of ellipse axes and centerline vectors

$$\mathbf{L} = \sum_{i=1}^{n-1} l(\vec{a}_i, \vec{b}_i, \vec{d}_i) \tag{15}$$

where the length element $l(\vec{a}_i, \vec{b}_i, \vec{d}_i)$ is

$$l(\vec{a}_i, \vec{b}_i, \vec{d}_i) = \frac{|\vec{l}_i \cdot \vec{d}_i|}{|\vec{l}_i|} \tag{16}$$

and

$$\vec{l}_i = \sum_{i^*=i_{\mathrm{LOW}}}^{i_{\mathrm{HIGH}}} \vec{d}_{i^*} \tag{17}$$

where the bounds $i_{\mathrm{LOW}} \leq i \leq i_{\mathrm{HIGH}}$ have to be selected in a way that satisfies the radius condition

$$|\vec{l}_i| \approx 2\frac{|\vec{a}_i| + \vec{b}_i|}{2} = |\vec{a}_i| + |\vec{b}_i|. \tag{18}$$

C. Data Acquisition

At the German Heart Institute of Berlin, two biplane Philips devices (frontal: Diagnost-C, lateral: L-ARC, both of type II as defined in [1]) are used. The biplane images are archived on 35-mm cine film with a rate of 12.5 (rare), 25 (coronary arteries), or 50 (ventricles) images per second. Two (6", 9") and three (5", 7", 9") image intensifier sizes can be chosen, depending on the device. Images of further interest may be selected and stored digitally in 512 × 512 pixel format on a Cardiac Workstation (CWS). The spatial resolution is within the range of 0.125 to 0.35 mm per pixel, depending on image intensifier size and focal distances.

The image data for the reconstruction process may be acquired in two ways: from the CWS directly in ACR-NEMA 2.0 format [14], from the 35-mm films using an ARRIPRO 35 projector delivering the video data for a DASM frame grabber. Pixel resolution and depth are the same for both digitally and conventionally acquired images. Of course, image contrast, distortion and noise differ. The required imaging data (e.g., distances, angulations, used catheters) can be retrieved from the patient information system (interventional data protocol).

In a preprocessing step, the images are rectified using regular grids [9]. In this way, any errors are eliminated that were caused by the unevenness of the image intensifier entrance fields and the geomagnetic field or by other effects during the acquisition and digitization process. Four lead markers mounted on the image intensifier entrance fields in known distances and orientations are used for further dewarping to obtain the correct image centers and orientations [15]. Furthermore, the real image intensifier sizes can be determined by these markers.

For each chain of image acquisition (used device, media, and correction processes), a unique set of device parameters is generated. Using these base parameters, for each image series the imaging geometry is derived.

D. Validation

Quantitative verifications were performed in several phantom studies. The imaging geometry approximation system was tested with both synthetically generated and real images. A virtual cube phantom with 40-mm edge length was used with a significantly distorted set of imaging parameters; the original parameters could be restored with a maximum error of 0.012 mm in isoaxis distances [5].

In a further study, we used a hexagonal phantom to determine the gantry sags. In standard frontal and lateral orientation, we measured an isocentric shift (i.e., distance of a projection axis to the rotational origin) of 10.4 mm for both systems. After establishing an exact isocenter in frontal/lateral orientation and moving the systems to 30°RAO/30°caud and 60°LAO/30°cran, there was a shift of 2.7 mm again. Even when using the frontal system for both angulations, there was still a sag of 1.7 mm. Significant distortions could be measured in longitudinal direction related to the projection axes: In theory, as far as our equipment is concerned, the distance of each focal spot to the isocenter is assumed to be constant ($D_S \approx 700$ mm) and not dependent on either rotation or total distance to the image intensifier. We found that the focal spot of the lateral system shifted by ± 9.5 mm during rotation, while the frontal focal spot had a tolerance of ± 20.1 mm in D_S. These distortions are not reproducible, i.e., after rotating from one into another and then back to the first orientation, the distorted parameters cannot be assumed to be the same again.

A comparison between the different single- and biplane calibration methods was performed using a cylindric solid phantom (40 mm in length by 6 mm in diameter) imaged in triple orthogonality. For calibration, a 7 F pigtail catheter was available with three markers of each 20-mm distance and a loop of 14.5 mm in diameter (Fig. 11). This pigtail catheter was inserted 1) in triple orthogonality, 2) oblique by approx. 30° and slightly curved, and 3) in a strong S-shaped curve with oblique orientations up to 60°. Additionally, angulated images with down to 70° inclination angle between the systems and ± 15° of skew were taken. After performing each calibration

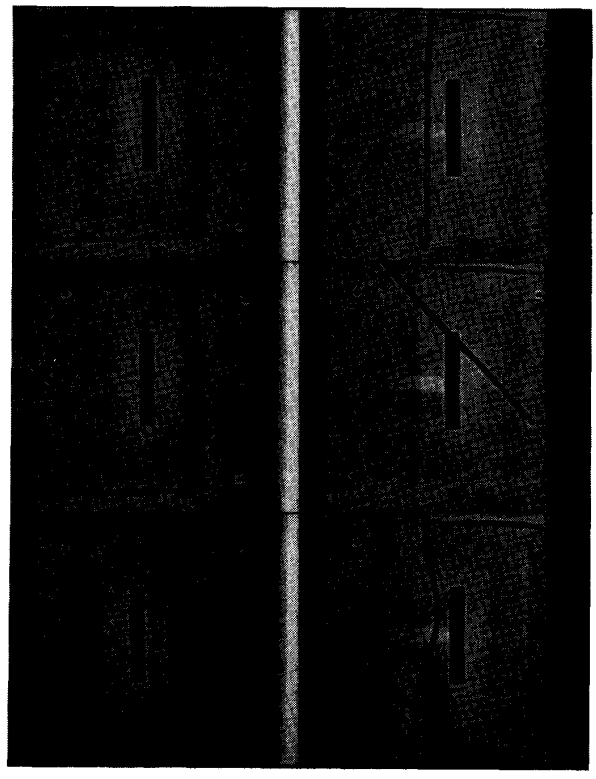

Fig. 11. Selected images of calibration study.

method, we reconstructed the cylinder and determined the errors in diameter and volume.

Using the conventional single-plane catheter diameter calibration method, volume measurement errors were in the range of 21–29%. The single-plane cardiomarker method yields good results only if the catheter is in triple orthogonality and adjusted in isocenter level; gross errors were caused by oblique catheters, thus the volume errors were in the range of 15–66%. The biplane methods should raise better results. As proposed by Büchi and Kirkeeide [3], the isocenter method yielded a mean volume error of 3.1%, whereas a maximum error of 9.7% was measured due to gantry sagging. Our biplane cardiomarker calibration (with edge detection applied to follow the catheter curvature) resulted in a comparable mean error of 3.5%, but within a more stable range of 3.0–4.6%. Finally, the biplane calibration using the pigtail loop minimized the volume errors to 0.8–4.4% (mean 2.6%).

While parallaxes do not cause significant further errors (volume errors using a spiral phantom of 76 mm in length and 5 mm in diameter: triple orthogonality 1.6%, 60° oblique to isoaxis 1.9%), inclination angles less than 30° between the X-ray systems raised the measured errors dramatically due to a high loss of spatial information. Within the inclination range of 60–120° used in medical practice, the additional volume errors kept below 1.5% (70°). In absence of overlapping, differences due to changes of the object position and orientation resulted in errors below 1%. Overlapping vessels, or if the vessels are strongly shortened in one or both projections, significant errors occur due to ambiguities and incorrect edge recognition (up to 8% in local diameters and up to 3% in vessel volumes).

The real phantom dimensions were obtained by manual measurements and/or water displacement.

III. Medical Application

A. Overview

There are many patients suffering from coronary artery disease without significant local stenosis and even more who have qualitatively obvious diffuse disease in addition to local stenoses. In some of these patients, e.g., post heart transplantation, luminographic X-ray projections may even show smooth vessel walls falsely suggesting absence of atherosclerotic disease, though those patients may be at high risk, eventually needing retransplantation. Qualitative alterations in the angiographic appearance of the coronary tree are of unknown significance. The assessment of their clinical impact implies the development of tools defining and quantifying these alterations. Even in patients with obvious diffuse disease, as in patients with dilating atherosclerotic arteries or with diffuse vessel narrowing (e.g., in diabetic patients), there is only a qualitative description possible, presented as an obstacle to assessment of severity of disease and the impact of therapeutic intervention on the progression.

Whereas the diagnosis and treatment of local stenosis are well established, assessment of diffuse disease remains difficult and time-consuming. There have been several approaches each suffering from various limitations. Conventional approach is usually serial measurement of absolute luminal diameters or cross-sections [16].

Recently, it was proposed to compare cross-sectional luminal area with the total distal length of the vascular tree since there is a strong correlation between the size of the coronary tree and regional mass perfused [17].

Chronic reduction in perfusion or progression in atherosclerosis should be associated with remodeling of trees and subtrees. The vascular tree in patients without atherosclerotic disease seems to obey certain scaling laws [17]–[19], complying with the principles of minimum viscous energy loss and limited adaptive vascular shear-stress [17]. The extent of deviation from this normal pattern should reflect the severity of disease. The observation that even diffuse disease is often not homogeneously distributed suggests that correlation analysis of dimensions in sets of coronary subtrees might be a suitable approach to measure progression in diffuse disease.

B. Methods

The purpose of this study is to quantify diffuse disease overall on total trees, which is to be well discerned from evaluating stenosis or reconstructing plaque locally. Thus, for testing this approach, LCA and RCA trees were analyzed retrospectively from three groups of patients selected according to clinical diagnosis:

1) Patients having no visible disease (controls).
2) Patients with CAD of the localized type post PTCA (CAD).

3) Patients with severe diffuse and dilating coronary artery disease (DCAD).

The patients, routinely imaged in the years 1992 and 1993 due to various diseases, were selected by their findings using the local patient information system. They had been imaged in standard projections (0–45°RAO, 45–90°LAO, with up to ± 20° skew) using either 6″, 7″, or 9″ (general views) image intensifier diameters. Patients had been catheterized by Judkins technique in local anaesthesia without special additional preparation. Manually injected Ultravist™ had been used as contrast agent. Analysis was done on end-diastolic frames, except a special study with 11 selected biplane angiographic pairs of different heart cycle phases of the same patient.

After performing the reconstruction process, the visible parts of the arteries are available as a 3-D tree (Fig. 12). This tree can be decomposed into a "stem" containing the segments from the root to the first bifurcation, and a corresponding "crown" consisting of the branches below the bifurcation. For example, the LCA is decomposed into the left main as the stem, and the combination of LAD and CX as the crown. The principal branches of a crown containing at least one additional bifurcation may be regarded as subtrees and are decomposed into stems and crowns in the same way as described above. A crown without any bifurcating branch cannot be decomposed. By the recursive application of this decomposing algorithm, every tree gives rise to a family of subtrees consisting each of a stem and a corresponding crown.

Assessment of Tree Destruction: Supposing a fractal vessel geometry in controls, the dimensions of the subtrees in terms of lengths, diameters, and volumes are scaled in a similar way [17]–[19]. Atherosclerotic disease due to inhomogeneous distribution is expected to be associated with increased variance in the scaling of individual subtrees. Angiographically visible destruction of the arterial tree seen in dilating coronary artery disease implies virtual abolishment of the normal fractal geometry. Thus, an effective measure for assessment of progressive destruction of fractal order in a coronary tree should assume well-separated values in the tree groups of patients and has to quantify the amount of similarity of scaling relations within a subtree. Correlations of the dimensions of the subtrees are suitable measures [20].

IV. Results

For every subtree, there are six corresponding values (length, diameter and volume, both for stem and for crown) which should be correlated. Graphical and numerical analyses showed that the relations are nonlinear. Logarithmic transformation turned out to be an appropriate preprocessing step linearizing data. Analysis using Bravais Pearsons correlation coefficient [20] was done in 67 RCA and 62 LCA subtrees in controls, 35 RCA and 83 LCA subtrees in the CAD group, and in 30 RCA and 42 LCA subtrees in the DCAD group.

There are 15 different combinations available to select a pair out of the six parameters mentioned above for a correlation analysis. The sum of these correlations gives a rough assessment of the degree of order inherent in the set of analyzed subtrees. Since some of these correlations are partially trivial (e.g., diameter of stem in relation to the volume of stem),

(a)

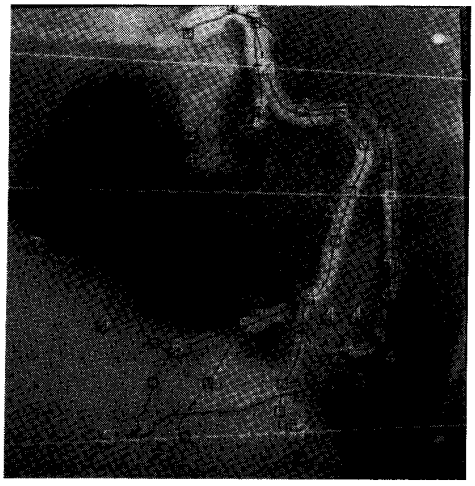

(b)

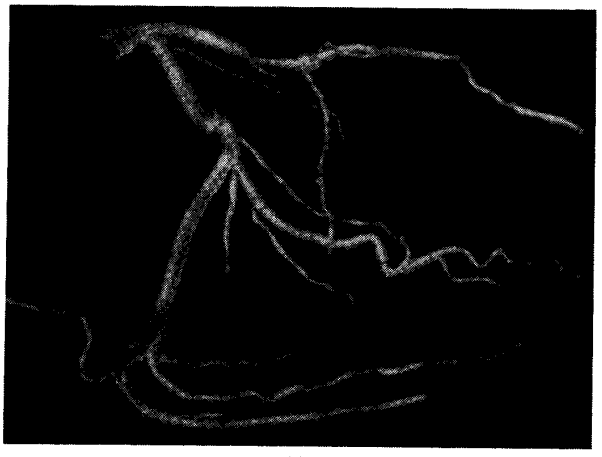

(c)

Fig. 12. RAO (a) and LAO (b) views of a left coronary artery (diff. CAD patient), reconstructed and shaded spatial model (c).

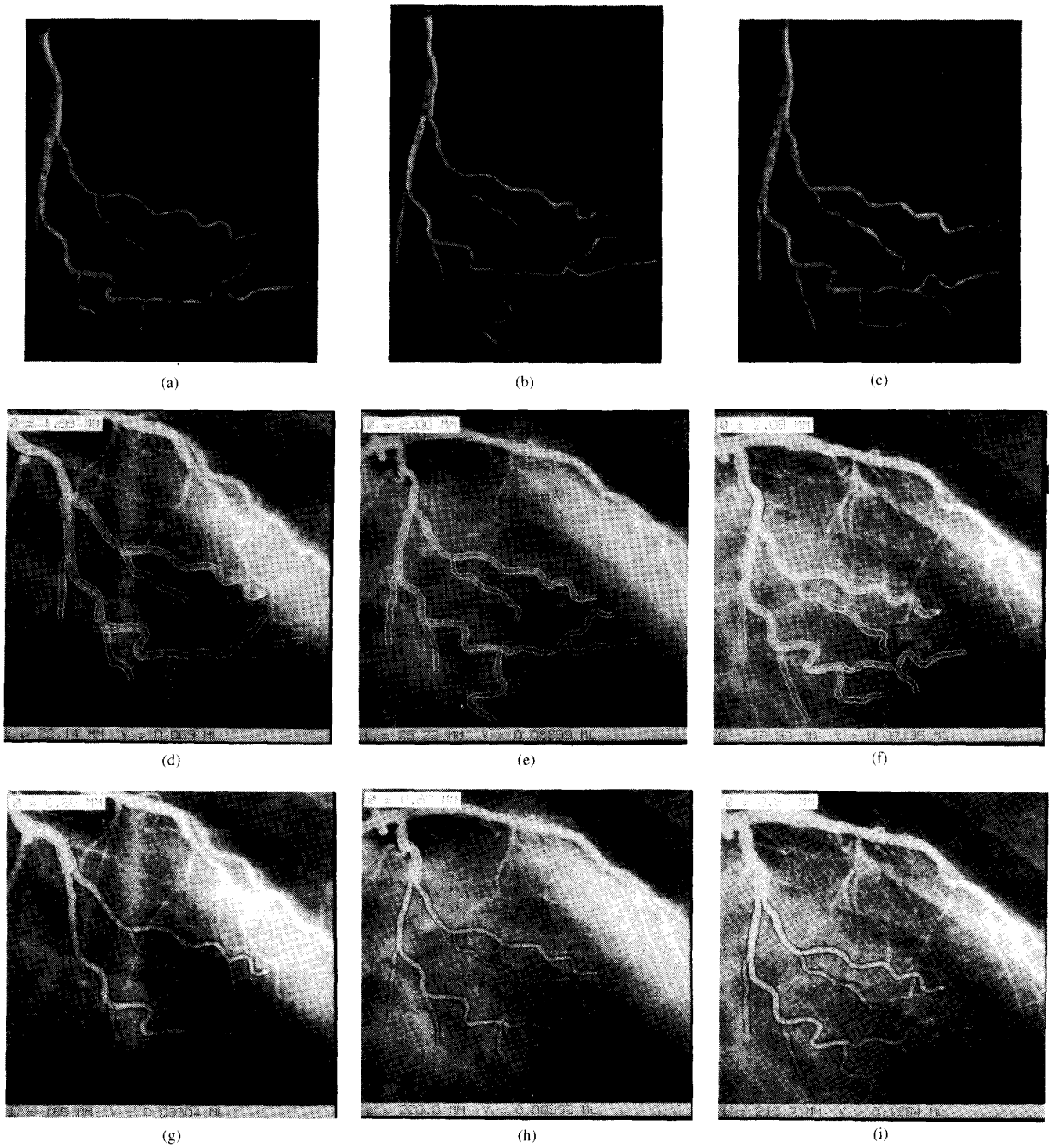

Fig. 13. Comparison and 3-D evaluations on a selected vessel subsystem (LCX) of a control patient. (a), (b), (c) The results of reconstruction and visualization. (d), (e), (f) The mean diameter (Ø), total lengths (L), and volumes (V) of the proximal vessel segment. (g), (h), (i) The corresponding values of the distal vessel subsystem. In (a), (d), and (g), no intervention was performed, in (b), (e), and (h), intervention by ergonovine was performed, and in (c), (f), and (i), intervention by nitroglycerine was performed.

retaining them is to be considered as giving additional weight to good correlations. We applied a weighting factor of zero to those correlations smaller than 0.5 in this sum to suppress bad correlations. The weighted sum of these 15 correlations (SUM) proved to be an effective measure of progressive destruction of order in the coronary tree with severity of atherosclerotic disease, as can be seen from Table I. Since weighted adding of measures yields again measures according to mathematical theory, the empirically defined parameter SUM remains a measure [21]. It is decreased if variance in the dimensions of the subtrees increases. Intervention with ergonovine (a test agent producing vascular spasm) decreases SUM by

TABLE I
CORRELATION ANALYSIS

Group	n	Length	Volume	Diam.	SUM
RCA					
Control	67	0.45	0.48	0.82	**3.67**
CAD	35	0.30	0.35	0.81	**2.80**
DCAD	30	0.25	0.28	0.40	**1.50**
LCA					
Control	62	0.57	0.61	0.82	**4.73**
CAD	83	0.42	0.45	0.79	**3.51**
DCAD	42	0.23	0.23	0.50	**1.65**

approximately 13%, whereas intervention with nitroglycerine (a vasodilating agent) increases SUM by approximately 12%.

Apart from the weighted sum of correlations, the correlations of the diameter of the stem with the diameter (D), length (L), and volume (V) of the corresponding crown are statistically significant (Table I). The correlations were generally better in the left coronary artery than in the right coronary artery.

V. DISCUSSION

Since ordinarily decomposition of the coronary tree yields more than 10 subtrees, calculating SUM on an individual basis seems feasible. Nevertheless, it would be desirable to have a local measure requiring only the evaluation of a part of the coronary tree.

The amount of time spent by the operator in evaluating a total tree varies widely according to the experience of the operator, complexity of the coronary anatomy, and technical factors, e.g., quality of the angiograms and the precision of the technical equipment and the interventional data protocol. A realistic estimation per total evaluation is 1 to 2 h.

Seiler *et al.* [17] found a correlation between area measured at any location in LCA and the total summed length of distal branches of $r = 0.93$ in controls and $r = 0.88$ in all patients. This parameter roughly corresponds to L. In a smaller series of 53 subtrees previously reported [22], we found correlations of $r = 0.802$ for L, whereas now in controls this value was only 0.57 in LCA subtrees.

The difference is attributed to several reasons. Apart from variance of r within a confidence interval due to sampling, Seiler's area calculation was based on diameters from selected segments of the coronary angiogram suitable for QCA, whereas our data include all segments (even those with ambiguous nodes, overlapping regions, areas of overexposure, and those containing stenoses). Correlation was worse in subtrees approaching the limits of angiographic resolution. Thus, suppressing the highest order of subtrees improves correlations. Based on our experience, ignoring subtrees with an order of higher than six, or—in other terms—with mean stem and crown diameters less than 0.5 mm, is recommended.

Comparing different phases of the cardiac cycle, there was a slight reduction of diameter and volume (2.31 mm, 0.865 mL) in early diastole as compared to systole (2.58 mm, 1.059 mL). The length of the tree varied about 3.4%. This variance was not systematic as in diameters and volumes and is within the limits of reproducibility.

As may be seen from Fig. 13, the length of the vascular stem changes under intervention with ergonovine as compared to controls and intervention with nitroglycerine. This phenomenon was investigated by a thorough analysis of this tree. Segments and subtrees were matched, thus the topologies of the considered subtrees were identical in both interventions and control. Effects due to cardiac cycle phase and patient motion could be excluded. A repositioning of the nodes in the proximal stem was done, minimizing possible segmentation errors at the bifurcation. The first two segments of the circumflex in the ergonovine tree remained 10–20% longer than the corresponding segments of the nitroglycerine intervented tree, in spite of minimizing variances due to other sources. Since there was no such difference in the remaining distal segments, this effect might be related to the thickness of the arterial wall. Due to the principle of conservation of mass of wall volume, dilation of a thin-walled artery should be associated with slight foreshortening

$$V = \pi\left(2d\,r + d^2\right)\cdot L$$

$$\Rightarrow\quad r = \frac{V}{2\pi}\cdot\frac{1}{d\cdot L} - \frac{d}{2} \tag{19}$$

$$\text{with } C = \frac{V}{2\pi} \text{ constant:}$$

$$\Rightarrow\quad r = C\,\frac{1}{d\cdot L} - \frac{d}{2}$$

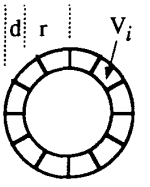

r inner radius of vessel;
d thickness of wall;
L length of segment;
V volume of the wall (sum of all wall cells V_i);
assuming a circular vessel cross-section.

If d is small and of limited variance, an increase in r is only possible if L becomes smaller.

More extensive clinical testing in different groups of patients is necessary to address these problems and to evaluate this approach further.

REFERENCES

[1] H. Wollschläger, P. Lee, A. Zeiher, U. Solzbach, T. Bonzel, and H. Just, "Mathematical tools for spatial computations with biplane isocentric X-ray equipment," *Biomedizinische Technik*, vol. 31, pp. 101–106, 1986.
[2] ——, "Improvement of quantitative coronary angiography by calculation of exact magnification factors," *IEEE Comput. Cardiol.*, pp. 483–486, 1985/86.
[3] M. Büchi, O. M. Hess, R. L. Kirkeeide, T. Suter, M. Muser, H. P. Osenberg, P. Niederer, M. Anliker, K. L. Gould, and H. P. Krayenbühl, "Validation of a new automatic system for biplane quantitative coronary arteriography," *Int. J. Cardiac Imag.*, vol. 5, pp. 93–103, 1990.
[4] J. W. Peifer, N. F. Ezquerra, C. D. Cooke, R. Mullick, L. Klein, M. E. Hyche, and E. V. Garcia, "Visualization of multimodality cardiac imagery," *IEEE Trans. Biomed. Eng.*, vol. 37, no. 8, pp. 744–756, 1990.
[5] A. Wahle, E. Wellnhofer, H. Oswald, and E. Fleck, "Biplane coronary angiography: Accurate quantitative 3-D reconstruction without isocenter," *IEEE Comput. Cardiol.*, London, pp. 97–100, 1993/94.
[6] D. L. Parker, D. L. Pope, K. S. White, L. R. Tarbox, and H. W. Marshall, "Three dimensional reconstruction of vascular beds," in *Information Processing in Medical Imaging*. Boston: Nihoff, 1986, pp. 414–430.

[7] A. Wahle, H. Oswald, G. A. Schulze, J. Beier, and E. Fleck, "3-D reconstruction, modeling and viewing of coronary vessels," in *Computer Assisted Radiology CAR'91*. Berlin: Springer-Verlag, 1991, pp. 669–676.

[8] L. E. Fencil and C. E. Metz, "Propagation and reduction of error in 3-D structure determined from biplane views of unknown orientation," *Med. Phys.*, vol. 17, no. 6, pp. 951–961, 1990.

[9] J. Beier, H. Oswald, and E. Fleck, "Edge detection for coronary angiograms: Error correction and impact of derivatives," *IEEE Comput. Cardiol.*, Venice, IT, pp. 513–516, 1991.

[10] A. Wahle, H. Oswald, and E. Fleck, "A new 3-D attributed data model for archiving and interchanging of coronary vessel systems," *IEEE Comput. Cardiol.*, London, pp. 603–606, 1993/94.

[11] D. L. Parker, D. L. Pope, R. van Bree, and H. W. Marshall, "Three dimensional reconstruction of moving arterial beds from digital subtraction angiography," *Comput. Biomed. Res.*, vol. 20, pp. 166–185, 1987.

[12] H. Wollschläger, A. Zeiher, P. Lee, U. Solzbach, T. Bonzel, and H. Just, "Computed triple orthogonal projections for optimal radiological imaging with biplane isocentric multidirectional X-ray systems," *IEEE Comput. Cardiol.*, Boston, MA, pp. 185–188, 1986/87.

[13] A. C. M Dumay, J. H. C. Reiber, and J. J. Gerbrands, "Determination of optimal angiographic viewing angles: Basic principles and evaluation study," *IEEE Trans. Med. Imag.*, vol. 13, no. 1, pp. 13–24, 1994.

[14] ACR-NEMA 300–1988, "Digital imaging and communications," *Nat. Elec. Manufacturers Assoc.*, Washington, D.C., pp. 11–20, 59-84, 1989.

[15] D. G. W. Onnasch and G. P. M. Prause, "Geometric image correction and isocenter calibration at oblique biplane angiographic views," *IEEE Comput. Cardiol.*, Durham, N.C., pp. 647–650, 1992/93.

[16] P. J. de Feyter, P. W. Serruys, M. J. Davies, P. Richardson, J. Lubsen, and M. F. Oliver, "Quantitative coronary angiography to measure progression and regression of coronary atherosclerosis," *Circ.*, vol. 84, pp. 412–423, 1991.

[17] C. H. Seiler, R. L. Kirkeeide, and K. L. Gould, "Basic structure function relations of the epicardial coronary vascular tree: Basis of quantitative coronary arteriography for diffuse coronary artery disease," *Circ.*, vol. 85, pp. 1987–2003, 1992.

[18] S. H. Zhou, E. Mateeva, and R. Collins, "The anatomy of human coronary vessels," in *Second International Symposium on Biofluid Mechanics and Biorheology*, D. Liepsch, Ed. New York: Springer-Verlag, 1990, pp. 463–470.

[19] J. H. G. M. van Beek, S. A. Roger, and J. B. Bassingthwaighte, "Regional myocardial flow heterogeneity explained with fractal networks," *Amer. J. Physiol.*, vol. 257, pp. H1670–1680, 1989.

[20] P. Armitage and G. Berry, *Statistical Methods in Medical Research*, 2nd ed. London: Blackwell Scientific, 1987, p. 150.

[21] H. Bauer, *Wahrscheinlichkeitstheorie und Grundzüge der Maβtheorie*, 2nd ed. Berlin/New York: Walter de Gruyter Verlag, 1974, pp. 22–23 (in German).

[22] A. Wahle, E. Wellnhofer, I. Mugaragu, H. U. Sauer, H. Oswald, and E. Fleck, "Quantitative volume analysis of coronary vessel systems by 3-D reconstruction from biplane angiograms," in *IEEE Medical Imaging Conference*, San Francisco, CA. New Jersey: IEEE Press, 1993/94, vol. 2, pp. 1217–1221.

2.1.2 Validation of an accurate method for three-dimensional reconstruction and quantitative assessment of volumes, lengths and diameters of coronary vascular branches and segments from biplane angiographic projections

Diese Arbeit stellt den zentralen Schritt der Validierung der unter 2.1.1 dargestellten Methode dar. Mit dieser Arbeit wurde die 3-D QCA als valide Messmethode für Herzkranzgefäße etabliert.

Es ließ sich zeigen, dass die 3-D QCA

- ein gegenüber der 2-D QCA genaueres Messverfahren (<3% Fehler) ist,
- mit moderater Interobserver- und - Intraobservervariabiliät (≤5%, Tabelle 2 und 3 und Fig. 6 und Fig.7),
- ein Messverfahren mit hoher Sensitivität ist, - durch den Herzzyklus (Tabelle 4) oder Medikamente (Tabelle 5) ausgelöste Diameter- und Volumenänderungen werden erfasst- ,
- mit signifikant geringerer Abhängigkeit von Projektionen (Verkürzungen) als die 2 D- QCA behaftet ist (Fig. 8 , Fig. 9 und Fig. 10)
- und neben Durchmessern, Längen, Winkel und Krümmungen der Gefäße exakt erfassen kann.

Schlussfolgerungen der Arbeit waren:

- Die 3-D QCA ist für retrospektive Verlaufsuntersuchungen geeignet, weil sie im Gegensatz zur 2-D QCA keine identischen Projektionen voraussetzt.
- Die 3-D QCA eignet sich besonders zur Beurteilung diffuser Veränderungen und Tonusschwankungen.
- Die 3-D QCA eignet sich darüber hinaus ausgezeichnet für eine erweiterte Geometrieanalyse mit Beurteilung von Krümmungen, Verzweigungen, Gefäßlängen und Volumina

Der Erstautor hat die Daten erhoben und statistisch analysiert. Er hat die Arbeit konzipiert, geschrieben und diskutiert. Neben der Zuarbeit von Herrn Wahle (Daten zu Phantommessungen) bestand der Beitrag der Herren Mugaragu und Gross in der Erstellung komplexer und zeitaufwändiger Rekonstruktionen und wertvollen methodischen Diskussionsbeiträgen.

Der Abdruck des folgenden Artikels erfolgte mit freundlicher Genehmigung der Springer Science+Business Media:

With kind permission from Springer Science+Business Media: International Journal of Cardiac Imaging, Validation of an accurate method for three-dimensional reconstruction and quantitative assessment of volumes, lengths and diameters of coronary vascular branches and segments from biplane angiographic projections. Vol 15, 1999, 339-353, Ernst Wellnhofer, Andreas Wahle, Ignace Mugaragu, Joachim Gross, Helmut Oswald, Eckart Fleck.

International Journal of Cardiac Imaging **15:** 339–353, 1999.

Validation of an accurate method for three-dimensional reconstruction and quantitative assessment of volumes, lengths and diameters of coronary vascular branches and segments from biplane angiographic projections

Ernst Wellnhofer[1], Andreas Wahle[2], Ignace Mugaragu[1], Joachim Gross[1], Helmut Oswald[1] & Eckart Fleck[1]
[1]*Department of Internal Medicine/Cardiology, Campus Virchow-Klinikum, Charité, Humboldt Universität zu Berlin and Deutsches Herzzentrum Berlin, Germany*
[2]*University of Iowa, Department of Electrical and Computer Engineering, USA*

Key words: coronary arteries, QCA, three-dimensional reconstruction

Abstract

The goal of the study was the validation of an accurate method for three-dimensional reconstruction and quantitative assessment of volumes, lengths and diameters of coronary vascular branches and segments from biplane angiographic projections. *Methods*: The accuracy was tested in a complex phantom. *In vivo*, inter- and intraobserver agreement were assessed by analysis of routine angiograms. The sensitivity was evaluated using angiograms of patients having diagnostic vasoactive pharmacological intervention. Two-dimensional quantitative coronary angiography (2-D QCA) and 3-D QCA were compared concerning the accuracy of diameter evaluation. *Results*: 3-D QCA yields accurate results (<3% error) even based on nonorthogonal views, provided that projections parallel to the object are avoided. The inter- and intra-observer variability is $\leqslant 5\%$. Significant ($p < 0.01$) changes of the volume (36–39%) and the diameter (19–21%) are detected following pharmacological intervention. 2-D QCA and 3-D QCA agree in short matched segments without foreshortening. 2-D QCA is rather sensitive to foreshortening and not suitable for evaluation of diameters of longer branches or total coronaries. *Conclusion*: 3-D QCA permits an accurate, reproducible and sensitive comprehensive three-dimensional geometric analysis of the coronaries and is superior to 2-D QCA with respect to extended diameter evaluation.

Introduction

The conventional approach to measure progression and regression of coronary atherosclerosis by two-dimensional quantitative coronary angiography (2-D QCA) is a serial measurement of absolute luminal diameters or cross-sections [1]. This method is limited to intraindividual comparison and hampered by the necessity to measure at the same positions in the same projections supposing identical imaging conditions, precluding retrospective studies. Quantitative analysis of three-dimensionally (3-D) reconstructed coronaries has the theoretical advantage of interindividual comparability and relative independence from position and imaging conditions. Moreover, extended three-dimensional geometric analysis becomes feasible, which may be relevant in the assessment of remodeling. 3-D reconstructions from coronary arteries of real patients may provide a basis for flow-simulation studies. The subsequent study provides an extended validation of a 3-D QCA algorithm reported previously [2–4]. Particular attention is given to the accuracy of diameter measurements of longer vascular segments comparing 3-D QCA to 2-D QCA.

Methods

Phantom study

The accuracy of determinations of diameter, length and volume, which had been previously validated in simple phantoms [3, 4], was tested in a complex phantom (hook ending in a screw, see Figure 1). Reference data for the volumes of the phantom were acquired by water displacement. Diameters and lengths were measured by caliper.

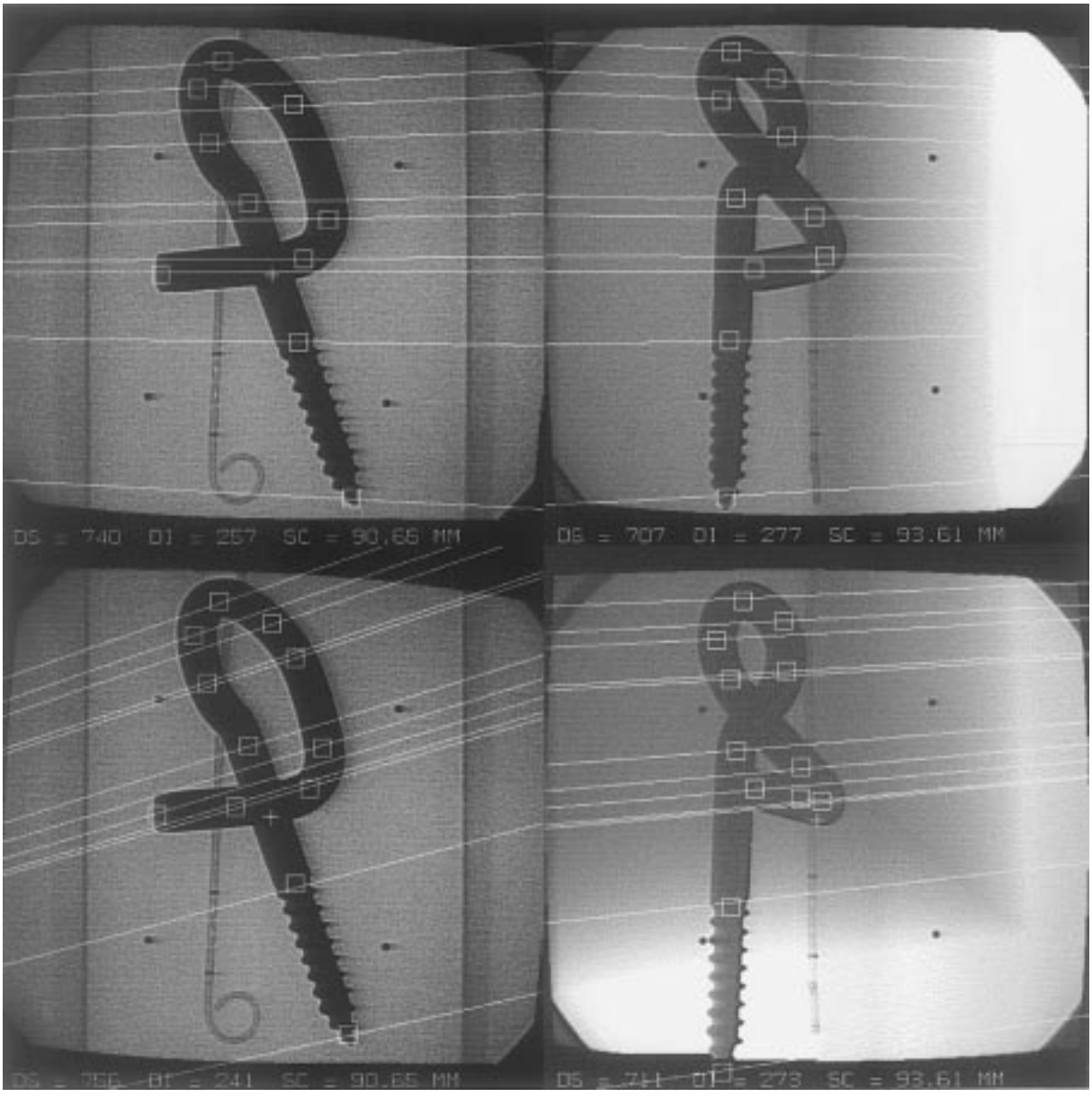

Figure 1. X-ray images of complex phantom with projection rays in two different nonorthogonal views.

Angiographic studies of routine angiograms

Inter- ($n = 32$ for segments and $n = 26$ for branches) and intraobserver ($n = 32$) agreement as well as the variability of the measurements during a cardiac cycle ($n = 6$) were assessed by retrospective analysis of routine angiograms from patients. The impact of the vascular tone was evaluated by a retrospective analysis of routine angiograms from patients, in whom coronary artery disease had been ruled out by angiography and who had been given ergonovine 0.3 mg i.v. followed by 0.15–0.3 mg nitroglycerine i.c. for the diagnosis of vasospastic disease.

Moreover, segmental diameter statistics derived from 3-D QCA were compared to corresponding evaluations using a validated 2-D QCA system (QANSAD^{TM}) in 30 coronary segments [5, 6] under optimal conditions (short matched medial segments without foreshortening, $n = 30$) and under suboptimal conditions comparing the two corresponding 2-D QCA evaluations with their respective 3-D QCA measurements on a segmental basis ($n = 41$). For comparison the segmental 2-D diameter statistics were taken from the projection with minor foreshortening. Calibration was performed by measuring catheter tips and by using X-ray source to image magnifier distances for monoplane isocenter calibration.

Image acquisition

Biplane angiograms (25 frames/s) were acquired digitally and by cinefilm on a standard biplane angiographic X-ray equipment (Philips DCI-System). Angulation, skew and distances of image magnifiers to X-ray sources were recorded by protocol. Frame numbers were used to identify corresponding pictures in LAO and RAO projections. Markers mounted on the magnifier and grid phantoms allowed a rectification of images and a correction of pincushion distortion [7].

3-D reconstruction

A 3-D model was reconstructed from digitized biplane angiographic projections using all geometric information provided by the imaging device. The reconstruction pipeline is delineated by the flow chart in Figure 2. The most important features of this method are summarized:

1. An iterative optimization of the imaging geometry starting from a model integrating protocol data, information regarding the specific X-ray device and corresponding projections is the base of the method [3, 4].

2. Calibration by 3-D reconstruction and retroprojection of objects of known length or

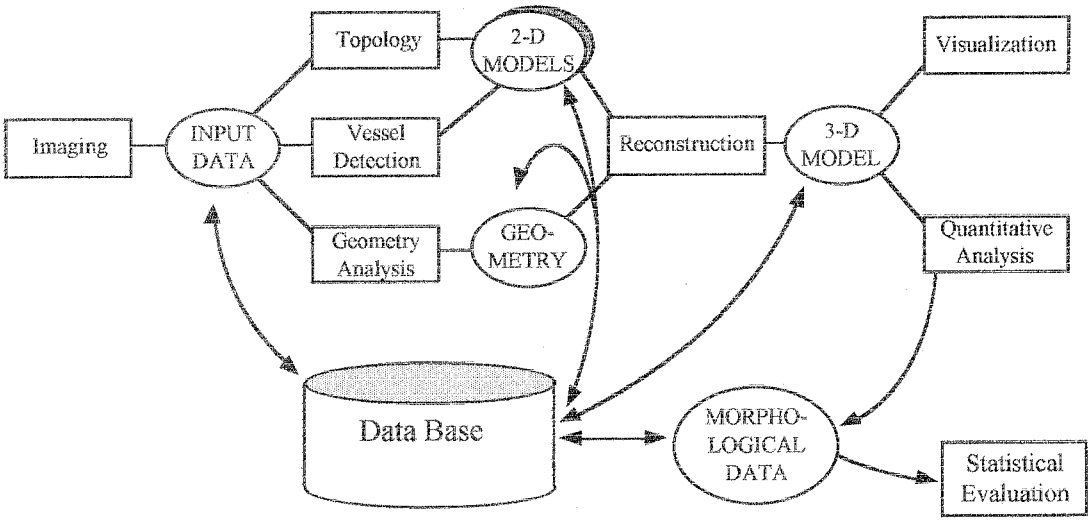

Figure 2. Flow-chart of 3-D reconstruction process.

diameter, e.g. catheter tip, markers or pigtail loops (3-D calibration) provides an improved calculation of image magnification [4, 8].

3. Special metric tools integrating comprehensive 3-D information, as elliptical modelling of cross-sections, volume determination by generalized elliptical conic sections and accurate vessel length calculation by running a caliper sphere along the vessel skeleton (centerline) were developed and validated in phantoms [3, 4]. For detailed presentation of the algorithm, see Wahle et al. [3, 4].

Reconstruction of small vessels of sixth order and higher nearly always necessitated manual corrections. To minimize manual interaction a filter automatically suppressing vessels smaller than 0.5 mm in diameter was used. The number of 3-D diameters per segment is given by the resolution of the 2-D diameter statistics in the angiogram with minor foreshortening. Missing diameters in the corresponding plane are interpolated. Thus the spatial resolution of 3-D QCA with respect to diameter statistics is equal to the resolution of 2-D QCA in the angiogram with minor foreshortening.

An example of matching RAO and LAO angiograms with projection lines and the reconstructed shaded spatial model is displayed in Figure 3.

Special efforts have been undertaken for exact quantitative analysis of the 3-D model based on angiograms. Segmentation of the coronary tree was performed by manual identification of nodes located at bifurcations. There is a unique identification of the segments by a set of numbers. The first number denotes branching order, the last number is identifying the branch at the actual segmentation level and the rest of the numbers contain complete information on previous nodes (see Figure 4).

Measurements of mean diameters, total lengths and volumes were done in each segment and in the related branches of the coronary tree perfused by this segment (see Figure 5).

The manual positioning of nodes is a source of variance affecting predominantly segmental measurements in short segments (a high relative error results from a small deviation). The influence of the projection angle on this error is limited by the fact that the reconstructed rays in 3-D space are bound to cross with limited minimal distance in a neighbourhood of the node.

Statistics

Apart from descriptive statistics (mean $\pm$ SD) paired comparisons were evaluated by mean difference, standard error of estimate of mean difference, *t*-test and correlation. A Bland–Altman plot [9] was employed to compare segmental diameter statistics.

Results

Accuracy in complex phantoms

In this test the algorithm was challenged by a suboptimal geometry in image acquisition. As may be seen from Table 1, changes in object orientation and small changes (20%) in angulation demonstrated minor influence on measurements (error $<3\%$). An additional skew of 15° led to a slight increase in estimated length. Extreme inclination was no problem if the projection axes were perpendicular to the object axis. In the case of parallel views the error of the volume increased by 31% and the error of the length by 33%. Simulated errors of the inclination angle (assumed values in parentheses) produced only a slight overestimation of all parameters, whereas a simulated error of the skew was associated with larger errors (5–12%).

Variability of measurements (angiograms from patients)

Interobserver variability (Table 2, Figure 6)
As shown in Table 2 the mean differences are small for all parameters, but, the variability between the interobserver pairs of measurements is rather high resulting in predominantly moderate correlations. Segmental lengths and volumes are critically dependent on the localization of the nodes, which are posed by manual interactions.

The agreement of the mean diameters of the total branches is deteriorated as a result of the necessity of manual corrections of the contours of the small vessels and the variability of the visible length of epicardial coronary arteries in the luminogram. The lengths of the total branches may be standardized by matching anatomical landmarks, e.g. vascular bifurcations.

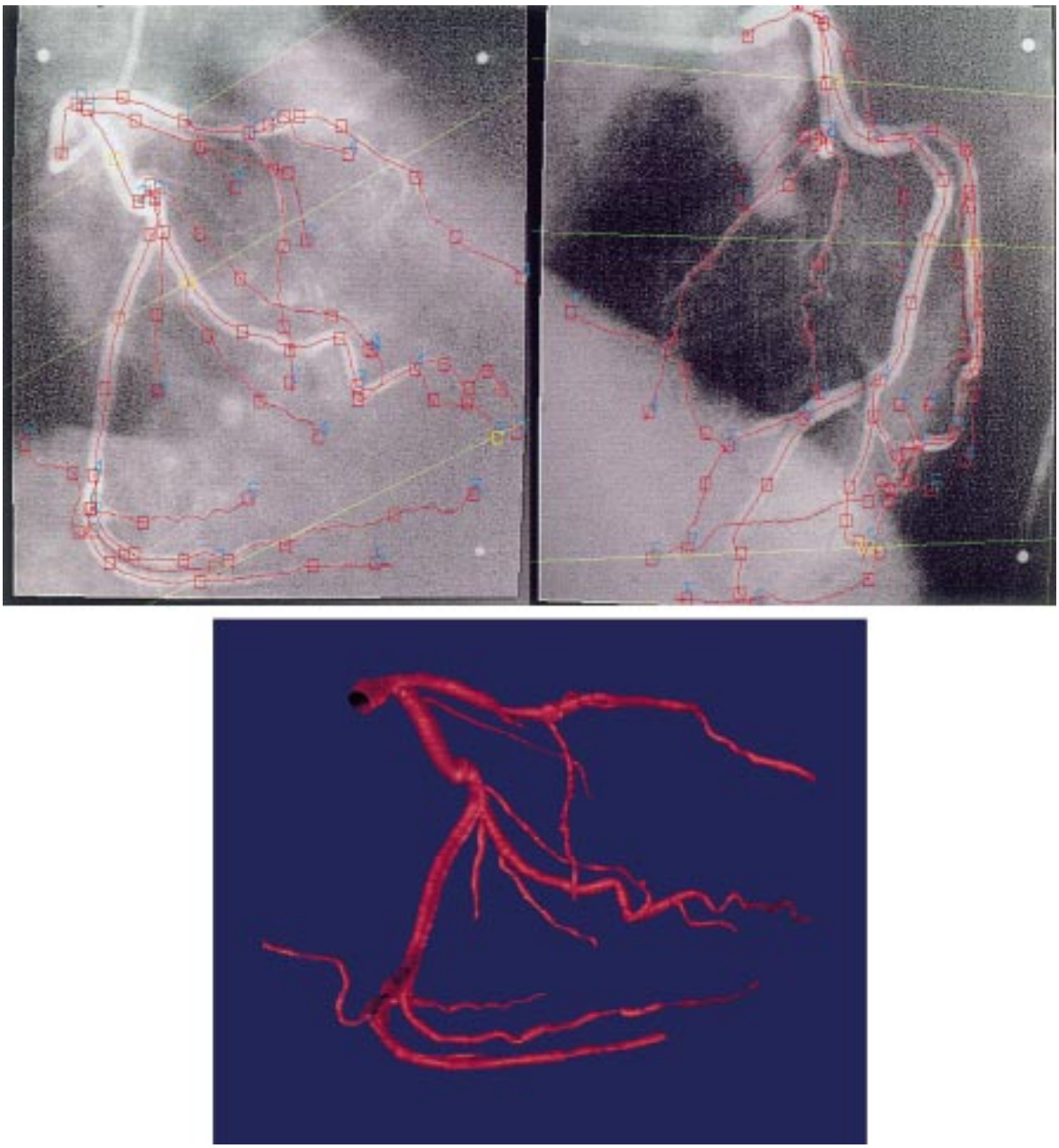

Figure 3. Shaded image of reconstruction in 3-D with corresponding angiograms. The green lines in the angiograms are corresponding projection rays.

Figure 4. Segmentation and identification of vascular branches. The LMCA bifurcates. The origin of the Cx (red centerline) is the first branch of second order and the LAD would be the second. At each new branching point (red squares) the order increases by 1. The first digit denotes the bifurcation order. The remaining digits serve to identify the branch. They are generated by appending an assigned running digit to the sequence of numbers identifying the parent vessel.

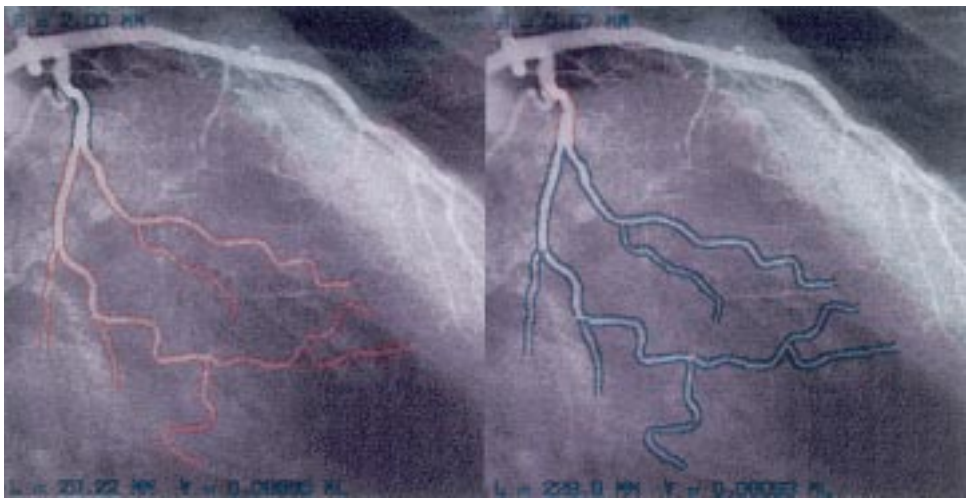

Figure 5. Example of evaluation printed on a projection as background for easy identification of measurements and respective vascular segment or branch. The evaluated segment is marked by blue contours. The length (L) and the volume (V) are depicted at the bottom and the diameter ($\varnothing$) at the top. The red contour marks the corresponding part of the vascular branch.

Table 1. Accuracy using a complex Phantom (hook).

	X-ray device	Volume (ml)	Diameter (mm)	Length (mm)
Reference values	–	19.5 ± 0.75	9.9 ± 0.1	250 ± 10
Baseline	0° F/90° L, no skew	19.12	9.89	248.8
Change in object orientation	0° F/90° L, no skew	19.43	9.97	248.8
Change in angulation	0° F/70° L, no skew	19.15	9.81	253.3
Change in skew	0° F/70° L, 15° cranial	19.70	9.91	255.5
View 20° perpendicular to object axis	70° L/90° L, no skew	19.31	9.80	255.8
View 15° parallel to object axis	70° L/70° L, 15° cranial	25.51	9.87	333.2
20° error in angulation (assumed values in parentheses)	0° F/70° L (90° L), no skew	20.02	10.05	252.2
15° error in skew (assumed values in parentheses)	0° F/70° L (skew + 15° cranial)	21.88	10.30	262.4

Table 2. Interobserver variation of measurements (n = 32 for segments and n = 26 for total branches, mean ± SEE).

	r	Mean difference	*t*-test	Evaluation A	Evaluation B
Segment					
Diameter (mm)	0.896	0.05 ± 0.32	n.s.	2.31 ± 0.67	2.26 ± 0.73
Length (mm)	0.997	0.28 ± 3.56	n.s.	56.27 ± 51.44	55.99 ± 50.66
Volume (ml)	0.975	0.021 ± 0.081	n.s.	0.21 ± 0.21	0.20 ± 0.19
Total branch					
Diameter (mm)	0.819	0.06 ± 0.22	n.s	1.87 ± 0.36	1.93 ± 0.36
Length (mm)	0.983	11 ± 26	n.s.	219 ± 134	208 ± 122
Volume (ml)	0.884	0.02 ± 0.24	n.s.	0.68 ± 0.50	0.68 ± 0.49

Intraobserver variability (Table 3, Figure 7)
The intraobserver agreement of repeated measurements was $\leq 5\%$ for all parameters as may be seen from Table 3. There are good correlations and small mean differences for all parameters. The volume and the length of the total branches demonstrate excellent agreement.

Changes in measurements during a cardiac cycle (Table 4)

One complete cardiac cycle was decomposed into nine phases beginning with the end of diastole. The respective measurements are displayed in Table 4. As expected there is no systematic variability of the length. As already noted in the intra- and interobserver testing the segmental measurements are more strongly affected by manual interaction than the measurements in the complete branches. The volumes and the diameters of the larger vessels demonstrate a slight increase in the systole and the mid-diastole and a decrease in the early diastole. These changes are not significant in a variance analysis using the phase as classification parameter probably as a result of the small sample size. The variability does not decrease with the size of the vessel. Thus, the relative errors in the smaller vessels are considerably larger than those in bigger vessels as may be seen from Table 4. Phase matching (usually selection of an end-diastolic frame) is necessary for a comparison of 3-D reconstructed coronaries.

Influence of vascular tone (Table 5)
As can be seen from Table 5 vasoconstriction after ergonovine (0.3 mg i.v.) and vasodilatation following nitroglycerine (0.2 mg i.c.) have a significant effect ($p < 0.01$) on the diameters (19–21%) and the volumes (36–39%) of the vessels in segmental evaluation as well as in assessment of the total branches. There is no significant effect on the segmental length. The length of total branches

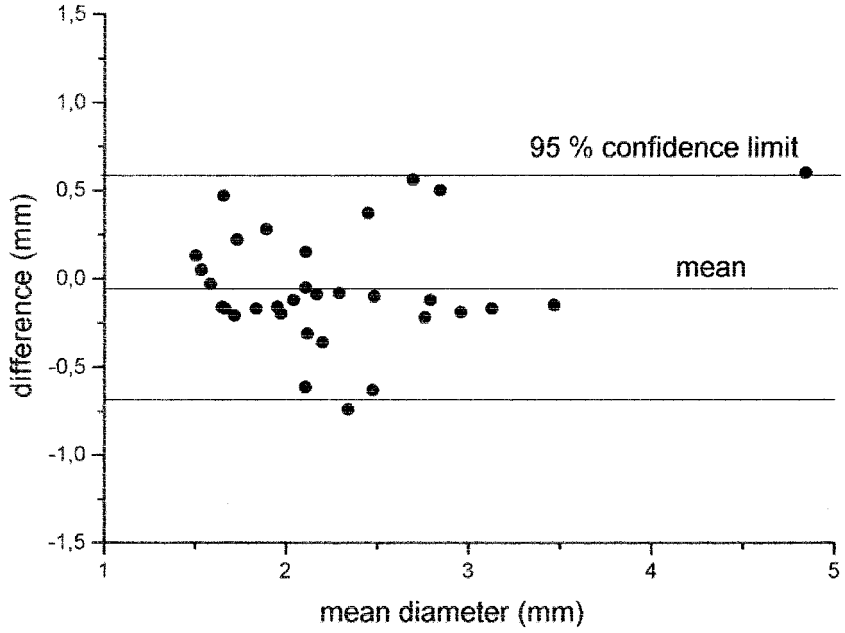

Figure 6. Bland–Altman plot of segmental diameter differences resulting from interobserver variability.

Table 3. Intraobserver variability of measurements (n = 32, mean ± SEE).

	r	Mean difference	*t*-test	Evaluation A	Evaluation B
Segment					
Diameter (mm)	0.984	0.04 ± 0.12	n.s.	2.63 ± 0.68	2.60 ± 0.67
Length (mm)	0.962	1.37 ± 4.90	n.s.	25.64 ± 17.99	24.27 ± 17.47
Volume (ml)	0.954	0.01 ± 0.10	n.s.	0.13 ± 0.11	0.12 ± 0.10
Total branch					
Diameter (mm)	0.960	0.05 ± 0.10	n.s.	1.78 ± 0.33	1.83 ± 0.37
Length (mm)	0.979	3 ± 28	n.s.	202 ± 136	198 ± 129
Volume (ml)	0.975	0.03 ± 0.11	n.s.	0.62 ± 0.50	0.58 ± 0.47

tends to be larger following injection of nitroglycerine. For comparison the small vessels only visible in the angiogram following administration of nitroglycerine had to be suppressed. Following administration of nitroglycerine increasing vessel diameter is associated with reconstruction of more distal small vessels resulting in an increased length of the tree. Ergonovine has the opposite effect. That the suppression of vessels only visible in the angiogram after administration of nitroglycerine has been effectively done is reflected by similar lengths of the total branches despite of an excellent correlation between the measurements.

Comparison with 2-D QCA (Figures 8–10)

As depicted in Figure 8, diameters evaluated by 3-D QCA and 2-D QCA do agree under optimal conditions without systematic difference. However, 2-D QCA measurements are very sensitive to imaging conditions. Even slight foreshortening causes a systematic overestimation of segmental diameters by 2-D QCA, which may be appreciated from the Bland–Altman plot in Figure 9. Further analysis of the effect of foreshortening on the 2-D QCA diameter statistics demonstrates an increase in systematic bias and variance with increased foreshortening (see Figure 10).

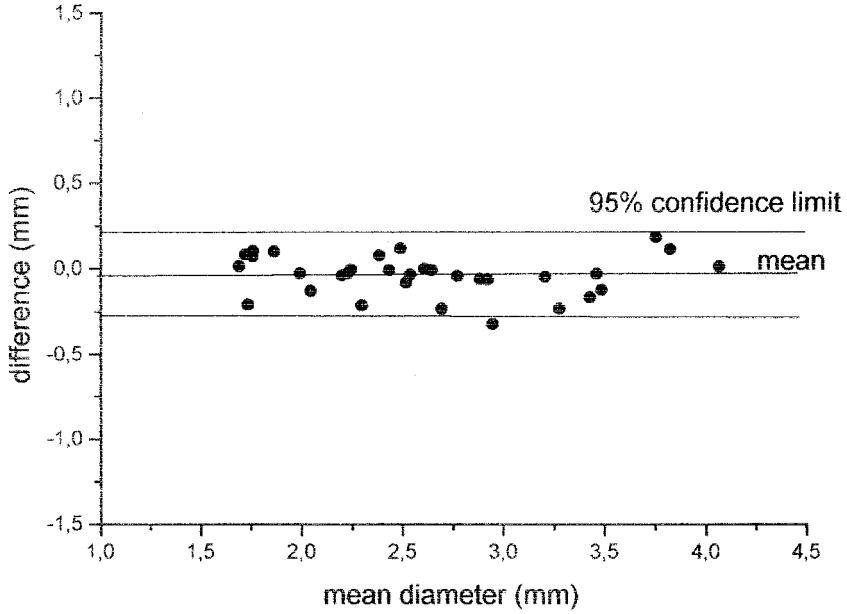

Figure 7. Bland–Altman plot of segmental diameter differences resulting from intraobserver variability.

Table 4. Variability related to cardiac cycle (percent variability and SEE, n = 6, phases = 9).

	Small vessel (%)	Large vessel (%)	SEE
Segment			
Diameter (mm)	9	4–18	0.14–0.72
Length (mm)	77	3–4	0.8–4.0
Volume (ml)	16–67	7–29	0.01–0.11
Total branch			
Diameter (mm)	20	4–8	0.1–0.25
Length (mm)	13	1–4	2.3–15.1
Volume (ml)	16–18	8	0.01–0.21

Discussion

Despite a rapidly expanding variety of methods providing 3-D reconstruction of blood vessels only few of these methods produce true 3-D reconstruction [10]. The evaluated method is a true 3-D reconstruction of vascular lumina [3] and provides special metric tools thereby qualifying to be entitled 3-D QCA. The most important results are:

1. The proposed method of 3-D QCA yields consistent and accurate results for volume, diameter and length using a complex phantom even in nonorthogonal and skewed views, provided that projections parallel to the object are avoided and angulation and skew of the imaging system are known.

2. The interobserver variability is moderate with respect to segmental lengths and volumes and fair with respect to the segmental diameters and the diameters, volumes and lengths of the total branches. The intraobserver agreement is fair.

3. There is some measurable variation of all parameters during the cardiac cycle. There are significant increases in the volume and the diameter from maximal constriction following administration of ergonovine to maximal vasodilatation following nitroglycerine, demonstrating the sensitivity of the 3-D measuring tools to functional alterations.

4. 2-D QCA and 3-D QCA agree in short matched segments without foreshortening. 2-D QCA is rather sensitive to foreshortening and not suitable for evaluation of diameters of larger branches or total coronaries.

Ad 1. (*accuracy*): The study of the complex phantom yielded a volume error <2%, a diameter

Table 5. Influence of vascular tone on the measurements (mean ± SEE, n = 24).

	r	Mean difference	*t*-test	Ergonovine	Nitrate
Segment					
Diameter (mm)	0.954	0.37 ± 0.29	$p < 0.001$	1.80 ± 0.85	2.17 ± 0.80
Length (mm)	0.831	0.60 ± 9.7	n.s.	20.1 ± 12.2	20.6 ± 12.5
Volume (ml)	0.940	0.029 ± 0.046	$p < 0.005$	0.065 ± 0.065	0.094 ± 0.098
Total branch					
Diameter (mm)	0.916	0.22 ± 0.17	$p < 0.001$	0.94 ± 0.39	1.16 ± 0.43
Length (mm)	0.991	13.4 ± 23.6	n.s.	196 ± 189	204 ± 196
Volume (ml)	0.976	0.11 ± 0.14	$p < 0.001$	0.22 ± 0.30	0.34 ± 0.44

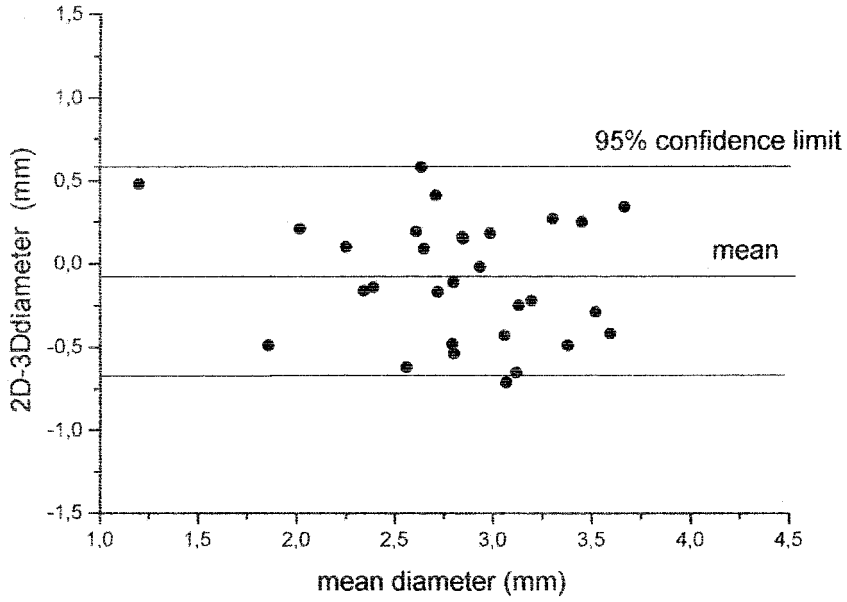

Figure 8. Bland–Altman plot of segmental diameter differences comparing 2-D QCA and 3-D QCA under optimal conditions (matched short medial segments and avoiding foreshortening).

error <1% (±0.1 mm) and a length error <3% using various projections demonstrating the excellent accuracy of the method even in nonorthogonal or slightly foreshortened projections. Extreme foreshortening of vessels in both projections (inclination angle 15° parallel to object axis), though, introduces considerable errors (>30%). The accuracy of the diameter measurements is comparable to results from validation studies assessing 2-D QCA [6, 11–16] and measurements on coronary latex casts using optical techniques [17]. Segments located in an epipolar plane, e.g. the plane parallel to the plane defined by the image intensifier midpoints and the isocenter, cannot be reconstructed. But, these cases may be usually avoided by the choice of an appropriate biplane projection. If angulation or skew of the imaging system are not known, considerable errors may be anticipated.

Ad 2. (*variability*): Inter- and intra-observer mean diameter differences in branches were 2% in segments and 3–4% in total branches comparable with data obtained for local measurements with 2-D QCA [12, 18]. However, the intraobserver values of the diameter demonstrated a better correlation and a smaller SEE of the differences than the interobserver measurements.

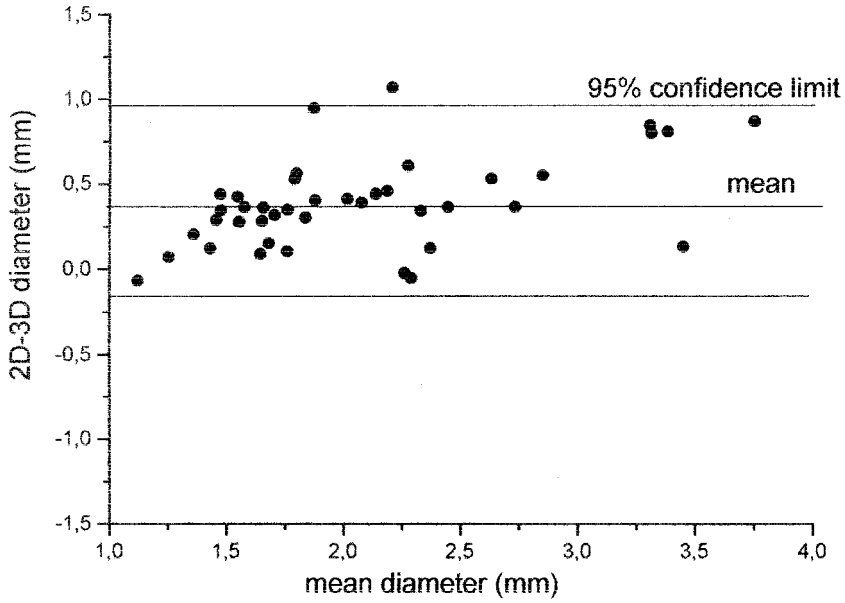

Figure 9. Bland–Altman plot of segmental diameter differences comparing 2-D QCA and 3-D QCA under suboptimal conditions (matched segments of a total LCA tree using the projection with minor foreshortening from both RAO and LAO angiograms).

Though the interobserver variability is acceptable, we expect major improvements. The storage of digital images on CD-R, which will be the standard in the future [19] resolves several problems. Parameters depicting the imaging geometry may be provided by the device, thus avoiding errors in the protocol by manual logging, and the grey-values are normalized. In contrast, digitizing films converted to video signals by frame grabbers is known to introduce a significant systematic error with respect to the vascular diameters in 2-D QCA as result of nonlinear and uncontrolled transformations of the grey-scale of the angiograms [20, 21]. Since the presented 3-D QCA algorithm uses 2-D edge detection it is affected by respective transformations of the grey-scale. Using different techniques, e.g. Fourier analysis or using additional densitometric information may enhance automatic vessel detection [14, 22–25] especially in small vessels. Supplanting manual positioning of the nodes by an automatic segmentation algorithm would reduce the interobserver variability resulting from differences of segmental lengths. Recent work has been perfomed on integration of a priori knowledge into anatomical models and the learning of variations of such models [26, 27]. Model-guided labeling of coronary structure [28] should be of value in automatic segmentation and data representation. In interpreting the presented data it should be kept in mind that we applied our algorithm retrospectively on routine angiograms, which had been filmed before. Such angiograms are often of suboptimal quality as is well known from literature [15, 29]. The 3-D QCA algorithm uses 2-D QCA edge detection, which is exposed to many confounding factors in a clinical setting, e.g. nonuniform radiographic background, low concentrations of contrast and overlap with cerclages, pacers, vascular side-branches and bones [29].

Ad 3. (*sensitivity*): The method is sensitive to cyclic variations in epicardial volume and diameter. Thus phase matched (usually enddiastolic) frames should be selected for evaluation, if cyclic variations of the epicardial vascular volume are not to be investigated. Diameter and volume measurements based on 3-D QCA may be used to assess the effect of vasoactive substances. Analysis of the segments and the branches is feasible with equal accuracy, but, suppression of some small branches only visible following administration of

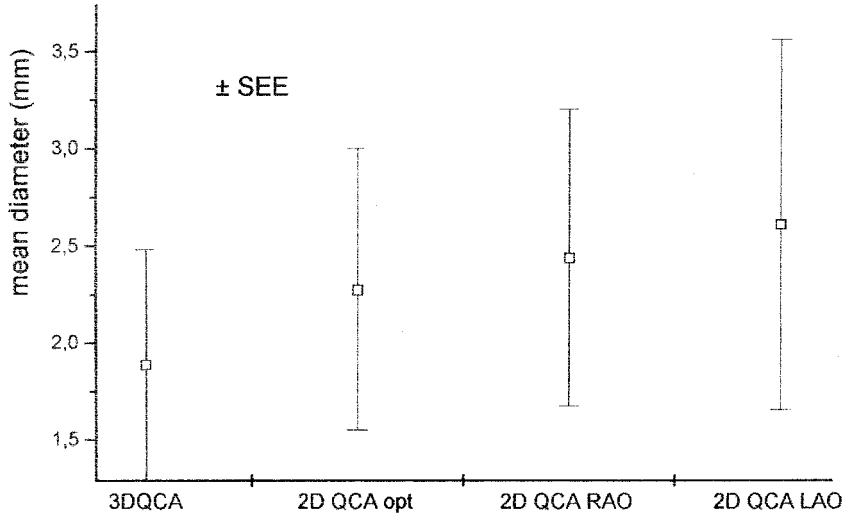

Figure 10. Further analysis of the effect of foreshortening. Mean diameters and standard deviations are depicted. At the left side the 3-D QCA measurement is depicted. At the right side the 2-D QCA measurements from the LAO projection are depicted. The 2-D QCA measurements from the angiogram with minor foreshortening (RAO or LAO) and from the RAO projection are arranged in between.

nitroglycerine may be necessary. The diameter increases following administration of nitroglycerine found in normal coronary arteries in 2-D QCA studies were dose dependent and amounted to 10–20% in a comparable dosage [30–32]. The diameter reduction following administration of ergonovine 0.4 mg i.v. in patients without vasospastic disease ranged between 10–20% [33–36]. Using 3-D QCA we found comparable diameter changes following administration of ergonovine 0.3 mg i.v.

Ad 4. (*comparison of 2-D QCA and 3-D QCA*): Though 2-D QCA is commonly used for the evaluation of local lesions this method has been used for assessing diffuse multi-segmental diameter changes of coronary vessels. The limitations of 2-D QCA with respect to this application, especially the critical dependence on the imaging geometry, are well known and have been discussed thoroughly by de Feyter et al. [1]. Thus, our findings are not surprising. Since 2-D QCA is widely available and might be less time consuming, for geometric evaluation of the coronary arteries a combination of 2-D diameter estimation in angiograms with minimal segmental foreshortening with the determination of the length of the coronary vascular tree from a wire-model has been used [37, 38]. Our data demonstrate that a correct assessment of multi-segmental diameter changes using 2-D QCA would necessitate several (>2) locally optimized angiograms. Otherwise considerable errors are to be expected. Practically all validation studies concerning 2-D QCA are confined to the assessment of phantoms or to the comparison of matched cross-sections or diameters or statistics relating relatively short segments [11, 12, 14, 16, 18, 39–42]. To the best of our knowledge there are no validation studies attempting to assess the accuracy of 2-D QCA with respect to the assessment of long and curved vascular segments or mean diameters of large coronary branches with complex geometry. The clinical and methodological restriction of the analysis of diameters to stenotic and adjacent reference segments greatly facilitates the choice of an optimal projection and limits the errors due to foreshortening and out-of-plane magnification in 2-D QCA validation studies. Integrating the data of two angiograms plus the information on imaging geometry 3-D QCA allows correction for moderate foreshortening, geometric distortion and out-of-plane magnification [3]. Thus the averaged and interpolated diameter information provided by 3-D QCA is expected to be more

accurate and less sensitive to local imaging problems than edge-detection based diameter statistics in 2-D QCA. Calibration should not contribute to the systematic differences between 2-D QCA and 3-D QCA. The use of visible catheter diameters as caliper for QCA has been validated extensively [43–46]. Though this convenient method has been found to be sufficiently accurate, there are some theoretical limitations. The catheter diameter should be measured without contrast. Thus the calibration cannot be performed in the same image as the measurement. The relative error is of increased importance in small objects as luminal diameters of catheters. In agreement with these limitations we found that 3-D calibration based on retro-projection of 3-D reconstructed images of catheter segments between markers or spheres embedding pigtail loops are even more accurate than the calibration using a catheter diameter and should be used for 3-D QCA [8].

Clinical implications: Do we need 3-D QCA?

3-D QCA is an accurate investigative tool for assessment of diameter, length and volume as well as vascular geometry in coronary artery disease. 3-D QCA may be applied to retrospectively selected angiograms and does not depend on identical imaging conditions as 2-D QCA. It is suited for comparison of groups and serial (retrospective) studies. Based on the presented data it should be superior to 2-D QCA in the evaluation of diffuse diameter changes due to vasoactive drugs or progessive diffuse atherosclerosis.

But the main advantage of 3-D QCA are not diameter statistics, but, the data on length, volume, angles at vascular branching points and tortuosity of vessels. This information allows a comprehensive geometric analysis of the coronary vascular tree and more sophisticated assessment of remodeling. This may be relevant in the evaluation of progressive atherosclerosis or other diseases, e.g. dilating coronary artery disease [37, 47, 48].

Further refinements of the method (automatic segmentation, improved artefact handling and contour detection) as well as improved quality of input (digital data CD-R) will simplify and accelerate 3-D QCA providing the basis for a broader clinical application of this method. Evaluation of local stenoses or QCA follow-up of interventional treatment will remain a domain of 2-D QCA. The three-dimensional approach provides a basis for combining different image modalities, e.g. intracoronary ultrasound with X-ray angiograms [10, 49, 50]. Image fusion is considered an important field of development, since it improves the modelling of the cross-sectional geometry and provides a basis for reconstruction and quantitative analysis of plaques.

Limitations and methodological considerations

Availability and the cost of time necessary for the evaluations of coronary angiograms (1–3 h) seem to be the most important limiting factors for application of 3-D QCA at the moment. Insufficient quality of angiograms and deficient protocols are major problems increasing evaluation time and error. The need for robust and accurate algorithms for determination of the imaging geometry based on limited prior information is well recognized [8, 51]. A more flexible approach integrating different a priori knowledge alternatively and including probabilistic elements is desirable. Such developments combined with the use of protocol data stored on CD-R may eventually result in an automatic determination of the imaging geometry. Together with improvements in user-independent contour detection and segmentation automatic 3-D QCA may be available in near future. Foreshortening is nearly inevitable in imaging complete coronary arteries or major branches. Whereas 2-D QCA is unable to cope with this problem, 3-D QCA is only affected by extreme foreshortening.

In conclusion, the evaluated 3-D QCA method provides a fairly accurate, reproducible and sensitive quantitative assessment the 3-D geometry of the coronary vascular tree, even if routine angiograms are used. It provides a valuable investigative tool for the assessment of diffuse luminal remodeling in progressive atherosclerosis and seems superior to 2-D QCA in the diameter assessment in total coronary branches.

Acknowledgement

The development of the 3-D QCA algorithm evaluated in this paper was supported by grant Fl 165/3-2 of the Deutsche Forschungsgemeinschaft [German Research Society], Bonn, Germany.

References

1. de Feyter PJ, Serruys PW, Davies MJ, Richardson P, Lubsen J, Oliver MF. Quantitative coronary angiography to measure progression and regression of coronary atherosclerosis. Circulation 1991; 84: 412–423.
2. Wahle A, Oswald H, Schulze GA, Beier J, Fleck, E. 3-D reconstruction, modelling and viewing of coronary vessels. In: Lemke HU, Rhodes ML, Jaffe CC, Felix R, editors. CAR '91; Berlin: Springer; 1991: 669–676.
3. Wahle A, Wellnhofer E, Mugaragu I, Sauer HU, Oswald H, Fleck E. Assessment of diffuse coronary artery by quantitative analysis of coronary morphology based upon 3-D reconstruction from biplane angiograms. IEEE Transactions on Medical Imaging 1995; 14: 230–241.
4. Wahle A. Präzise dreidimensionale Rekonstruktion von Gefäßsystemen aus biplanen angiographischen Projektionen und deren klinische Anwendung. 1997. Technische Universität Berlin, Fortschr.-Ber. VDI Reihe 17 Nr.152, Düsseldorf: VDI-Verlag.
5. Beier J. Automatische Quantifizierung von Koronarstenosen aus angiographischen Roentgenbildern. 1993. Dissertation Technical University Berlin. Fortschr.-Ber. VDI Reihe 17 Nr.95, Düsseldorf: VDI-Verlag.
6. Hausleiter J, Jost S, Nolte CW et al. Comparative *in vitro* validation of eight first- and second-generation quantitative coronary angiography systems. Coron Artery Dis 1997; 8: 83–90.
7. Wahle A, Krauss U, Oswald H, Fleck E. Inter- and extrapolation of correction coefficients in dynamic image rectification. IEEE Comp in Card 97: 521–524.
8. Wahle A, Wellnhofer E, Oswald H, Fleck E. Biplane coronary angiography: Accurate quantitative 3-D reconstruction without isocenter. IEEE Comp in Card 93: 97–100.
9. Bland JM, Altman DG. Statistical methods for assessing agreement between two methods of clinical measurements. Lancet 1986; i: 307–317.
10. Slager CJ, Wentzel JJ, Oomen JA et al. True reconstruction of vessel geometry from combined X-ray angiographic and intracoronary ultrasound data. Semin Interv Cardiol 1997; 2: 43–47.
11. Beauman GJ, Reiber JH, Koning G, Vogel RA. Comparisons of angiographic core laboratory analyses of phantom and clinical images: interlaboratory variability [see comments]. Cathet Cardiovasc Diagn 1996; 37: 24–31.
12. Dietz U, Rupprecht HJ, Brennecke R et al. Comparison of QCA systems. Int J Card Imaging 1997; 13: 271–280.
13. Keane D, Haase J, Slager CJ et al. Comparative validation of quantitative coronary angiography systems. Results and implications from a multicenter study using a standardized approach. Circulation 1995; 91: 2174–2183.
14. Lievre M, Finet G, Maupas J. Validation of a new quantitative coronary angiography analysis system used to evaluate densitometric lumen remodelling. Int J Card Imaging 1997; 13: 15–22.
15. Seissl H, Peukert K, Geiger B, Verstraelen BJ. Quantitative coronary angiography: impact of imaging parameters on accuracy and confidence interval. Heart Vessels 1997; Suppl 12: 212–216.
16. van der Geest RJ, Morris KG, Cusma JT, Reiber JH. Postmortem validation of the automated coronary analysis (ACA) software package. Int J Card Imaging 1994; 10: 95–102.
17. Zhang Q, Parker DL, Wu J. Optical lumen measurement of coronary artery latex casts. Med Phys 1993; 20: 463–468.
18. Sirnes PA, Myreng Y, Molstad P, Golf S. Reproducibility of quantitative coronary analysis, Assessment of variability due to frame selection, different observers, and different cinefilmless laboratories. Int J Card Imaging 1996; 12: 197–203.
19. Reiber JH, Goedhart B, Brand GJ, Schiemanck L, van der Zwet PM. Quantitative coronary arteriography: current status and future. Heart Vessels 1997; Suppl 12: 209–211.
20. Reiber JH. QCA and cine film exposure [editorial; comment]. Cathet Cardiovasc Diagn 1996; 39: 137.
21. Robert N, Yaffe MJ, Langer A. Variations in measured vessel diameters using coronary measurement system [see comments]. Cathet Cardiovasc Diagn 1996; 39: 131–136.
22. Molloi SY, Ersahin A, Roeck WW, Nalcioglu O. Absolute cross-sectional area measurements in quantitative coronary arteriography by dual-energy DSA. Invest Radiol 1991; 26: 119–127.
23. Molloi S, Ersahin A, Hicks J, Wallis J. In-vivo validation of videodensitometric coronary cross-sectional area measurement using dual-energy digital subtraction angiography. Int J Card Imaging 1995; 11: 223–231.
24. Weber DM, Molloi SY, Folts JD, Peppler WW, Mistretta CA. Geometric quantitative coronary arteriography. A comparison of unsubtracted and dual energy-subtracted images. Invest Radiol 1991; 26: 649–654.
25. Muhlestein JB, Zhang Q, Parker DJ, Horn SD, Parker DL, Anderson JL. A comparison of the accuracy and reproducibility of digital three-dimensional coronary artery reconstructions using edge detection or videodensitometry. Comput Biomed Res 1997; 30: 415–426.
26. Hall P, Ngan M, Andreae P. Reconstruction of vascular networks using three-dimensional models. IEEE Trans Med Imaging 1997; 16: 919–929.
27. Windyga P, Garreau M, Shah M, Le Breton H, Coatrieux JL. Three-dimensional reconstruction of the coronary arteries using a priori knowledge. Med Biol Eng Comput 1998; 36: 158–164.
28. Ezquerra N, Capell S, Klein L, Duijves P. Model-guided labeling of coronary structure. IEEE Trans Med Imaging 1998; 17: 429–441.

29. Herrington DM, Siebes M, Walford GD. Sources of error in quantitative coronary angiography. Cathet Cardiovasc Diagn 1993; 29: 314–321.
30. Feldman RL, Pepine CJ, Curry RCJ, Conti CR. Coronary arterial responses to graded doses of nitroglycerin. Am J Cardiol 1979; 43: 91–97.
31. Gensini GG, Kelly AE, Da CB, Huntington PP. Quantitative angiography: the measurement of coronary vasomobility in the intact animal and man. Chest 1971; 60: 522–530.
32. Jost S, Reil G, Knop I et al. Coronary vasodilation with nitrocompounds – is there a maximum? Z Kardiol 1989; 78 (Suppl 2): 38–40; discussion 64–67.
33. Curry RCJ, Pepine CJ, Sabom MB, Feldman RL, Christie LG, Conti CR. Effects of ergonovine in patients with and without coronary artery disease. Circulation 1977; 56: 803–809.
34. Cipriano PR, Guthaner DF, Orlick AE, Ricci DR, Wexler L, Silverman JF. The effects of ergonovine maleate on coronary arterial size. Circulation 1979; 59: 82–89.
35. Heupler FAJ, Proudfit WL, Razavi M, Shirey EK, Greenstreet R, Sheldon WC. Ergonovine maleate provocative test for coronary arterial spasm. Am J Cardiol 1978; 41: 631–640.
36. Hoshio A, Kotake H, Mashiba H. Significance of coronary artery tone in patients with vasospastic angina. J Am Coll Cardiol 1989; 14: 604–609.
37. Seiler C, Kirkeeide RL, Gould KL. Basic structure-function relations of the epicardial coronary vascular tree – basis of quantitative coronary arteriography for diffuse coronary artery disease. Circulation 1992; 85: 1987–2003.
38. Klein JL, Hoff JG, Peifer JW, et al. A quantitative evaluation of the three dimensional reconstruction of patients' coronary arteries. Int J Card Imaging 1998; 14: 75–87.
39. Achenbach S, Moshage W, Ropers D, Bachmann K. Comparison of vessel diameters in electron beam tomography and quantitative coronary angiography. Int J Card Imaging 1998; 14: 1–7.
40. Desmet W, De SI, Beatt K, Huehns T, Piessens J. In vivo comparison of different quantitative edge detection systems used for measuring coronary arterial diameters. Cathet Cardiovasc Diagn 1995; 34: 72–80.
41. Syvanne M, Nieminen MS, Frick MH. Accuracy and precision of quantitative arteriography in the evaluation of coronary artery disease after coronary bypass surgery. A validation study [see comments]. Int J Card Imaging 1994; 10: 243–252.
42. McPherson DD, Johnson MR, Collins SM, Kieso RA, Marcus ML, Kerber RE. Validation by high-frequency epicardial echocardiography of a new method of analyzing coronary angiography quantitatively in coronary artery disease. Am J Cardiol 1993; 71: 28–32.
43. Legrand V, Raskinet B, Martinez C, Kulbertus H. Variability in estimation of coronary dimensions from 6F and 8F catheters. Cathet Cardiovasc Diagn 1996; 37: 39–45.
44. Reiber JH, Jukema W, van Boren A, van Houdt RM, Lie KI, Bruschke AV. Catheter sizes for quantitative coronary arteriography [see comments]. Cathet Cardiovasc Diagn 1994; 33: 153–155.
45. Herrman JR, Keane D, Ozaki Y, den Boer A, Serruys PW. Radiological quality of coronary guiding catheters: a quantitative analysis. Cathet Cardiovasc Diagn 1994; 33: 55–60.
46. Koning G, van der Zwet PM, von LC, Reiber JH. Angiographic assessment of dimensions of 6F and 7F Mallinckrodt Softouch coronary contrast catheters from digital and cine arteriograms. Int J Card Imaging 1992; 8: 153–161.
47. Wellnhofer E, Gross J, Wahle A, Oswald H, Fleck E. Quantitative Progression Der Koronaratherosklerose. Serielle Morphometrische Analyse an Aus Angiogrammen 3-D Rekonstruierten Linken Koronararterien. [abstract]. Z Kardiol 1998; 87 (Suppl I): 2–2.
48. Labarbera M. Principles of Design of Fluid Transport Systems in Zoology. Science 1990; 249: 992–1000.
49. Prause GP, De Jong SC, McKay CR, Sonka M. Towards a geometrically correct 3-D reconstruction of tortuous coronary arteries based on biplane angiography and intravascular ultrasound. Int J Card Imaging 1997; 13: 451–462.
50. Wahle A, Prause GPM, DeJong SC, Sonka M. 3-D fusion of biplane angiography and intravascular ultrasound for accurate visualization and volumetry. In: Wells WM, Colchester A, Delp S, editors. Medical image computing and computer-assisted intervention – MICCAI '98. Lecture Notes in Computer Science, vol. 1496. Berlin: Springer 1998: 146–155.
51. Chen SY, Metz CE. Improved determination of biplane imaging geometry from two projection images and its application to three-dimensional reconstruction of coronary arterial trees. Med Phys 1997; 24: 633–654.

2.1.3 Progression of coronary atherosclerosis quantified by analysis of 3- D reconstruction of left coronary arteries

Nachdem das Verfahren entwickelt und die Methodik validiert worden war, wurde das Verfahren auf eine klinische Fragestellung angewandt. Zum einen sollten Normalwerte für Gefäßdiameter, - Längen und -Volumina bestimmt werden, zum anderen der atherosklerotische Umbau des Koronargefäßbaums an zwei länger auseinander liegenden Zeitpunkten punktuell erfasst werden.

Es handelt sich hierbei um die erste klinische Anwendung der 3-D QCA in einer Kohortenstudie. Da es sich bei der koronaren Herzerkrankung in der Regel um eine über Jahre progrediente Erkrankung handelt, die wiederholt zu lokalen Interventionen führt, bot es sich an geeignete bei entsprechenden Interventionen in längeren Abständen erfasste Koronarangiogramme auszuwählen und die Erkrankung der Patienten unabhängig von der erfassten Morphologie klinisch zu charakterisieren. Das Besondere an dieser Arbeit ist die klinische Definition der Atherosklerose, für die der Autor eine sorgfältige retrospektive Recherche durchführte.

Ergebnisse:

- Normalbefunde für die 3-D QCA in Kontrollen mit Ausschluss einer relevanten Herzerkrankung und Vergleichsdaten zur 2-D- QCA aus der Literatur sind in Tabelle 3 dargestellt.

- Querschnitte und Volumina wurden entsprechend einem Modell aus der Literatur (11) auf einen Schätzwert der Masse des zugehörigen Perfusionsgebiets bezogen. Die entsprechenden Daten im Verlauf und zum Vergleich Normalwerte sind in Tabelle 4, - leider mit verrutschter Kopfzeile- , dargestellt. Die entsprechenden Querschnitte und Volumina sind sowohl bezogen auf Segmente als auch auf Unterbäume bereits initial bei KHE- Patienten signifikant gegenüber den Normalwerten verringert und nehmen im Verlauf weiter signifikant ab.

- Die Veränderungen korrelieren signifikant mit der Summe der Risikofaktoren und der Dauer des Follow- up

- Die Veränderungen der Querschnitte korrelierten nicht mit den Ausgangswerten oder dem Gensini Score (197), was als Hinweis auf diffuse Progression zu werten ist.

- Korrelationen und Regressionen der Volumen- und- Querschnittsmaße mit der Masse der regionalen Perfusionsgebiete sind in Tabelle 2 dargestellt.

Beurteilung:

Es ließ sich nachweisen, dass sich eine Zunahme atherosklerotischer Wandveränderungen mit 3- D-QCA bereits bei wenigen Patienten mit statistischer Signifikanz nachweisen lässt im Unterschied zur zweidimensionalen QCA (Tabelle 4). Die wesentlich größere Genauigkeit hat u. a. praktische Bedeutung im Hinblick auf die erforderliche Probandenzahl für eine Studie mit 3-D QCA im Vergleich zu 2-D- QCA. Die Reduktion der mittleren Koronargefäßdiameter von im Mittel 0.04±0.13 mm pro Jahr stimmte überraschend gut mit den Ergebnissen der REGRESS- Studie (198) überein.

Die Veränderungen der Gefäßquerschnitte sind diffus und reflektieren nicht die Progression einzelner Stenosen, da sie sonst mit dem Gensini- score oder/ und dem Ausgangsgefäßquerschnitt korrelieren müssten

ELSEVIER

Atherosclerosis 160 (2002) 483–493

ATHEROSCLEROSIS

www.elsevier.com/locate/atherosclerosis

Progression of coronary atherosclerosis quantified by analysis of 3-D reconstruction of left coronary arteries

Ernst Wellnhofer [a,*], Andreas Wahle [b], Eckart Fleck [a]

[a] *Department of Internal Medicine/Cardiology, Deutsches Herzzentrum Berlin, Augustenburger Platz 1, 13353 Berlin, Germany*
[b] *University of Iowa, Department of Electrical and Computer Engineering, Iowa City, IA 52242, USA*

Received 11 May 2001; received in revised form 18 July 2001; accepted 20 July 2001

Abstract

Objectives: Quantitative measurements on three-dimensional (3-D) reconstructed coronary trees permit accurate evaluation of vascular volumes, lengths and diameters. We applied this technique to investigate diffuse luminal narrowing in patients with the clinical manifestation of progressive atherosclerosis. *Methods:* In 13 patients who presented repeatedly for coronary angioplasty (at least 4 years of invasive follow-up), left coronary arteries were reconstructed in 3-D from biplane coronary angiograms. Mean diameter, cross-sectional areas, total length, and volume were calculated for segments and branches. Five patients without coronary artery disease served as controls. *Results:* Patients with progressive coronary atherosclerosis demonstrated a significant reduction of total vascular volumes, mean diameters and cross-sectional areas at the initial investigation when compared with controls. Progressive luminal shrinkage occurred during follow-up (-0.04 ± 0.13 mm per year and per segmental diameter). The progress of luminal narrowing in patients with coronary artery disease is related to the number of coronary risk factors and the duration of follow-up. *Conclusion:* Quantitative measurements on 3-D reconstructed coronary trees are a useful investigative tool for the assessment of progression of coronary atherosclerosis.

Keywords: Atherosclerosis; Coronary artery disease; Angiography

1. Introduction

The conventional assessment of progression of coronary artery disease (CAD) by quantitative coronary angiography (QCA) is based on serial measurements of diameters. This method is limited to intra-individual comparison and hampered by the necessity to measure the same sites in the same projections assuming identical imaging conditions, which precludes retrospective studies [1,2]. Quantitative analysis of three-dimensionally reconstructed coronaries (three-dimensional QCA) has the advantage of compensating for moderate foreshortening, provides improved calibration and is independent from changes in gantry settings, provided the actual settings are recorded [3]. Moreover, measurements of length and volume of coronary segments and branches becomes feasible [3,4]. The subsequent serial retrospective study applies three-dimensional QCA to assess progression of atherosclerosis. For this study, we intentionally selected patients with clinical manifestations of progressive CAD.

2. Methods

2.1. Patients

2.1.1. Controls

A control group of patients (see Table 1) without angiographically visible coronary wall irregularities or calcifications and no more than two cardiovascular risk factors were investigated. These patients presented for coronary angiography between 1992 and 1993. There was no invasive follow-up of these patients for ethical reasons.

* Corresponding author. Tel.: +49-30-4593-2400; Fax: +49-30-4593-2500.
E-mail address: ewellnhofer@t-online.de (E. Wellnhofer).

0021-9150/02/$ - see front matter
PII: S0021-9150(01)00609-8

2.1.2. Patients with clinical manifestations of progression of coronary atherosclerosis

2.1.2.1. Selection criteria. Patients with clinical manifestations of progressive coronary atherosclerosis were assumed to present repeatedly with angina and signs of coronary ischaemia that eventually would lead to cardiac catheterization and result in the diagnosis of new or advanced coronary stenoses. As a consequence, appropriate patients for this study were found among patients who underwent repeated revascularization.

A database search was performed. Patients with a history of repeated revascularization and angiographic follow-up of at least 4 years were selected. Their files were examined for clinical manifestations of progressive CAD. An exact protocol of distance of image intensifier to X-ray source, rotation and skew for both planes (error $< 1\%$) had to be available. The complete left coronary artery had to be clearly visible on both angiograms. The following cardiovascular risk factors were checked in all patients from the patient file: diabetes, hypercholesterolemia, hypertension, smoking, and family history of cardiovascular disease. Eventually, 13 patients (see Table 1), who presented repeatedly for percutaneous transluminal angioplasty between 1989 and 1997, were selected.

2.2. Procedure

Informed consent was given by all patients prior to examination. Coronary catheterization and angioplasty were performed according to standard clinical practice. There had been primary procedural success without complications in all selected cases.

Biplane angiograms (25 frames/s) had been acquired on cine film with standard biplane angiographic X-ray equipment (Philips Integris-System) using standard projections. Rotation, angulation, image intensifiers used and distance of image intensifiers to X-ray sources had been routinely documented by protocol. Frame numbers were used to identify corresponding pictures in the left anterior oblique and the right anterior oblique projections. Four markers mounted on each magnifier were used to rectify the images. Measurements on grid phantoms allowed a correction of pincushion distortion in each plane.

2.2.1. Three-dimensional reconstruction

A 3-D model was reconstructed from biplane angiographic projections digitized from cine film by the use of protocol information on imaging geometry. In all cases, final angiograms following intracoronary application of 0.1–0.2 mg nitroglycerin were used (adequate dilatation). An elliptical lumen geometry is assumed, which allows modeling not only of circular, but also oval lumina with eccentric plaque. For detailed information about the algorithms for three-dimensional reconstruction and quantitative evaluation, see Wahle et al. [3]. The accuracy of the algorithm is high (volume error $< 2\%$, diameter error $< 1\%$) and the reproducibility is reasonable [3–5].

Biplane calibration, as performed in this study, reconstructs a three-dimensional object, e.g. catheter, out-of-plane in real space from projections of this object visible in both angiograms. The known real dimensions of this object are used to get the correct size. Back-projections of the reconstructed and correctly sized object on both

Table 1
Patient groups

	CAD patients ($N = 13$)			Controls ($N = 5$)
	Initial evaluation	Follow-up investigation	Comments	
Gender	11 male/2 female	Mean follow-up, 5.2 ± 1 (4–7) years		2 male/3 female
Age (years)	63.0 ± 6.8			54.4 ± 12.8
Height (cm)	174 ± 7			165 ± 6
Weight (kg)	81 ± 11			66 ± 9
Body mass index (kg/m^2)	26.6 ± 2.2			24.2 ± 2.3
Left ventricular mass (g)	260 ± 49			148 ± 32
Ejection fraction (%)	60 ± 12	55 ± 12	Decrease $>10\%$ in 6/13 patients	70 ± 9
Number of PTCAs	2.2 ± 1.9	5.2 ± 1.3	42 LAD, 24 Cx, 19 RCA	–
ACVB/TMLR	1	3/1	Scheduled	–
Gensini score (6)	24 ± 22	17 ± 27		0
Angina CCS (7)	2 ± 1	2.6 ± 1.2		–
History of infarction	9/13			
3/13 in LCA region	3 additional infarctions		No events	

ACVB, Aorto-coronary venous bypass; TMLR, transmyocardial laser revascularization; CCS, Canadian Cardiovascular Society Functional Classification [8].

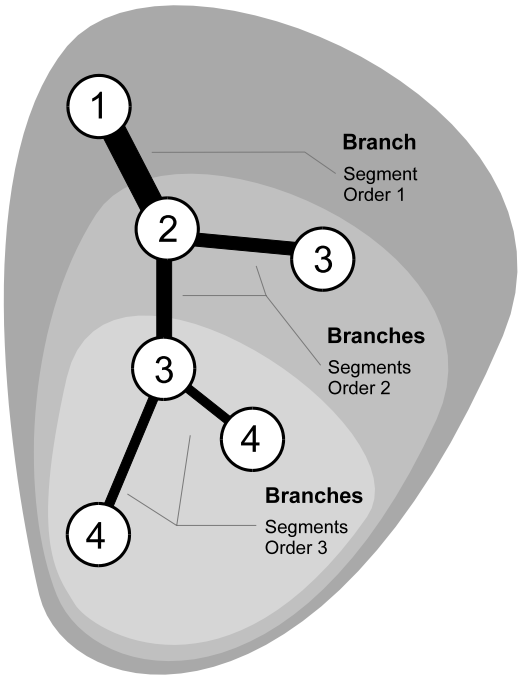

Fig. 1. The order of the branching nodes starts with one at the origin of the left main artery and increases by one at each branching node. A segment was defined as the part of the vessel between two successive branching nodes. A branch was defined as the total visible coronary artery with origin at a certain branching node. Branches include the parent segment. Orders of segments and branches were defined as demonstrated.

angiograms provide a calibration in both imaging planes [3]. This type of calibration needs no correction for out-of-plane location of the scaling object or foreshortening, which is an unsolved problem in two-dimensional QCA. Vessels smaller than 0.5 mm in diameter were suppressed by a filter. Previous studies without using this filter demonstrated that reconstruction of all visible small vessels may be subject to the visionary skills of the investigator. Comparative studies without and with a filter in the same set of data demonstrated that the average results are similar but investigator related differences of reconstructions of individual small branches were suppressed by use of the filter.

The origin and the branching nodes of the coronary were marked interactively using both angiographic projections. Segments, branches and orders were defined as explained in Fig. 1.

Volume, cross-sectional area (CSA), diameter and length of segments and branches were evaluated by three-dimensional QCA. Complete sampling of all visible branches and segments ≥ 0.5 mm was performed for each investigated coronary artery. Since right coronary angiograms were not performed at every follow-up in the CAD group, in these patients only serial measurements of branches and segments of the left coronary artery (LCA), matched by suppressing vascular branches not visible in both angiograms, were performed (total number of matched segments/branches $N = 115$, 8.8 segments/branches per LCA). In 7/12 patients, one branch visible in the first angiogram was not visible at follow-up and had to be suppressed. In controls in addition to the LCA (total number of segments/branches $N = 81$, 16.2 segments/branches per LCA), the right coronary artery (RCA) (total number of segments/branches $N = 55$, 11 segments/branches per RCA) was evaluated. As no visible segments had to be excluded as not suitable for analysis, the average number of reconstructed segments of RCA and LCA in controls doubles the total number of the segments of RCA and LCA assessed in the REGRESS study, which refers to ten segments in the LCA and three segments in the RCA [16]. In patients with CAD, some vessels were occluded and not visible, especially at the second angiogram and had to be suppressed. Vessels that underwent a percutaneous transluminal coronary angioplasty (PTCA) were not suppressed. Evaluation was performed in the last control angiograms after PTCA. In the REGRESS study, 6.6 ± 3 segments per patient (RCA + LCA) could be reconstructed [16] as compared with 8.8 (range, 6–12) reconstructed segments per LCA in our study. In order to reduce the variance due to different vessel size, the volume and CSA were standardized per cardiac mass. Regional masses m_r were calculated according to the method proposed by Seiler et al. [6]:

$$m_r = M_{LV}(L_T/L_{LV})$$

where M_{LV} is left ventricular mass determined by biplane angiography using a validated Simpson algorithm [7], and L_T is the total length of the branch and L_{LV} is the total length of the left coronary artery. The results of the analysis are given in Table 2.

2.3. Statistics

Mean $\pm$ standard deviation is presented for comparison with reference data and median and range for evaluation of group differences and serial changes. The significance of changes between initial evaluation and follow-up was evaluated by paired comparison of volumes and areas of corresponding segments and branches by parametric and non-parametric tests (paired t-test and Wilcoxon's rank test). Inter-group differences between controls and CAD patient groups were tested by multivariance analysis with Bonferroni correction. In order to assess the impact of the duration of follow-up and the number of individual cardiovascular risk factors on the decrease in vascular volume of coronary branches, general multifactorial linear modeling that used the software package SPSS (version 7.0) is performed. Branching order and total length were included in the model as a first-order correction for vessel size.

3. Results

3.1. Clinical characteristics of patients and controls

As may be seen from Table 1, the controls comprise a higher percentage of female patients than the CAD group. Mean age is lower and body mass index tends to be lower in controls. Left ventricular mass is normal in controls and elevated in CAD patients. Mean ejection fraction of CAD patients is lower than in controls but still normal at initial evaluation.

Progression of CAD was clinically reflected by the necessity for multiple coronary interventions, a slight increase in the grade of angina [8], an increase in nitrate medication, a slight deterioration in ventricular function and four additional scheduled surgical revascularizations at the end of the follow-up period.

All patients had at least two cardiovascular risk factors, 3/13 three and 4/13 four or more. Of the three diabetic patients, two were on insulin treatment. The mean cholesterol level was 247 ± 21 mg/dl, and 4/13 patients were taking cholesterin synthetase inhibitors.

3.2. Controls

3.2.1. Normal volumes, diameters and lengths

A summary of the measurements of lengths, diameters and volumes classified by the order is given in Table 3. Reference values for diameters [9,10] derived by two-dimensional QCA are given in the final column. Values of volumes, lengths and diameters of segments and branches did not differ significantly between circumflex artery (Cx) and left anterior descendant artery (LAD). As a result, Cx and LAD measurements were pooled for comparison with CAD patients. Mean values and standard deviations of the segments and branches in controls in Table 3 were calculated by averaging N (column 2 of Table 3) samples. The average length of the segments ranges from about one to two centimetres independent from branching order, whereas all other parameters (volumes, diameters and lengths of branches) are correlated with branching order. The volume of the branches demonstrates the best correlation with branching order (Spearman's correlation for individual coronaries $r = -0.591$ to $r = -0.983$).

3.3. Patients with progressive atherosclerosis

A summary of the measurements of CSA and volume of coronary segments and branches per regional mass is given in Table 4. The data are stratified with respect to branching order. In addition to the initial values and the measurements at follow-up, the respective values of the controls are given for comparison.

3.3.1. Comparison with controls

At the initial evaluation LCA volume, left main CSA and total left coronary length is significantly ($P < 0.05$) smaller in patients with coronary artery disease (1.53 ± 0.55 ml, 11.3 ± 3.5 mm^2 and 489 ± 101 mm) than in the control group (1.72 ± 0.36 ml, 14.0 ± 4.4 mm^2 and 902 ± 98 mm). Median CSA and volume of branches and segments standardized per regional mass is significantly lower in the patients with CAD than in controls (Table 3). For comparison with canine data from the literature (1.25–1.5 ml/100 g total cardiac mass) [11], mean LCA volumes in controls (1.15 ml/100 g total cardiac mass) and in patients with CAD (initially, 0.59 ± 0.22 ml/100 g; at follow-up, 0.45 ± 0.17 ml/100 g total cardiac mass) are given. Median values given in Table 4 differ only slightly.

3.4. Progression of diffuse coronary atherosclerosis

Examples of paired angiograms separated by a time interval > 4 years are shown in Figs. 2 and 3. CSA and volume per cardiac mass decreased significantly ($P < 0.005$) in branches and segments from the initial evaluation to follow-up (Table 4). The mean reduction of the

Table 2
Relation of cross-sectional areas (A) and volumes (V) to calculated regional mass (m_r)

		Volume of branch	Area of branch	Volume of segment	Area of segment	Reference for area of segment [6]
Controls	Correlation	$r = 0.91$	$r = 0.73$	$r = 0.63$	$r = 0.85$	$r = 0.93$
	Regression	$V = 0.0037 m_r^{1.22}$	$A = 0.28 m_r^{0.40}$	$V = 0.0041 m_r^{0.76}$	$A = 0.24 m_r^{0.80}$	$A = 0.0004 + 0.0029 m_r^{0.76}$
CAD first evaluation	Correlation	$r = 0.90$	$r = 0.78$	$r = 0.59$	$r = 0.76$	$r = 0.88$
	Regression	$V = 0.0008 m_r^{1.37}$	$A = m_r(24 + 0.14 m_r)$	$V = m_r(1200 + 3.68 m_r)$	$A = 0.25 m_r^{0.67}$	$A = 0.0051 + 0.0012 m_r^{0.81}$
CAD follow-up	Correlation	$r = 0.91$	$r = 0.69$	$r = 0.58$	$r = 0.77$	
	Regression	$V = 0.0005 m_r^{1.41}$	$A = m_r(32 + 0.17 m_r)$	$V = m_r(1645 + 2.46 m_r)$	$A = 0.15 m_r^{0.74}$	

Table 3
Volumes, diameters and lengths (mean ± S.D.) in controls and reference diameters by two-dimensional (2-D) QCA

Branching order	*N*	Vessel	Length of branch (mm)	Volume of branch (ml)	Diameter of branch (mm)	Length of segment (mm)	Volume of segment (ml)	Diameter of segment (mm)	Diameters 2-D QCA (mm)	
									[10]	[9]
1	7	RCA prox.	687 ± 126	1.167 ± 0.363	1.47 ± 0.27	15.8 ± 16.9	0.167 ± 0.182	3.58 ± 0.59	3.0 ± 0.5/3.4 ± 0.7	3.6 ± 0.8
2	10	mid RCA	447 ± 255	0.718 ± 0.541	1.24 ± 0.44	15.6 ± 8.2	0.084 ± 0.051	2.81 ± 1.07		3.2 ± 0.6
3	9	mid RCA	416 ± 213	0.662 ± 0.480	1.25 ± 0.46	19.2 ± 12.5	0.110 ± 0.081	2.78 ± 0.94		
4	10	RCA dist.	302 ± 148	0.455 ± 0.338	1.29 ± 0.42	25.7 ± 17	0.123 ± 0.097	2.46 ± 0.86	2.5 ± 0.6/2.9 ± 0.7	2.9 ± 0.6
5	11	RCA dist.	207 ± 137	0.287 ± 0.301	1.14 ± 0.44	18.3 ± 15.2	0.068 ± 0.050	2.25 ± 0.79		
6	8	RCA dist.	205 ± 96	0.306 ± 0.233	1.20 ± 0.53	18.9 ± 13.6	0.106 ± 0.091	2.42 ± 0.82		2.3 ± 0.5
1	5	LCA(LMA)	902 ± 102	1.718 ± 0.364	1.53 ± 0.11	12.7 ± 7.2	0.132 ± 0.085	3.56 ± 0.25	3.5 ± 0.7/4.3 ± 0.6	4.2 ± 0.7
2	6	LAD prox.	381 ± 137	0.726 ± 0.352	1.43 ± 0.20	21.5 ± 5.4	0.173 ± 0.076	3.19 ± 0.80	2.9 ± 0.4/3.5 ± 0.5	3.5 ± 1.0
3	11	mid LAD	194 ± 128	0.303 ± 0.281	1.16 ± 0.34	14.3 ± 14.6	0.081 ± 0.108	2.24 ± 0.92		2.8 ± 0.6
4	9	LAD dist.	151 ± 56	0.206 ± 0.121	1.18 ± 0.21	23.0 ± 9.9	0.079 ± 0.047	2.03 ± 0.56	1.8 ± 0.2/2.0 ± 0.4	1.9 ± 0.5
5	5	LAD dist.	103 ± 51	0.134 ± 0.079	1.10 ± 0.17	21.5 ± 21.6	0.057 ± 0.049	1.90 ± 0.44		
6	6	LAD dist.	72 ± 40	0.035 ± 0.049	0.96 ± 0.17	14.7 ± 5.9	0.024 ± 0.013	1.46 ± 0.42		
2	5	LCX prox.	423 ± 75	0.640 ± 0.272	1.34 ± 0.22	8.9 ± 6.7	0.064 ± 0.047	3.10 ± 0.42	2.6 ± 0.6	3.0 ± 0.6
3	7	mid LCX	261 ± 95	0.394 ± 0.256	1.25 ± 0.15	27.6 ± 8.9	0.157 ± 0.124	2.55 ± 0.57		2.6 ± 0.6
4	11	LCX dist.	133 ± 87	0.139 ± 0.126	1.04 ± 0.17	22.7 ± 11.5	0.057 ± 0.046	1.70 ± 0.58	1.9 ± 0.2	2.1 ± 0.5
5	7	LCX dist.	108 ± 78	0.084 ± 0.087	0.88 ± 0.14	18.5 ± 8.2	0.036 ± 0.032	1.49 ± 0.45		
6	9	LCX dist.	82 ± 55	0.046 ± 0.047	0.76 ± 0.13	13.1 ± 8.2	0.017 ± 0.016	1.19 ± 0.51		

'Mid RCA' includes right ventricular branches, 'RCA dist.' includes descendent posterior and posterolateral branches, 'mid LAD' and 'LAD dist.' include septal and diagonal branches, 'Mid LCX' and 'LCX dist.' include marginal branches; *N* is number of evaluated branches and segments of respective order.

Table 4
Serial follow-up of volumes and areas standardized per regional mass with values in controls as reference

	Order	CSA (mm^2/100 g)				Volume (ml/100 g)			
		Controls[a]		CAD[a]		Controls[a]		CAD[a]	
		N1		N2	Initial evaluation[b]	Follow-up[b]		Initial evaluation[b]	Follow-up[b]
Branches	1	5	1.13 (0.66–2.16)	13	1.04 (0.88–1.81)	1.01 (0.54–1.40)	1.053 (0.488–2.174)	0.481 (0.345–1.089)	0.462 (0.222–0.764)
	2	11	2.49 (0.99–4.43)	24	2.11 (0.91–8.20)	1.69 (0.53–4.69)	0.997 (0.460–2.157)	0.483 (0.238–1.073)	0.388 (0.184–0.802)
	3	18	4.11 (1.92–6.68)	28	3.09 (1.12–8.12)	2.56 (0.68–7.66)	0.768 (0.213–2.235)	0.406 (0.233–1.176)	0.330 (0.131–1.002)
	4	20	5.02 (2.90–23.3)	24	3.30 (1.44–7.91)	2.54 (0.94–8.27)	0.762 (0.290–1.790)	0.344 (0.074–1.221)	0.248 (0.033–0.703)
	5	12	5.30 (2.57–19.5)	17	3.82 (1.91–12.66)	2.60 (1.39–5.61)	0.552 (0.254–2.296)	0.299 (0.111–0.938)	0.233 (0.078–0.624)
	>5	15	7.28 (3.87–14.3)	9	4.02 (1.95–9.93)	2.84 (1.64–5.44)	0.506 (0.271–0.828)	0.335 (0.125–0.486)	0.226 (0.121–0.339)
Segments	1	5	6.6 (4.3–9.9)	13	4.9 (1.3–6.8)	3.3 (1.8–8.3)	0.064 (0.034–0.168)	0.043 (0.008–0.100)	0.031 (0.006–0.098)
	2	11	12.1 (4.8–26.4)	24	5.1 (2.5–14.0)	4.8 (1.3–12.4)	0.155 (0.023–0.499)	0.099 (0.008–0.508)	0.069 (0.006–0.301)
	3	18	13.1 (5.8–27.7)	28	5.4 (2.4–14.5)	5.3 (0.9–13.0)	0.243 (0.037–1.278)	0.104 (0.018–0.374)	0.079 (0.006–0.376)
	4	20	14.4 (5.5–31.2)	24	6.1 (3.0–14.6)	5.3 (1.6–13.2)	0.320 (0.084–1.549)	0.148 (0.042–0.281)	0.101 (0.030–0.322)
	5	12	15.9 (10.3–30.3)	17	5.9 (4.0–20.1)	4.6 (3.2–10.8)	0.214 (0.080–1.627)	0.138 (0.049–0.737)	0.105 (0.025–0.450)
	>5	15	17.5 (6.9–27.3)	9	7.2 (1.8.0–48.2)	5.8 (3.1–9.4)	0.252 (0.061–0.360)	0.089 (0.010–0.219)	0.060 (0.017–0.165)

Data presented as median values and ranges in parentheses. N1 (N2) denotes the number of segments for a given branching order in controls (in CAD patients).

[a] Differences between controls and patients with coronary artery disease were significant ($P<0.05$) for normalized areas and volumes in branches and segments (variance analysis with Bonferroni correction for multiple comparisons).

[b] Differences between initial measurements and follow-up of patients with coronary artery disease were significant ($P<0.005$) for normalized areas and volumes in branches and segments (paired t-test and Wilcoxon's rank test).

average segmental diameter per year was 0.04 ± 0.13 mm. Whereas in the branches, the upper and lower limits of the range of CSA and volume decrease during follow-up in CAD patients, there is a considerable variability and overlap of CSA and volume of the segments during follow-up. For example, for the complete LCA (branching order 1; first line in Table 4), the upper limit (lower limit) of the CSA is 1.81 mm^2/100 g (0.88 mm^2/100 g) at the initial evaluation in CAD patients and 1.40 mm^2/100 g (0.54 mm^2/100 g) at follow-up. The corresponding segment of order 1 in line 7 is the left main and does not demonstrate a corresponding change of the ranges of CSA despite a decrease in median CSA from 4.9 mm^2/100 g to 3.3 mm^2/100 g.

3.4.1. Further analysis of factors related to the progression of diffuse coronary atherosclerosis

We found a correlation ($r = 0.52$, $P < 0.05$) of volume and CSA decrease with the duration of follow-up (see group comparison in Fig. 4).

The shrinkage of the CSA of the branches was correlated with the sum of the individual risk factors ($r = 0.41$, $P < 0.01$; see group comparison in Fig. 5). There was a significant main effect ($F = 5.8$, $P < 0.02$) of the sum of risk factors on branch volume decrease in a general linear factorial model.

3.4.2. Spatial pattern of progressive luminal changes

Segmental CSA and volume reductions showed no correlation with branching order or baseline CSA. These results imply a diffuse pattern of progressive decrease of vascular lumina. However, segmental CSA and volume of the first and the second angiogram demonstrated only a moderate correlation ($r = 0.647$), which suggested some inhomogeneity of luminal narrowing (Fig. 6). The slope of the regression line is significantly smaller than one ($P < 0.05$), which reflects the systematic diameter decrease during follow-up. The data pairs above the line of identity represent segments with positive remodeling. Mean decreases of the diameters of segments and total

branches were not correlated with changes or absolute values of the Gensini score [12], a measure of severity and extent of local stenoses.

4. Discussion

Current two-dimensional QCA was developed for the assessment of local stenoses. It may fail to account for the true severity of diffuse CAD. In view of the methodological limitations of two-dimensional QCA, a recent validated method for three-dimensional QCA [3–5] was evaluated in a retrospective study of serial biplane angiograms of patients with advanced coronary atherosclerosis and in a control group.

Agreement of LCA volumes per cardiac mass in controls and canine reference data [11] is fair. The slightly smaller volumes in our study may be explained by the suppression of the small arteries (< 0.5 mm) and some systematic overestimation of the left ventricular mass perfused by the LCA, as the contribution of the right coronary artery to perfusion of the left ventricle was neglected. Left main coronary artery CSA and segmental diameter values in the controls agree rather well with the reference values derived by two-dimensional QCA [9,10,13,14].

A further significant reduction of vascular lumen occurred in the patients with advanced atherosclerosis during follow-up. The mean reduction of the average segmental diameter per year (0.04 ± 0.13 mm) was comparable with values measured by two-dimensional QCA in the control groups of large studies on the progression of atherosclerosis, such as the REGRESS study (0.05 ± 0.11 mm), the SCRIP study (0.04 ± 0.14) and other intervention studies with QCA end points [2,15,16]. The progress of luminal shrinkage correlated with the duration of follow-up and the number of cardiovascular risk factors as found in other studies [2,15]. Differences of remodeling between segments are probably the main reason for the variability of segmental CSA as reflected by the large range of segmental CSA values in Table 4 Positive remodeling may even cause a local diameter increase [17,18]. As a result variability and overlap of CSA and volume of the segments of CAD patients during follow-up are much higher than in branches, as illustrated in the results section in the paragraph on progression of diffuse atherosclerosis with reference to Table 4. In case of small vessels becoming less than 0.5 mm at follow-up, we have to consider two cases. If a total branch is occluded, the branch is suppressed for matched comparison of the remaining branches. If only a part of the daughter vessels of a branch is affected there is a small reduction in the total length of the branch, which may give rise to slight overestimation of the mean CSA of the branch. The effect on total volume may be neglected as, due to the small diameter (< 0.5 mm), the volume of the filtered part of the vessel is minimal, even if its length is some centimetres. The volume of total vascular branches may be the best measurement of the overall effects. The vascular narrowing found in these patients with advanced CAD was not explained by an increasing number and severity of stenoses, otherwise the Gensini score [12] would have correlated with volume and CSA. Thus, volume and CSA of coronary branches must provide information that is different from the evaluation of local stenoses.

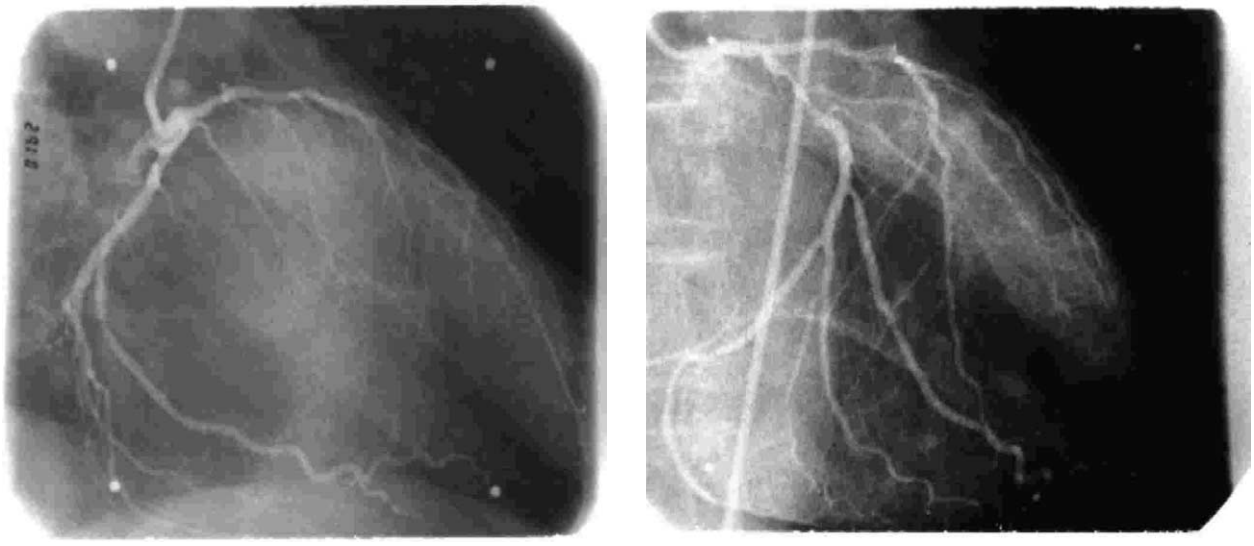

Fig. 2. Pair of angiograms of a patient with a significant ($P < 0.05$) decrease in total coronary volume of 0.6 ml (left, first angiogram; right, last angiogram). The patient suffered from hypertension, hyperlipidemia and insulin-dependent diabetes. The difference in diameter is not visible. Due to projection, even a diameter increase may be suspected in monoplane evaluation.

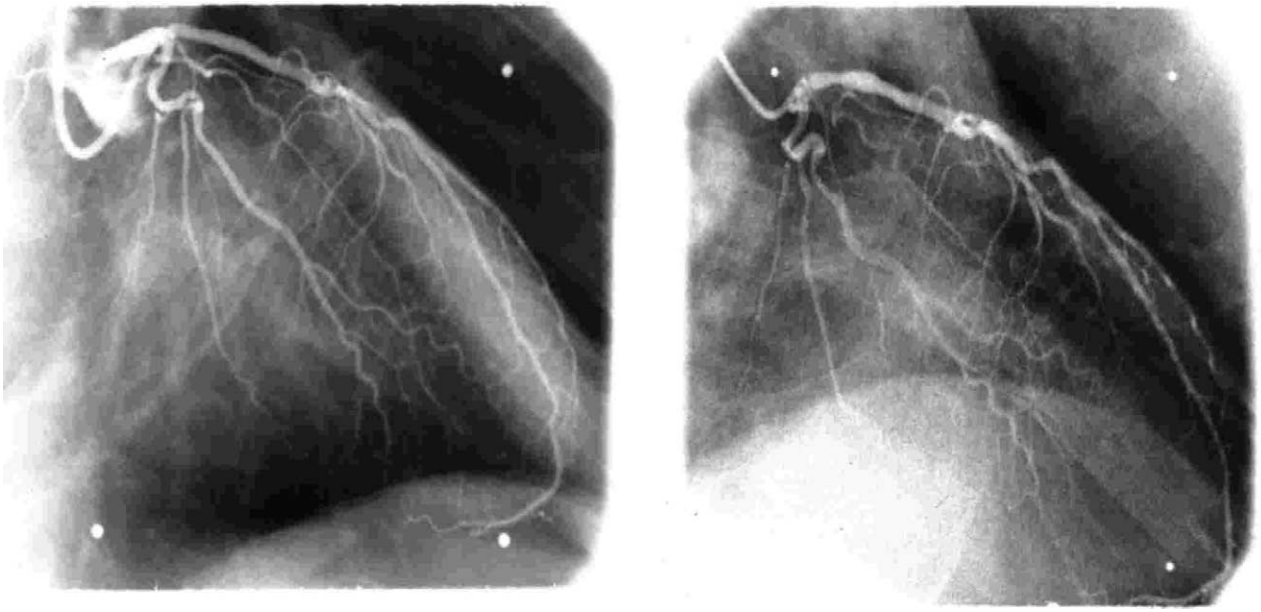

Fig. 3. Pair of angiograms of a patient with nearly no progression of luminal narrowing (left, first angiogram; right, last angiogram). Only one risk factor (hyperlipidemia) was present. The difference in diameter is not visible. Due to projection, even a diameter increase may be suspected in monoplane evaluation.

4.1. Advantages of quantitative three-dimensional coronary angiography as compared with two-dimensional QCA.

Serial two-dimensional QCA is subject to many methodological sources of error and provides only segmental diameter statistics as an appropriate parameter for the assessment of diffuse atherosclerosis [1,2]. Out-of-plane magnification and foreshortening may produce large errors in two-dimensional QCA [3,4] but not in three-dimensional QCA with biplane calibration. Three-dimensional QCA accounts for eccentric luminal geometry and integrates information from two projection planes. As a result of the enhanced accuracy of three-dimensional measurements there is a smaller standard deviation, e.g. of progressive changes of diameter as related to the investigated number of patients (0.13 mm per year in 12 patients as compared with 0.19 (0.21) mm/per 2 years in 323 (330) patients in the REGRESS study [16]). This means a reduction of study size and costs of trials. It should be noted that a comprehensive two-dimensional QCA study as performed in the REGRESS trial may not consume less time per case and may not be less costly than a three-dimensional study. In view of methodological shortcomings of two-dimensional QCA, Seiler et al. [6] proposed that local CSA, calculated from diameters measured by two-dimensional QCA, should be related to total length of the corresponding distal branch estimated from a three-dimensional model. The variability of the segmental CSA is considerable, however, due to local remodeling (see also Table 4). Moreover, total length of a vascular branch depends on imaging conditions and the limiting criteria used for the reconstruction of tiny vessels.

4.2. Quantitative three-dimensional coronary angiography for assessment of diffuse atherosclerosis as compared with other methods

Three-dimensional intravascular ultrasound has the advantage of providing data on plaque volume [19,20] and may help to assess the composition of plaques and their surface properties [21–23]. It may be combined

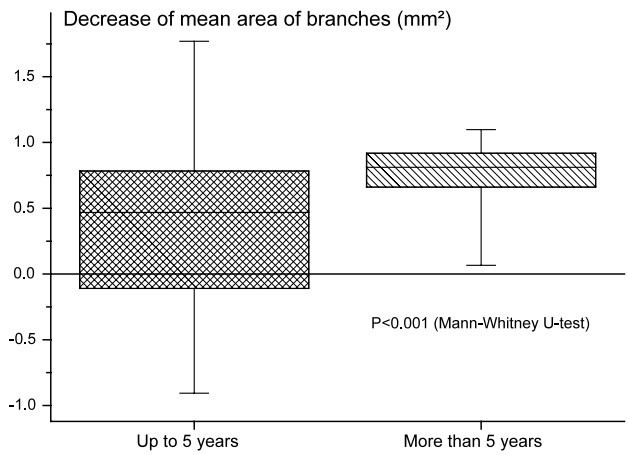

Fig. 4. Median decrease, and 75% (hatched areas) and 95% confidence intervals of mean areas of the left coronary artery branches grouped with respect to the time interval between the first and last evaluation ($N = 115$).

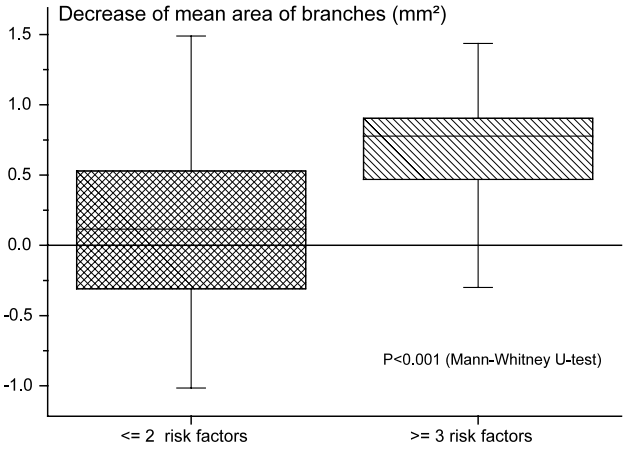

Fig. 5. Median decrease, and 75% (hatched areas) and 95% confidence intervals of mean diameters of the left coronary artery branches grouped with respect to the number of cardiovascular risk factors ($n = 115$).

with, and enhanced with respect to geometric accuracy, by three-dimensional angiographic reconstruction [24,25]. The main limitation of this technique is the size of the probes. New miniaturized devices may be available in the future, however [26]. Optical coherence tomography is another developing technique for intravascular assessment of plaque morphology with a higher axial resolution and a wider dynamic range than intravascular ultrasound [21].

Magnetic resonance imaging is a rapidly developing non-invasive technique for the evaluation of plaque volume, plaque composition and lumen area [27]. As far as the investigation of coronary arteries in vivo is concerned, there are still problems with combined spatial and time resolution and correction of motion artifacts, which have to be resolved by technical improvements [28–31]. Electron beam tomography provides a quantitative assessment of calcified plaque [32,33]. This may be important adjunctive information, but it is no surrogate for the assessment of lumina and plaque volume [34]. Contrast-enhanced electron beam tomography allows curved multiplanar reconstruction of the coronary arteries [35]. However, image quality is not always adequate for technical reasons [36]. The feasibility of a comprehensive assessment of all epicardial coronaries, the relative cost-effectiveness (no additional investigations, devices or investments) and the fact that only two angiographic projections and some protocol data are needed constitute the major advantage of three-dimensional QCA as compared with other methods.

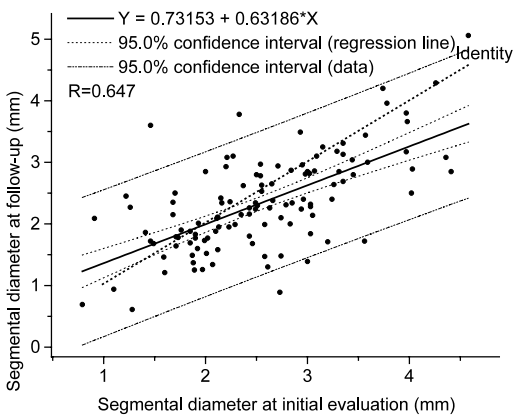

Fig. 6. Correlation of diameters of segments and branches at initial investigation and at follow-up ($n = 115$). The data demonstrate a considerable variability of the diameter decrease for branches and segments that is not related to vessel size. The dotted line represents the identity. Segments with positive remodeling are represented by data pairs above this line, and those with negative remodeling correspond to data pairs below this line. Negative remodeling prevails, as is reflected by the slope of the regression line.

4.3. Limitations and methodological considerations

The controls were defined angiographically by the absence of coronary luminal irregularities, which does not rule out angiographically silent atherosclerosis. This limitation does not appear to be critical, since the luminal volumes, areas and diameters in the controls agree with reference data from literature as already discussed. The investigated groups were rather small as a result of the selection criteria and the cumbersome reconstruction technique. However, the size was sufficient to demonstrate the potential clinical use of this technique, provided further technical developments facilitate the application of three-dimensional QCA. Differences due to sampling were excluded by paired comparison of all serial measurements, stratification with respect to branching order, normalization per regional mass and the three-dimensional approach, which provides a unique geometry of a given vascular tree. Controls were not tested twice because in our previous validation study [4] serial investigations of volumes, lengths, and diameters of segments by different investigators agreed within 0.05 ± 0.32 mm, 0.28 ± 0.356 mm and 0.021 ± 0.081 ml. Similar results were found for branches.

4.4. Clinical impact

Currently, three-dimensional QCA is an investigative tool. Due to the accuracy, sensitivity and relative independence of imaging conditions of this method [4], it should be useful for studies that assess the influence of lifestyle changes or medication on the progression of coronary atherosclerosis. Some major limitations of the method—standardized image and protocol quality and time-consuming manual interaction—may be overcome by current developments in digital imaging and automation and further improvements of the method. For a more comprehensive quantitative evaluation of

atherosclerosis in large coronary vessels, three-dimensional intravascular ultrasound or other imaging modalities, e.g. magnetic resonance imaging, may be combined with and enhanced with respect to geometric accuracy by three-dimensional angiographic reconstruction [24,25].

Acknowledgements

The authors are grateful for editorial assistance from Tonie Derwent.

References

[1] de Feyter PJ, Serruys PW, Davies MJ, Richardson P, Lubsen J, Oliver MF. Quantitative coronary angiography to measure progression and regression of coronary atherosclerosis. Circulation 1991;84:412–23.
[2] Jukema JW, Bruschke AVG, Reiber JHC. Lessons learned from angiographic coronary atherosclerosis trials. In: Reiber JHC, van der Wall EE, editors. Cardiovascular Imaging, 1st ed. Dordrecht: Kluwer Academic, 1996:119–32.
[3] Wahle A, Wellnhofer E, Mugaragu I, Sauer HU, Oswald H, Fleck E. Assessment of diffuse coronary artery by quantitative analysis of coronary morphology based upon 3-D reconstruction from biplane angiograms. IEEE Trans Med Imaging 1995;14:230–41.
[4] Wellnhofer E, Wahle A, Mugaragu I, Gross J, Oswald H, Fleck E. Validation of an accurate method for 3-dimensional reconstruction and quantitative assessment of volumes, lengths and diameters of coronary vascular branches and segments from biplane angiographic projections. Int J Cardiac Imaging 1999;15:339–53.
[5] Wahle A. Präzise dreidimensionale Rekonstruktion von Gefäßsystemen aus biplanen angiographischen Projektionen und deren klinische Anwendung. 1-185, Technische Universität Berlin. Düsseldorf: VDI-Verlag, 1997.
[6] Seiler C, Kirkeeide RL, Gould KL. Basic structure–function relations of the epicardial coronary vascular tree — basis of quantitative coronary arteriography for diffuse coronary artery disease. Circulation 1992;85:1987–2003.
[7] Beier J, Wellnhofer E, Oswald H, Fleck E. Accuracy and precision of angiographic volumetry methods for left and right ventricle. Int J Cardiol 1996;53:179–88.
[8] Goldman L, Hashimoto B, Cook EF, Loscalzo A. Comparative reproducibility and validity of systems for assessing cardiovascular functional class: advantages of a new specific activity scale. Circulation 1981;64:1227–34.
[9] Lichtlen P, Rafflenbeul W. Intravitale Morphometrie von Koronargefäßen. In: Lichtlen PR, editor. Koronarangiographie, 2nd ed. Erlangen: Perimed, 1990:371–404.
[10] MacAlpin RN, Abbasi AS, Grollman JHJ, Eber L. Human coronary artery size during life. A cinearteriographic study. Radiology 1973;108:567–76.
[11] Douglas JE, Greenfield JC. Epicardial coronary artery compliance in the dog. Circulat Res 1970;27:921–9.
[12] Gensini G. The pathological anatomy of the coronary arteries in man—the coronary artery disease scoring and retrieval system of Gensini (cardscores). In: Gensini G, editor. Coronary Angiography. New York: Futura, 1975:271–4.
[13] Brown BG, Bolson E, Frimer M, Dodge HT. Quantitative coronary arteriography: estimation of dimensions, hemodynamic resistance, and atheroma mass of coronary artery lesions using the arteriogram and digital computation. Circulation 1977;55:329–37.
[14] Gensini GG, Kelly AE, Da Costa BC, Huntington PP. Quantitative angiography: the measurement of coronary vasomobility in the intact animal and man. Chest 1971;60:522–30.
[15] Haskell WL, Alderman EL, Fair JM, et al. Effects of intensive multiple risk factor reduction on coronary atherosclerosis and clinical cardiac events in men and women with coronary artery disease. The Stanford Coronary Risk Intervention Project (SCRIP). Circulation 1994;89:975–90.
[16] Jukema JW, Bruschke AV, van Boven AJ, et al. Effects of lipid lowering by pravastatin on progression and regression of coronary artery disease in symptomatic men with normal to moderately elevated serum cholesterol levels. The Regression Growth Evaluation Statin Study (REGRESS). Circulation 1995;91:2528–40.
[17] Glagov S, Weisenberg E, Zarins CK, Stankunavicius R, Kolettis GJ. Compensatory enlargement of human atherosclerotic coronary arteries. N Engl J Med 1987;316:1371–5.
[18] Shircore AM, Mack WJ, Selzer RH, Lee PL, Azen SP, Alaupovic P, Hodis HN. Compensatory vascular changes of remote coronary segments in response to lesion progression as observed by sequential angiography from a controlled clinical trial. Circulation 1995;92:2411–8.
[19] von Birgelen C, Slager CJ, Di Mario C, de Feyter PJ, Serruys PW. Volumetric intracoronary ultrasound: a new maximum confidence approach for the quantitative assessment of progression–regression of atherosclerosis? Atherosclerosis 1995;118(suppl):S103–13.
[20] von Birgelen C, van der Lugt A, Nicosia A, et al. Computerized assessment of coronary lumen and atherosclerotic plaque dimensions in three-dimensional intravascular ultrasound correlated with histomorphometry. Am J Cardiol 1996;78:1202–9.
[21] Brezinski ME, Tearney GJ, Weissman NJ, et al. Assessing atherosclerotic plaque morphology: comparison of optical coherence tomography and high frequency intravascular ultrasound. Heart 1997;77:397–403.
[22] de Korte CL, Cespedes EI, van der Steen AFW, Pasterkamp G, Bom N. Intravascular ultrasound elastography: assessment and imaging of elastic properties of diseased arteries and vulnerable plaque. Eur J Ultrasound 1998;7:219–24.
[23] Erbel R, Ge J, Gorge G, et al. Intravascular ultrasound classification of atherosclerotic lesions according to American Heart Association recommendation. Coronary Artery Dis 1999;10:489–99.
[24] Wahle A, Prause GPM, von Birgelen C, Erbel R, Sonka M. Fusion of angiography and intravascular ultrasound in vivo: establishing the absolute 3-D frame orientation. IEEE Trans Biomed Eng 1999;46:1176–80.
[25] Wahle A, Prause GPM, DeJong SC, Sonka M. Geometrically correct 3-D reconstruction of intravascular ultrasound images by fusion with biplane angiography—methods and validation. IEEE Trans Med Imaging 1999;18:686–99.
[26] Hiro T, Hall P, Maiello L, et al. Clinical feasibility of 0.018-inch intravascular ultrasound imaging device. Am Heart J 1998;136:1017–20.
[27] Shinnar M, Fallon JT, Wehrli S, et al. The diagnostic accuracy of ex vivo MRI for human atherosclerotic plaque characterization. Arterioscler Thromb Vasc Biol 1999;19:2756–61.
[28] Huber A, Nikolaou K, Gonschior P, Knez A, Stehling M, Reiser M. Navigator echo-based respiratory gating for three-dimensional MR coronary angiography: results from healthy volunteers and patients with proximal coronary artery stenoses. Am J Roentgenol 1999;173:95–101.

[29] Nagel E, Bornstedt A, Schnackenburg B, Hug J, Oswald H, Fleck E. Optimization of realtime adaptive navigator correction for 3D magnetic resonance coronary angiography. Magn Reson Med 1999;42:408–11.
[30] Sandstede JJ, Pabst T, Beer M, Geis N, Kenn W, Neubauer S, Hahn D. Three-dimensional MR coronary angiography using the navigator technique compared with conventional coronary angiography. Am J Roentgenol 1999;172:135–9.
[31] Botnar RM. A fast 3D approach for coronary MRA. J Magn Reson Imaging 1999;10:821–5.
[32] Callister TQ, Raggi P, Cooil B, Lippolis NJ, Russo DJ. Effect of HMG-CoA reductase inhibitors on coronary artery disease as assessed by electron-beam computed tomography. N Engl J Med 1998;339:1972–8.
[33] Callister TQ, Cooil B, Raya SP, Lippolis NJ, Russo DJ, Raggi P. Coronary artery disease: improved reproducibility of calcium scoring with an electron-beam CT volumetric method. Radiology 1998;208:807–14.
[34] Doherty TM, Detrano RC, Mautner SL, Mautner GC, Shavelle RM. Coronary calcium: the good, the bad, and the uncertain. Am Heart J 1999;137:806–14.
[35] Achenbach S, Moshage W, Ropers D, Bachmann K. Curved multiplanar reconstructions for the evaluation of contrast-enhanced electron beam CT of the coronary arteries. Am J Roentgenol 1998;170:895–9.
[36] Achenbach S, Moshage W, Ropers D, Nossen J, Daniel WG. Value of electron-beam computed tomography for the noninvasive detection of high-grade coronary-artery stenoses and occlusions. N Engl J Med 1998;339:1964–71.

2.2 Flow-Profiling

2.2.1 Shear Stress and Vascular Remodeling: Study of Cardiac Allograft Coronary Artery Disease as a Model of Diffuse Atherosclerosis

Der Rückschluss von der morphologischen Momentaufnahme auf den Prozess stützt sich auf die experimentell belegte Theorie des flussmechanischen regulatorischen von der Endothelfunktion übersetzten Steuersignals Schubspannung an der Gefäß Innenwand. Zwischen Schubspannung, Geschwindigkeit und Geometrie bestehen strömungsmechanisch determinierte Beziehungen. Die biologische Wirkung der Schubspannung im Regelkreis setzt funktionsfähige Endothelzellen voraus.

Als bed-side Forscher untersuchten wir deshalb die Beziehungen zwischen am Patienten invasiv gemessenen Parametern im Koronarsystem wie Blutflussgeschwindigkeit, Gefäßdiameter, aus Laborparametern berechneter Vollblutviskosität und Endothelfunktion. Entsprechend dem klinischen Charakter der Untersuchung musste ein etwas vereinfachtes Konzept der Schubspannungsberechnung zugrunde gelegt werden. Da dieses Konzept lokalisierte Veränderungen an Stenosen oder Stents nicht adäquat erfasst, bot es sich an, diffuse Entzündungs- und Remodelingprozesse zu untersuchen. Solche Prozesse sind z. B. bei der Transplantatvaskulopathie bekannt. Da das DHZB eines der führenden Herztransplantationszentren ist, waren auch entsprechende Daten aus klinischen Studien verfügbar.

Methodik:

In der Arbeit wurden vier Gruppen von Patienten verglichen:

- Nicht herztransplantierte Kontrollen mit Ausschluss einer organischen Herzerkrankung,
- Herztransplantierte ohne Wandveränderungen im intravaskulären Ultraschall (IVUS),
- Herztransplantierte mit Intimaproliferation im IVUS aber ohne höhergradige Stenosen bzw. Revaskularisationsindikation,
- Herztransplantierte mit perkutaner koronarer Intervention.

Querschnitte wurden mittels 2-D QCA bestimmt. Flussgeschwindigkeiten mit einem Dopplerdraht erfasst (199). Zudem wurde die Endothelfunktion erfasst durch den Vergleich der Wirkung von intrakoronarer Gabe von 25 pmol Substanz P (endothelabhängige Vasodilation im Wesentlichen über endogenes NO) mit 0,2 mg Nitroglycerin (endothelunabhängige Vasodilatation). Für die Berechnung der WSS

wurde ein Hagen Poiseuille Modell mit nicht- Newtonscher kinematischer Viskosität verwendet (Details siehe Methodik).

Ergebnisse:

Es zeigte sich, dass die WSS

- invers mit dem Gefäßdurchmesser korreliert,
- direkt mit der Endothelfunktion korreliert,
- bei Herztransplantierten gegenüber Kontrollen erhöht ist
- und bei Herztransplantierten mit Intimahyperplasie oder perkutaner koronarer Intervention höher als bei Herztransplantierten mit Koronarien ohne Wandveränderung ist,
- dass also eine erhöhte koronare Ruheblutflussgeschwindigkeit in Abwesenheit von lokalen Stenosen auf Negativremodeling und/oder Vasokonstriktion hinweist, während sehr niedrige Blutflussgeschwindigkeiten Positivremodeling und/oder Vasodilatation implizieren.

Schlussfolgerung:

Anhand der Transplantatvaskulopathie wurde ein Modell zur Beurteilung von Remodelingprozessen mittels intravaskulärer Geschwindigkeitsmessungen etabliert. Auch unter Berücksichtigung einer gewissen Stellgrößengrundvariabilität einzelner Regelkreise (19), hat dieser Ansatz erhebliche Vorteile insbesondere bei Verlaufsuntersuchungen bei diffusen Wandveränderungen, da hier der klassische Durchmesser- oder- Querschnittsvergleich mit einem Referenzsegment nicht mehr valide ist.

Shear Stress and Vascular Remodeling: Study of Cardiac Allograft Coronary Artery Disease as a Model of Diffuse Atherosclerosis

Ernst Wellnhofer, MD,[a] Wolfgang Bocksch, MD,[a] Nicola Hiemann, MD,[b] Michael Dandel, MD,[b] Waldemar Klimek, MD,[a] Roland Hetzer, MD, PhD,[b] and Eckart Fleck, MD[a]

Background: The assessment of remodeling in diffuse atherosclerosis by intravascular ultrasound is hampered by the lack of an appropriate reference segment. Transplant coronary artery disease is an accepted model of diffuse atherosclerosis. Flow-dependent remodeling is regulated by shear stress. Thus, normal levels of shear stress at baseline flow reflect adequate regulation and provide a functional assessment of flow-dependent remodeling.

Methods: The approach was evaluated in 91 patients with transplant coronary artery disease and in 9 non-transplanted controls and 16 control transplant recipients. Quantitative coronary angiography, intracoronary ultrasound and intracoronary velocity studies were performed at baseline and after pharmacologic intervention. Calculated shear stress was compared between these groups and a sub-group with coronary angioplasty at follow-up (8 of 60 patients with control angiography after 23 ± 8 months). The relation of shear stress to flow, diameter, flow/area ratio and endothelial function was analyzed.

Results: Normal shear stress was found in non-transplanted controls and transplant recipients without coronary artery disease. Patients with coronary angioplasty at follow-up had elevated shear stress and enhanced endothelial dysfunction on the initial investigation. Shear stress was not correlated with flow ($r = 0.062$, non-significant), but with diameter ($r = -0.654$), flow/area ratio ($r = 0.814$) and endothelial dysfunction ($r = 0.722$).

Conclusion: Calculated local shear stress appears to be useful for the assessment of the adequacy of flow-dependent macrovascular remodeling in diffuse atherosclerosis. Elevated blood flow/area ratio is a potential clinical marker of increased shear stress that reflects inadequate flow-dependent remodeling. J Heart Lung Transplant 2002; 21:405–416.

From the [a]Departments of Internal Medicine/Cardiology and [b]Department of Cardiothoracic and Vascular Surgery, Deutsches Herzzentrum Berlin, Berlin, Germany.

Submitted March 15, 2001; revised May 23, 2001; accepted July 26, 2001.

Reprint requests: Dr. Ernst Wellnhofer, Deutsches Herzzentrum Berlin, Augustenburger Platz 1, 13353 Berlin, Germany. Fax: 49-30-4593-2500. Telephone: 49-30-4593-2400. E-mail: ewellnhofer@t-online.de

1053-2498/02/$–see front matter PII S1053-2498(01)00374-6

Regional remodeling of atherosclerotic arteries has been found to be a major determinant of the clinical manifestations of the disease,[1–3] especially in heart transplant recipients.[4,5] Clinical evaluation of remodeling is usually performed by intravascular ultrasound and compares the target vascular segment to a reference segment.[1,6] There are inherent limitations of this approach due to the assumption of a "normal" reference segment, which are well recognized, and this precludes its application in diffuse vascular disease.[1–3,7] Transplant coronary artery disease is a model of diffuse coronary atherosclerosis[8,9] suitable for the evaluation of new concepts for the clinical assessment of remodeling.[7]

Shear stress is the principal fluid-mechanical signal that regulates flow-dependent remodeling and therefore provides functional assessment of the adequacy of flow-dependent remodeling. Signal transduction and processing are supposed to be endothelium dependent.[10-15] However, shear-dependent remodeling has been found to occur even in vessels with severely impaired endothelial function,[2,3] which suggests that assessment of the adequacy of flow-dependent remodeling by shear stress may be feasible in diffuse atherosclerosis as it is in transplant coronary artery disease.[16]

Whereas experimental studies that investigate flow-dependent remodeling vary flow to induce changes in shear stress, in most clinical settings local flow is fixed as a result of perfusion demands in combination with the principle of conservation of mass.[17] Encroachment of the vascular lumen as a result of local inflammation of the vascular wall and thrombosis results in a relative mismatch between luminal area and flow and should be an important trigger of local flow-dependent remodeling in clinical situations. The ratio of local flow to luminal area increases as adaptation fails and is independent of plaque burden. This ratio is a velocity and its value is identical to mean velocity. The relationship of the flow/area ratio to shear stress is easily seen in Figure 1. Inadequate remodeling implies an increase in this ratio as local flow has to be conserved[17] and shear stress remains elevated due to increased velocity and reduced diameter. If complete regulation occurs, both parameters assume normal values.

The objective of our cohort study is to evaluate whether shear stress is clinically useful to assess the adequacy of flow-dependent remodeling in diffuse atherosclerosis. Coronary interventions during follow-up in a group with documented diffuse coronary artery disease, but without angiographic lesions at initial evaluation, served as a test.

METHODS

Patients

Between September 1996 and June 1999, 107 orthotopic heart transplant recipients, who underwent surveillance cardiac catheterization without angiographic lesions,[18] were included in the study (see Table I).

Control Group of Heart Transplant Recipients

The control group consisted of 16 transplant recipients with a normal flow reserve and without coronary intimal thickening >0.3 mm, as diagnosed by intracoronary ultrasound.

Sub-group Serving as Model for Diffuse Disease

The sub-group of diffuse disease comprised 91 patients with transplant coronary artery disease as diagnosed by intracoronary ultrasound. Of these patients, all had a clinical follow-up at 24 ± 10 months and 60 patients also had angiographic follow-up at 23 ± 8 months. Eight transplant recipients had to be treated by angioplasty at follow-up.

Group of Non-Transplanted Controls

Non-transplanted controls consisted of 9 non-transplanted patients who presented with suspected angina but normal coronary angiograms and normal coronary flow reserve (i.e., >2.5).

General Procedures

Written informed consent was obtained from all patients prior to examination. The study was approved by the local institutional review committee. Vasoactive medication was discontinued 24 hours prior to catheterization. Diagnostic right and left heart catheterization, coronary angiography and right ventricular endomyocardial biopsy were performed according to standard clinical practice using the transfemoral approach. Biplane angiograms of coronary arteries were acquired using a non-ionic contrast agent and standard angiographic X-ray equipment (Integris /LARC System, Philips).

Following the administration of 5000 IU of heparin, ultrasound was performed using an Endosonics device with 3F to 3.4F Visions Five-64 F/X catheters. A manual pull-back was continuously recorded on video-tape, which started in the distal LAD, ran through the middle and proximal left anterior descending coronary arteries and finished at the origin of the left main coronary artery.

Subsequently, a 0.014-in. Doppler guide wire[19] (Cardiometrics) was introduced into the left ante-

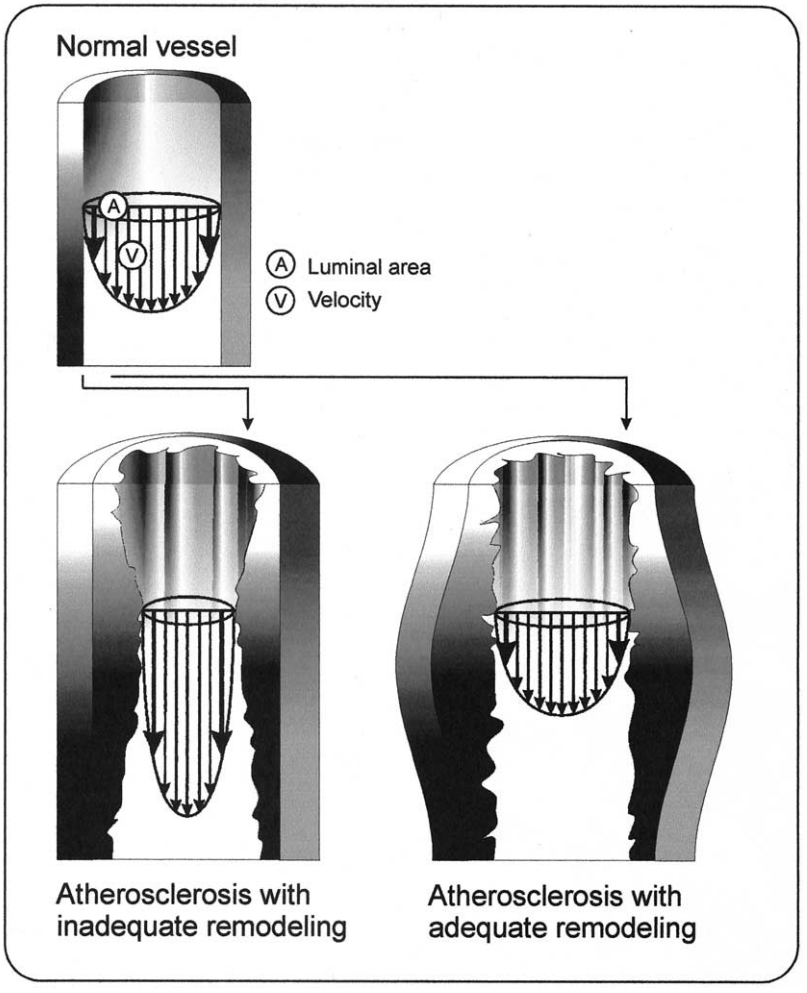

FIGURE 1 Schematic diagram illustrating the effect of remodeling on local velocity. At the top a normal vessel is displayed. Volume flow is equal to mean velocity × area. At the bottom are two vascular segments with a similar volume of plaque perfused by an identical volume flow as the normal segment at the top. On the left side adaptive remodeling is assumed to be absent. In this case luminal narrowing is necessarily associated with increased velocity to preserve flow. On the right side, perfect adaptive remodeling is assumed. Because the luminal area is equal to that of the normal vessel, mean velocity is identical assuming the same flow. It should be noted that relative increases in shear stress are even more pronounced if remodeling is inadequate, because shear stress is inversely proportional to the root of the area and proportional to velocity, whereas velocity is only inversely proportional to the area at a given flow.

rior descending coronary artery through a 7F or 8F guiding catheter.

Baseline measurements of average peak velocity (APV), 3 to 5 minutes after the control angiogram, were followed by intracoronary bolus injections of 5 ml of 0.9% NaCl, 25 pmol of substance P (Clinalfa [C-601]) in 1 ml of 0.9% NaCl, 30 μg of adenosine (Sanofi Withrop Adrekar) in 1 ml of 0.9% NaCl and finally 0.15 mg of nitroglycerin in 1.5 ml of 0.9% NaCl, followed by a wait of at least 2 minutes after each test. Bolus injections were followed by flushing with 4 ml of 0.9% NaCl. Angiograms were recorded 40 to 60 seconds after each bolus.

Velocity measurements were performed continuously. For calculations, angiographic diameters and velocity measurements immediately before the injection of contrast agent were combined. Representative measurements are given in Figure 2.

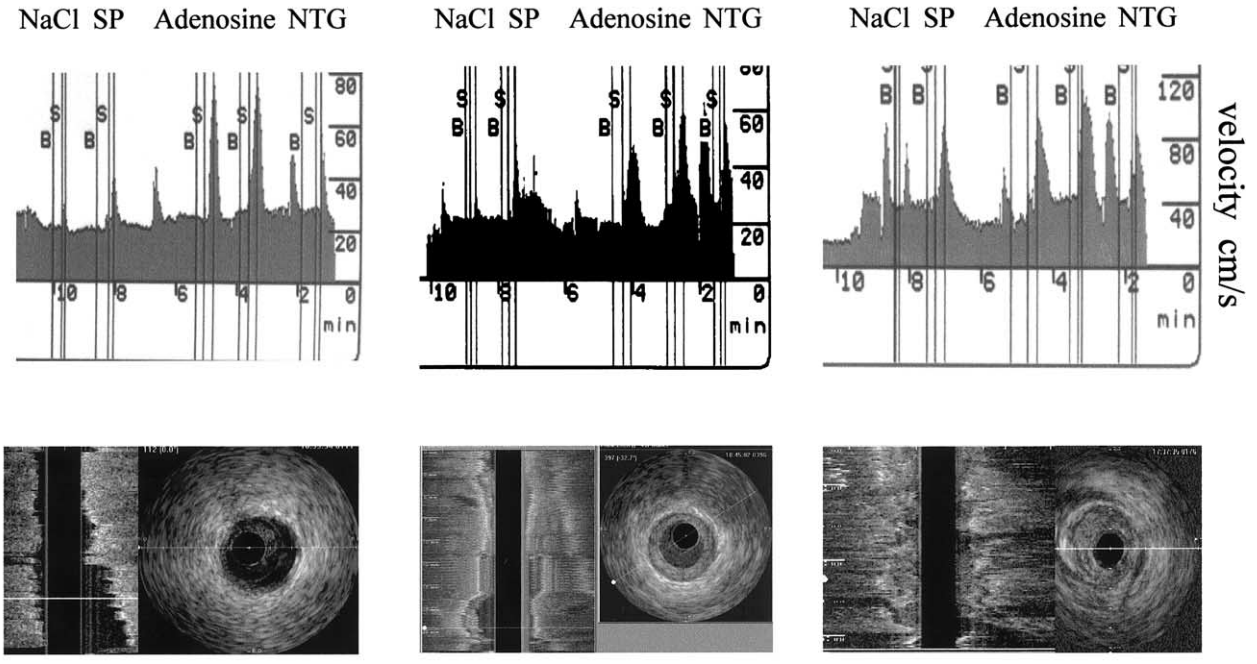

FIGURE 2 Representative examples. (Left) Recording taken from the transplanted control group. Baseline flow velocity varies slightly during the investigation of vascular function but remains <30 cm/sec. The velocity peaks not related to pharmacologic testing are due to contrast injections. (Middle) Registration from another patient with diffuse transplant coronary artery disease (Stanford Class IV) in the proximal and medial left anterior descending coronary arteries and adequate remodeling. Again, baseline flow velocity remains below 30 cm/sec. The corresponding IVUS shows a remarkably well-preserved luminal area despite diffuse intimal thickening of the whole vessel. (Right) Registration from patient with diffuse transplant coronary artery disease (Stanford Class IV) in the proximal and medial left anterior descending coronary arteries and inadequate remodeling. In this case, part of a pull-back of the Doppler wire from the distal LAD is seen on the left- hand side of the velocity scan. At the beginning of plaque baseline flow velocity increases abruptly to about 40 cm/sec. The corresponding IVUS shows a reduced luminal area and diffuse intimal thickening of the proximal and medial LAD.

Quantitative Coronary Angiography

Diameters of a proximal segment of the LAD, which comprised the Doppler sample and delimited by defined landmarks, and ejection fraction were measured by QANSAD, a state-of-the-art second generation QCA system with an accuracy of within ± 0.028 mm.[20] Calibration was performed with guiding catheters. Pin-cushion distortion was corrected.

Intracoronary Ultrasound

Minimum luminal areas (LA), maximum intimal thickening (MIT) and total vessel areas (VA) were determined from video-tapes or CD-ROMs at the sites of minimum luminal areas by the use of resident software. The intimal area (IMA) was calculated as VA − LA. The intimal index was calculated as IMA/VA.[21] A recently proposed remodeling index for evaluation of remodeling in transplant coronary artery disease was calculated as VA/IMA.[7]

Biopsies were graded according to the ISHLT classification.[22]

Hemodynamics and Rheologically Relevant Laboratory Data

Blood pressure, heart rate and electrocardiogram (ECG) data were monitored continuously and recorded digitally. For estimating dynamic viscosity the hematocrit and total protein values were collected.[23]

Documentation

Average peak flow velocity was documented on S-VHS video, on hard copies, and recorded by

computer together with the arterial pressure and ECG. Angiograms were stored on CD-ROM in DICOM format and on 35-mm cine film. ICUS pull-backs were stored on S-VHS video and on CD-ROM in DICOM format.

Calculations

Mean perfusion pressure = mean aortic pressure − left ventricular end-diastolic pressure (mm Hg).

Area at baseline ($A_{baseline}$) and after nitroglycerin (A_{NTG}) was calculated from diameter at baseline ($D_{baseline}$) and following intracoronary application of nitroglycerin (0.15 mg) (D_{NTG} mm), assuming a circular lumen.[24]

$$A_x = (\pi/4) \cdot D_x^2 \, [mm^2]$$

(where × denotes NTG or baseline). For calculation of shear stress at minimal tone mean velocity (V_{NTG}) was determined from APV values 30 seconds after injection of nitroglycerin (APV_{NTG}) to avoid transient bolus effects.[25] For calculation of baseline flow and shear stress at baseline tone, mean velocity ($V_{baseline}$) was determined from mean baseline APV:

$$V_x = APV_x/2 \, [cm/sec]^{17,19}$$

where *x* denotes nitroglycerin (NTG) or baseline. Volume flow (F) was calculated as:

$$F = V_x \cdot A_x \, [mm^2 \cdot cm/sec]$$
$$= V_x \cdot A_x \cdot (0.01 \cdot 60) \, [ml/min]^{17,19,26}$$

Shear rate (S) was calculated as:

$$S = 32 \cdot F_x/(\pi \cdot D_x^3) = 8 \cdot V_x/D_x \, [cm/sec \cdot /mm]$$
$$= 10 \cdot 8 \cdot V_x/D_x \, [Hz]^{27}$$

Dynamic viscosity, μ (cP), where 1 cP = 0.001 Pa·sec, was calculated from shear rate, hematocrit and total protein according to the regression equations given by de Simone et al.[23] Shear stress, τ, was calculated as:

$$\tau = (10 \cdot 0.001) \, \mu \cdot S \, [dyn/cm^2]^{26}$$

A non-dimensional index of endothelial dysfunction relates diameter increase after substance P to diameter increase after NTG as reference:

$$I_{EdysF} = (D_{NTG} - D_P)/(D_{NTG} - D_{baseline})$$

with D_P diameter after substance P. This index is zero if the action of substance P equals the action of nitroglycerin. It assumes the value of 1 if there is no effect of substance P.

Statistics

For a description of data, means and standard deviations, median values and ranges or counts and percentages are given as appropriate. Intergroup differences were assessed by distribution-free methods (Mann–Whitney *U*-test and Kruskal–Wallis test), because the distribution of nearly all parameters demonstrated significant deviation from a normal distribution. Trends were evaluated by product-moment correlation. Significance was assumed at $p \leq .05$.

RESULTS

Clinical Characteristics

Table I contains a survey of the data. All transplant recipients were on standard immunosuppressive treatment with cyclosporine, 2 to 4 mg/kg, which maintained a trough level of 250 ng/ml; prednisolone 0.1 to 0.5 mg/kg, and azathioprine, 1 to 5 mg/kg, adjusted for the white blood cell count. Donor age ($p < .03$) was higher in patients who underwent angioplasty during follow-up and was lowest in transplant recipients without coronary disease, the latter comprising relatively more female patients ($p < .02$). There were no significant differences between the groups with respect to other risk factors or concomitant medication.

There were two complications during the initial investigations in the transplant recipients: one dissection and one spontaneous thrombosis, despite anti-coagulation with heparin in a patient with acute rejection. All complications were treated successfully by angioplasty or stenting.

Hemodynamic, Laboratory and Ultrasound Data

Baseline hemodynamics and laboratory data are shown in Table II. There were no significant intergroup differences within transplant recipients, especially with respect to perfusion pressure. In the reference group, blood pressure, heart rate, left ventricular end-diastolic pressure and estimated perfusion pressure were slightly lower, whereas hematocrit and total protein were lower in the transplant recipients. Diffuse atherosclerosis, defined by polyfocal or diffuse intimal thickening that comprised more than one vascular segment, was present in 70 of the 91 patients with transplant coronary artery disease. There was only a small group (13 patients) with a single lesion. Because this small group did not differ significantly from the total

TABLE I Clinical characteristics

	Controls	Tx controls	TxCAD		*p*-Value (Kruskal–Wallis)
			Event-Free	PTCA	
N	9	16	83	8	—
Gender M/F	7/2	10/6*	66/17	8/0*	0.02*
Age (years)	59 ± 4	47 ± 15	52 ± 12	54 ± 9	n.s.
Body surface area (m^2)	1.86 ± 0.14	1.82 ± 0.18	1.94 ± 0.20	2.04 ± 0.15	n.s.
Ischemic origin, n (%)†	—	1 (6)	18(22)	2 (25)	n.s.
Time post-transplant (months)	—	31 ± 33	49 ± 33	43 ± 25	n.s.
Donor age (years)	—	25 ± 7	35 ± 13	42 ± 14	0.03
Ischemic time (minutes)	—	147 ± 38	177 ± 46	165 ± 28	n.s.
Biopsy grade (0/1A/1B/2)	—	15/1/−/−/−	74/7/1/1	7/1/−/−	n.s.
Average cyclosporine trough level (ng/dl)	—	234 ± 113	272 ± 117	240 ± 90	n.s.
Cholesterol (mg/dl)	225 ± 60	260 ± 75	247 ± 58	243 ± 74	n.s.
Body mass index (kg/m^2)	26 ± 3	24 ± 5	27 ± 4	26 ± 3	n.s.
Diabetes, n (%)	0 (0)	2 (13)	16 (19)	1 (12)	n.s.
Hypertension, n (%)	3 (33)	9 (56)	71 (86)	8 (100)	n.s.
Lipid-lowering agents, n (%)	4 (44)	2 (13)	27 (33)	2 (25)	n.s.
Acetylcholinesterase inhibitors, n (%)	3 (33)	9 (56)	55 (67)	8 (100)	n.s.
Ca^{++} antagonists, n (%)	1 (11)	3 (19)	50 (61)	6 (75)	n.s.

*There was a significant difference between Tx controls and patients with PTCA only during follow-up (n.s., $p > .05$).
†Ischemic origin applies to the etiology of the cardiomyopathy in the transplant recipients.

transplant coronary artery disease group with respect to shear stress and related parameters (see Figure 3), for statistical reasons focal and diffuse coronary artery diseases were not further investigated as different groups. There seemed to be a non-significant trend, however, indicating worse endothelial function and remodeling in diffuse disease (see Figure 3).

Group Comparison

Diameters, velocities and calculated values are summarized in Table III. In the reference group (non-transplant patients with normal coronary arteries) and in control transplant recipients velocities *and* shear stress values remained well within the normal range (<30 cm/sec and <15 to 20 dyn/cm^2).[12,14,28,29]

TABLE II Hemodynamics, laboratory data and ultrasound measurements

	Controls	Tx controls	TxCAD		*p*-Value* (Kruskal–Wallis)
			Event-Free	PTCA	
N	9	16	83	8	—
Perfusion pressure (mm Hg)	85 ± 17	102 ± 15	98 ± 15	97 ± 15	n.s.
Ejection fraction	71 ± 4	71 ± 7	69 ± 6	66 ± 6	n.s.
Left ventricular end-diastolic pressure (mm Hg)	8 ± 3	11 ± 5	13 ± 4	11 ± 2	0.005
Aortic pressure (mm Hg)	96 ± 15	112 ± 15	111 ± 16	108 ± 14	n.s.
Heart rate (beats/min)	78 ± 9	92 ± 17	91 ± 14	82 ± 13	0.03
Hematocrit (%)	41 ± 3	34 ± 3	35 ± 5	38 ± 3	0.01
Total protein (g/dl)	7.8 ± 0.5	6.4 ± 1.0	6.2 ± 0.5	6.2 ± 0.1	<0.001
Intimal index (%)	—	0 (0–18)	41 (13 ± 67)	48 (27–70)	<0.001
Remodeling ratio	—	—	2.4 (1.5–6.6)	2.07 (1.4–3.6)	n.s.
Maximum plaque thickness (mm)	—	0 (0–0.3)	1.08 (0.4–2.0)	1.24 (0.5–1.6)	<0.001

*Not significant (n.s;), $p > 0.05$.

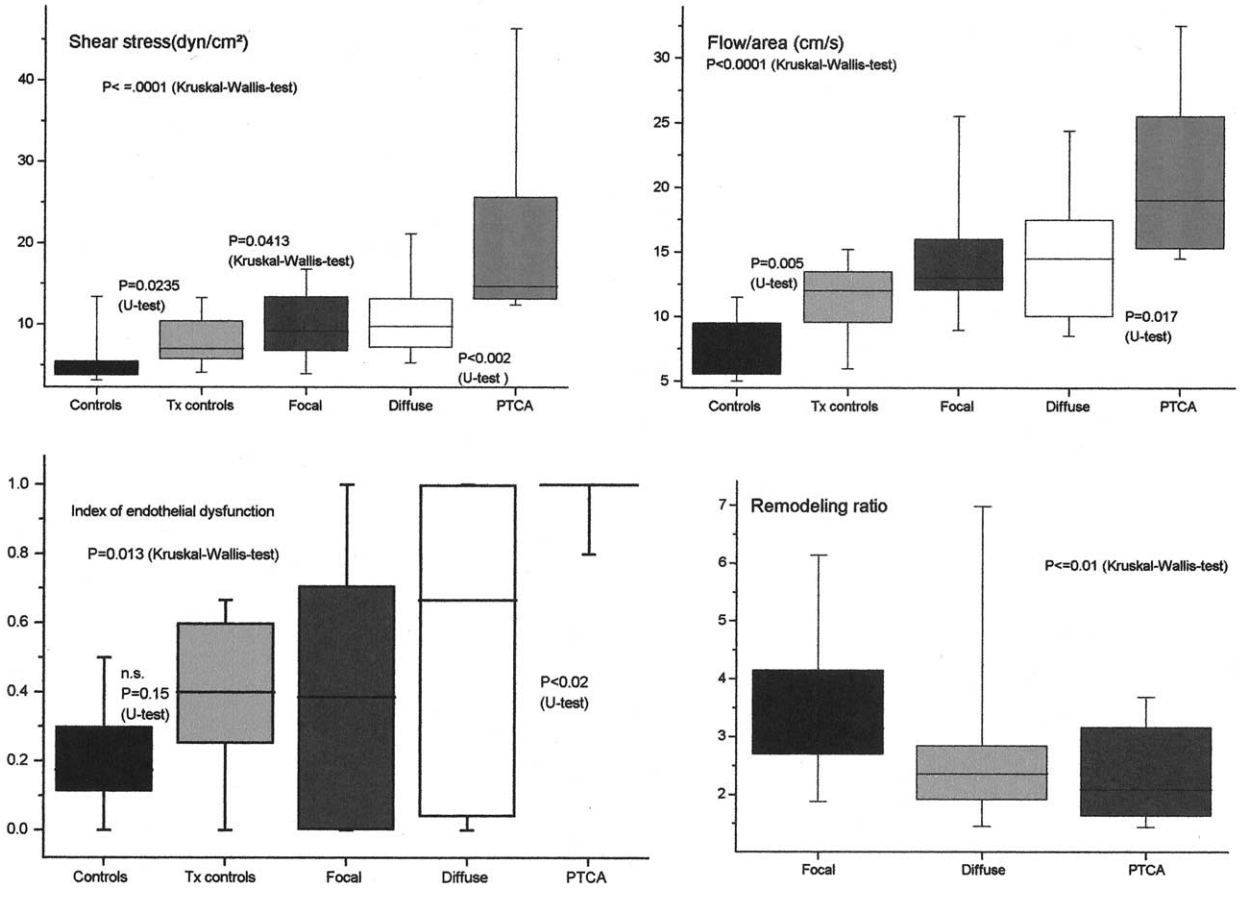

FIGURE 3 Group comparison of shear stress (left top), flow/area ratio (right top), index of endothelial dysfunction (bottom left) and remodeling ratio (bottom right). Box-plot with median values, 75% (areas) and 95% percentiles (bars). Shear stress and flow/area ratio were determined at the minimal tone (after nitroglycerin). Further subgroups were analyzed in patients with transplant coronary artery disease (91 patients). Eight patients had percutaneous transluminal coronary angioplasty (PTCA) during follow-up. Diffuse atherosclerosis, defined as polyfocal or diffuse intimal thickening that comprised more than one vascular segment, was present in all patients with subsequent PTCA and in 70 other patients. Focal disease, defined as plaque confined to single coronary segment, was diagnosed in 13 patients.

As can be seen from Figure 3 (top) shear stress and flow/area ratio behaved similarly. The lowest shear stress values and flow/area ratios were found in the controls and the highest values in transplant recipients who underwent an intervention procedure during follow-up. These values were significantly elevated when compared with the values in patients with diffuse transplant coronary artery disease without events during follow-up. As suggested by the 75% (boxes) and 95% (whiskers) confidence intervals of data in Figure 3, calculated shear stress might provide a better separation of the group at risk for future coronary angioplasty than F/A ratio. Although the intravascular ultrasound (IVUS)-based remodeling ratio (bottom right) was significantly lower in diffuse disease than in focal disease, it did not discriminate between patients who had an intervention during follow-up and those with an event-free follow-up.

The increased range and median values of shear stress in the angioplasty group (Figure 3, top left) indicated failure of regulation and corresponded well with the enhanced endothelial dysfunction in this group (Figure 3, bottom left). It should be noted that in non-transplanted controls moderate endothelial dysfunction does occur and endothelial func-

TABLE III Velocities, quantitative coronary angiography data and calculated values (mean values and range)

	Controls	Tx Controls	TxCAD		*p*-Value (Kruskal–Wallis)
			Event-Free	PTCA	
N	9	16	83	8	—
Mean baseline APV (cm/s)	16 (10–21)	22 (11–31)	27 (13–47)	32 (28–62)	<0.001
Maximum APV after substance P (cm/s)	35 (20–48)	40 (24–69)	51 (20–100)	73 (44–96)	<0.001
Maximum APV after nitroglycerin (cm/s)	41 (25–60)	48 (22–80)	54 (27–110)	68 (55–142)	<0.001
APV 30 s after nitroglycerin (cm/s)	17 (10–23)	23 (11–31)	29 (15–90)	38 (29–65)	<0.001
Coronary flow velocity reserve (adenosine)	3.5 (2.9–4.5)	3.1 (2.5–5.0)	2.7 (1.1–4.3)	2.6 (2.0–3.2)	0.003
Diameter at baseline (mm)	3.5 (1.8–4.9)	3.4 (2.2–6.8)	3.3 (2.1–4.5)	2.8 (2.0–4.1)	n.s.
Diameter after substance P (mm)	4.2 (2.1–5.8)	3.8 (2.5–7.4)	3.6 (2.2–5.1)	2.8 (2.1–4.2)	0.02
Diameter after nitroglycerin (mm)	4.4 (2.3–6.0)	3.9 (2.5–7.8)	3.6 (2.4–5.1)	3.2 (2.1–4.6)	0.04
Viscosity (cP)	4.7 (4.0–5.5)	3.4 (2.8–4.4)	3.2 (2.4–4.4)	3.5 (3.1–4.3)	0.04
Flow at baseline (ml/min)	55 (20–118)	694 (21–288)	72 (25–173)	78 (31–186)	n.s.
Flow at minimal tone (ml/min)	85 (28–169)	94 (31–219)	94 (32–171)	100 (47–234)	n.s.
Shear rate at baseline (Hz)	180 (92–366)	281 (129–480)	358 (169–617)	558 (346–1128)	<0.001
Shear rate at minimal tone (Hz)	133 (71–304)	226 (99–400)	307 (175–705)	411 (342–1083)	<0.001
Shear stress τ at baseline (dyn/cm^2)	7 (4–16)	9 (5–15)	11 (5–29)	20 (13–48)	<0.001
Shear stress τ at minimal tone (dyn/cm^2)	5 (3–13.0)	7 (4–13)	10 (5–22.0)	15 (12–46)	<0.001
Diameter increase substance P (%)	18 (14–22)	8 (0–20)	7 (0–27)	1 (0–5)	<0.001
Diameter increase nitroglycerin (%)	19 (16–21)	13 (4–25)	12 (2–28)	8 (3–18)	0.04
Index of endothelial dysfunction	0.2 (0.0–0.5)	0.4 (0.0–0.7)	0.6 (0.0–1.0)	1.0 (0.8–1.0)	0.002

*Not significant (n.s.), $p > .05$.

tion in transplant recipients without coronary disease is only moderately compromised.

Correlation Analysis

As can be seen in Figure 4 (top left) there was no correlation between shear stress and flow. This agrees with the assumption of different regulation mechanisms for flow and shear stress. Flow is determined by regulation mechanisms related to the perfused region[17] and shear stress is determined by local adaptation to flow.[12,14] As a result we found a good correlation of shear stress with local endothelial function (Figure 4, bottom right). The overall correlation of shear stress with diameter (Figure 4, top right) was moderate and improved by 0.10 to 0.15 in the regulated groups (e.g., non-transplanted controls). There was a good correlation of shear stress with the flow/area ratio (Figure 4, bottom left). This correlation was 0.10 lower in the control groups, where shear stress was supposed to be regulated and enhanced by 0.05 in transplant recipients who had an intervention during follow-up, and where failure of regulation could be assumed.

DISCUSSION

The importance of remodeling as the primary determinant of lumen size in atherosclerotic vessels has been pointed out in several recent reviews.[1–3,30] Regulation is complex and involves nitric oxide and metalloproteinases and mitogenic and fibrogenic growth factors, and may depend on elastin and connexin turnover. Most mediators of shear-sensitive remodeling are also mediators or targets of the inflammatory response to vascular injury in atherosclerosis and are linked to plaque vulnerability.[2,3,30] Vessel morphology is the result of both remodeling and inflammation and thus provides only implicit and limited information on the remodeling itself. Apart from the fundamental problem resulting from the assumption of a normal reference segment in atherosclerotic vessels, conventional morphologic assessment of remodeling provides no valid information as to whether the remodeling process attains adequate luminal area with respect to local flow. Such information may not be provided by either measurement of luminal area or vessel area alone

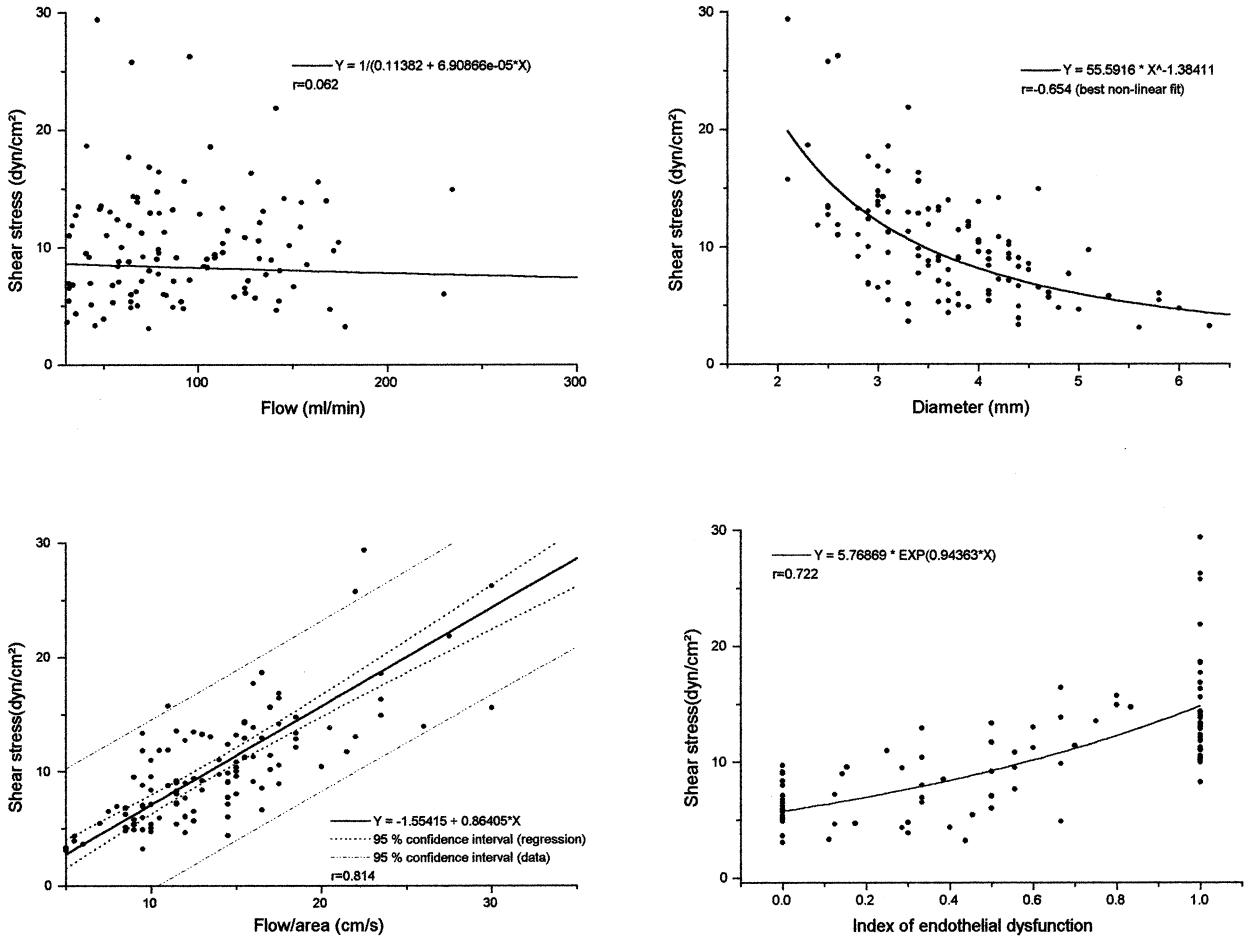

FIGURE 4 Correlations, regressions and scatterplots of shear stress and flow (top left), diameter (top right), flow/area ratio (bottom left) and index of endothelial dysfunction (bottom right). Shear stress, diameter and flow/area ratio were determined at minimal tone (after nitroglycerin).

without assessment of actual local flow. Functional assessment of flow-dependent remodeling by shear stress provides this information, which may be clinically important for two reasons. First, adequate flow-dependent remodeling implies the absence of luminal obstructions irrespective of plaque volume and it probably depends on some residual endothelial function, which may be vasoprotective even in an atherosclerotic vascular segment. Moreover, this analytical approach provides a framework for an interpretation of clinical findings as to the comparison of vascular function to vessel morphology. It should be clear that adequate remodeling in terms of morphologic assessment and adequate flow-dependent remodeling are different concepts and may not coincide. This has potential clinical implications as illustrated by comparison of the following studies.

A recent longitudinal ultrasound study in transplant recipients found a progressive decrease of luminal area,[31] and another ultrasound study detected an initial decrease and late increase of the luminal area of the proximal coronary arteries.[32] On the contrary, baseline coronary blood flow was found to be elevated early after transplantation when compared with controls,[33,34] and to normalize after 3 years.[34] Obviously the interpretation of the aforementioned intravascular ultrasound studies might be different if functional assessment of remodeling in relation to flow had been performed. A reduction of luminal area may be considered as constrictive remodeling by morphologic criteria. If flow decreases concomitantly such a reduction might be adequate with respect to flow.

Functional assessment of flow-dependent remod-

eling provides different and possibly complementary insight into morphologic assessment, which may give more information on local inflammation than on other specific aspects of remodeling such as flow-dependent luminal enlargement.

Definition of Adequate Remodeling With Respect to Flow

The most important clinical feature of this approach is that calculated shear stress provides a physiologic definition of a normal vascular lumen or adequate remodeling with respect to flow. This obviates the problematic use of a reference site in a more or less generally diseased vessel to define adequate remodeling.[1–3,6]

Prognostic Relevance

A potential prognostic value of assessment of luminal remodeling by calculated shear stress was demonstrated in contrast to assessment by the remodeling ratio.[7] Due to statistical and methodologic reasons we did not define an a priori cutoff point for calculated shear stress in this investigation. The upper limit of shear stress was 13 dyn/cm^2 in both control groups and was in good agreement with the literature,[14] and the lower limit of shear stress was 12 dyn/cm^2 in the group with intervention during follow-up. Seventy-five percent of the transplant recipients with diffuse coronary artery disease without angioplasty during follow-up had shear stress of $\leq$13 dyn/cm^2. The optimal cutoff value should range from around 12 to 14 dyn/cm^2, but remains to be specified by further study.

Flow-Dependent Remodeling as a Parameter Reflecting Endothelial Function

Failure of regulation of shear stress was clearly related to enhanced endothelial dysfunction in our study, which was in agreement with the literature.[13,35–37] Persistently elevated shear stress at baseline flow implies a failure of flow-dependent remodeling or advanced vascular dysfunction, whereas overshoot enlargement in early atherosclerosis[1,38] indicates an error in the regulation of the feedback loop between the shear stress signal and adaptive vascular remodeling. The latter should be a sign of early endothelial dysfunction, as suggested by studies with acetylcholine.[39]

Clinical Significance of Resting Flow Velocity

Under normal conditions the coronary flow/area ratio depends on coronary flow, which is related to the size of the perfusion bed, and on total vascular area determined by branching geometry of the vascular tree. Given a constant flow and a slight increase of vascular area at each branching level, a slight decrease of intracoronary velocity may be anticipated.[40] The physiologic concept behind this argument assumes adequate local adaptation of the vascular bed to flow. If local flow-dependent regulation of the luminal area fails, then flow/area ratio varies with shear stress as noted earlier and confirmed by our investigation. As a result of the failure of local flow-dependent regulation of the luminal area, higher resting velocity values have been found in patients with coronary artery disease, even in vessels without local stenoses.[17,41] Viscosity does affect the flow/area ratio (compare shear stress and flow/area ratio in Figure 3). The non-transplanted controls had a significantly higher viscosity (Table III) than the transplant recipients. The flow exerted a stronger force on endothelial cells at lower shear rates in non-transplanted controls as compared with transplant recipients. As a result, the transplanted controls demonstrated higher flow/area ratios. Correction was performed by calculating the shear stress instead of a shear rate or flow/area ratio. The difference in shear stress between the control groups was less than the difference between flow/area ratios and represented the true functional deviation.

Limitations and Methodologic Considerations

A major limitation is that the study was performed only in one vessel. A further extension of the protocol to include additional measurements in other coronary vessels was not feasible for ethical and logistic reasons. We would expect, however, similar findings in these vessels. We considered only elevated shear stress, but this was not a principal restriction. Angiographic Type B1 lesions in accelerated transplant coronary artery disease[18] provide a perfect example of low shear stress adaptation failure. There was some endothelial dysfunction in the control groups and angiographically silent atherosclerosis cannot be completely ruled out in the non-transplanted control group. Because regulation did work in these groups, it turned out to be no real limitation. Simultaneous IVUS and Doppler velocity studies would have been methodologically preferable as they allow a more accurate local assessment of shear stress, flow, endothelial function and luminal area. Local shear stress and changes in endothelial function may be similar, however, in a larger local environment in diffuse atherosclerosis, especially in transplant coronary artery disease. As a

result, precisely localized measurements would not be as important as in focal disease. The calculations used for flow, shear rate and shear stress assumed a steady laminar flow in a circular, rigid, non-tapering tube. With respect to flow a slight to moderate error was associated with these assumptions (30% at 30 ml/min to 13% at 160 ml/min).[26] Calculated Womersley numbers for our data ranged from 1.3 to 7.0, and steady flow model and pulsatile flow model calculations (not presented) yielded nearly identical results.[27] Tapering increased shear rate and shear stress, which likely led to minor systematic underestimation of both parameters. Curvatures and bifurcations gave rise to asymmetric shear distributions and should not have had too much impact on the mean values of shear rate and shear stress. Coronary blood flow increase at minimal tone as compared to baseline tone may be calculated from the data presented in Table III. It tended to be lower in transplanted recipients (31%) than in non-transplanted controls (54%) and coincided fairly well with data from Sudhir et al.[25] (39% after 0.1 mg and 50% after 0.2 mg of nitroglycerin). At baseline, tone shear stress values were slightly higher than at minimal tone. Shear stress at minimal tone is an artificial pharmacologically induced condition. Shear stress at baseline tone should be the clinically relevant signal. The difference between these shear stress values is generally small, however, as can be seen from Table III. Concomitantly, increased vessel area compensated for increased flow at minimal tone with respect to shear rate and flow/area ratio. Stronger elevations of vascular tone at baseline may have had an influence on these measurements at baseline in individual cases, which can be detected by a nitroglycerin test.

CONCLUSION

Functional assessment of flow-dependent remodeling in coronary arteries by calculation of shear stress provides additional information and a more comprehensive clinical analysis of remodeling. Elevation of baseline velocity is a good predictor of elevated shear stress, because velocity reflects flow/area ratio. Elevated shear stress is associated with an increased rate of interventions during follow-up in initially angiographically silent diffuse transplant-associated atherosclerosis. If baseline velocity is found to be elevated, we suggest that a shear stress calculation should be done in addition to morphologic assessment of remodeling.

The authors are grateful for editorial assistance from Tonie Derwent.

REFERENCES

1. Birnbaum Y, Fishbein MC, Luo H, Nishioka T, Siegel RJ. Regional remodeling of atherosclerotic arteries: a major determinant of clinical manifestations of disease. J Am Coll Cardiol 1997;30:1149–64.
2. Pasterkamp G, de Kleijn DP, Borst C. Arterial remodeling in atherosclerosis, restenosis and after alteration of blood flow: potential mechanisms and clinical implications. Cardiovasc Res 2000;45:843–52.
3. Ward MR, Pasterkamp G, Yeung AC, Borst C. Arterial remodeling: mechanisms and clinical implications. Circulation 2000;102:1186–91.
4. Pethig K, Heublein B, Wahlers T, Haverich A. Mechanism of luminal narrowing in cardiac allograft vasculopathy: inadequate vascular remodeling rather than intimal hyperplasia is the major predictor of coronary artery stenosis. Working Group on Cardiac Allograft Vasculopathy. Am Heart J 1998;135:628–33.
5. Lim TT, Liang DH, Botas J, Schroeder JS, Oesterle SN, Yeung AC. Role of compensatory enlargement and shrinkage in transplant coronary artery disease. Serial intravascular ultrasound study. Circulation 1997;95:855–9.
6. von Birgelen C, Mintz GS, de Vrey EA, et al. Atherosclerotic coronary lesions with inadequate compensatory enlargement have smaller plaque and vessel volumes: observations with three dimensional intravascular ultrasound in vivo. Heart 1998;79:137–42.
7. Schwarzacher SP, Uren NG, Ward MR, et al. Determinants of coronary remodeling in transplant coronary disease: a simultaneous intravascular ultrasound and Doppler flow study. Circulation 2000;101:1384–9.
8. Ventura HO, Mehra MR, Smart FW, Stapleton DD. Cardiac allograft vasculopathy: current concepts. Am Heart J 1995; 129:791–8.
9. Gordon D. Transplant arteriosclerosis. In: Fuster V, Ross R, Topol EJ, eds. Atherosclerosis and coronary artery disease. Philadelphia: Lippincott-Raven, 1996:715–26.
10. Gnasso A, Carallo C, Irace C, et al. Association between intima-media thickness and wall shear stress in common carotid arteries in common carotid arteries in healthy male subjects. Circulation 1996;94:3257–62.
11. Cines DB, Pollak ES, Buck CA, et al. Endothelial cells in physiology and in the pathophysiology of vascular disorders. Blood 1998;91:3527–61.
12. Gotlieb AI, Langille BL. The role of rheology in atherosclerotic coronary artery disease. In: Fuster V, Ross R, Topol EJ, eds. Atherosclerosis and coronary artery disease. Philadelphia: Lippincott-Raven, 1996:595–606.
13. Ben Driss A, Benessiano J, Poitevin P, Levy BI, Michel JB. Arterial expansive remodeling induced by high flow rates. Am J Physiol 1997;272:H851–8.
14. Tedgui A, Lehoux S, Levy B. Mechanical factors and vascular biology. In: Levy BI, Tedgui A, eds. Biology of the arterial wall. Dordrecht: Kluwer, 1999:71–100.
15. Hudlicka O, Brown MD, Egginton S. The role of hemodynamic and mechanical factors in vascular growth and remodeling. In: Lelkes PI, ed. Mechanical forces and the endothelium. Amsterdam: Harwood, 1999:291–359.
16. Gibbons GH. The pathogenesis of graft vascular disease:

implications of vascular remodeling. J Heart Lung Transplant 1995;14:149–58.
17. Anderson HV, Stokes MJ, Leon M, Abu-Halawa SA, Stuart Y, Kirkeeide RL. Coronary artery flow velocity is related to lumen area and regional left ventricular mass. Circulation 2000;102:48–54.
18. Gao SZ, Alderman EL, Schroeder JS, Silverman JF, Hunt SA. Accelerated coronary vascular disease in the heart transplant patient: coronary arteriographic findings. J Am Coll Cardiol 1988;12:334–40.
19. Doucette JW, Corl PD, Payne HM, et al. Validation of a Doppler guide wire for intravascular measurement of coronary artery flow velocity. Circulation 1992;85:1899–911.
20. Hausleiter J, Jost S, Nolte CW, et al. Comparative in-vitro validation of eight first- and second-generation quantitative coronary angiography systems. Coron Artery Dis 1997;8:83–90.
21. St Goar FG, Pinto FJ, Alderman EL, et al. Intracoronary ultrasound in cardiac transplant recipients: in vivo evidence of "angiographically silent" intimal thickening. Circulation 1992;85:979–87.
22. Billingham ME, Cary NRB, Hammond ME, et al. A working formulation for the standardization of nomenclature in the diagnosis of heart and lung rejection: Heart Rejection Study Group. J Heart Lung Transplant 1990;9:587–93.
23. de Simone G, Devereux RB, Chien S, Alderman MH, Atlas SA, Laragh JH. Relation of blood viscosity to demographic and physiologic variables and to cardiovascular risk factors in apparently normal adults. Circulation 1990;81:107–17.
24. Berglund H, Luo H, Nishioka T, et al. Highly localized arterial remodeling in patients with coronary atherosclerosis: an intravascular ultrasound study. Circulation 1997;96:1470–6.
25. Sudhir K, MacGregor JS, Barbant SD, et al. Assessment of coronary conductance and resistance vessel reactivity in response to nitroglycerin, ergonovine and adenosine: in vivo studies with simultaneous intravascular two-dimensional and Doppler ultrasound. J Am Coll Cardiol 1993;21:1261–8.
26. Doriot P, Dorsaz P, Dorsaz L, Chatelain P. Accuracy of coronary flow measurements performed by means of Doppler wires. Ultrasound Med Biol 2000;26:221–8.
27. Samet MM, Lelkes PI. The hemodynamic environment of endothelium in vivo and its simulation in vitro. In: Lelkes PI, ed. Mechanical forces and the endothelium. Amsterdam: Harwood, 1999:1–32.
28. Caracciolo EA, Wolford TL, Underwood RD, et al. Influence of intimal thickening on coronary blood flow responses in orthotopic heart transplant recipients. A combined intravascular Doppler and ultrasound imaging study. Circulation 1995;92:II182–90.
29. Duffy SJ. Contribution of vasodilator prostanoids and nitric oxide to resting flow, metabolic vasodilation, and flow-mediated dilation in human coronary circulation. Circulation 1999;100:1951–7.
30. Herity NA, Ward MR, Lo S, Yeung AC. Review: clinical aspects of vascular remodeling. J Cardiovasc Electrophysiol 1999;10:1016–24.
31. Kobashigawa J, Wener L, Johnson J, et al. Longitudinal study of vascular remodeling in coronary arteries after heart transplantation. J Heart Lung Transplant 2000;19:546–50.
32. Pethig K, Heublein B, Meliss RR, Haverich A. Volumetric remodeling of the proximal left coronary artery: early versus late after heart transplantation. J Am Coll Cardiol 1999;34: 197–203.
33. Kofoed KF, Czernin J, Johnson J, et al. Effects of cardiac allograft vasculopathy on myocardial blood flow, vasodilatory capacity, and coronary vasomotion. Circulation 1997;95:600–6.
34. Kushwaha SS, Narula J, Narula N, et al. Pattern of changes over time in myocardial blood flow and microvascular dilator capacity in patients with normally functioning cardiac allografts. Am J Cardiol 1998;82:1377–81.
35. Langille BL, O'Donnell F. Reductions in arterial diameter produced by chronic decreases in blood flow are endothelium-dependent. Science 1986;231:405–7.
36. Zarins CK, Glagov S, Giddens DP. Adaptive Enlargement of Arteries in Response to Increased Flow and Increased Intimal Plaque. In: Yoshida Y, Yamaguchi T, Caro CG, Glagov S, Nerem RM, eds. Role of blood flow in atherogenesis—proceedings of the international symposium, Hyogo, October 1987. Tokyo: Springer, 1988:185–8.
37. Kamiya A, Togawa T. Adaptive regulation of wall shear stress to flow change in the canine carotid artery. Am J Physiol 1980;239:H14–21.
38. Glagov S, Weisenberg E, Zarins CK, Stankunavicius R, Kolettis GJ. Compensatory enlargement of human atherosclerotic coronary arteries. N Engl J Med 1987;316:1371–5.
39. Lerman A, Cannan CR, Higano SH, Nishimura RA, Holmes DRJ. Coronary vascular remodeling in association with endothelial dysfunction. Am J Cardiol 1998;81:1105–9.
40. Seiler C, Kirkeeide RL, Gould KL. Basic structure–function relations of the epicardial coronary vascular tree—basis of quantitative coronary arteriography for diffuse coronary artery disease. Circulation 1992;85:1987–2003.
41. Kern MJ, Bach RG, Mechem CJ, et al. Variations in normal coronary vasodilatory reserve stratified by artery, gender, heart transplantation and coronary artery disease. J Am Coll Cardiol 1996;28:1154–60.

2.2.2 In-vivo coronary flow profiling based on biplane angiograms: influence of geometric simplifications on the three- dimensional reconstruction and wall shear stress calculation

Für eine Anwendung des Verfahrens in größerem Stil war es aus Gründen des Zeitaufwands erforderlich zu prüfen, welche Vereinfachungen im 3-D Rekonstruktionsprozess möglich waren, d.h. keine größeren Fehler bei der WSS verursachten.

Methodik: In einer stratifizierten Stichprobe wurden Auswirkung geometrischer Vereinfachungen, wie die Annahme eines zirkulären Querschnitts und geringe Reduktion der räumlichen Auflösung auf die WSS untersucht.

Die absolute WSS hängt zudem stark von der Größe der Flüsse ab, die ihrerseits eine Funktion des absoluten Gefäßquerschnitts und der absoluten Geschwindigkeit sind. Dies verbietet einen direkten Vergleich der Wandschubspannung bei unterschiedlichen Patienten, wo große Unterschiede dieser Parameter erwartet werden müssen. Für einen Vergleich muss ein Ansatz gewählt werden, bei dem mehrere Parameter so in Beziehung gesetzt werden, dass eine reine Größenskalierungsänderung per se zu keiner Änderung der Bewertung führt. Neben der methodischen Vereinfachung der 3-DRekonstruktion wurden deshalb auch normalisierte Histogramme der Wandschubspannung bei Gefäßbäumen mit deutlich unterschiedlicher Geometrie untersucht.

Ergebnisse:

Wir konnten zeigen, dass einfache geometrische Vereinfachungen, wie die Annahme eines zirkulären Querschnitts und eine geringe Reduktion der räumlichen Auflösung nur einen begrenzten Effekt auf die Strömungssimulation und die berechnete Wandschubspannung hat, aber deutlich Rechenzeit bei der Aufbereitung der Finite Elemente Modelle einspart. Die Unterschiede der Wandschubspannungswerte zwischen elliptischer und zirkulärer Querschnittsrekonstruktion waren 4.6% ±5.3% (maximal 14.3 %).

Es zeigten sich erhebliche Gruppenunterschiede in den dimensionslosen Verteilungsmustern.

Schlussfolgerungen:

- Die Annahme eines zirkulären Querschnitts und geringe Änderungen der räumlichen Auflösung haben wenig Einfluss auf die WSS und gestalten die Aufbereitung der Daten effizienter.
- Die Annahme eines zirkulären Querschnitts und geringe Änderungen der räumlichen Auflösung haben minimalen Einfluss auf die entwickelten dimensionslosen Verteilungshistogramme.

Der Stichprobenumfang war etwas klein. Deshalb konnten die in der Arbeit entwickelten dimensionslosen Verteilungsfunktionen nur vorläufig evaluiert werden. Es zeigte sich, dass doch erhebliche Gruppenunterschiede bestanden.

BioMedical Engineering OnLine

BioMed Central

Research

Open Access

In-vivo coronary flow profiling based on biplane angiograms: influence of geometric simplifications on the three-dimensional reconstruction and wall shear stress calculation

Ernst Wellnhofer†[1], Leonid Goubergrits*†[2], Ulrich Kertzscher[2] and Klaus Affeld[2]

Address: [1]German Heart Institute of Berlin, Berlin, Germany and [2]Biofluid Mechanics Laboratory, Charité-Universitätsmedizin Berlin, Berlin, Germany

Email: Ernst Wellnhofer - wellnhofer@dhzb.de; Leonid Goubergrits* - leonid.goubergrits@charite.de; Ulrich Kertzscher - ulrich.kertzscher@charite.de; Klaus Affeld - klaus.affeld@charite.de

* Corresponding author †Equal contributors

Published: 14 June 2006

BioMedical Engineering OnLine 2006, **5**:39 doi:10.1186/1475-925X-5-39

Received: 08 December 2005
Accepted: 14 June 2006

This article is available from: http://www.biomedical-engineering-online.com/content/5/1/39

Abstract

Background: Clinical studies suggest that local wall shear stress (WSS) patterns modulate the site and the progression of atherosclerotic lesions. Computational fluid dynamics (CFD) methods based on in-vivo three-dimensional vessel reconstructions have recently been shown to provide prognostically relevant WSS data. This approach is, however, complex and time-consuming. Methodological simplifications are desirable in porting this approach from bench to bedside. The impact of such simplifications on the accuracy of geometry and wall shear stress calculations has to be investigated.

Methods: We investigated the influence of two methods of lumen reconstruction, assuming circular versus elliptical cross-sections and using different resolutions for the cross-section reconstructions along the vessel axis. Three right coronary arteries were used, of which one represented a normal coronary artery, one with "obstructive", and one with "dilated" coronary atherosclerosis. The vessel volume reconstruction was performed with three-dimensional (3D) data from a previously validated 3D angiographic reconstruction of vessel cross-sections and vessel axis.

Results: The difference between the two vessel volumes calculated using the two evaluated methods is less than 1 %. The difference, of the calculated pressure loss, was between 2.5% and 8.5% for the evaluated methods. The distributions of the WSS histograms were nearly identical and strongly cross-correlated (0.91–0.95). The good agreement of the results was confirmed by a Chi-square test.

Conclusion: A simplified approach to the reconstruction of coronary vessel lumina, using circular cross-sections and a reduced axial resolution of about 0.8 mm along the vessel axis, yields sufficiently accurate calculations of WSS.

Introduction

Based on the hypothesis that information on local wall shear stress (WSS) patterns has a prognostic value with respect to the progression and risk of coronary artery disease, in vivo profiling of the endothelial shear stress in coronary arteries has been performed recently in several studies [1-7]. Published serial invasive investigations in the last years support the prognostic impact of local WSS evaluations [8,9]. Most of these studies were performed by three-dimensional (3D) reconstruction of coronary artery segments fusing intravascular ultrasound images (IVUS) and angiograms with subsequent numerical flow simulation studies. The IVUS is used because it provides detailed information of the circumferential endo-luminal border and also additional information of the vessel wall that is derived from imaging the local plaque. Numerical flow simulation is used since measurements of velocity profiles, and especially of wall shear stress distribution in the coronary arteries, are not feasible.

3D-reconstruction of coronary artery segments fusing IVUS-images and angiograms with subsequent numerical flow simulation studies is an invasive, expensive and time consuming approach that is limited to dedicated studies and rather small numbers of investigated vessel lesions. Further limitations of this method are size of the segments (> 1 mm), which may be assessed by the IVUS catheter. Thus the assessment of side branches and distal coronary arteries is not feasible. We do not know whether the costs of the accuracy of the reconstruction approach translate into the amount of additional clinical diagnostic impact. Simpler approaches may provide clinically relevant prognostic information [9]. Thus, research on simpler techniques is required. Furthermore, we would like to characterize coronary artery disease in the coronary trees as is shown in figures 2 and 3. We propose to use 3D-reconstruction of coronary trees based on biplane angiograms with subsequent numerical flow simulations.

Coronary artery disease is clinically diagnosed by symptoms related to impaired myocardial perfusion and invasively diagnosed by detection of wall irregularities or local obstructions in selective angiograms (luminograms). The luminal contour is the net result of the encroachment of plaque into the vascular lumen and compensatory vessel wall remodeling [10,11]. Luminal remodeling is localized and preserves a circular lumen even in the majority of eccentric atherosclerotic lesions [12]. The irregular lumina occur rarely, generally at severely diseased sites. These advanced lesions imply a failure of local remodeling. This in turn suggests a loss of endothelial function and of WSS responsiveness [13]. Luminal geometry and flow determine wall shear stress. IVUS-data shows that wall thickness and wall composition have no direct impact on WSS.

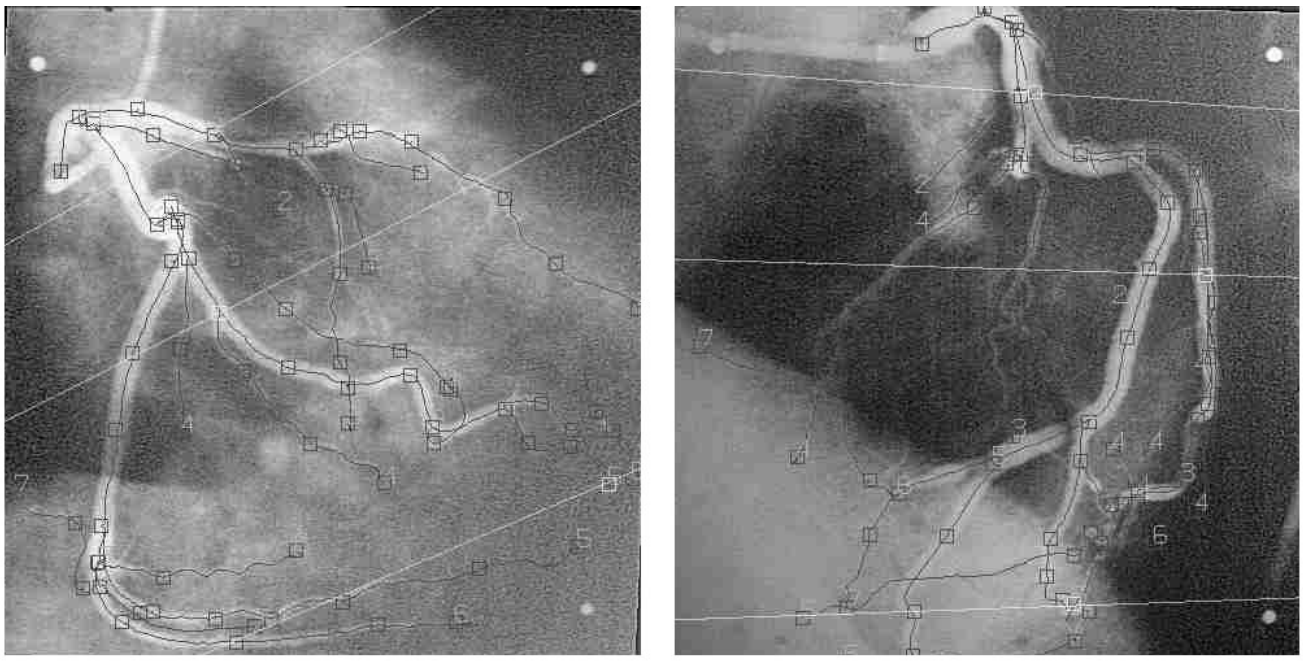

Figure 1
Example of a pair of corresponding LAO and RAO projections. The three straight lines in each image show corresponding projection lines in the two projections. These lines are used to match the two projections. Numerated squares mark nodes used for segmentation and identification of vascular branches.

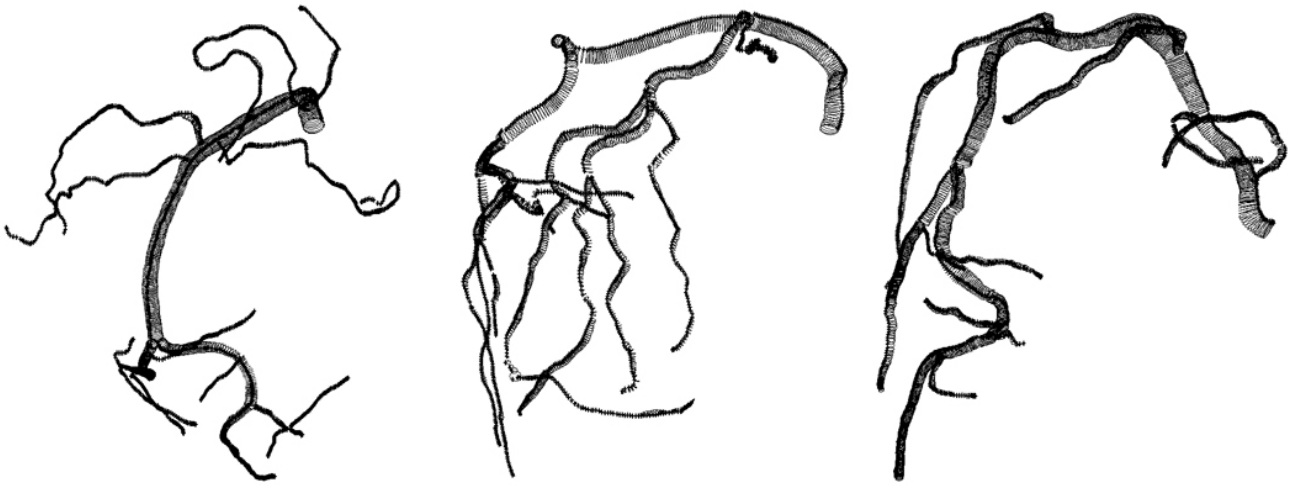

Figure 2
Wire representation of the three right coronary arteries investigated in our study. From left to right: normal right coronary artery, right coronary artery with "obstructive" atherosclerotic disease and right coronary artery with "dilated" atherosclerotic disease. Circular cross-sections are supposed. The reconstructions were done by use of the software Gambit™.

Thus, wall shear stress estimation from standard luminograms using fast semi-automatic geometric reconstructions and flow calculations should be feasible and may be an important step from bench to bedside in providing clinically relevant WSS-data in vivo.

The proposed approach implies simplifications of geometric reconstructions and model assumptions with respect to flow simulation in geometries reconstructed from biplane angiograms. A methodological investigation of the impact of these simplifications on WSS calculations using in vivo data is necessary. The goal of this paper is an assessment of the impact of two different time saving simplifications of geometric reconstruction on cycle-averaged WSS. Furthermore, a new method of WSS distribution characterization is proposed – analysis of WSS histograms. A further goal of this paper is to investigate the impact of reconstruction simplifications on the proposed method of the WSS characterization.

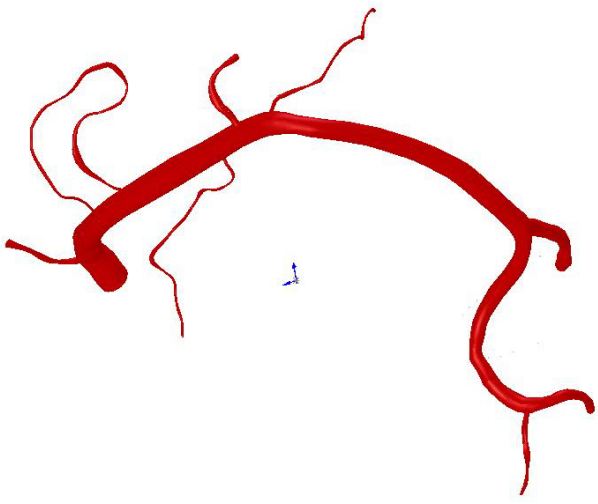

Figure 3
Geometry of the reconstructed endo-luminal surface of the normal coronary artery using Method 1 and the software SolidWorks™. A normal right coronary artery is presented.

Methods

Data

Three distinct cases of coronary artery luminal geometries reconstructed from biplane patient angiograms were used: a normal right coronary artery (control), and right coronary arteries (RCA) with atherosclerosis with "dilated" versus "obstructive" remodeling. The concept of "dilated" versus "obstructive" coronary atherosclerosis was introduced by Schoenhagen et al. [14,27]. The concept of Schoenhagen addresses the fact that remodeling is an important factor affecting the luminal width which is only loosely related to plaque growth. He says: "Traditionally, the development of coronary artery disease was described as a gradual growth of plaques within the intima of the vessel. The outer boundaries of the intima, the media and the external elastic membrane, were thought to be fixed in size. However, histologic studies demonstrated that certain plaques do not reduce luminal size because of expansion of the media and the external elastic membrane during atheroma development. This phenomenon of "arterial remodeling" was confirmed in necropsy specimens of human coronary arteries. [14]" Even though in his review Schoenhagen focuses on local remodeling

assessed by IVUS and IVUS-specific definitions of remodeling, he sees a clinical analogy between positive remodelling and coronary ectasia. We apply his concept on atherosclerotic coronary ectasia ("dilated") and non-ectatic coronary artery disease ("obstructive"). The underlying hypothesis of our choice of these three particular coronary arteries is that vascular remodeling is intrinsically related to atherosclerotic inflammation and affects environments at multiple sites rather than localized foci. Thus profiles of WSS within whole segments or vessels might identify different patterns of remodeling associated with characteristic changes in the distribution of WSS. This is why three different vessels were used to study the impact of reconstruction simplifications on WSS characterization.

Three-dimensional reconstruction

Biplane angiograms (25 frames/s) had been acquired on cine-film by a standard biplane angiographic X-ray device (Philips DCI-System) during end diastole. Rotation and angulations of the C-arms, distances of image intensifiers to X-ray sources and size of image intensifiers had been recorded. Frame numbers were used to find the corresponding images in the left anterior oblique (LAO) and in the right anterior oblique (RAO) projections. These protocol data were used to estimate the three-dimensional geometry. A two-dimensional (2D) model was reconstructed for each projection by a combination of interactive topology marking and automatic vessel detection. Vessel bifurcations were manually identified and used for both segmentation and vessel detection (see figure 1). 2D data is organized in segments consisting of coordinates of centerline and related radii, defining both edge points of the vessel projection for the corresponding 2D models of LAO and RAO projections. The 3D reconstruction is calculated from 2D projections in the three-dimensional space estimated from protocol data. Each data set representing a particular 3D reconstruction segment consists of a discrete set of vector triplets that represent the 3D coordinates of the segment centerline and the two radii R1 and R2 obtained from two projections. For a more detailed description of the 2-D models and the 3-D reconstruction procedures, please refer to [15, 16]. The accuracy of the used reconstruction software was tested and validated in phantom studies with well defined geometries and were described elsewhere [17]. The diameter and volume measurements in this model were performed by three-dimensional calipers (spheres and generalized cones). The resulting accuracy yields an error for diameters of <3%. The inter- and intra-observer variability is <5%. In these phantom studies a reconstruction procedure using elliptical cross-sections was applied.

There are two simplifications suggested by these considerations that speed up the reconstruction and circumvent the reconstruction problems with vector triplets representing degenerated ellipses and non-orthogonal (tilted) and unevenly spaced cross-sections. The first one is a reduction of the spatial resolution by using only every second vector triplet for interpolation. The cross-sections defined by the original vector triplets are tilted, because the radius vectors are not orthogonal to the longitudinal axis of the vessel. Thus neighboring cross-sections may intersect and unevenly spaced tilted cross-sections occur. The analysis of the 3000 cross-sections of the coronary artery represented in figure 2 left demonstrated that the mean angle between cross-section planes defined by vector triplets and longitudinal vessel axis was 90° ± 6.5° (SD). However, some cross-sections were angulated by less than 30°. A 3D caliper approach is necessary to construct cross-sections orthogonal to the longitudinal axis from the original vector triplets. As most of the cross-sections defined by vector triplets are nearly orthogonal, an approximate solution is to neglect one of two intersecting cross-sections or respective vector triplets. The axial resolution is only slightly reduced by this approach. The resulting models were defined as high fidelity models (HF). Two further resolution models were also studied – low fidelity models (LF) with a relative to HF models halved number of reconstructed cross-sections and double low fidelity model (DLF) with a relative to LF models halved number of cross-sections. The provided 3D reconstruction data defines only 4 points on the vessel cross-section. Interpolation algorithms are necessary to reconstruct surface and volume geometry and to construct a sufficiently fine grid of this vessel lumen for CFD study.

Although the biplane views were chosen orthogonal or near orthogonal, the radii are not orthogonal due to foreshortening. Vector triplets may even represent ellipses with high eccentricity. The data provides only an estimate of the real vascular eccentricity, however, since vessel foreshortening causes fake eccentricity. The analysis of the 3000 cross-sections reconstructed for the coronary artery presented in figure 2 left showed that the mean eccentricity of elliptical cross-sections, defined as the relationship between the two radii R1 and R2, was relatively small with 1.13 ± 0.34 (SD). The assumption of a circular lumen is supported by this data and data from IVUS studies that report the preservation of nearly circular lumina due to highly localized remodeling [12]. The second simplification is the assumption of a circular cross-section (Method 1) instead of an elliptic one (Method 2). These two methods proposed for cross-section reconstruction procedure are described in detail below:

Method 1 (circular lumen)

The radius R of the circles defining cross-sections was chosen as the geometric mean radius ($R = (R1 \cdot R2)^{1/2}$). In this case, the cross-sectional area of the resulting circle is equal

to the area of the ellipse where the major and minor axes equal to the two radii (R1 and R2). To convert data with original radii into the circular model the radii vectors R1 and R2 had to be scaled by factors R/R1 and R/R2 respectively. This calculation was done automatically using a macro written in MS Excel™. With the macro, obtained data is rewritten in a journal file format. This allows an automatic generation of all cross-section circles in 3-D-space with three defined points (center point and two points on the circle) by the software Gambit™ (Fluent Inc., Lebanon, USA). Figure 2 shows the resulting wire grid reconstructions of the coronary lumina. The resulting geometries were subsequently exported in commonly used IGES format.

Method 2 (elliptic lumen)

These vectors can be used directly as the axes of elliptic contours only in the case of orthogonality of two radius vectors. Otherwise, the shape of the ellipses is ambiguous due to a loss of spatial information. Ambiguity increases with a decreasing angle between the two radii. Three specific points are needed for an unambiguous definition of elliptic contours in 3-D space. The first point is the center of the ellipse. The second point together with first point must define the major axis of the ellipse, whereas the third point is located on the elliptical contour and does not coincide with the second point. Since both radius vectors were defined using the projection edges of vessel lumina, each may initially be considered as the major axis. If neither of both projections is orthogonal to the major axis of the real elliptic cross-section, then neither of the radius vectors represents the direction or length of the real major axis radius. The larger radius of R1 and R2 is the best approximation, however. For non-orthogonal radius vectors including an angle of less than 45°, a circular cross-section was assumed by Wahle et al. [15]. In this case, the procedure is the same as for Method 1 and was automatically performed using an MS Excel macro. Finally, a Gambit journal file was generated and exported in IGES file format.

The ultimate generation of endo-luminal surface and volume geometry from cross-sections defined in IGES file format was done with the CAD-program SolidWorks™ (Solidworks Inc., Concord, USA). The IGES files were imported into SolidWorks™. The volume of each segment was then generated by interpolation using the "Loft" tool in SolidWorks™ with the segment centerline as a guide line. Bifurcations were modeled by extrusion. The branch segment was extruded toward the parent segment starting from the first cross-section of the branch segment until the start of the branch segment was completely inside of the parent segment. Figure 3 shows an example of a complete coronary artery reconstructed according to Method 1.

The CFD study described in this paper was limited to the reconstruction of the right coronary artery without branches (see figure 4). In order to smooth the outlet geometry for CFD and to eliminate the influence of outlet boundary conditions, we generated an additional 10 mm long segment by extruding the last cross-section of the reconstructed vessel in the direction normal to itself.

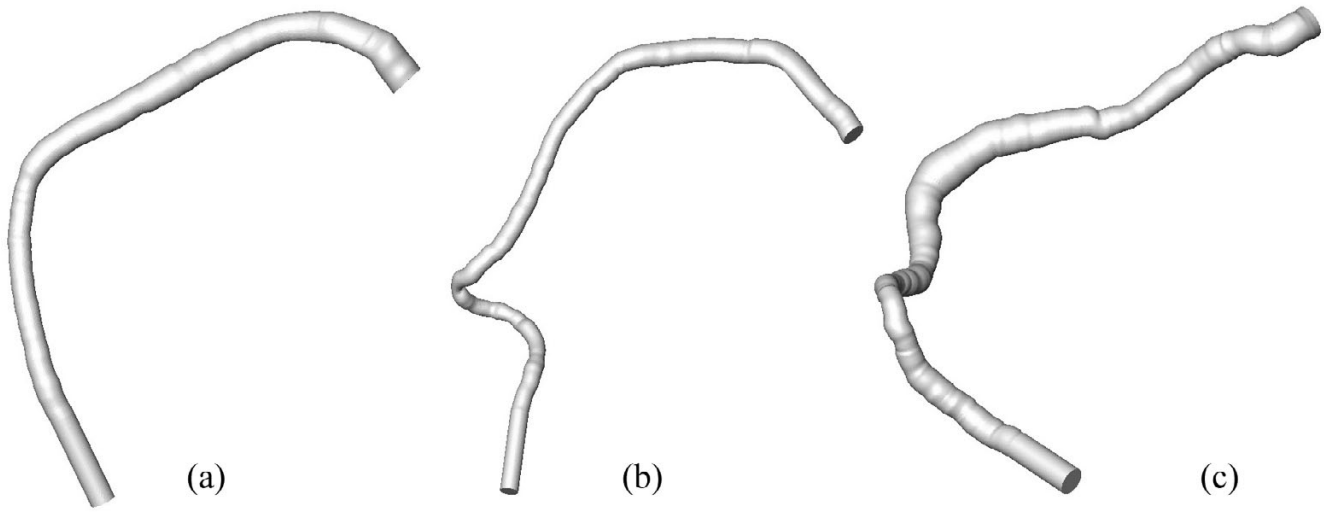

Figure 4
Endo-luminal surfaces of the three right coronary arteries reconstructed without branches: (a) – normal right coronary artery, (b) –, right coronary artery with "obstructive" atherosclerotic disease, and (c) – right coronary artery with "dilated" atherosclerotic disease. These geometries correspond to images shown in figure 1.

For the comparative study presented in this paper the following models were reconstructed: three HF models of three different coronary vessels with circular cross-sections, three HF models of three different coronary vessels with elliptical cross-sections, three LF models of three different coronary vessels with circular cross-sections and one DLF model of the normal coronary artery with a circular cross-section. Table 1 gives an overview of the main geometric parameters of the reconstructed segments.

Computational fluid dynamics

The numerical solution of steady Navier-Stokes equations for momentum and mass conservation governing fluid motion under defined boundary conditions were solved by a control volume finite element method (FEM) implemented in FLUENT 6 (Fluent Inc., Lebanon, USA). For finite element numerical simulation the vessel volume had to be represented by a mesh grid. This transformation of the volume data was done by Gambit (software). The surface of the vessel was triangulated with a node distance between 0.1 and 0.2 mm (1:20 of the mean diameter). Based on this surface mesh, a grid composed of tetrahedral elements was generated in the reconstructed vessels. The total number of nodes exceeded 50,000. The average number of elements per cross-section was 350. Recently, some detailed studies were performed regarding the mesh resolution required to appropriately simulate the blood flow in coronary arteries using finite element methods [18,19]. The authors found that a high mesh resolution near the walls was needed in order to get accurate values of WSS. Based on the results of these studies [19,20], we generated a mesh which was refined in the near wall region. A boundary layer consisting of 4 rows, with a growth factor of 1.2 (ratio between two consecutive layers near the wall) and a total depth of 0.2 mm, was generated (see figure 5). The quality of the generated mesh grid was assessed using different approaches. The maximal skew of their distribution was, for example, below 0.75, which is fully satisfactory. The resulting number of grid volume elements ranged between 270,000 and 390,000 for the different vessels. Stationary laminar flow was simulated presuming rigid motionless walls. A no-slip condition was assumed at the wall. The pressure value was not imposed at the outlet. Blood was modeled as a Newtonian fluid with a kinematic viscosity of $3.5\ 10^{-6}\ m^2/s$. A second order discretization scheme and a SIMPLE model for pressure flow coupling were used. A plug velocity profile was assumed at the inlet, because coronary arteries originate from a large compartment (sinus of the aortic root). The mean flow rate for each investigated vessel was estimated based on our flow rate measurements. These were recorded by the simultaneous measurement of pressure and velocity in these patients by a miniaturized ultrasound Doppler probe positioned within the coronary artery. The mean inlet velocities, 0.17 m/s for the normal patient, 0.27 m/s for the patient with "obstructive" coronary atherosclerosis and 0.09 m/s for the patient with "dilated" coronary atherosclerosis, were used, which resulted in the Reynolds numbers of 184, 228, and 117 respectively, for the three investigated geometries. The mass flows were 112.9 ml/min for the patient with a normal coronary artery, 111.8 ml/min for the patient with "obstructive" coronary artery disease and 88.5 ml/min for the patient with "dilated" coronary artery disease. The mass flows were calculated by multiplying the mean inlet velocity with the inlet cross-section areas obtained as the result of reconstructions. The smaller mass flow in the last patient is due to the smaller perfusion territory of the right coronary artery in this patient. The convergence criteria for relative errors in velocity components and pressure were set as 10^{-5}.

Statistics

In order to quantify the differences between the resulting WSS distributions, we generated distribution histograms. The whole range of calculated wall shear stress values was divided into 100 classes. For each class, the area corresponding to the WSS range was calculated and normalized as a percent of the total wall surface area. The sum of the calculated values from all classes was then equal to 100%. Cross-correlations and Chi-square tests were used to compare distribution histograms.

Results

Three different coronary vessels were reconstructed using two different reconstruction methods (I and II) with a higher resolution – HF models. The reconstruction method I (circular cross-sections) was also used to generate LF models for all three coronary arteries. A DLF model was generated for the normal coronary vessel. Altogether, 10 models of three different coronary vessels were studied. The analysis of the reconstructed models shows that the number of cross-sections used in generating the high fidelity (HF) models resulted in a rather fine resolution of

Table 1: Geometric parameters of the three reconstructed right coronary arteries. D stands for diameter.

Parameters	Volume, mm^3	Length, mm	Inlet D: mm	Outlet D: mm	Range of D: mm	Mean D: mm
"normal"	483	62	3.78	2.58	2.22 – 3.78	3.14
"stenosed"	413	94	2.97	2.19	1.78 – 2.97	2.36
"dilating"	1586	120	4.56	3.87	2.88 – 5.86	4.10

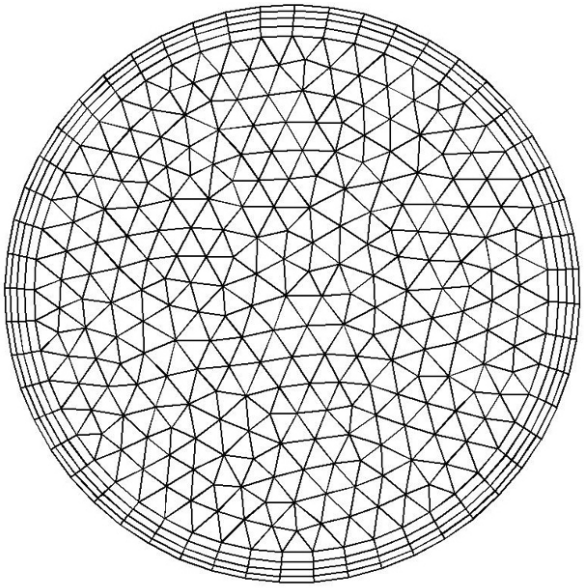

Figure 5
Grid in the inlet region of the right coronary model of the normal coronary artery.

about 0.3–0.4 mm. This equals the resolution of the original data obtained by a reconstruction of biplane angiograms with software developed at the DHZB (German Heart Institute of Berlin). The resolution of low fidelity (LF) models was about 0.8 mm. However, the comparison of volumes and surfaces between HF and LF models yields an error of <1%.

Steady numerical flow simulations of steady flow were done for the 10 reconstructed models of the three different coronary vessels. The corresponding distributions of WSS are visualized in figures 6, 7, and 8. The distributions of WSS for the reconstructions with high and low resolution appear identical.

Histogram curves were generated from calculated WSS distributions. The distribution curves agree well (see figures 9a, b and 9c), and demonstrate a strong cross-correlation (0.91 – 0.95) for each of the investigated three coronary arteries. In the Chi-square test for the comparison of histograms, no significant difference was found ($p = 0.995$).

The calculated pressure loss was slightly lower (2.5–8.5%) in LF models. Pressure drops strongly depended on the type of geometry (normal control: 6 mmHg, "obstructive" disease: 25.4 mmHg, or "dilated" disease: 1.83 mmHg).

The effect on the distribution of WSS, if a circular cross-section (Method 1) is assumed as opposed to an elliptic cross-section (Method 2), is also displayed in figures 6, 7, and 8. The comparison was performed for HF models. The distribution histograms shown in figures 9a, b and 9c are similar, and also demonstrate a high cross-correlation (0.87 – 0.94). Again, in the Chi-square test for the comparison of histograms, no significant difference was found ($p = 0.995$). The difference between the volumes was less than 0.017 ml (< 2%), the difference in wall area was less than 13 mm^2 (< 1%) and the pressure loss was slightly higher (3.6–5.3%) with the elliptical cross-sections in coronary artery disease. It should be noted that there are also some differences between the inlet diameters of models reconstructed with different methods (< 1.5 %). The differences between the outlet diameters of models reconstructed with different methods were even higher but remained below 5 %.

The three distinct varieties of coronary vessel geometry are characteristically reflected by the WSS histograms. The mean WSS was 4.6 Pa in the normal patient and the range was between 0 Pa and 10 Pa. The mean WSS was higher in the sample with "obstructive" atherosclerotic disease with 8.8 Pa, and had a wide range (0 Pa to 20 Pa). On the contrary, the mean WSS in the sample with "dilated" atherosclerotic disease was lower with 1.3 Pa, and had a rather narrow range (0 Pa to 6 Pa). However, the obtained WSS histogram curves also revealed characteristic shape differences (see figure 9d) which were shown by normalizing the WSS ranges. The histogram of the control patient is a symmetrically distributed curve with a single peak of WSS at 4 Pa that is nearly in the middle of the WSS range and is close to the mean value of 4.6 Pa (see figure 9a). These small differences between mean, median and peak values are also reflected in the low skew value for the histograms of the normal patient – 0.16. The histogram of the patient with "obstructive" atherosclerotic disease demonstrates an asymmetric distribution where the peak is at 5 Pa, which is located near to the peak seen in the histogram of the patient without coronary disease. However, there is a strong right-sided hump in the histogram curve (see figure 9b) which is assumed to correspond to stenotic parts of the vessel. This results in the rather large difference between peak (5 Pa), mean (8.8 Pa), and median (10 Pa) values of WSS. The asymmetry of the histogram curve of the patient with "obstructive" atherosclerotic disease is also reflected by a higher skew value – 0.7. The wide range of WSS values reflects multifocal disease and inhomogeneous remodeling. For the patient with "dilated" atherosclerotic disease, the histogram of WSS distribution is very asymmetric (one-sided), with the peak of WSS having shifted to low values at 0.9 Pa. This results in the strong difference between peak (0.9 Pa), mean (1.3 Pa) and median (3 Pa) values of WSS. The excessive asymmetry of the histogram curve of the patient with "dilated" atherosclerotic disease is reflected by a very high skew value –

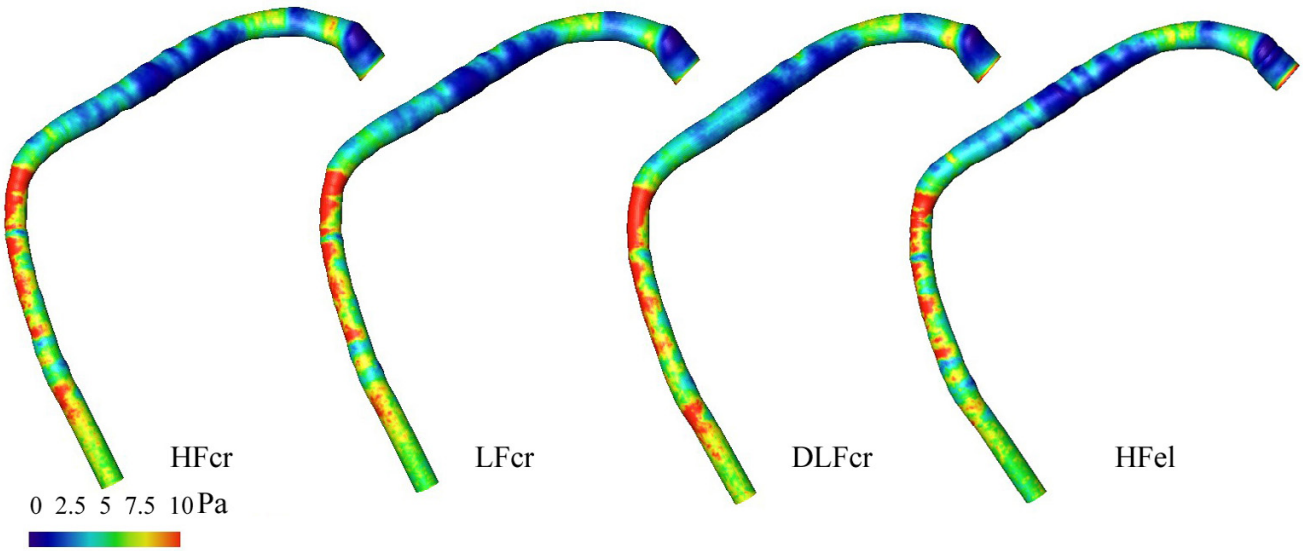

Figure 6
WSS distributions in the reconstructed normal coronary artery. From the left to the right: HF model reconstructed by Method 1, LF model reconstructed by Method 1, DLF model reconstructed by Method 1 and HF model reconstructed by Method 2 of the normal right coronary artery. The Reynolds number was Re = 184.

0.97. The confinement of WSS to a narrow range of low values means diffuse negative remodeling. It should be noted that the simplified reconstruction approaches had no impact on the shape differences of these curves.

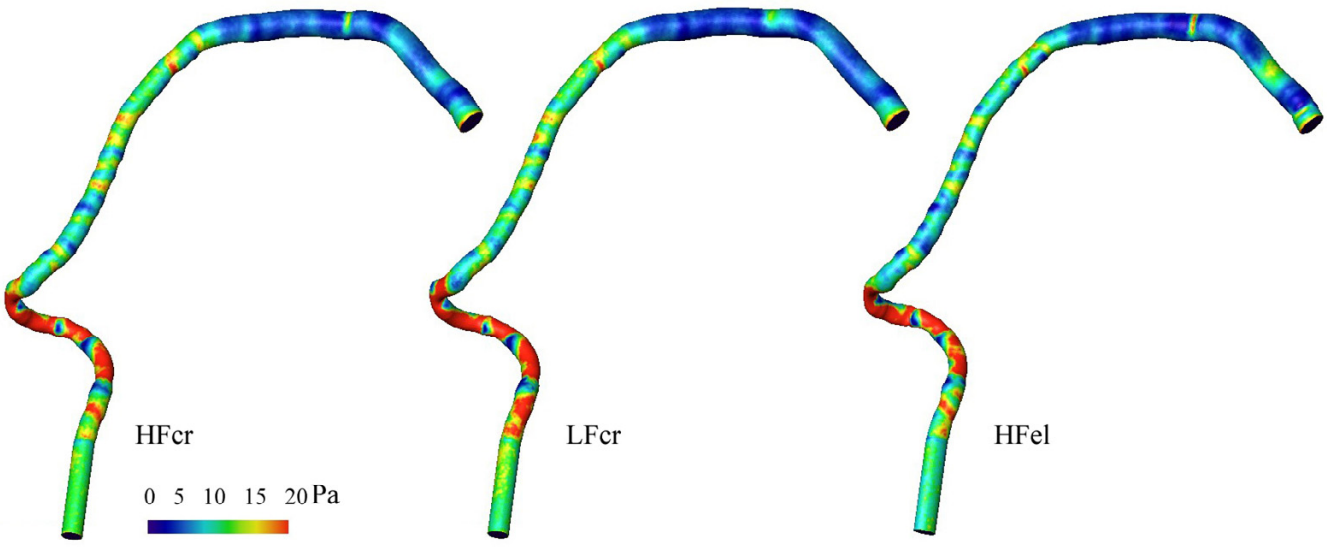

Figure 7
WSS distributions in the reconstructed right coronary artery with "obstructive" atherosclerotic disease. From the left to the right: HF model reconstructed by Method 1 (left), LF model reconstructed by Method 1 (middle), and HF model reconstructed by Method 2 (right) of the right coronary artery with "obstructive" atherosclerotic disease. The Reynolds number was Re = 228.

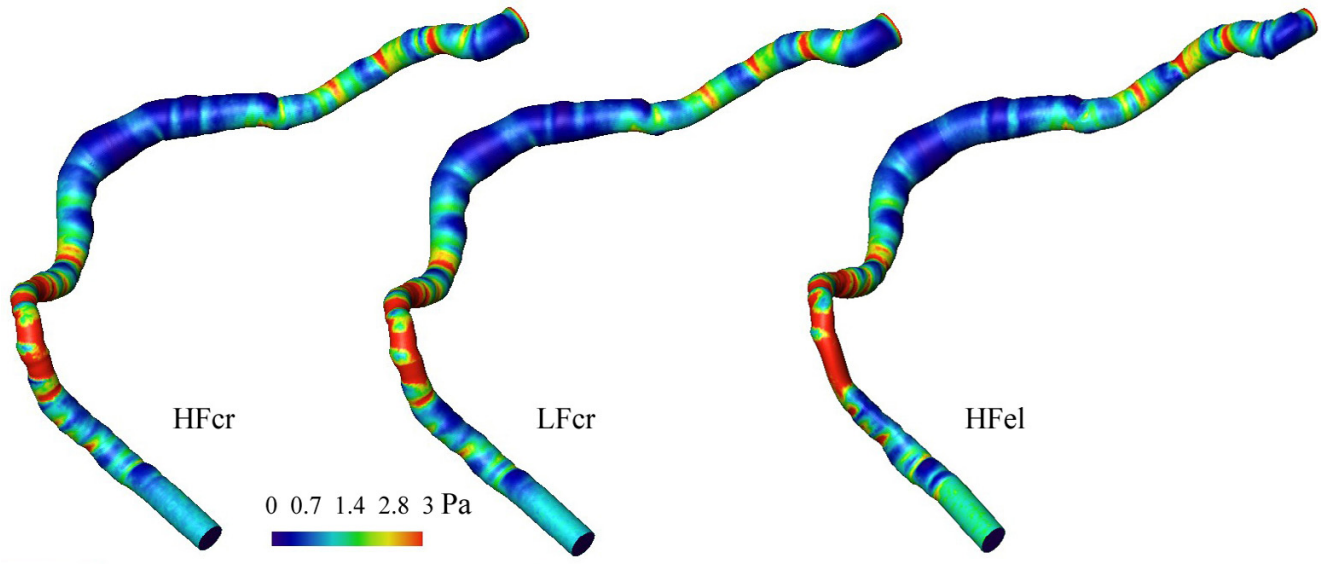

Figure 8
WSS distributions in the reconstructed right coronary artery with "dilated" atherosclerotic disease. From left to right: HF model reconstructed by Method 1 (left), LF model reconstructed by Method 1 (middle), and HF model reconstructed by Method 2 (right) of the right coronary artery with "dilated" atherosclerotic disease. The Reynolds number was Re = 117.

In order to quantify the effect of geometric simplifications on the local WSS distributions, we investigated the WSS distributions in the coronary artery of the normal patient, reconstructed by different methods, in more detail. A part of the wall surface of the normal patient coronary artery was divided by x-constant planes into 36 sections (see figure 10) for each of the three models (HF and LF models reconstructed with Method 1 and HF model reconstructed with Method 2). The distance between the planes was 1 mm. The mean WSS was calculated for each section. Figure 11 shows a comparison of the curves of the mean WSS values for different models along the x-axis (x-position). The difference in WSS values between HF and LF models (see figure 11b) reconstructed by Method 1, for all evaluated 36 sections, was 2.2% ± 1.7%. The maximal difference for one site was 6.6 %. The difference in WSS values between HF models reconstructed by Method 1 and Method 2 (see figure 11a) was 4.6% ± 5.3%. The maximal difference for one site was 14.3 %.

In order to assess the effect of further reduction of the spatial resolution of geometric reconstruction, we investigated the WSS distributions in the double low fidelity model (DLF) of the coronary artery of the normal patient reconstructed with Method 1. The mean distance between two cross-sections in this model was 1.6 mm. The comparison of volumes and surfaces between HF and DLF models yielded an error of about 1%. The corresponding distribution of WSS is visualized in figure 6. The distribution of WSS in the reconstructions with high and double low resolution appear identical in the proximal and middle parts of the coronary model. The differences in the distal part are more impressive. However, the distribution curves agree well (see figure 9a), and demonstrate a strong cross-correlation (0.93). In the Chi-square test for comparison of histograms, no significant difference was found ($p = 0.995$). The more detailed comparison of the local WSS values of the 36 vessel wall parts (middle part of the coronary artery) from the HF and DLF models revealed higher differences than between the HF and LF models reconstructed with Method 1 or than between the models reconstructed with Method 1 and Method 2. The difference in WSS values between HF and DLF models (see figure 11b) reconstructed by Method 1 for all 36 evaluated sections was 5.3% ± 5.2%. The maximal difference at any site was 26 %.

Discussion

Wall shear stress is the most important mechanical regulatory signal which links flow to adaptive changes of the vascular wall and atherosclerotic lesions [21]. Three-dimensional reconstruction of coronary artery segments, with subsequent numerical flow simulation studies based on individual patient data, are currently the standard approach to in vivo flow profiling and WSS measurements in coronary arteries [1-9]. The prognostic clinical value of this approach is supported by the results of two recent clinical serial studies [8,9]. We do not know

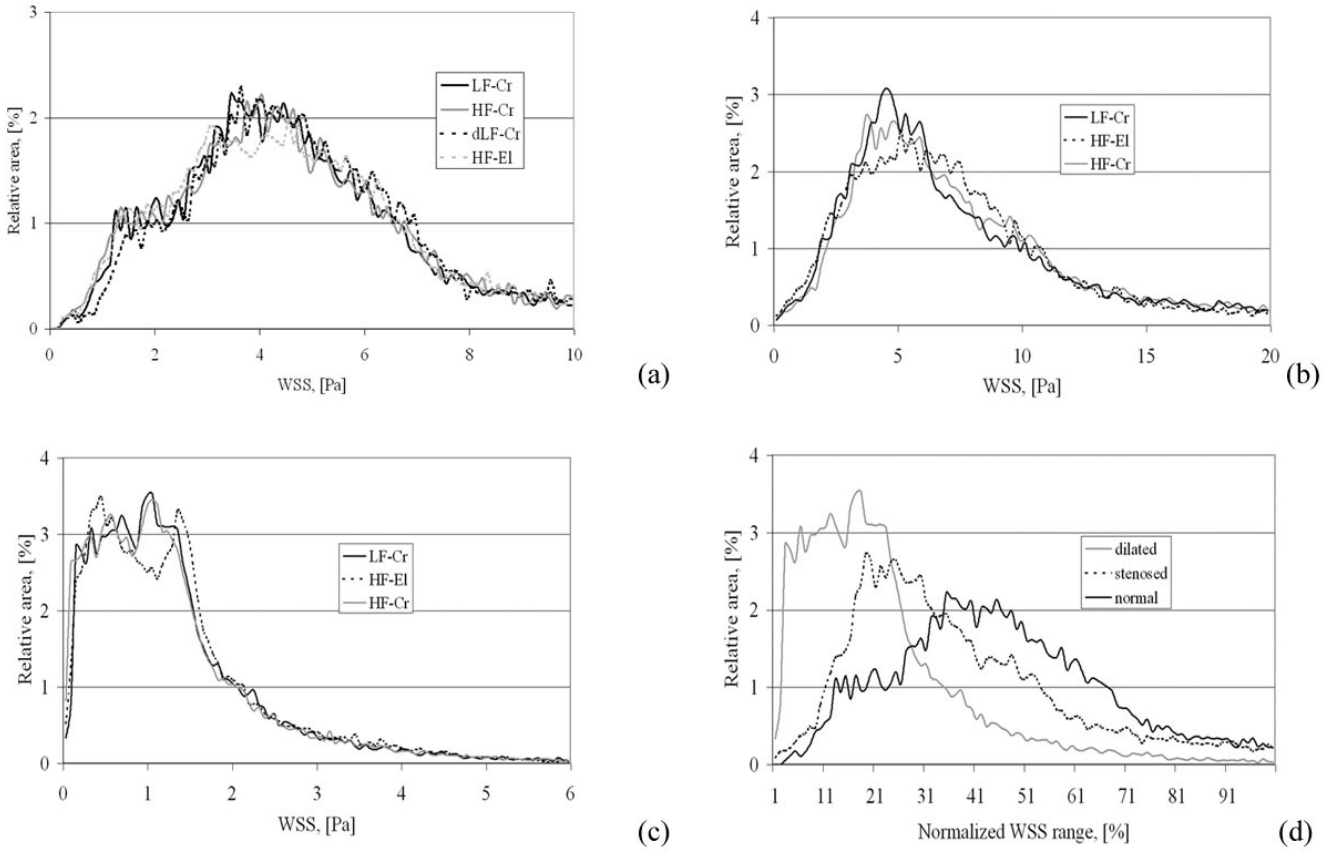

Figure 9
Images (a), (b) and (c) show histograms of the WSS distributions depicted in figures 6, 7 and 8 respectively. Image (d) shows a comparison of three histograms of the three different vessels with normalized WSS ranges for LF models reconstructed with Method 1. Cr stands for models with circular cross-sections. El stands for models with elliptic cross-sections.

whether the costs of the enhanced accuracy of the complex modeling approach to WSS estimation proposed in [8] translates into an additional clinical diagnostic impact as compared to the simplified approaches [9]. A calculation based on a simplified geometric reconstruction would be an important step beyond exemplary studies from bench to bedside. Moreover, routine catheterization data, which do not supply the high resolution circumferential data (e.g. by IVUS) necessary for the complex approach, should be sufficient for a simplified model with a lower resolution. We investigated the impact of two simplifications of the geometric reconstruction of 3-D vessel lumina on the accuracy of flow simulation in coronary arteries.

Using a LF model reduces the spatial resolution by a factor of two; however, it also reduces the time for the 3-D geometry reconstruction by nearly a factor of 3. This time saving results from the fact that reconstruction problems due to intersecting cross-sections are avoided. The low resolution (LF) model demonstrated a negligible impact on the vessel wall area and the WSS distribution as compared to the results for the HF model. The differences in pressure drops between the HF and LF model were small compared to the differences related to the type of geometry (normal, obstructive or dilated). The deviation of the distribution histograms, caused by the reduced resolution in the LF model, was not significant and small compared to the differences due to the type of geometry. Hence, the HF resolution neither improves the results nor adds additional clinical information. Consequently, LF models are preferred. The LF models smooth the surface geometry. As a result, some local information is lost that may be important. Since the difference between HF and LF models is equivalent to a reduction of the spatial resolution by a factor of two, we studied the impact on the accuracy of the local geometric variability (see figure 11) and found that a sufficient accuracy of reconstruction is preserved. The LF model has a mean distance of 0.8 mm between the two cross-sections used for reconstruction. This resolution of the vessel reconstruction along the vessel axis is of the same order as the slice thickness of the standard CT

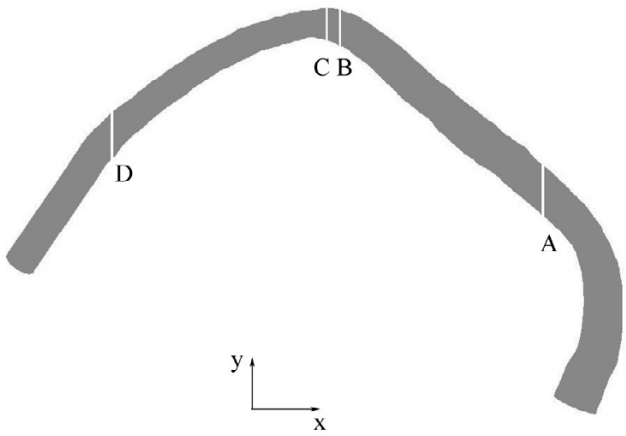

Figure 10
Normal coronary artery of the normal patient used for the analysis of the impact of evaluated simplifications on the local WSS distribution. The letter A marks the x position (x = 18 mm) of the first x-constant plane whereas the letter D marks the x position (x = -18 mm) of the last x-constant plane defining the region of the vessel wall used for the analysis of the local WSS distribution. Letters B and C mark two neighboring x-constant planes which define one of the 36 evaluated vessel wall parts.

devices and better than the resolution of IVUS and MRI imaging. Further reduction of the spatial resolution by a factor of four in the DLF model revealed a significant loss of local information about the WSS distribution.

The comparison of HF models of coronary arteries, reconstructed by Method 1 and Method 2, demonstrated only minor differences in the vessel wall area and the WSS distribution. The maximal error of the calculated pressure drop was 6.8 % for simulations in the coronary artery of the normal patient, which is much lower than the variability of the pressure drop in the different types of geometry. The deviations in the histograms of WSS were much larger between the three coronary arteries with a different geometry than the variability caused by the reconstruction method. On the other hand, the differences caused by the reconstruction method were higher than the differences caused by the reduction of model resolution. This is reflected by the lower cross-correlation coefficients (0.91–0.95) that were found by analyzing the effect of resolution and 0.87–0.94 that were found by analyzing the effect of the reconstruction method. One reason for the deviation of the pressure drop between different models of the same vessel is the use of hydraulic radii (radii calculated from the cross-sectional area) in the elliptical cross-sections with non-orthogonal radii. The geometric mean radius is equal to the hydraulic radius only if the radii are orthogonal. For example, the inlet diameters of the coronary models reconstructed with Method 1 were 3.78 mm in the coronary artery of the control patient, 2.96 mm in the coronary artery of the patient with "obstructive" disease and 4.54 mm in the coronary artery of the patient with "dilated" disease. The hydraulic diameters of the coronary models reconstructed with Method 2 were 3.73 mm, 2.97 mm, and 4.53 mm respectively. Note that a difference of 1% in the vessel radius causes a difference of about 2% in the pressure drop for the same inlet velocity. The second, and more important, reason for the differences in pressure

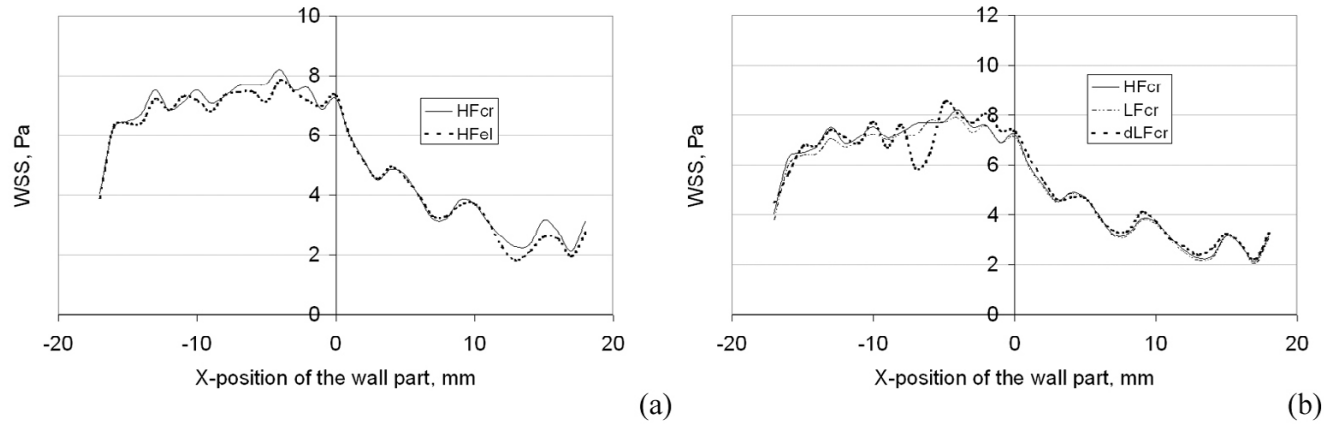

Figure 11
Comparison of the distribution of the WSS averaged over 36 local vessel wall sites for four of the models (the HF model reconstructed with Method 1 – HFcr; the LF model reconstructed with Method 1 – LFcr; the DLF model reconstructed with Method 1 – DLFcr and the HF model reconstructed with Method 2 – HFel) of the coronary artery of the control (normal) patient.

drop and WSS caused by reconstruction Method 2, as opposed to Method 1, are irregularities in the cross-sections reconstructed with Method 2. For non-orthogonal radius vectors including an angle of less than 45°, a circular cross-section was assumed by Wahle et al. without any interpolation or smoothing with respect to cross-sections in the neighborhood [15]. A circular cross-section, instead of an elliptic one, occurs in about 30% of all the cross-sections (3000 cross-sections were analyzed). These artificial wall irregularities cause artifactual local flow disturbances and WSS artifacts that are avoided by the smoother reconstruction technique (Method 1), which uses a circular shape for all reconstructed cross-sections. Thus, the use of Method 1 for geometry reconstruction should provide fewer artifacts, and hence, more accurate and realistic results from the CFD calculations. Furthermore, Method 1 is more suitable for further automatization of the reconstruction algorithm and may be implemented by macro programming in SolidWorks™. Last but not least, Method 1 reflects the physiology of luminal remodeling which is highly localized and preserves a circular lumen even in the majority of eccentric atherosclerotic lesions [12].

The problems of the geometry reconstruction using the software developed by DHZB (intersecting cross-sections and irregularities in cross-sections and therefore irregularities in the interpolated surface caused by the use of elliptical and circular shapes) are mainly due to the fact that the primary goal of the software was an assessment of the vessel diameters and volumes, and that a further use for numerical flow simulations was not considered at that stage. The above mentioned problems may be alternatively resolved by an algorithmic approach. However, this implies a time-consuming modification of the existing software. The proposed simplifications for studying WSS profiling in a coronary reconstruction, allows immediate and statistically relevant profiling in a larger sample of available data (about 60 coronary arteries).

Since the geometry is the main factor influencing the WSS distribution, it is important to consider the impact of neglecting branch flows. Surprisingly, it was shown that branch flows are of minor importance in determining WSS patterns in the trunk of the right coronary artery [18].

One of the important issues of WSS profiling is the validation of WSS profiling based on biplane angiograms. Unfortunately, we can not consider 3-D-IVUS as a gold standard for our method. None of these methods provides a direct measurement. IVUS provides a better resolution for an assessment of the vessel cross-section. However, the resolution is worse with regard to the reconstruction of geometry along the vessel axis in the main flow direction. Furthermore, IVUS is not suitable for studying complex vessel trees similar to the vessels shown in figure 2.

Further simplifications in our study concerned the numerical model. The momentum and mass conservation equations have to be solved under difficult boundary conditions in order to fully model the blood flow in arteries. All physiological parameters have to be accounted for, i.e. wall compliance, pulsatile flow, and non-Newtonian behavior of the blood. In addition, in a coronary artery, cardiac contraction induces a continuous, site specific motion and deformation of the vessel. All these aspects may affect flow patterns and were thoroughly studied in the last years [18,22-26]. The impact of the assumption of rigid or non-rigid arterial walls has been well investigated and discussed in the literature [22,23]. The authors of these studies agree that the assumption of a rigid wall is sufficiently accurate for WSS profiling in investigating atherosclerosis for clinical purposes. This judgment is based on their calculations with regard to reconstructions of the first bifurcation of the left coronary artery. However, these results are also valid for right coronary arteries, since there are no significant differences between these two arteries from a hemodynamic point of view (Reynolds and Strouhal numbers, Womersley parameter, pressure pulse wave and vessel thickness). Among the deformations of the coronary arteries due to cardiac surface motion, only torsion is assumed to have a small effect on local WSS. The effect of pulsatility was also found to be small and to have a limited effect on local WSS. No differences were found between steady-state calculations of the WSS distribution and time-averaged calculations over a whole heart cycle [18,26]. Average calculated Womersly parameters ($Wo = R(2\pi f/\nu)^{0.5}$, where R is the artery radius, f is the heart frequency and ν is the kinematic viscosity of blood) were found to be low in coronary arteries ($Wo = 3.05 \pm 1.00$, $N = 117$) due to the small radii of the coronary arteries (own unpublished results based on in-vivo coronary hemodynamic data and quantitative coronary angiography data acquired by cardiac catheterization). Since flow unsteadiness associated with pulsatility has a significant impact on the local WSS only, if $Wo >> 1$ (cut-off 5). Pulsatile flow modeling is not necessary in coronary arteries, if we study time-averaged WSS. The WSS distribution averaged over one heart cycle is considered as the main hemodynamic parameter that links flow to adaptive changes of the vascular wall and atherosclerotic lesions. There are other parameters, which are held to be important: e.g. temporal (WSSGt) and spatial WSS gradients (WSSG), and the oscillating WSS index (OSI) [18]. Many of the above-mentioned aspects (e.g. pulsatility, wall elasticity, non-Newtonian blood behavior), do apply for these parameters (OSI, WSSGt, WSSG). Last but not least, it should be noted that atherosclerotic wall alterations reduce wall elasticity and eventually lead to a rigid wall model.

The most interesting findings of this study are the differences between the WSS histogram curve shapes. These differences seem to be characteristic for these three different coronary arteries which represent three different entities of coronary pathology (normal patients, patients with "obstructive atherosclerosis" and patients with "dilated" atherosclerosis) and might have diagnostic value. However, further studies with a larger number of coronary arteries are necessary to assess the clinical value of these findings. Local information about WSS distribution may be smoothed by our approach. Such local information is thought to be very important for the study of the correlation between WSS distribution and the distribution of atherosclerotic wall alterations or intimal thickening. However, a low WSS value does not imply that wall alterations will necessarily be present at the corresponding site. The relation between WSS and biologic vascular response is modulated by many other factors. The assessment of this relation needs a probabilistic and multi-factorial approach. We know that clinically symptomatic coronary atherosclerosis usually shows a multimodal, or even diffuse distribution, and demonstrates distinct varieties of positive or negative remodeling associated with different geometries. According to the statistical principle of stratified sampling, extreme varieties of coronary geometries were selected to identify characteristic features of the impact of global geometry on flow and WSS. A characteristic global parameter is mean WSS. The mean WSS may be estimated from the mean vessel radius R and the mean velocity V as $\tau = \mu(4\ V/R)$ (Eq. 1), where μ is the dynamic blood viscosity. Using this equation, the mean WSS may be calculated as 1.49 Pa for the coronary of the normal patient, 2.95 Pa for the coronary from the patient with "obstructive" atherosclerotic disease and 0.6 Pa for the coronary from the patient with "dilated" atherosclerotic disease. The average WSS values calculated from the CFD results are 4.6 Pa, 8.8 Pa and 1.3 Pa respectively. Thus a simplified approach based on the mean radius and mean velocity results in significantly lower values of WSS as compared to values based on the CFD calculations. Moreover, the information of the WSS histograms on scatter, distribution, skew, and peak values of WSS provides quantitative information on the diffuseness, the inhomogeneity and the progress of the atherosclerotic disease and the extent and type of associated remodeling as reflected by the resultant luminal geometry. It should be emphasized that the histograms obtained from the CFD solution characterize a very complex flow pattern, including flow separations and flow recirculations caused by the vessel curvature and local narrowings or enlargements. Such histograms cannot be obtained by a simplified approach as the calculation of WSS for each reconstructed cross-sectional volume slice is based on the Hagen-Poiseuille equation (Eq. 1). Furthermore, the WSS estimation, by using the Hagen-Poiseuille equation, is not able to predict the existence of the wall areas with low wall shear stress values ($\tau < 0.5$ Pa), as it is done by the CFD results. These values are included in our histograms. These low WSS values are very important for our study, since they correlate with the loss of endothelial function and WSS responsiveness [13,28].

The distinct differences in the distribution of WSS values obtained from histograms may help to distinguish between, and assess the severity of, different coronary artery diseases. Further analysis is currently being performed in our 3-D coronary database consisting of right and left coronary arteries from 6 control patients, 10 patients with "obstructive" atherosclerotic disease, and 8 patients with "dilated" atherosclerotic disease.

There were a lot of investigations which considered the problem of reconstruction procedure on the accuracy of the numerical flow simulation in vessels, and especially for coronary arteries [18,20,22]. The novel aspects of the presented study are the following: we used a non-dimensional allometry approach (WSS histogram curve) to characterize and compare WSS in different coronary arteries, we studied the impact of two reconstruction simplifications on wall shear stress characterization using the WSS histogram curve, we used circular instead of elliptical cross-sections, and we used a reduced number of cross-sections for volume reconstruction. The study was applied to three different right coronary arteries representing three different geometries of this vessel: a right coronary artery of a control patient, a right coronary of a patient with "obstructive" atherosclerotic disease and a right coronary of a patient with "dilated" atherosclerotic disease. The study of three different vessels allowed us to show that the proposed simplifications are not significant for the differentiation of these coronary arteries by the proposed method.

As we mentioned above, there are no significant differences between right and left coronary arteries from a hemodynamic point of view. Hence, the results obtained in this study with right coronary arteries should also be valid for studies with left coronary arteries.

Conclusion

A simplified approach to the reconstruction of coronary vessel lumina from biplane angiograms, by assuming circular cross-sections and using only every second vector triplet of the original data with the mean distance of 0.8 mm between cross-sections, yields sufficiently accurate calculations of vessel volumes, surfaces, wall shear stress distributions, and pressure drops. The resolution of 0.8 mm is accurate enough for the global (histogram) and local characterization of the wall shear stress in coronary arteries. This is valid also for other geometry reconstruction meth-

ods (3-D-IVUS or magnet resonance imaging). Lower resolution results in non significant deviations for the global characterization parameter of the WSS and in significant local alterations in WSS calculations. The issue, which remains to be validated, is: May we use biplane angiograms for WSS profiling? A final decision on this subject requires a study with a phantom of a real coronary artery, for which an exact computer model exists. This study is under way in our group.

Profiles of WSS within whole segments or vessels might identify different patterns of remodeling associated with characteristic changes in the distribution of WSS and quantify the extent and diffuseness of coronary artery disease. However, this issue needs further investigation in a larger number of patients with different coronary geometries in each group (controls, "obstructive" and "dilated" coronary atherosclerosis).

Competing interests

The author(s) declare that they have no competing interests.

Authors' contributions

Dr. Wellnhofer from German Heart Institute of Berlin performed biplane patient angiograms and velocity measurements with a miniaturized ultrasound Doppler probe. He is also one of the developers of the reconstruction software. Dr. Goubergrits developed the reconstruction software further that allowed performing a volume reconstruction, which may be used for numerical simulations with a CFD code. He performed also the numerical simulations with CFD code FLUENT and proposed the analysis of the WSS distributions by the WSS histograms. Dr. Kertzscher was involved in the statistical analysis of the obtained results. Prof. Dr. Affeld is a supervisor of the project and was also involved in the analysis and the discussion of the obtained results.

Acknowledgements

The authors gratefully acknowledge the German Research Foundation for the financial support of this project (Grant DFG GO 1067/2-1). The Authors wish to express their thanks to the Carolyn Christensen for her assistance in preparing of this paper.

References

1. Bom N, de Korte CL, Wentzel JJ, Krams R, Carlier SG, van der Steen AW, Slager CJ, Roelandt JR: **Quantification of plaque volume, shear stress on the endothelium, and mechanical properties of the arterial wall with intravascular ultrasound imaging.** *Z Kardiol* 2000, **89(Suppl 2):**105-111.
2. Goubergrits L, Affeld K, Wellnhofer E, Zurbrugg R, Holmer T: **Estimation of wall shear stress in bypass grafts with computational fluid dynamics method.** *Int J Artif Organs* 2001, **24:**145-151.
3. Hoffmann KR, Wahle A, Pellot-Barakat C, Sklansky J, Sonka M: **Biplane X-ray angiograms, intravascular ultrasound, and 3D visualization of coronary vessels.** *Int J Card Imaging* 1999, **15:**495-512.
4. Ilegbusi OJ, Hu Z, Nesto R, Waxman S, Cyganski D, Kilian J, Stone PH, Feldman CL: **Determination of Blood Flow and Endothelial Shear Stress in Human Coronary Artery in Vivo.** *J Invasive Cardiol* 1999, **11:**667-674.
5. Krams R, Wentzel JJ, Oomen JA, Vinke R, Schuurbiers JC, de Feyter PJ, Serruys PW, Slager CJ: **Evaluation of endothelial shear stress and 3D geometry as factors determining the development of atherosclerosis and remodeling in human coronary arteries in vivo. Combining 3D reconstruction from angiography and IVUS with computational fluid dynamics.** *Arterioscler Thromb Vasc Biol* 1997, **17:**2061-2065.
6. Stone PH, Coskun AU, Yeghiazarians Y, Kinlay S, Popma JJ, Kuntz RE, Feldman CL: **Prediction of sites of coronary atherosclerosis progression: In vivo profiling of endothelial shear stress, lumen, and outer vessel wall characteristics to predict vascular behavior.** *Curr Opin Cardiol* 2003, **18:**458-470.
7. Feldman CL, Ilegbusi OJ, Hu Z, Nesto R, Waxman S, Stone PH: **Determination of in vivo velocity and endothelial shear stress patterns with phasic flow in human coronary arteries: a methodology to predict progression of coronary atherosclerosis.** *Am Heart J* 2002, **143:**931-939.
8. Stone PH, Coskun AU, Kinlay S, Clark ME, Sonka M, Wahle A, Ilegbusi OJ, Yeghiazarians Y, Popma JJ, Orav J, Kuntz RE, Feldman CL: **Effect of endothelial shear stress on the progression of coronary artery disease, vascular remodeling, and in-stent restenosis in humans: in vivo 6-month follow-up studym.** *Circulation* 2003, **108:**438-444.
9. Wellnhofer E, Bocksch W, Hiemann N, Dandel M, Klimek W, Hetzer R, Fleck E: **Shear stress and vascular remodeling: study of cardiac allograft coronary artery disease as a model of diffuse atherosclerosis.** *J Heart Lung Transp* 2002, **21:**405-416.
10. Glagov S, Weisenberg E, Zarins CK, Stankunavicius R, Kolettis GJ: **Compensatory enlargement of human atherosclerotic coronary arteries.** *N Engl J Med* 1987, **316:**1371-1375.
11. Hirose M, Kobayashi Y, Mintz GS, Moussa I, Mehran R, Lansky AJ, Dangas G, Kreps EM, Collins MB, Stone GW, Colombo A, Leon MB, Moses JW: **Correlation of coronary arterial remodeling determined by intravascular ultrasound with angiographic diameter reduction of 20% to 60%.** *Am J Card* 2003, **92:**141-145.
12. Berglund H, Luo H, Nishioka T, Fishbein MC, Eigler NL, Tabak SW, Siegel RJ: **Highly localized Arterial remodeling in Patients with coronary atherosclerosis – An intravascular ultrasound study.** *Circulation* 1997, **96:**1470-1476.
13. Wentzel J, Janssen E, Vos J, Schuurbiers JC, Krams R, Serruys PW, de Feyter PJ, Slager CJ: **Extension of increased atherosclerotic wall thickness into high shear stress regions is associated with loss of compensatory remodeling.** *Circul* 2003, **108:**17-23.
14. Schoenhagen P, Ziada KM, Vince DG, Nissen SE, Tuzcu EM: **Arterial remodeling and coronary artery disease: the concept of "dilated" versus "obstructive" coronary atherosclerosis.** *J Am Coll Cardiol* 2001, **38:**297-306.
15. Beier J, Oswald H, Fleck E: **Edge detection for coronary angiograms: Error correction and impact of derivatives.** In *IEEE Comput Cardiol* Venice, IT; 1991:513-516.
16. Wahle A, Oswald H, Fleck E: **A new 3-D attributed data model for archiving and interchanging of coronary vessel systems.** In *IEEE Comput Cardiol* London; 1993:603-606.
17. Wellnhofer E, Wahle A, Mugaragu I, Gross J, Oswald H, Fleck E: **Validation of an accurate method for 3-D reconstruction and quantitative assessment of volumes, lengths and diameters of coronary vascular branches and segments from biplane angiographic projections.** *Int J Card Imag* 1999, **15:**339-353.
18. Myers JG, Moore JA, Ojha M, Johnston KW, Ethier CR: **Factors influencing blood flow patterns in the human right coronary artery.** *Annals of Biomedical Engineering* 2001, **29:**109-120.
19. Prakash S, Ethier CR: **Requirements for mesh resolution in 3-D computational hemodynamics.** *Journal of Biomedical Engineering* 2001, **123:**26-38.
20. Berthier B, Bouzerar R, Legallais C: **Blood flow patterns in an anatomically realistic coronary vessel: influence of three different reconstruction methods.** *Journal of Biomechanics* 2002, **35:**1347-1356.
21. Cunningham KS, Gotlieb AI: **The role of shear stress in the pathogenesis of atherosclerosis.** *Lab Invest* 2004. advance online publication, 29.11.2004
22. Perktold K, Hofer M, Rappitsch G, Loew M, Kuban BD, Friedman MH: **Validated computation of physiologic flow in a realistic coronary artery branch.** *J Biomech* 1998, **31:**217-228.

23. Perktold K, Kenner Th: **Flow and stress characteristics in rigid walled and compliant carotid artery bifurcation models.** In *Medical-Biological Engineering-Computing* Graz, Austria; 1993:1-20.
24. Moore JEJ, Guggenheim N, Delfino A, Doriot PA, Dorsaz PA, Rutishauser W, Meister JJ: **Preliminary analysis of the effects of blood vessel movement on blood flow patterns in the coronary arteries.** *J Biomech Eng* 1994, **116:**302-306.
25. Perktold K, Resch M, Florian H: **Pulsatile non-Newtonian flow characteristics in a three-dimensional human carotid bifurcation model.** *Biomechanical Engineering* 1991, **113:**464-475.
26. LaDisa JF, Olsona LE, Gulere I, Hettricka DA, Kerstenb JR, Warltiera DC, Pagela PS: **Circumferential vascular deformation after stent implantation alters wall shear stress evaluated with time-dependent 3D computational fluid dynamics models.** *J Appl Physiol* 2005, **98(3):**947-957.
27. Feldman CL, Coskun AU, Yeghiazarians Y, Kinlay S, Wahle A, Olszewski ME, Rossen JD, Sonka M, Popma JJ, Orav J, Kuntz RE, Stone PH: **Remodeling characteristics of minimally diseased coronary arteries are consistent along the length of the artery.** *Am J Cardio* 2006, **97:**13-16.
28. Malek A, Alper S, Izumo S: **Hemodynamic shear stress and its role in atherosclerosis.** *JAMA* 1999, **282:**2035-42.

2.2.3 Novel non-dimensional approach to comparison of wall shear stress distributions in coronary arteries of different groups of patients

Nach diesen Vorarbeiten erfolgte wie bereits bei der 3-D-Rekonstruktion eine Arbeit zum klinischen Anwendungspotential.

Die absolute WSS hängt stark von der Größe der Flüsse ab, die ihrerseits eine Funktion des absoluten Gefäßquerschnitts und der absoluten Geschwindigkeit sind. Dies verbietet einen direkten Vergleich der Wandschubspannung bei unterschiedlichen Patienten, wo große Unterschiede dieser Parameter erwartet werden müssen. Aufgrund der Variabilität der Koronaranatomie ist eine lokale Zuordnung der Wandschubspannung im Patientenvergleich nur äußerst grob, z. B. bezogen auf ganze Segmente der Herzkranzgefäße möglich. Die dimensionslose Charakterisierung hat sich in der Strömungslehre (z. B. Reynoldszahl) und in der Medizin (z. B. Auswurffraktion) als sehr effektive und effiziente Methode zur Lösung solcher Skalierungsprobleme erwiesen. Jedenfalls muss ein Ansatz gewählt werden, bei dem mehrere Parameter so in Beziehung gesetzt werden, dass eine reine Größenskalierungsänderung per se zu keiner Änderung der Bewertung führt.

Ziel war somit eine mehr oder weniger skaleninvariante Charakterisierung der strömungsbedingten Auswirkungen der Gefäßgeometrie auf die Strömungsfelder.

Methodik:

Mindestens je 5 rechte Koronararterien von drei Patientengruppen wurden untersucht:

- Patienten ohne koronare Herzerkrankung,
- Patienten mit normaler Koronaratherosklerose (stenosierende Gefäße),
- Patienten mit aneurysmatischer (Gefäßerweiterung) Koronaratherosklerose.

Der Einfluss unterschiedlicher Größen der Einlaufströmung auf die dimensionslosen Verteilungsfunktionen wurde in Extremstichproben analysiert.

Zur Unterscheidung der Gruppen wurden dimensionslose Verteilungsfunktionen der WSS und weitere statistische Methoden (z. B. Diskriminanzanalyse) benutzt. Im Übrigen wurde die Methodik aus der vorangegangenen Validierungsarbeit benutzt (123).

Ergebnisse:

- Der Einfluss unterschiedlicher Größen der Einlaufströmung auf die dimensionslosen Verteilungsfunktionen in Extremstichproben war gering.
- Eine Unterscheidung der Gruppen gelang mit einer Diskriminanzfunktion fast vollständig (eine falsche Klassifikation). Der Trennung der Angiogramme von KHE-Patienten mit Negativremodeling von den Kontrollen ist allerdings deutlich schlechter als die Abgrenzung der Angiogramme von Patienten mit aneurysmatischer Koronaratherosklerose.

Schlussfolgerung

Diese Charakterisierung könnte unabhängig von lokalen Stenosen eine erweiterte Definition der koronaren Herzerkrankung erlauben, die insbesondere zur Erkennung und Einordnung früher Verlaufsstadien oder diffuser Verlaufsformen der koronaren Herzerkrankung ohne stärkere Veränderungen im Luminogramm und ihrer potentiellen Verläufe beitragen könnte.

ELSEVIER

Atherosclerosis 202 (2009) 483–490

ATHEROSCLEROSIS

www.elsevier.com/locate/atherosclerosis

Novel non-dimensional approach to comparison of wall shear stress distributions in coronary arteries of different groups of patients

E. Wellnhofer[a,*,1], L. Goubergrits[b,1], U. Kertzscher[b], K. Affeld[b], E. Fleck[a]

[a] *German Heart Institute of Berlin, Berlin, Germany*

[b] *Biofluid Mechanics Laboratory, Charité-Universitätsmedizin Berlin, Berlin, Germany*

Received 8 February 2008; received in revised form 6 May 2008; accepted 19 May 2008

Available online 9 July 2008

Abstract

Background: Local wall shear stress (WSS) has an impact on local remodelling of the vessel wall. WSS in turn strongly depends on local geometry. Our aim was to characterize patterns of local wall shear stress associated with distinct types of remodelling in coronary arteries. Vessel size and flow rates are different between patients, however. To compare distribution patterns of WSS in analogy to fluid-dynamic modelling, non-dimensional WSS/area functions are calculated.

Methods: Right coronary arteries from seven controls, five patients with coronary artery disease (CAD) and five patients with aneurysmatic CAD (AnCAD) were analyzed. Flow simulations were performed in three-dimensionally reconstructed coronary vessels from biplane angiographic projections. Local WSS was normalized as percentage of maximum value in a histogram (100 classes) and corresponding area was expressed as percentage of total area.

Results: The normalized WSS distribution was characterized by a single peak with a large lower tie in controls, a loss of the single peak and a stochastic distribution in AnCAD and a narrowing of the lower tie in CAD. Correct classification of 16/17 coronary arteries was feasible by Fisher's discriminant functions based on median WSS, mean diameter, percentage of area with WSS ≤ 0.4 Pa and with WSS ≥ 15 Pa.

Conclusion: Normalized WSS distribution might be an efficient tool in comparing wall shear stress between different patient groups. Whether normalized WSS distribution curves are apt to grade severity of disease remains to be investigated.

Keywords: Coronary artery; Image-based flow modelling; 3D vessel reconstruction; Wall shear stress; Computational fluid dynamics

1. Introduction

Coronary artery disease (CAD) is confirmed by local obstructions in selective angiograms (luminograms). The luminal contour is the net result of the encroachment of plaque into the vascular lumen and compensatory remodelling [1]. Luminal geometry and flow determine wall shear stress (WSS). WSS is the most important mechanical regulatory signal that links flow to adaptive changes of the vascular wall and atherosclerotic lesions [2,3].

Three-dimensional (3D) reconstruction of coronary artery segments with subsequent numerical flow simulation studies based on individual patient data are currently the standard approach to flow and WSS profiling in coronary arteries [4–8]. Such studies were very cumbersome in the past and thus restricted to single specimens, models or small study samples. Most of these studies were performed by combining angiography and intravascular ultrasound (IVUS). IVUS provides some additional local accuracy and the measurement of wall thickness. Though wall thickness is an important parameter in assessing atherosclerosis it has no direct impact on the calculation of WSS. Recently, we evaluated a simplified approach to 3D-modelling of the geometry of coronary arteries based on angiograms only [9] that allows retrospective studies in angiographic data-bases. The method may be used with 3D-data from different (fast) reconstruction algorithms,

* Corresponding author at: German Heart Institute of Berlin, Internal Medicine/Cardiology, Augustenburger Platz 1, Berlin 13353, Germany. Tel.: +49 174 9677265; fax: +49 30 45932500.

E-mail address: Ewellnhofer@t-online.de (E. Wellnhofer).

[1] These authors equally contributed to the work.

0021-9150/$ – see front matter © 2008 Elsevier Ireland Ltd. All rights reserved.
doi:10.1016/j.atherosclerosis.2008.05.044

e.g. CAAS 5.2™ (Pie Medical Imaging BV, Maastricht, The Netherlands). Improvements in imaging modalities provide alternative non-invasive data sources [10–13].

There are principal problems in evaluating WSS studies, however. Although a point-to-point comparison of WSS within serial studies of patients may be achieved by meticulous matching, a point-to point comparison of WSS between different individuals or groups of patients is not feasible altogether, due to gross differences in size and geometry of coronary arteries and coronary flow. Similarity modelling and the use of non-dimensional parameters is an approach to treat such problems. The Reynold's number is a famous example from fluid-mechanics and the ejection fraction was a success in cardiology. There are two quantities that have to be normalized: WSS and the luminal vessel area. This paper presents a first evaluation of this novel approach to characterize remodelling in a sample of 17 right coronary arteries with 3 different geometries: controls, aneurysmatic disease (AnCAD) [14], and CAD with negative remodelling.

2. Methods

2.1. Data and patients

We used previously (1990–1994) reconstructed 3D-data sets of right coronary arteries from digitized biplane routine angiograms. All patients had a history of angina at moderate or slight exertion, had been catheterized because of suspected or known coronary artery disease, and had signed informed consent prior to the procedure. Since the study is a retrospective data analysis, the approval of an institutional review committee was not required.

The selection was based on clinical diagnosis and quality of angiograms assessed by experienced cardiologists. Representative 3D-reconstructions are given in Fig. 1. The box-plot of mean diameters calculated from vessel length and vessel volume within the groups (left bottom) suggests a sufficiently correct clinical separation of aneurysmatic disease from CAD and controls.

Controls are seven patients (four female, age 52 ± 17 years, height 165 ± 8 cm, weight 75 ± 15 kg, ejection fraction >60%). Three patients had 3, two patients had 2 and only one patient had no cardiovascular risk factors. All had normal coronary morphology, but three had functional abnormalities indicating vasospastic angina (ergonovine test).

The CAD group includes five patients (one female, age 50 ± 10 years, height 176 ± 15 cm, weight 89 ± 11 kg, ejection fraction 53 ± 7%). One patient had 2, one 3, one 2 and two had no cardiovascular risk factors. All but one patient with two-vessel disease suffered from three-vessel disease. Maximal local area obstruction in the right coronary artery was about 75%.

The group of aneurysmatic CAD comprises five patients (one female, age 58 ± 14 years, height 175 ± 6 cm, weight 101 ± 8 kg, ejection fraction 48 ± 10%). Two patients presented with 2, and the rest with 3 cardiovascular risk factors. Three patients had three-vessel disease, one two- and one one-vessel disease. Maximal local area obstruction in the right coronary artery was less than 75%.

2.2. Three-dimensional reconstruction

Biplane angiograms (25 frames/s) had been acquired on cine-film by a standard biplane angiographic X-ray device (Philips DCI-System) during end diastole. Rotation and angulations of the C-arms, distances of image intensifiers to X-ray sources and size of image intensifiers had been recorded. These protocol data were used to estimate the three-dimensional (3D) geometry. A two-dimensional (2D) model was reconstructed for each projection by a combination of interactive topology marking and automatic vessel detection.

Vessel bifurcations were manually identified and used for both segmentation and vessel detection. Two-dimensional data is organized in segments consisting of coordinates of centreline and related radii, defining both edge points of the vessel projection for the corresponding 2D models of LAO and RAO projections. The 3D-reconstruction is calculated from 2D-projections in the three-dimensional space estimated from protocol data. Each data set representing a particular 3D reconstruction segment consists of a discrete set of vector triplets that represent the 3D coordinates of the segment centreline and the two radii $R1$ and $R2$ obtained from two projections [15]. The accuracy of the used reconstruction software was tested and validated in phantom studies with well-defined geometries and clinical studies [16]. The resulting accuracy yields an error for diameters of <3%. The inter- and intra-observer variability is <5%. The resolution of the 3D-reconstruction along the vessel axis based on the original data is 0.2 mm.

Two simplifications were introduced to improve the efficiency of 3D surface generation from these data: a reduction of the spatial resolution by using only every second vector triplet for interpolation (resolution along the vessel axis: 0.4 mm) and the assumption of a circular cross-section instead of an elliptic one. The radius R of the cross-sectional circles was chosen as the geometric mean radius ($R = (R1R2)^{1/2}$). Both simplifications speed up the reconstruction and circumvent the reconstruction problems with vector triplets representing degenerated ellipses and non-orthogonal (tilted) and unevenly spaced cross-sections. The difference in the calculated vessel volumes is lower than 1%. The difference of calculated pressure loss is between 2.5% and 8.5%. There is no significant impact on WSS [9].

Obtained data is rewritten in a journal file format with a macro written in MS Excel™. In this way all cross-section circles in 3D-space are generated from three defined points (centre point and two points on the circle)

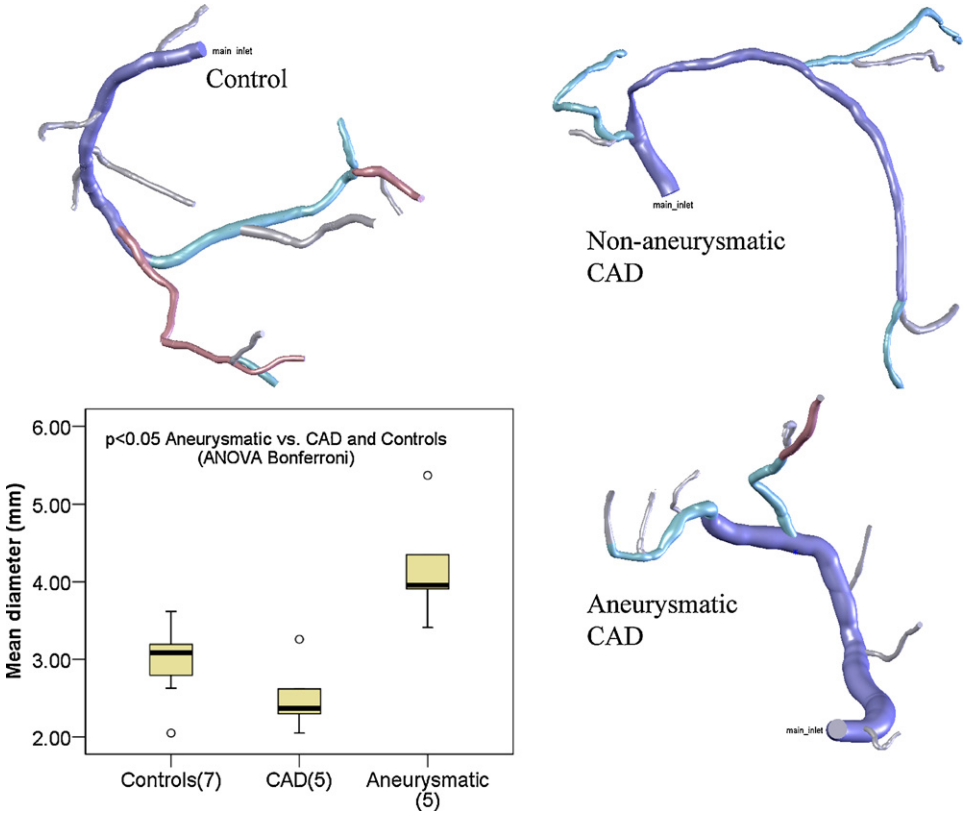

Fig. 1. Representative specimens of reconstructed coronary arteries. A group comparison for mean diameters is presented on bottom left as box-plot (median, 75%, 95% confidence and outliers).

by the software Gambit™ (ANSYS-Fluent Inc., Lebanon, USA). The resulting geometries are subsequently exported in IGES format. The ultimate generation of endo-luminal surface and volume geometry from cross-sections defined in IGES file format is done with the CAD-program SolidWorks™ (Solidworks Inc., Concord, USA). The IGES files are imported into SolidWorks™. The volume of each segment is subsequently calculated by interpolation using the "Loft" tool in SolidWorks™ along the segment centreline.

This computational fluid dynamics (CFD) study was limited to the reconstruction of the right coronary artery without branches. In order to smooth the outlet geometry for CFD and to eliminate the influence of outlet boundary conditions, we generated an additional 10-mm long segment by extruding the last cross-section of the reconstructed vessel in the normal direction. The reconstructed geometries were used for mesh generation and numerical flow modelling. The main geometric parameters of the reconstructed segments for controls/CAD/aneurysmatic CAD were the inlet diameters 3.6 ± 0.8 mm/3.3 ± 0.6 mm/4.1 ± 1.1 mm, the length of the investigated segment 117 ± 21 mm/128 ± 13 mm/122 ± 28 mm and the mean segment diameter 3.0 ± 0.5 mm/2.5 ± 0.5 mm/4.0 ± 1.0 mm derived from the length and the calculated volume of the vessel segment $855 \pm 370\,mm^3$/$669 \pm 306\,mm^3$/$1647 \pm 912\,mm^3$.

2.3. Computational fluid dynamics

Steady flow Navier–Stokes equations for momentum and mass conservation were solved by a control volume finite element method implemented in FLUENT 6 (ANSYS-Fluent Inc., Lebanon, USA). Calculation of local WSS is an integral part of the software based on partial differentiation of local velocity near wall perpendicular to the corresponding surface element (WSS = μ(∂(velocity)/∂(↓ surface). For finite element numerical simulation the vessel volume was transformed to a mesh grid using the software Gambit™(ANSYS-Fluent Inc., Lebanon, USA). The surface of the vessel was triangulated with a node distance between 0.1 mm and 0.2 mm or 0.05 mm of the segment mean diameter. Based on this surface mesh, a grid composed of tetrahedral elements was generated in the reconstructed vessels (total number of nodes >50,000). The average number of elements per cross-section was 350. Recently, some detailed studies assessed the mesh resolution required to appropriately simulate the blood flow in coronary arteries using finite element methods [17–19]. Based on these studies the authors performed own experiments with an anatomically realistic model of the coronary artery. Four different meshes with and without boundary layer mesh were investigated. The number of cells varied between 460,000 and 1,300,000. A high mesh resolution near the walls was needed for accurate val-

ues of WSS. Thus the mesh was refined in the near-wall region. A boundary layer consisting of four rows of prisms, with a growth factor of 1.2 (ratio between two consecutive layers near the wall) was generated. With such a mesh the error is below 3.5% for velocity calculations and below 5.1% for WSS calculations. The resulting number of grid volume elements ranged between 300,000 and 1,400,000. Stationary laminar flow was simulated presuming rigid motionless walls. A no-slip condition was assumed at the wall. The pressure value was not imposed at the outlet. Blood was modelled as a Newtonian fluid with a kinematic viscosity of 3.5×10^{-6} m^2/s. A second order discretization scheme and a SIMPLEC model for pressure-flow coupling were used. The convergence criteria for relative errors in velocity components and pressure were set as 2×10^{-5}. Further reduction of the convergence criteria results in a difference <1%. A plug velocity profile was assumed at the inlet, because coronary arteries originate from a large compartment (sinus Valsalvae of the aortic root). The mean flow rate for each investigated coronary artery group was derived from intravascular flow velocity measurements in these patients [20]. The mean inlet velocities used were 0.17 m/s for controls, 0.27 m/s for CAD and 0.09 m/s for aneurysmatic CAD. The mass flows, 108 ± 47 ml/s (controls), 139 ± 48 ml/s (CAD), and 75 ± 36 ml/s (aneurysmatic CAD) (p = n.s.), were calculated by multiplying the mean inlet velocity with the inlet cross-section areas obtained as the result of reconstructions. The corresponding Reynold's numbers were 175 ± 39 (controls), 252 ± 48 (CAD), and 105 ± 28 (aneurysmatic CAD) ($p < 0.01$).

2.4. WSS profiling

We generated non-dimensional distribution histograms to characterize the differences between the resulting WSS distributions. The whole range of calculated WSS values was divided into 100 classes. For each class, the area corresponding to the WSS range was calculated as the percentage of the total wall surface area subject to the corresponding WSS. The impact of variations in coronary flow on these normalized histograms was evaluated in two coronaries (see Fig. 2). As expected there is no relevant change in the histograms. Moreover, we evaluated the percentage of luminal area exposed to WSS ≤ 0.4 Pa, WSS ≥ 1.5 Pa, and WSS ≥ 15 Pa.

2.5. Statistics

Continuous variables are described by mean $\pm$ S.D. (standard deviation) or displayed as box-plots with median and 75% and 95% ranges. Group differences were assessed by ANOVA with Bonferroni correction and a Kruskal–Wallis test. Significance was assumed at $p \leq 0.05$. A Kolmogoroff–Smirnov test was performed to assess deviations from a normal distribution. A discriminant analysis was performed by the statistical package SPSS^{TM} V.12).

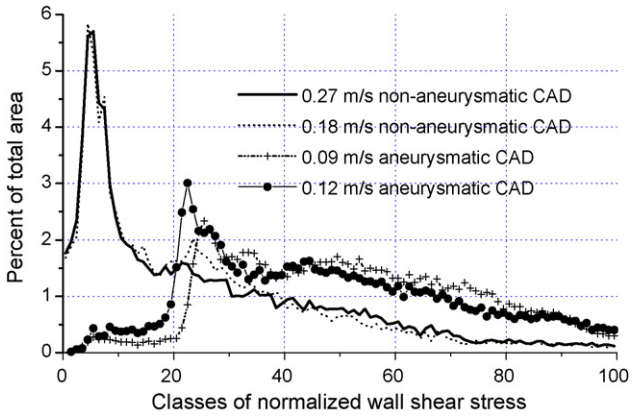

Fig. 2. The impact of variations in coronary flow on two normalized histograms.

3. Results

3.1. WSS

Representative WSS distributions are displayed as colour code models in Fig. 3. Aneurysmatic disease is characterized by the lowest range of mean WSS (less than 1.03 Pa in example and <2 Pa in all specimens). On the contrary mean WSS in the obstructive disease sample ranges from 4.5 up to 10 Pa (19.5 Pa outlier). A group comparison with medians, percentiles and outliers is given in the box-plot (see Fig. 3).

3.2. Normalized WSS distributions

Individual and mean distributions (bold) are presented in Fig. 4. Control curves (top left) show a single flat peak at classes 20–30 with a slow ascent and a decaying descent. Obstructive CAD curves (top right) demonstrate a single acute peak at classes <10 with a sharp ascent and a rapidly decaying descent. The tallest peak corresponds to the RCA with severe diffuse obstruction displayed in Figs. 1 and 3 on top right. Aneurysmatic CAD curves (bottom right) show multiple small peaks between classes 10 and 50. The distribution is not significantly different from a normal (stochastic) distribution in four/five cases in contrast to the other groups. The curve with the extremely flat distribution in the range of classes 1–20 corresponds to the example of aneurysmatic disease at the bottom right in Figs. 1 and 3. We evaluated the percentage of luminal area exposed to WSS ≤ 0.4 Pa, WSS ≥ 1.5 Pa, and WSS ≥ 15 Pa (bar graph at bottom left of Fig. 4). Aneurysmatic CAD is characterized by a large area exposed to low WSS, whereas CAD demonstrates a trend to an increased area exposed to strongly elevated WSS.

3.3. Discriminant analysis

A discriminant analysis (Fig. 5) was performed. There was only one misclassification. The angiogram of the CAD

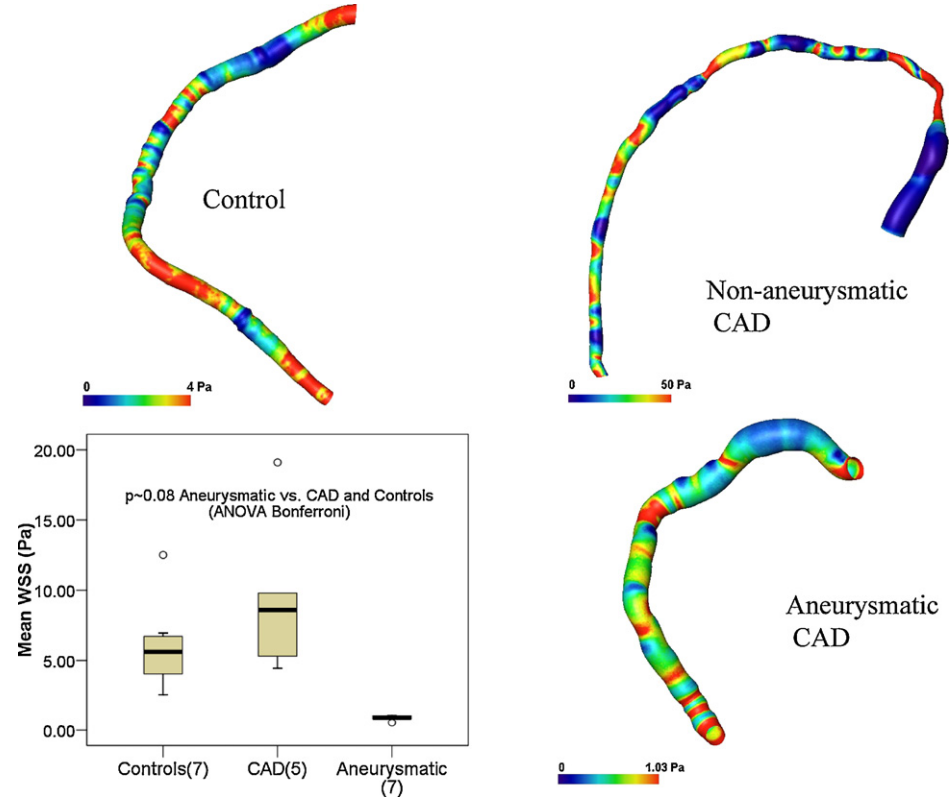

Fig. 3. Representative WSS results are displayed as colour code models. In the box-plot on bottom left a group comparison of median WSS values is given (median, 75%, 95% confidence and outliers).

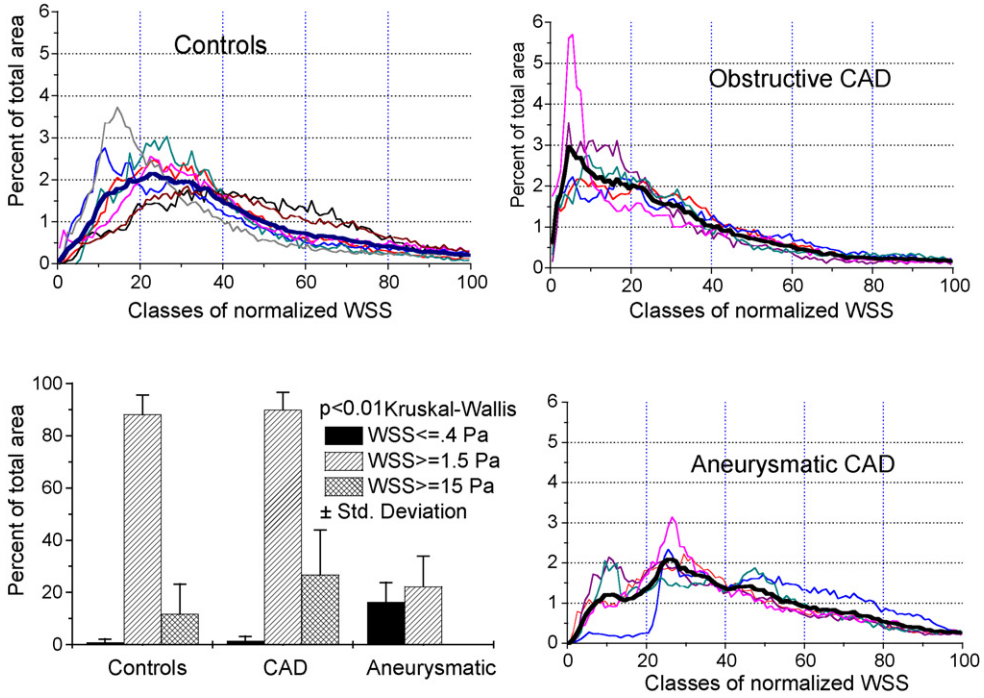

Fig. 4. Individual and mean distributions (bold) of normalized WSS. A group comparison of percentage of luminal area exposed to WSS $\leq$0.4 Pa, WSS $\geq$1.5 Pa, and WSS $\geq$15 Pa is given in the bar graph on bottom left.

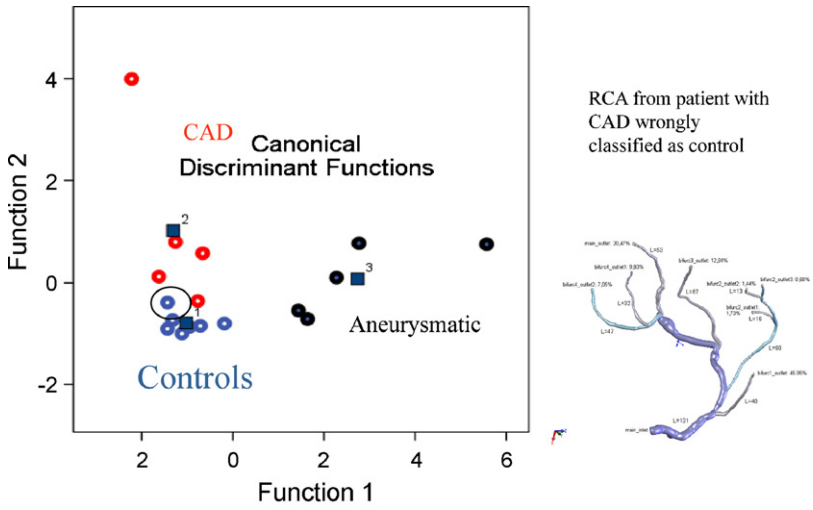

Fig. 5. Plot and standardized discriminant functions for discriminant analysis with median WSS (WSSm), mean diameter (*D*), percentage of area with WSS ≤0.4 Pa($WSS_{\leq 0.4}$), and WSS ≥15 Pa ($WSS_{\geq 15}$).

patient misclassified as control is depicted in Fig. 5 and is marked by a circle in the discrimination plot.

4. Discussion

A large body of evidence demonstrates the influence of WSS on vascular endothelial cells as well as on vascular smooth muscle cells resulting in as different events as flow mediated vasodilatation, atherosclerosis, thrombus formation and vascular remodelling [2,3]. Low WSS values are known to stimulate a pro-atherogenic endothelial phenotype, whereas moderate WSS induces endothelial quiescence and an athero-protective gene expression profile [2,8]. This is a first evaluation of a novel approach for inter-individual comparison of WSS distributions.

A whole vessel approach not restricted to segments was adopted in this study. This is based on the hypothesis that vascular remodelling is intrinsically related to atherosclerotic inflammation and affects environments at multiple sites rather than localized foci. Thus profiles of WSS might identify different patterns of remodelling associated with characteristic changes in the distribution of WSS. Positive remodelling was found to be related to endothelial dysfunction combined with active inflammation and/or early plaque [21,22]. The normalized WSS distribution of aneurysmatic disease is associated with the loss of the single peak and stochastic distribution. This might reflect a dispersion of the set-point in wall shear stress dependent remodelling. Moreover, a severe increase in the relative area exposed to WSS <0.4 Pa is found. In patients with obstructive disease a loss in the low range of the normalized distribution is combined with an increase of the area exposed to WSS >15 Pa. This observation might be explained by a loss of remodelling reserve or functional endothelium [23].

4.1. Selection of groups

As WSS only depends on luminal geometry irrespective of wall thickness remodelling is crucial for this parameter. Positive as well as negative remodelling deviating from simply compensatory changes have opposite impact on this parameter. The concept of “dilated” versus “obstructive” coronary atherosclerosis was introduced by Schoenhagen et al. [1]. We expand his concept on atherosclerotic coronary ectasia (“dilated”) and non-ectatic coronary artery disease (“obstructive”).

4.2. Limitations of the study

The inlet flow was about 30% higher in obstructive disease and 30% lower in aneurysmatic disease as compared to controls (p = n.s.), whereas the length as indicator of the size of the artery and its perfusion bed [24,25] was similar in all three groups. The inlet flow was calculated from geometry and previous peak flow-velocity measurements with a Doppler flow-wire [20]. The ratio of peak velocity/mean velocity may be elevated in a narrow artery with parabolic or skewed profile and decreased in a wide artery with flat profile.

The adopted geometric model simplifications have no significant impact on normalized WSS-distribution as shown in a previous methodological evaluation. The difference in WSS values due to assumption of a circular vessel geometry was 4.6 ± 5.3% (maximal 14.3% at one site) [9].

The momentum and mass conservation equations would have to be solved under difficult boundary conditions in order to fully model the blood flow in arteries. Wall com-

pliance, pulsatile flow, and non-Newtonian behaviour of the blood would have to be accounted for. In addition, cardiac contraction induces a continuous, site-specific motion and deformation of the coronary vessel. The impact of these boundary conditions on flow pattern was thoroughly investigated in prior studies [18,26–30]. The assumption of a rigid wall is sufficiently accurate for WSS profiling for clinical purposes [27]. Moreover, atherosclerosis reduces wall elasticity and eventually leads to a rigid wall model. No differences were found between steady-state calculations of the WSS distribution and time-averaged calculations over a whole heart cycle [18]. The effect of pulsatility was found to be small and to have a limited effect on local WSS. Average calculated Womersley numbers ($Wo = R(2\pi f/\nu)^{0.5}$, where R is the artery radius, f is the heart frequency and ν is the kinematic viscosity of blood) were found to be low in coronary arteries ($Wo = 3.05 \pm 1.00$, $N = 117$) due to the small radii (own unpublished data based on in vivo intra-coronary measurements, QCA and blood analysis). Since flow unsteadiness associated with pulsatility has a significant impact on the local WSS only, if $Wo \gg 1$ (cut-off 5) pulsatile flow modelling is not necessary in coronary arteries to study time-averaged WSS. Cyclic torsion and curvature changes have a limited effect on local WSS [18,26,30]. Cyclic deformations of the right coronary artery are small as the vessel is situated in the atrio-ventricular groove [28]. A potential chronic effect even of insignificant differences in local WSS on local remodelling over decades may not be completely excluded, but, is beyond the scope of this study. In obstructive disease with local stenosis, flow may be disturbed or even turbulent. But the maximal local area obstruction in this study was about 75%. Reynold's numbers were 617 ± 464 in coronaries with $62 \pm 12\%$ area obstruction (own unpublished data based on in vivo intra-coronary measurements, QCA and blood analysis). Thus, fully developed turbulence may not be expected. In case of turbulence WSS would be increased and the chaotic nature of turbulence implies a loss of WSS direction thus providing endothelial cells with ambiguous signals.

Studies that link hemodynamics with atherogenesis should replicate the patient-specific coronary geometry [18].

4.3. Assessment of results and perspectives

Obstructive and aneurysmatic CAD may be differentiated from controls by normalized and semi-normalized WSS distribution parameters, median WSS and mean diameter. The distribution curves (histograms) seem to reflect the severity of disease. The examples of severe remodelling deviations in Figs. 1 and 3 had the most abnormal distribution within their group. But this hypothesis remains to be tested, e.g. in a serial study.

An important investigation currently under way is the evaluation of the impact of integrating side branches into the flow study.

New commercially available software, e.g. CAAS 5.2™, allows efficient generation of 3D-data for coronary arteries and prospective investigations in larger patient groups will become feasible in future. Recent advances in imaging technology (rotational angiography, CT and MRI) provide non-invasive sources of geometric data for flow-simulation studies in future [10,12,13]. Last not least improvements in software and hardware will speed up flow-simulation studies.

Funding source: The study was supported by the German Research Foundation (G 01067/2-2).

Appendix A. Supplementary data

Supplementary data associated with this article can be found, in the online version, at doi:10.1016/j.atherosclerosis.2008.05.044.

References

[1] Schoenhagen P, Ziada KM, Vince DG, Nissen SE, Tuzcu EM. Arterial remodelling and coronary artery disease: the concept of "dilated" versus "obstructive" coronary atherosclerosis. J Am Coll Cardiol 2001;38:297–306.

[2] Chatzizisis YS, Coskun AU, Jonas M, Edelman ER, Feldman CL, Stone PH. Role of endothelial shear stress in the natural history of coronary atherosclerosis and vascular remodelling: molecular, cellular, and vascular behavior. J Am Coll Cardiol 2007;49:2379–93.

[3] Cunningham KS, Gotlieb AI. The role of shear stress in the pathogenesis of atherosclerosis. Lab Invest 2005;85:9–23.

[4] Coskun AU, Yeghiazarians Y, Kinlay S, et al. Reproducibility of coronary lumen, plaque, and vessel wall reconstruction and of endothelial shear stress measurements in vivo in humans. Catheter Cardiovasc Interv 2003;60:67–78.

[5] Goubergrits L, Affeld K, Wellnhofer E, ZurbruggR, Holmer T. Estimation of wall shear stress in bypass grafts with computational fluid dynamics method. Int J Artif Organs 2001;24:145–51.

[6] Lee BK, Kwon HM, Hong BK, et al. Hemodynamic effects on atherosclerosis-prone coronary artery: wall shear stress/rate distribution and impedance phase angle in coronary and aortic circulation. Yonsei Med J 2001;42:375–83.

[7] Stone PH, Coskun AU, Yeghiazarians Y, et al. Prediction of sites of coronary atherosclerosis progression: in vivo profiling of endothelial shear stress, lumen, and outer vessel wall characteristics to predict vascular behavior. Curr Opin Cardiol 2003;18:458–70.

[8] Stone PH, Coskun AU, Kinlay S, et al. Regions of low endothelial shear stress are the sites where coronary plaque progresses and vascular remodelling occurs in humans: an in vivo serial study. Eur Heart J 2007;28:705–10.

[9] Wellnhofer E, Goubergrits L, Kertzscher U, Affeld K. In vivo coronary flow profiling based on biplane angiograms: influence of geometric simplifications on the three-dimensional reconstruction and wall shear stress calculation. Biomed Eng Online 2006;5(39):39.

[10] Cademartiri F, Palumbo AA, Maffei E, et al. Non invasive imaging of coronary arteries with 64-slice CT and 1.5T MRI: challenging invasive techniques. Acta Biomed 2007;78:6–15.

[11] de Feyter PJ, Meijboom WB, Weustink A, et al. Spiral multislice computed tomography coronary angiography: a current status report. Clin Cardiol 2007;30:437–42.

[12] Jahnke C, Paetsch I, Nehrke K, et al. Rapid and complete coronary arterial tree visualization with magnetic resonance imaging: feasibility and diagnostic performance. Eur Heart J 2005.

[13] Goubergrits L, Kertzscher U, Schoneberg B, Wellnhofer E, Petz C, Hege HC. CFD analysis in an anatomically realistic coronary artery model based on non-invasive 3D imaging: comparison of magnetic resonance imaging with computed tomography. Int J Cardiovasc Imaging 2007.
[14] Hartnell GG, Parnell BM, Pridie RB. Coronary artery ectasia. Its prevalence and clinical significance in 4993 patients. Br Heart J 1985;54:392–5.
[15] Wahle A, Wellnhofer E, Mugaragu I, Sauer HU, Oswald H, Fleck E. Assessment of diffuse coronary artery disease by quantitative analysis of coronary morphology based upon 3D reconstruction from biplane angiograms. IEEE Trans Med Imaging 1995;14:230–41.
[16] Wellnhofer E, Wahle A, Mugaragu I, Gross J, Oswald H, Fleck E. Validation of an accurate method for three-dimensional reconstruction and quantitative assessment of volumes, lengths and diameters of coronary vascular branches and segments from biplane angiographic projections. Int J Cardiovasc Imaging 1999;15:339–53.
[17] Berthier B, Bouzerar R, Legallais C. Blood flow patterns in an anatomically realistic coronary vessel: influence of three different reconstruction methods. J Biomech 2002;35:1347–56.
[18] Myers JG, Moore JA, Ojha M, Johnston KW, Ethier CR. Factors influencing blood flow patterns in the human right coronary artery. Ann Biomed Eng 2001;29:109–20.
[19] Prakash S, Ethier CR. Requirements for mesh resolution in 3D computational hemodynamics. J Biomech Eng 2001;123:134–44.
[20] Doucette JW, Corl PD, Payne HM, et al. Validation of a Doppler guide wire for intravascular measurement of coronary artery flow velocity. Circulation 1992;85:1899–911.
[21] Lerman A, Cannan CR, Higano SH, Nishimura RA, Holmes DRJ. Coronary vascular remodelling in association with endothelial dysfunction. Am J Cardiol 1998;81:1105–9.
[22] Saihara K, Hamasaki S, Okui H, et al. Association of coronary shear stress with endothelial function and vascular remodelling in patients with normal or mildly diseased coronary arteries. Coronary Artery Dis 2006;17:401–7.
[23] Wentzel JJ, Janssen E, Vos J, et al. Extension of increased atherosclerotic wall thickness into high shear stress regions is associated with loss of compensatory remodelling. Circulation 2003;108:17–23.
[24] Halmann M, Sideman S, Lessick J, Beyar R. Relating coronary perfusion to myocardial function using three-dimensional reconstruction of heart and coronary arteries. Med Biol Eng Comput 1994;32:S144–50.
[25] Seiler C, Kirkeeide RL, Gould KL. Basic structure-function relations of the epicardial coronary vascular tree. Basis of quantitative coronary arteriography for diffuse coronary artery disease. Circulation 1992;85:1987–2003.
[26] Prosi M, Perktold K, Ding Z, Friedman MH. Influence of curvature dynamics on pulsatile coronary artery flow in a realistic bifurcation model. J Biomech 2004;37:1767–75.
[27] Perktold K, Hofer M, Rappitsch G, Loew M, Kuban BD, Friedman MH. Validated computation of physiologic flow in a realistic coronary artery branch. J Biomech 1998;31:217–28.
[28] Liao R, Chen SY, Messenger JC, Groves BM, Burchenal JE, Carroll JD. Four-dimensional analysis of cyclic changes in coronary artery shape. Catheter Cardiovasc Interv 2002;55:344–54.
[29] LaDisa Jr JF, Olson LE, Douglas HA, Warltier DC, Kersten JR, Pagel PS. Alterations in regional vascular geometry produced by theoretical stent implantation influence distributions of wall shear stress: analysis of a curved coronary artery using 3D computational fluid dynamics modelling. Biomed Eng Online 2006;5(40):40.
[30] Zeng D, Ding Z, Friedman MH, Ethier CR. Effects of cardiac motion on right coronary artery hemodynamics. Ann Biomed Eng 2003;31:420–9.

3. Diskussion

3.1. Simulation und Transfer von Strömungssimulationen in Koronargefäßen aus der Wissenschaft in die klinische Diagnostik

Mit wachsenden technischen Möglichkeiten werden Simulation und virtuelle diagnostische Modelle weiter in die medizinische Diagnostik und Therapie, aber auch in die wissenschaftliche Methodik vordringen (200). Die Entwicklung der medizinischen Bildgebung und der Computertechnik erlauben einen Transfer aufwändiger und anspruchsvoller Modellbildungs- und Simulationstechniken aus der Forschung in die Klinik (54;110;144;150;152;154;174).

Dies gilt insbesondere für die Simulation des „Risikofaktors" Blutströmung in den Koronargefäßen. Umfassende Forschung belegt die Wirkung der Wandschubspannung auf Endothelzellen und glatte Muskelzellen und ihre mittelbare Rolle in den Prozessen der flussabhängigen Vasodilatation, des (mal)adaptiven Gefäßumbaus der Atherosklerose und der Bildung von Thromben. Insbesondere niedrige und oszillierende Wandschubspannungen sind ein pro-atherogener Risikofaktor, wohingegen physiologische Strömung protektiv wirkt (8;21;24;25;33;43-46;50;51;56;60;62;63;74;114;201-210).

Durch Kontraktion und Füllung kommt es notwendigerweise zu erheblichen Volumenschwankungen des Herzens, die ihrerseits mit zyklischen Verkleinerungen und Vergrößerungen der epikardialen Oberfläche verbunden sind. Die Herzkranzgefäße verlaufen deshalb in Bögen und Gegenbögen, um diese Bewegungen auszugleichen. Diese Krümmungen verursachen eine hohe Komplexität der Strömung in den Koronargefäßen, so dass einfache Modelle basierend auf geraden Rohren (Hagen-Poiseuille Strömung) nicht oder nur sehr bedingt anwendbar sind. Eigene Vergleiche von Schätzungen der WSS mittels der Hagen-Poiseuille Formel aus mittleren Geschwindigkeiten und Durchmessern und Berechnungen aus Strömungssimulationen zeigten erheblich niedrigere WSS bei Schätzung nach Hagen-Poiseuille, wobei allerdings relative Gruppenunterschiede erhalten bleiben. Der Hauptvorzug der Schätzung nach Hagen- Poiseulle ist, dass sie ohne 3-D Rekonstruktion, Gittererstellung und Strömungssimulation durchführbar ist. Der Ansatz wurde deshalb in Untersuchungen an transplantierten Patienten als Modell einer diffusen Intima Verdickung verwendet (121).

Eine Lösung der für alle Strömungen geltenden Navier Stokes'schen Differentialgleichungssysteme (Erhalt von Masse und Moment) ist generell, mit Ausnahme von Sonderfällen, nur durch eine Simulation in einem Finite Elemente Modell möglich. Ein Finite Elemente Modell ist ein Gitter von kleinen Zellen, womit das Bett

der Strömung bzw. das Gefäß aufgerastert wird. Ist wie in unserem Fall die Strömung an der Wand besonders wichtig, können die Gitter an der Wand verfeinert werden (123). Die hierzu erforderliche möglichst exakte Rekonstruktion des Strömungsbettes bedeutet für die Koronargefäße eine exakte 3- D Rekonstruktion (18;137;144;174).

Viele Arbeitsgruppen auf dem Gebiet der Simulation des „Risikofaktors“ Blutströmung in den Koronargefäßen konzentrieren sich auf lokale (vulnerable) Plaques mit serieller Untersuchung. Da hier morphologische Veränderungen im Verlauf insbesondere der Plaques Ergebnisse der lokalen Beströmung der Gefäßwand sind, werden diese Untersuchungen durchweg mit IVUS ausgeführt (21;47;51;112;144). Hierfür wurden mehrere Methoden entwickelt und validiert (140;143;144;161;177;180;211). Für uns waren folgende Gründe maßgeblich, uns auf aus Koronarangiographien rekonstruierte Gefäßbäume zu konzentrieren:

- Zur Berechnung der Wandschubspannung und zur Beurteilung der strömungsrelevanten Nettowirkung von Plaquewachstum und Remodeling auf das Gefäßlumen ist eine Darstellung der Wand (IVUS) nicht erforderlich. Strömungssimulationen basierend auf rein angiographischen Lumen-Darstellungen wurden auch von anderen Arbeitsgruppen durchgeführt (18).

- Die neuen kommerziell erhältlichen 3-D- Angiographiesysteme wurden im Vergleich mit einer validierten IVUS/Angiographie Fusionsmethode (ANGUS) (142) bzw. IVUS als Goldstandard mit gutem Ergebnis getestet (161;212). Sie zeigen hohe Korrelationen von Durchmessern und Querschnitten mit diesem Goldstandard und geringe systematische Abweichungen (CAAS QCA 3D™ versus ANGUS: 0.45±1.49 mm² (161), CardiOp- B™ minimaler Querschnitt : 3.42 ± 1.66 mm, IVUS minimaler Querschnitt : 3.78 ± 1.60 mm).

- Nur mit angiographischen Daten sind auch retrospektive und ergänzende nachträgliche klinisch interessierende Strömungssimulationen möglich. Kommerzielle angiographische 3-D Rekonstruktionssystem sind online verfügbar und zukünftige Versionen von CAAS QCA 3D™ werden eine automatische Rekonstruktion ganzer Bäume mit Verzweigungen bei geringem interaktivem Aufwand und mit der Möglichkeit, bis zu 6 Projektionen zu nutzen, erlauben.

- Der mit IVUS kaum mögliche Blick auf den gesamten Baum ergänzt den interventionellen Blick auf fokale Plaques und erlaubt möglicherweise auch Früherkennung und Verlaufsbeurteilung einer koronaren

Herzkranzgefäßerkrankung anhand einer Definition von Kriterien jenseits des Rückgriffs auf lokale Stenosen (54;120-122). Zudem zeigt sich, dass Verzweigungen nicht vernachlässigbar sind (siehe auch Diskussion Strömungssimulation). Hierzu wurde bereits vorgeschlagen IVUS und Angiographie zur Rekonstruktion der Seiten Äste ohne IVUS in einem Hybridmodell zu kombinieren (145).

- Angiogramme,- und in Zukunft CT (161;163;213), MRT (164;213-215) und Rotationsangiographie (171;172)-, sind in wesentlich breiterem Umfang der klinischen Diagnostik zugänglich als die selteneren IVUS – Untersuchungen.

- Eine fokale Berindung des Baums mit Wandstücken aus dem IVUS ist grundsätzlich möglich. Das kardiale MRT wird in Zukunft Wanddarstellungen in die geometrischen Modelle mit einbringen.

3.2. Methodische Teilaspekte zur Datenauswahl und zum Datenvergleich: Interindividuelle Vergleiche von WSS mittels Statistik und dimensionsloser Modellierung, Testmodellgruppen als stratifizierte Stichprobenerhebung

Ziel unserer Untersuchungen war unabhängig von lokalen Stenosierungen Messparameter für die frühzeitige Erkennung und Graduierung der Schwere obstruktiver und die dilatierender Verlaufsformen zu entwickeln (54;120-122). Daher diente das Konzept der Kontrollgruppe im Vergleich zu Negativ- und Positivremodeling als Grundlage für eine stratifizierte Stichprobenerhebung für unsere Simulationsansätze (54;123). Wir vergleichen aneurysmatische atherosklerotische Koronarien (118;119;216) mit obstruktiv ggf. diffus stenotisch veränderten Koronararterien und Kontrollen, bei denen ein Ausschluss einer koronaren Herzerkrankung erfolgte.

Das Konzept der „dilatierten“ im Vergleich zur „obstruktiven“ Variante der Koronaratherosklerose wurde bezogen auf lokale Läsionen von Schoenhagen basierend auf IVUS-Untersuchungen eingeführt (117). Für unsere Stichproben erweiterten wir das Konzept auf das Remodeling Verhalten ganzer Gefäße. Dem liegt die Hypothese zugrunde, dass das Remodeling eng mit der atherosklerotischen Entzündung verbunden ist und auf Nachbarschaften übergreift. Das scheint zumindest für Anfangsstadien der Atherosklerose zu gelten (110). Positivremodeling konnte klinisch in Verbindung mit Endotheldysfunktion und früher Plaqueentwicklung nachgewiesen werden (217;218). Möglicherweise handelt es sich hier zum Teil um unterschiedliche Stadien. So scheint der klassische Glagov-Effekt (109) offensichtlich eine frühe Dysregulation (kompensatorische Entgleisung) bei endothelialer Dysfunktion (218) und bei florider Entzündung (219;220) darzustellen. Ausgebrannte

fibrosierte Narben scheinen hingegen mit einem Verlust der kompensatorischen Gefäßerweiterung verbunden zu sein (112). Mindestens teilweise scheint es sich jedoch auch um genetisch bedingte unterschiedliche Gefäßregulationsmuster bzw. teils genetisch bedingte Krankheitsvarianten zu handeln (221-223).

Ein direkter Vergleich der WSS zwischen mehreren Patienten(Gruppen) ist in der Regel nicht möglich, da die Herzkranzgefäße große Variationen bzgl. Anatomie und Größe aufweisen und die ins Ostium einströmenden Flüsse und peripheren Widerstände sehr unterschiedlich sind. Dimensionslose Modellierungsverfahren (z. B. Auswurffraktion in der Medizin oder Reynoldszahl in der Strömungslehre) und statistische Modelle bieten jedoch Wege diese Problematik zu umgehen. Dimensionslose bzw. statistische Charakterisierungen von WSS-Profilen sind damit ein weiteres wesentliches methodisches Instrument zur Entwicklung einer von lokalen Stenosegraden unabhängigen Definition und Erkennung von Frühformen, Verläufen und Remodeling Mustern koronarer Atherosklerose (54;120-122).

In unseren Untersuchungen (54) fanden wir, dass die normalisierte WSS Verteilung bei aneurysmatischer Koronarathersoklerose gegenüber Kontrollen keinen klaren Gipfel mehr zeigt und stochastischer ist. Dies könnte eine Dispersion oder den Verlust eines einheitlichen Sollwerts im WSS- abhängigen Remodeling reflektieren. Darüberhinaus ist die Gefäßfläche, die sehr niedrigem WSS exponiert ist, im Verhältnis zu den anderen Gruppen sehr hoch. Koronargefäße von Patienten mit obstruktiver Atherosklerose zeichneten sich durch eine Verschiebung zu hohem WSS in den Häufigkeitsklassen in der normalisierten Verteilung aus. Diese Beobachtung ist konsistent mit dem partiellen Verlust der Fähigkeit zum kompensatorischen Remodeling bzw. funktionellen Endothels (112).

Ergebnisse aus unserer „fraktalen“ Analyse und der Verlaufsuntersuchung mittels 3-D QCA bei KHE-Patienten weisen daraufhin, dass die Atherosklerose die pseudo-fraktalen Ordnungseigenschaften des Koronargefäßbaums zunehmend zerstört (120;122). Korrelationsfunktionen von 3-D QCA- Maßen eignen sich nur bei Frühformen der koronaren Atherosklerose zur Diagnostik, da mit zunehmender Anzahl der Gefäßverschlüsse keine ausreichende Anzahl von Korrelationen auf einem Baum zur Verfügung steht. Direkte Vergleiche der Querschnitte und Volumina eignen sich deshalb besser zur Quantifizierung für Verlaufsuntersuchungen bei fortgeschrittenen Veränderungen (122). Die gefundene Korrelation der Veränderung mit der Anzahl der allgemeinen Risikofaktoren stützt die Einbeziehung einer entsprechenden Varianz erklärenden Größe auch in das lokale Risikoprädiktionsmodell.

3.3. Baumstrukturmodell

Für unsere Analysen benutzten wir ein modifiziertes Weibel Modell (126). Die Modifikation besteht darin, dass für jede Ordnung die distale Verzweigung auch bei kleinen asymmetrischen Abzweigen als Ganzes dem Stamm zugeordnet wird. Das modifizierte Weibel Modell liefert eine funktionsgerechte Interpretation (129). Dieses vom Autor entwickelte Modell wurde von Kassab in „Scaling Laws of Vascular Trees: Of Form and Function" der Strukturanalyse des koronaren Gefäßbaums zugrunde gelegt bzw. übernommen (131), obwohl diese Arbeitsgruppe basierend auf morphometrischen Untersuchungen an Koronarien von Schweinen ursprünglich ein modifiziertes Strahler Modell (diameter- defined Strahler model) zur Beschreibung des koronaren Gefäßbaums verwendete (127;128). Die wesentlichen Unterschiede der Verzweigungsmodelle bestehen darin, wie den Gefäßsegmenten eine hierarchische Ordnung zugeteilt wird. In Strahler Modellen entspricht die Ordnung 0 der niedrigsten Ebene, z. B. den Kapillaren. Wenn sich 2 Gefäße vereinigen, entsteht ein neues Element mit einer um 1 höheren Ordnungszahl genau dann und nur dann, wenn die sich vereinigenden Elemente dieselbe Ordnung aufweisen. Ansonsten wird das Element mit der höheren Ordnung um das betreffende Segment verlängert. Da selbst bei Einhaltung dieser Regel im Koronargefäßbett eine große Durchmesservarianz der Elemente mit bestimmter Ordnung auftritt (durch asymmetrische Verzweigungen), erscheint es sinnvoll, die mittleren Durchmesser und Standardabweichungen der Elemente bestimmter Ordnung zu berechnen und eine Neuzuweisung der Ordnung auf Basis dieser Berechnung durchzuführen. Das Verfahren kann wiederholt werden, bis die Verteilung der Durchmesser von Elementen einer bestimmten Ordnung eine gewünschte Form hat. Dieses Verfahren wird Diameter-definiertes Strahler Modell genannt (128). Die Korrelation zwischen Diameter von Segmenten und Elementen und Ordnung wird durch diese Reklassifikation bzgl. der Ordnung basierend auf dem Durchmesser natürlich verbessert und verliert an Aussage. Das Strahler Modell als „wahres" Modell wird nicht nur durch morphometrische Daten sondern auch durch morphogenetische Untersuchungen gestützt, nach denen sich die Koronargefäße im Myokard an mehreren Stellen beginnend auf kapillärer Ebene stückweise entwickeln und später aneinander und an die Aorta Anschluss finden (224). Trotzdem ist eine Strahler Ordnung für Angiogramme nicht geeignet, wo nur Elemente der Ordnung 9-11 entsprechend dem Kassab Modell (128) sich darstellen. Wenn die Segmente als Teile von Elementen zwischen 2 kleinen Seitenästen definiert sind, ist die Anzahl der Segmente pro Element in Leitungsgefäßen sehr hoch. Dementsprechend nimmt dieses Verhältnis in Kassabs Daten bei den Ordnungen 9-11 stark zu. Das bedeutet, dass das Diameter-definierte Strahler Modell im Bereich angiographisch erkennbarer Gefäße nicht brauchbar ist.

3.4. 3-D Rekonstruktion

Die DFG Anträge [Fl 165/3-1 und Fl 165/3-2] liefen in einer Zeit in der die Pionierarbeiten zur 3-D Rekonstruktion von Koronarien erfolgten. Die Rekonstruktionen waren aufwändig, erwiesen sich allerdings als wesentlich genauer hinsichtlich quantitativer Vermessung (3-DQCA) als 2 D Bilder (137;173). Die 3-D QCA war in kleinen Stichproben geeignet eine Progredienz von diffusen luminalen Verengungen im Sinne einer fortschreitenden Koronaratherosklerose nachzuweisen (122).

Die Rekonstruktionen erwiesen sich als geeignet zur Aufbereitung für und Durchführung von Strömungssimulationen (123;147-149). Von anderen Arbeitsgruppen wurden andere oder in Einzelheiten differierende Ansätze entwickelt und evaluiert (139;179;181;225-242). Die Kombination aus Entwicklung der numerischen und theoretischen Mathematik der Bildverarbeitung (155;169;170;181;243-248), der Computertechnologie und der Verbesserung hoch auflösender 3- D Bildgebungsverfahren (MRT, CT, Rotationsangiographie) führte dazu, dass sich der Schwerpunkt der Forschung zu 3-D Rekonstruktionen von Gefäßen auf MRT, CT und Rotationsangiographie verlagert hat (163;165;167-172;181). Die Weiterentwicklung der Algorithmen erfolgt heute großenteils für die oder in den Forschungs- und Entwicklungsabteilungen (F&E) der großen Hersteller von CT-, MR- und- Röntgenanlagen (z.B. Philips, Siemens) und spezialisierter Zuliefer-Software-Entwicklungsfirmen (z.B. Pie-Medical und Paieon). Wir führten deshalb im Phantommodell methodische Machbarkeitsstudien zur Strömungssimulation aus Koronarien unter Verwendung von CT- und MR- Aufnahmen (148) bzw. biplanen Angiographie Aufnahmen, die mit auf dem Markt verfügbarer Software dreidimensional rekonstruiert wurden (149), durch. Im Ergebnis zeigten diese Arbeiten, dass die entsprechenden 3 D- Datensätze sich grundsätzlich als geometrische Modelle für eine genaue Strömungssimulation eignen.

Die 3-D Rekonstruktion aus angiographischen Bildern erlebt allerdings eine Renaissance durch die kommerziell erhältliche schnelle (on- line) Software (CAAS 3-D QCA™, und CardiOp- B™). Sie wird bei Interventionen zur Vermessung der Länge von Gefäßabschnitten die mit Stent ersorgt werden sollen (159;249), zur Beurteilung und Behandlung von Läsionen an Verzweigungen (250;251), zur Wiedereröffnung chronischer Verschlüsse (252) und zur Strömungssimulation empfohlen (161). Validierungsuntersuchungen der genannten Systeme (CAAS 3D QCA™, und CardiOp- B™) im Vergleich zu IVUS (212), Fusionsbildgebung mit IVUS und Angiographie (161), Stents (159) sowie Phantomen bekannter Größe im Tierversuch (160;162) zeigten eine Tendenz zu einer geringen systematischen Unterschätzung der Gefäßquerschnitte durch die 3-D QCA bei starker Trendkopplung beider Methoden (r~0.9). Während bei der CAAS 3-D QCA™ die Kalibration meist geometrisch erfolgte,

wurde bei CardiOp- B™ die Kalibration teilweise mit der Katheterspitze ausgeführt. Das könnte einen Teil des schlechteren Abschneidens von CardiOp- B™ im direkten Vergleich (160) erklären. Nach eigenen Messungen war die geometrische Kalibration der Kalibration durch Vermessung der Katheterspitze deutlich überlegen, konnte aber durch Vermessung eines kugelförmigen Elements (Hüllkugel einer Pigtail Schlaufe) weiter verbessert werden (137).

Eine weitere Einflussgröße ist die Wahl des Querschnitts orthogonal zur Achse, die bei IVUS und Angraphie nicht identisch ist und eigentlich ein spezielles Messtool erfordert. Darüberhinaus sind in Abhängigkeit von Informationsverlusten durch Verkürzung Fehler in der angiographischen Rekonstruktion des Querschnitts zu erwarten, die möglicherweise künftig durch Einstellung geeigneter Projektionen (253) und/oder die Verwendung multipler Projektionen reduziert werden können.

Herausforderungen in der digitalen Bildverarbeitung sind weiter Randbedingungen, Mehrdeutigkeiten und ungleichmäßige Qualität der Ausgangssignale, automatische Gefäßerkennung und Segmentierung (254) sowie die dreidimensionale Bewegungsverfolgung (169;170;178;235;246;255). Einen Ausflug in die neue Welt der Mathematik der 3-D Rekonstruktion konnte der Autor in Zusammenarbeit mit Prof. Reinhold Orglmeister und Herrn Steffen Zeiler machen.

Die moderne Bildverarbeitung ist ein komplexer Erkennungsprozess der von unterschiedlichen Datenquellen über Datenbearbeitungs- und Datenkontextanalyseverfahren ggf. mit externem Zusatzwissen zu einer, - im medizinischen Bereich möglichst diagnostisch relevanten -, Interpretation oder Information führt. Die Struktur dieser Datenflüsse, Prozesse und des Wissens unter der Oberfläche des erkannten Bildes sind in dem folgenden Schema zum Weg vom digitalen Bild zur Bilderkennung adaptiert nach Jähne (245) skizziert.

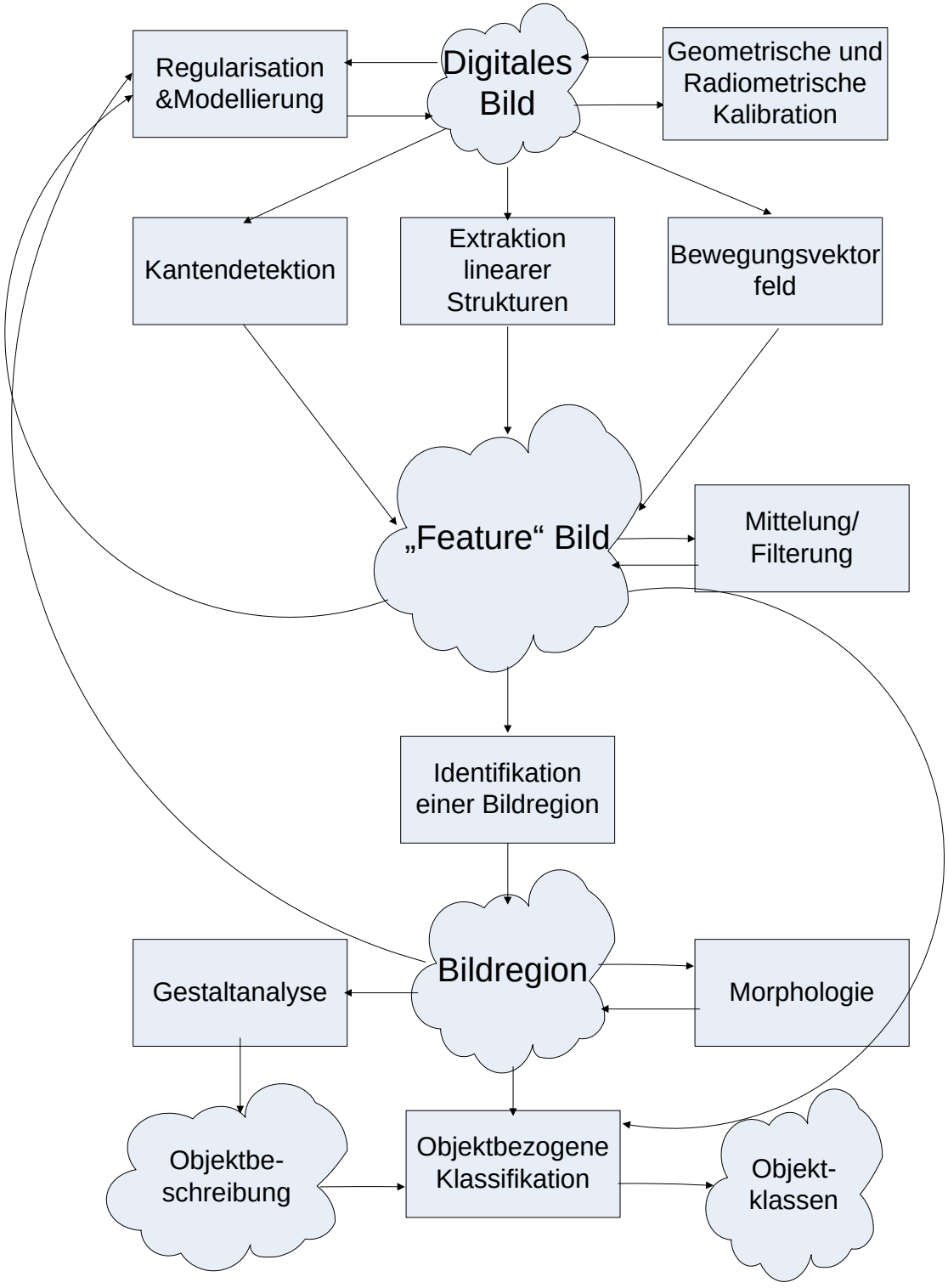

Abbildung 6: Schema zum Weg vom digitalen Bild zur Bilderkennung adaptiert nach Jähne (245)

Eine 3-DRekonstruktion beinhaltet folgende Schritte:

i. Bildakquisition in mehreren Projektionen über mehrere Herzzyklen (spatio- temporal image acquisition).
ii. Bestimmung der Geometrie
iii. Detektion des Gefäßbaums in den Projektionen
iv. 3- D Rekonstruktion
v. 3-D Repräsentation
    a. Segmentierung und/oder Labeling
    b. Visualisierung und Datenaufbereitung

Schritt (i) ist entscheidend für die Qualität der Eingangssignale. Neben Bewegungsartefakten durch Eigenbewegung des Herzens und Bewegung des Tisches (panning), stellen Überlagerungen, inhomogene Strahlenabschwächung im Hintergrund (z. B. durch Zwerchfell und Lunge), magnetische nichtlineare Bildverzerrung (pincushion distortion (256)) etc. Herausforderungen für Bildaufnahme und Bild Vorverarbeitung dar (257). Für das am DHZB entwickelte 3- D Rekonstruktionsverfahren wurde zur Bildentzerrung Algorithmen aus einem früheren DFG-Projekt zu QCA verwendet (258). Eine Entzerrung auf den Rohdaten vermehrt allerdings das Bildrauschen (Filter: Pixelauflösung), weshalb in neueren Methoden die Integration einer rein rechnerischen Korrektur in den Rekonstruktionsalgorithmus vorgeschlagen wird (Filter: numerische Rechengenauigkeit bzw. Rundungsfehler) (225).

Nach unseren Erfahrungen waren die häufigsten vermeidbaren Probleme ein Verschieben des Tisches während der Aufnahme und ein Abschneiden des Koronarbaums (Bildverstärkung + exzentrische Position) in mindestens einer Ebene. Am besten erwiesen sich folgende biplane Darstellungen zur Akquisition überlagerungsfreier Projektionen:

LCA: Projektion 1: Rotation 30° RAO, Angulation 25-30° kaudal; Projektion 2: Rotation 60-70° LAO, Angulation 30° kranial)

RCA: Projektion 1: Rotation 30° RAO, Angulation 25° kaudal; Projektion 2: Rotation 30° LAO mit Angulation 30° kranial oder Rotation 50% LAO ohne Angulation.

Bei Abweichung der beiden Aufnahmeebenen um bis zu 20° zeigten sich bei Untersuchungen am Phantom begrenzte Fehler (137).

(ii, iii, iv) Die Schritte ii, iii und iv sind nicht unabhängig und beeinflussen sich gegenseitig.

(ii) Eine Aufzeichnung der Aufnahmegeometrie (Rotation, Angulation, Abstände von Bildverstärker und Objekt vom Fokus, Verstärkung und Auflösung) wird auf modernen Anlagen elektronisch mitprotokolliert. Weil Ungenauigkeiten eines solchen Protokolls oder Messfehler im Protokoll oder Einstellungsfehler (z. B. Verschiebung der Röntgensysteme oder des Tisches) angenommen werden müssen, ist der Standardansatz, dass man mit einer initialen Geometrie Annäherung startet und durch Rückprojektion rekonstruierter Strukturen

oder Punkte die Geometrieschätzung iterativ verbessert (259-263). Leider sind oft nur wenige eindeutige Projektionspunktpaare in mindestens 2 Projektionsebenen vorhanden. Insbesondere die exakte Markierung ist leider meist nur bei wenigen Verzweigungs-, Abgangspunkten oder sonstigen Objekten möglich. Lineare Regressionen und nichtlineare Schätzmethoden sind aber sehr ungenau bei sehr wenigen Messpunkten. Die beste Statistik für kleine Messreihen ist der Mittelwert, dessen Standardfehler sehr schnell konvergiert (Beitrag des Autors: mean value approach (263)).

Das klassische Geometriemodell für Rekonstruktionen ist das Modell der Epipolargeometrie mit einem eindeutigen Isozentrum.

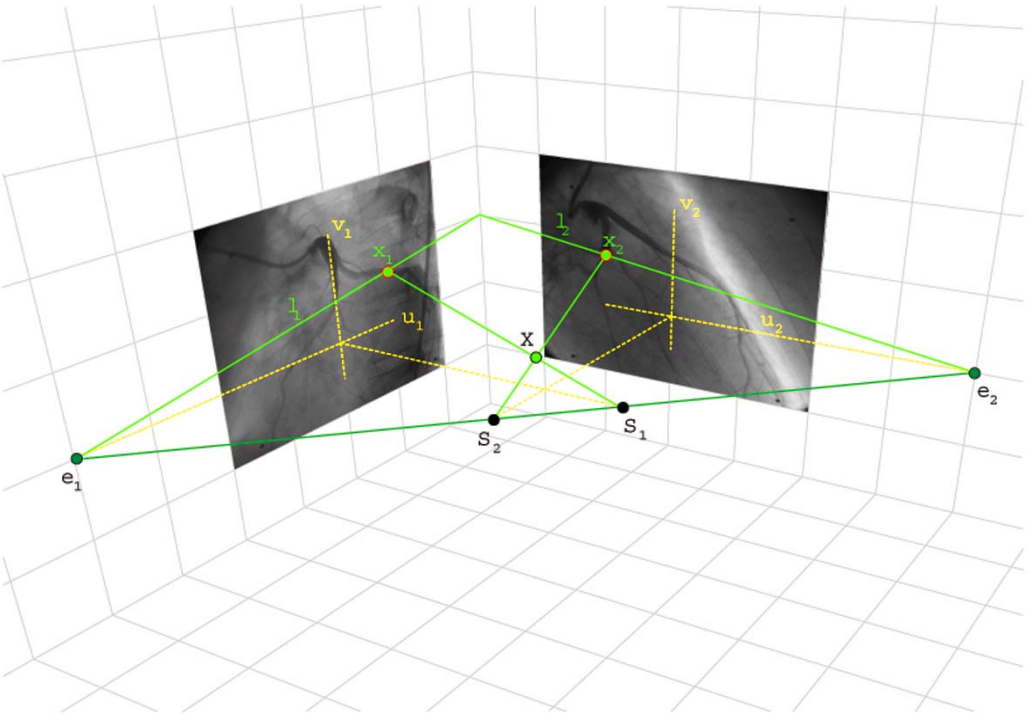

Abbildung 7: Epipolargeometrie, mit S_1, S_2 Projektionszentren, e_1 und e_2 den beiden Epipolen, den beiden Bildpunkten x_1 und x_2, dem 3-D Punkt X (mit freundlicher Genehmigung von Steffen Zeiler, TU- Berlin, Elektronics and Medical Signal Processing (EN3))

Problem ist, dass sich die Rotationszentren der beiden C-Bögen nur ungenau zur Deckung bringen lassen und Projektionslinien aus zwei oder mehreren Richtungen sich häufig nicht in einem Isozentrum schneiden (bis zu 18 mm Distanz nach Messungen am DHZB 1993!). Durch die zu beiden Projektionen orthogonale Raumachse wird eine Isoachse definiert und erlaubt eine Anpassung des Zentrums des Koordinatensystems (263). Eine andere Alternative zur Umgehung

des Problems ist z. B. das unten beschriebene Verfahren der iterativen Geometrieoptimierung mit Konvergenz auf eine 3-D Mannigfaltigkeit[i] im 4-DVereinigungsraum (241).

(iii) Die Detektion des Gefäßbaums in den Projektionen ist ein Problem, das auch heute noch unterstützende manuelle Interaktion (Markierung von Punkten, region of interest etc.) erfordert. Gefäßbewegung, hohe Kontrastunterschiede, inhomogener Hintergrund, Überlagerungen und andere lineare Strukturen im Bild erschweren eine automatische Gefäßfindung.

Für das am DHZB entwickelte 3-D Rekonstruktionsverfahren wurden zur Gefäßerkennung Algorithmen aus einem früheren DFG-Projekt zu QCA integriert (173;258). Topologische Eigenschaften (z. B. Verzweigungen) unterscheiden Gefäßbäume von anderen linearen Strukturen im Bild. Zentrales Problem in allen Bildverfahren zur medizinischen Gefäßdarstellung ist die Rekonstruktion der Gefäßachsen (181). Grundsätzlich orientieren sich Verfahren zur Extraktion linearer Gefäßstrukturen aus Bildern entweder an relativen Intensitätsmaxima (pixelorientiert) oder an Gradientenfeldern (Kantenerkennung) (228). Ein 3-D Tracking der Koronargefäße ggf. unter Einbeziehung weiterer Randbedingungen (z. B. konvexe Myokardoberfläche) hat den Vorteil, dass die meisten Uneindeutigkeiten in 2-DProjektionsbildern gelöst werden können. 3- D Modelle können als deformierbare parametrische Modelle gestaltet und im Bewegungsfeld verfolgt werden (235).

Die Bestimmung der Gefäßmerkmale kann z. B. mit einem Multiskalenverfahren erfolgen (236), da entsprechende Bildmerkmale von Gefäßen in unterschiedlichen Auflösungsstufen im Bild vorliegen können. Störende Bildstrukturen, die sich in ihrer Ausdehnung charakteristisch von denen der Arterien unterscheiden, können allein durch die Auswahl geeigneter Skalen unterdrückt werden. Neben dem Merkmal der Gefäßzugehörigkeit sind weitere für die Rekonstruktion wichtige Merkmale wie Orientierung, Größe und Stärke einer Bildstruktur ableitbar. Die Rekonstruktion selbst ist nicht an ein spezielles Segmentierungsverfahren gebunden. Die Eigenwertanalyse der Hessematrix (Matrix der partiellen Ableitungen 2. Ordnung) eignet sich u.a. zur Kantenerkennung und zum Filtern linearer Strukturen (264). Sie hat den Vorteil, für 3D und 2D Daten gleichermaßen anwendbar zu sein. Bei der Fourier Transformation lassen sich u. a. Vorteile für die Berechnung der Ableitung, der Konvolution mit Filtern und der Normalisierung erreichen (265;266).

Im Rahmen einer Zusammenarbeit des Autors mit Prof. Orglmeister, TU- Berlin, hat der Autor im Hinblick auf dieses Problem Herrn Zeiler anonymisierte Angiogramme aus der täglichen Routine des Herzkatheter-Labors („Härtetestdaten) für die Entwicklung einer automatischen 3-DRekonstruktion zur Verfügung gestellt. Aus dem in Abbildung 8 gezeigten Ergebnis ist

[i] Der mathematische Begriff Mannigfaltigkeit bezeichnet topologische Räume mit abzählbarer Basis und lokal Euklidischer Metrik, für deren Elemente kleine disjunkte Umgebungen existieren. Z.B. ist die Kugeloberfläche eine Mannigfaltigkeit, wobei lokal die Oberfläche auf ein x-y Koordinatensystem (Euklidische Metrik) als Karte abgebildet werden kann.

ersichtlich, dass das Regionen-Wachstumsverfahren im Bereich der Überlagerung durch Zwerchfell oder Wirbelsäule Erkennungsprobleme hat, die sich auch durch einen Multiskalenansatz (240;245) nur teilweise lösen lassen.

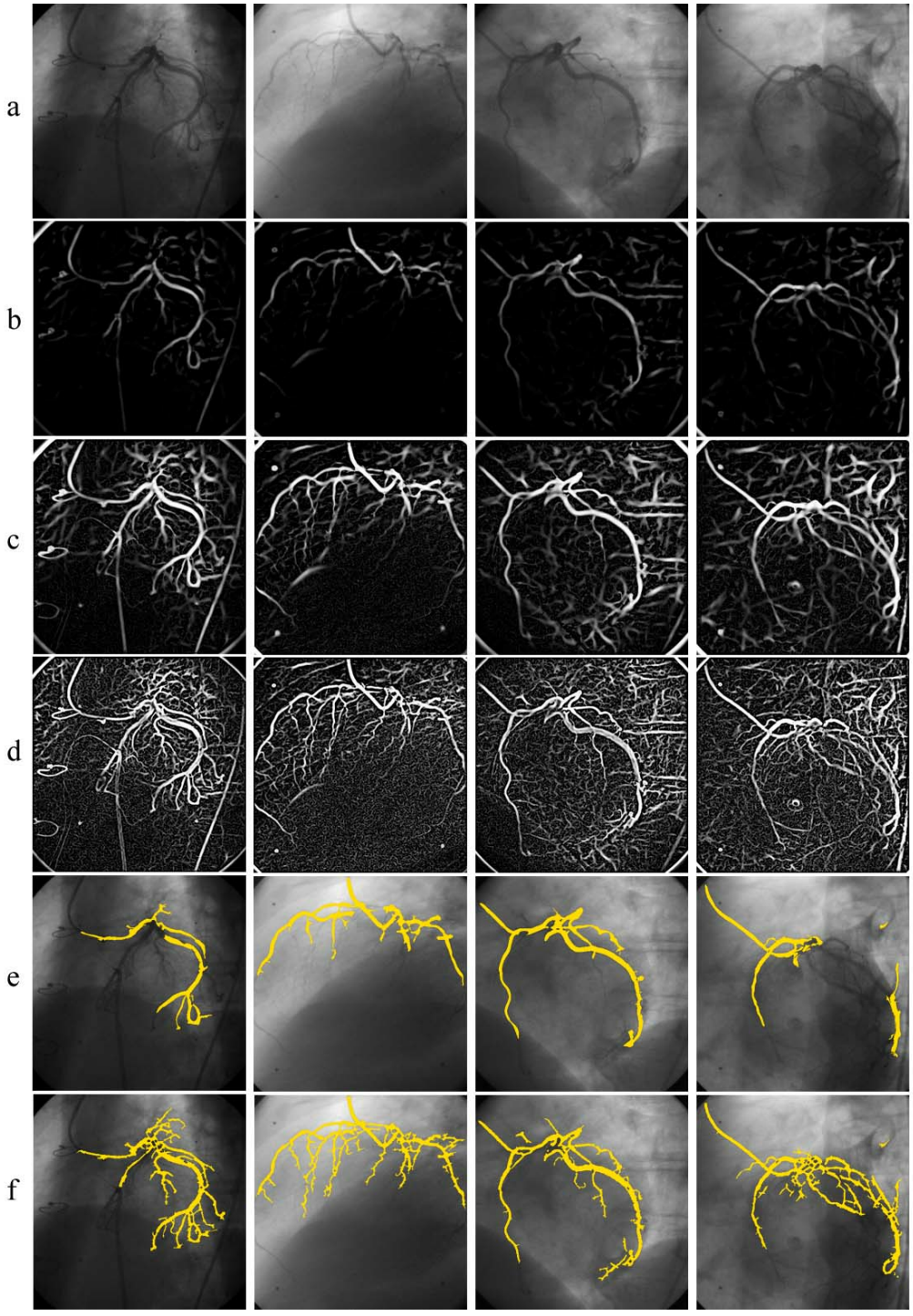

Abbildung 8: Ergebnisse des Regionen-Wachstumsverfahrens zur Segmentierung der Arterien für vier Beispielbilder. a) Originalaufnahmen, b) Merkmalsbilder in niedrigen Skalen, c) Merkmalsbilder für mittlere Skalen, d) Merkmalsbilder in hohen Skalen, e) Ergebnisse nach Segmentierung auf Grundlage des groben Skalenbildes, f) Endergebnis nach Hinzunahme der kleinen Skalen (mit freundlicher Genehmigung von Steffen Zeiler, TU- Berlin, Elektronics and Medical Signal Processing (EN3))

Ein weiteres Verfahren ist die Pfadsuche, die zweckmäßigerweise dreidimensional erfolgt und mit einer Geometrieverbesserung kombiniert wird. Die Problemstellung ist korrespondierende Punkte in 2 Projektionsbildern mit unbestimmter Geometrie zuzuordnen.

Bei der iterativen Pfadsuche erfolgt ausgehend von einem Startpunkt die Suche bis zu einem durch den Anwender definierten Endpunkt. Eine Kostenfunktion soll die Einbeziehung nicht korrespondierender 2- dimensionaler Punktepaare in den Pfad unterdrücken. Sie wird für Prioritätsentscheidungen bei Alternativen benötigt. Die Wichtigkeit dieser Kostenfunktion im 4 D-Raum ist aus folgender Abbildung ersichtlich. Die Kreuzung des Diagonalastes mit dem Ramus interventrikularis anterior ist im 2 D- Bild nicht eindeutig und führt zu einem falschen Weg! Nach jedem Schritt vorwärts wird das neue korrespondierende Punktepaar zur Verbesserung der Geometrieschätzung benutzt (156;241).

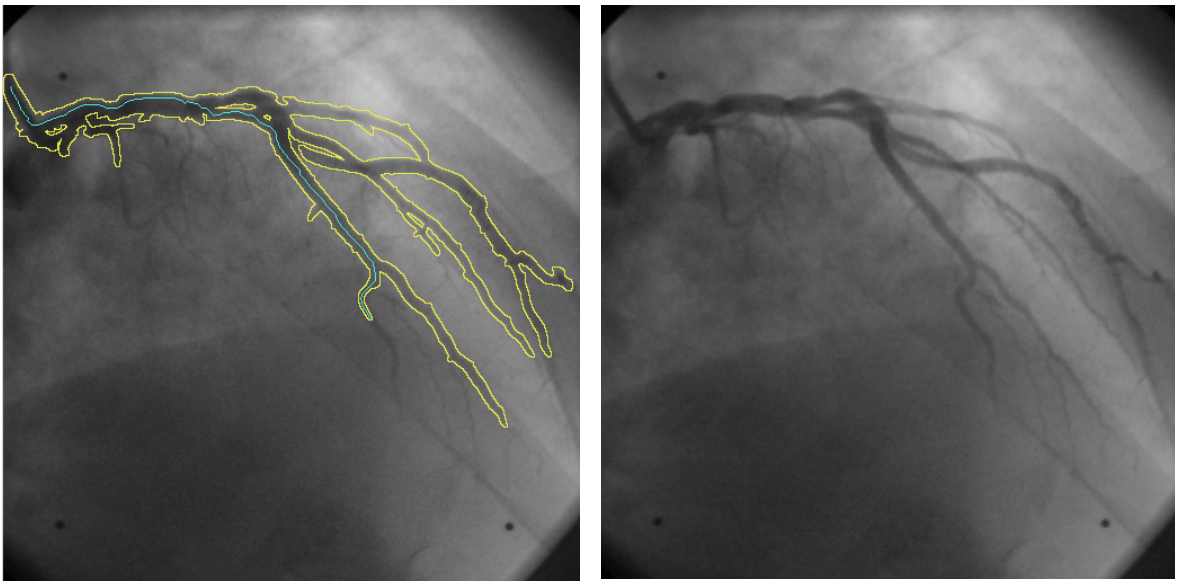

Abb 9: 2-D Pfadsuche (mit freundlicher Genehmigung von Herrn Steffen Zeiler, TU-Berlin, Elektronics and Medical Signal Processing (EN3))

Für die 3-D Rekonstruktion wurde ein sehr allgemeiner Ansatz entwickelt. Wichtigstes Merkmal ist die Trennung von Objekttopologie und -Geometrie. Dies ist notwendig, um die Schwierigkeiten bestehender Ansätze bei der Lösung des Korrespondenzproblems zu umgehen. Bei der biplanen Angiographie sind die Kameras in der Regel um 90° zueinander versetzt angeordnet. Dadurch enthalten die Aufnahmen viele räumliche Informationen. Die unterschiedlichen perspektivischen Projektionen führen aber zu einem vollkommen anderen Aussehen des Objektes in den Projektionen. Unabhängig davon wie unterschiedlich ein Objekt (Körper) in zwei Aufnahmen erscheint, die Topologie bleibt unter dem Einfluss der Transformationen bei der Bildentstehung erhalten.

Im Raum aller Hypothesen über die Objektkonfiguration, wird nach jener Konfiguration gesucht, die aufgenommene Bilddaten am besten erklären kann. Um den Suchraum zu begrenzen und die

Suche zu beschleunigen, werden alle zusätzlich verfügbaren Informationen integriert. Der eigentliche Rekonstruktionsprozess wird von der Topologie bestimmt. Verfügbare Informationen, wie z. B. Bildmerkmale und Geometrie, werden genutzt um die Anzahl in Frage kommender Hypothesen einzuschränken.

Zum Einsatz kommen dabei Methoden der dynamischen Programmierung und Pfadverfolgung, wie sie z. B. in der künstlichen Intelligenz verwendet werden. Sie bieten die Möglichkeit lokale Information in einem globalen Modell zu integrieren. Das Korrespondenzproblem, wie es bei der biplanen Angiographie auftritt, ist nicht immer eindeutig lösbar. Liegt ein Gefäß in einer Epipolarebene, so ist kein eindeutiger Gefäßverlauf zu ermitteln. Die topologischen Eigenschaften der Gefäße erlauben es aber, geometrische Information aus anderen Bildbereichen, die eine eindeutige Zuordnung erlauben, auf Gebiete mit Mehrdeutigkeiten zu übertragen, um damit einen eindeutigen Gefäßverlauf zu ermitteln.

Eine weitere Anwendung, bei der die Methode der Pfadverfolgung erfolgreich eingesetzt werden konnte, ist die Bewegungsschätzung von Arterien. Auch unter dem Einfluss eines unbekannten Bewegungsvektorfeldes bleibt die Topologie der Gefäße erhalten. Bei der Bewegungsschätzung von Arterien tritt das Blendenproblem auf. Es ist nicht möglich einen eindeutigen Bewegungsvektor zu bestimmen, da nur die senkrechte Komponente des Bewegungsvektors aufgrund mangelnder Strukturinformation bestimmt werden kann. Auch hier hat sich die Methode der Pfadverfolgung bewährt, indem sie Informationen aus weiter entfernten Gebieten mit genügend Strukturinformation, in Bereiche mit mehrdeutigen Lösungen überträgt und damit eine eindeutige Bestimmung des Bewegungsvektorfeldes für die Gefäßpunkte ermöglicht.

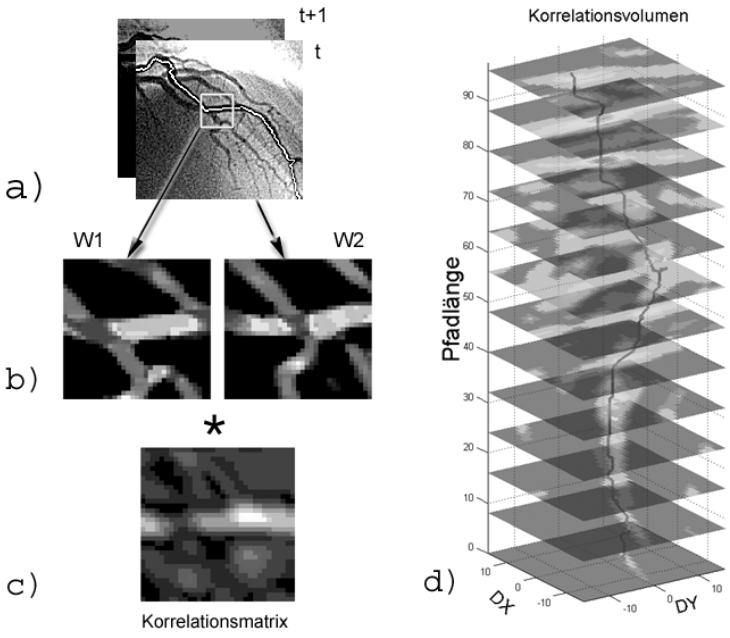

Abbildung 10: Beispiel einer Pfadsuche zur Bewegungsschätzung (mit freundlicher Genehmigung von Steffen Zeiler, TU- Berlin, Elektronics and Medical Signal Processing (EN3))

(v) a 3 D- Repräsentation

Segmentierung und Labeling

Die dreidimensionalen Objekte haben in der Regel komplexe Strukturen, da sie neben der Rekonstruktion, Markierungen, Strukturverweise und ggf. weitere topologische und geometrische Informationen beinhalten. Das am DHZB verwendete „3-D Attributed Data Model for Achiving and Interchanging of Coronary Vessel Systems“ ist ein solches Modell (173;267). In der gewählten Darstellung sind Stamm und Zweige Teil des 3-D Objekts, wobei die Zweige und Stämme jeweils ihrerseits Verweise auf weitere Objekte beinhalten, worin die Zweige als Stämme und die Stämme als Zweige auftreten. So entsteht ein Netzwerk basierend auf dem Grundelement der Bifurkation mit Stamm und Zweigen. Den Elementen lässt sich zwanglos eine Ordnung zuweisen, wenn man den Hauptstamm mit der Ordnung 0 und bei jeder neuen Verzweigung eine Zunahme der Ordnungszahl um 1 zuordnet. Verzweigungen gleicher Ordnung werden sequentiell im Uhrzeigersinn nummeriert. Dies ist ein modifiziertes Weibel Modell (126). Die Modifikation besteht darin, dass für jede Ordnung die distale Verzweigung auch bei kleinen asymmetrischen Abzweigen als Ganzes dem Stamm zugeordnet wird. Basierend auf morphometrischen Untersuchungen an Koronarien von Schweinen schlugen Kassab et al. ein modifiziertes Strahler Modell (diameter-defined Strahler model) zur Beschreibung des koronaren Gefäßbaums vor (127;128). Ein solches Modell bezieht sich auf die kapilläre Ebene als Nullebene und ist bestenfalls sinnvoll, wenn die Kapillaren in „Sicht“ sind.

(v) b Visualisierung und Datenaufbereitung

Die Visualisierung und Datenaufbereitung wird heute häufig unter Verwendung browserfähiger Standardtools durchgeführt. Hierdurch wird eine plattformunabhängige Anwendung und Visualisierung erreicht. Hierfür kann die Virtual Reality Modelling Language (VRML) verwendet werden. Die Kombination von VRML Prototypen mit JavaScript Knoten erlaubt die Implementierung umfassender Anwenderoberflächen bei Beibehaltung der Standardbrowserfunktionen (154;268). Insbesondere ist in jüngerer Zeit das VRML basierte „High Dynamic Range Image Texture Mapping“ fortentwickelt worden (269).

Grundsätzlich ist die räumliche Visualisierung gekennzeichnet durch

- die Projektionsgeometrie (perspektivisch oder parallel),
- 3 D Eigenschaften (Tiefe, Maximum Intensity Projection, Shading, Opacity etc.)
- und die Implementierung.

Bei der Implementierung unterscheidet man

- ein indirektes Verfahren. Der „marching cube“ Algorithmus z. B., erstellt zuerst eine geometrische Repräsentation von Isoflächen mit Intensitätsschwellen. Das erstellte Polygongitter erlaubt ein effizientes Rendering mit Graphik Hardware.

- Bei den direkten Verfahren wird das Volumen ohne intermediäre geometrische Repräsentation verarbeitet. Bei den Objektordnungsalgorithmen („splatting“) wird das Volumen systematisch Voxel für Voxel aufgearbeitet. Bei Bildordnungsalgorithmen (ray-casting) werden Projektionsstrahlen von jedem Bildpixel in der Bildebene ins Volumen konstruiert. Entsprechende ggf. gewichtete Projektionsstrahlfunktion erlauben die Modellierung der oben erwähnten 3-D Eigenschaften. Für dieses Ray-Casting gibt es unterschiedliche Beschleunigungsalgorithmen, z. B. den Inter-Frame Coherence Algorithmus (270).

3.4. WSS und „Flow-profiling“

Die numerische Simulation von Strömungen in dreidimensionalen Rekonstruktionen von Koronararterien „Flow-Profiling“ ist der derzeitige Standard der Untersuchung der Wandschubspannung in Herzkranzgefäßen (47;78;144;150;152;174;215). Der prognostische klinische Wert dieser immer noch sehr aufwändigen Methode konnte in aktuellen Studien belegt werden (21;43;44;51;55;271).

In den genannten Studien wurden im wesentlichen Ausschnitte des Koronarengefäßsystems im Verlauf betrachtet. Unser Ziel war die Untersuchung ganzer Bäume mit dem Ziel, interindividuell vergleichbarer Charakteristika, die eine vom Vorliegen höhergradiger lokaler Stenosen unabhängige Klassifizierung beginnender und fortschreitender Atherosklerose erlaubt. Hierfür wurde auf statistische Methoden zur Klassifikation von Mustern und dimensionslose Größen aus normalisierten WSS-Verteilungsdiagrammen zurückgegriffen.

In die Simulation gehen als wichtigste Randbedingungen die Strömungsgrößen und Drücke sowie die lokale Geometrie ein. Eine erste Betrachtung gilt deshalb den Messvarianzen und vereinfachenden Annahmen für diese Hauptrandbedingungen.

Die Inlet-Flüsse wurden aus Gefäßquerschnitten und intravaskulären ostialen Dopplermessungen (199) geschätzt. Die Methode eignet sich grundsätzlich auch für die pulsatile Simulation, da sie die relevanten zeitlichen Gradienten der Blutflussgeschwindigkeit als wesentliche Determinante der Scherrate abbildet (77;208). Da die Geschwindigkeit in kleineren Umgebungen ziemlich konstant ist, sofern keine lokalen Stenosen vorliegen (siehe Schemabild Abb. 11), können ostiale Geschwindigkeiten, durch Geschwindigkeiten in den proximalen großen Gefäßen näherungsweise ersetzt werden. Alternativ wurde in einer neuen Untersuchung aufgrund von Simulationsberechnungen in Koronarekonstruktionen eine direkte Schätzung des Flusses aus der Geometrie vorgeschlagen (130).

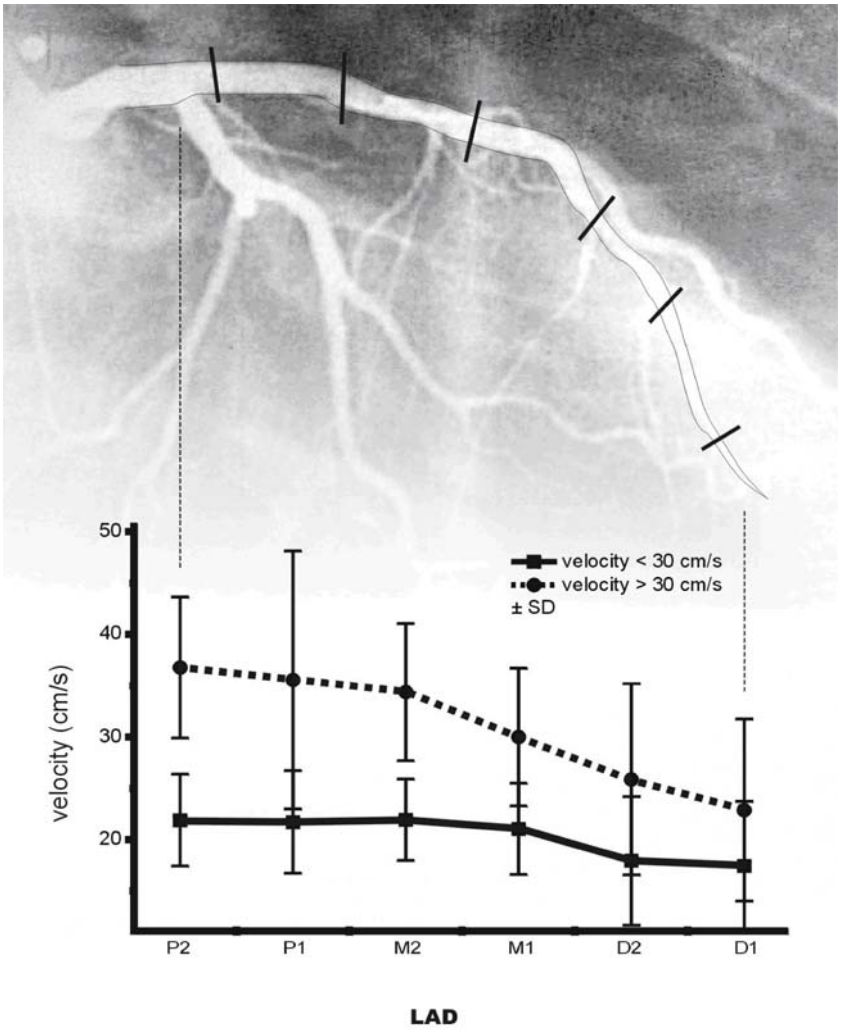

Abbildung 11: Geschwindigkeiten bei Rückzug im Ramus interventricularis anterior

Die Schätzung der Flussgrößen aus berechnetem Gefäß Lumen und Dopplerspitzen-geschwindigkeit sind Näherungen, weil das exakte räumliche Strömungsprofil in vivo nicht gemessen werden kann. Da der Messung der Flussgeschwindigkeit am Gefäßabgang die Annahme zugrunde liegt,dass die maximale Flussgeschwindigkeit das doppelte der mittleren Flussgeschwindigkeit beträgt (199), treten systematische Fehler in Abhängigkeit von der Gefäßgröße auf (123). Das Verhältnis von lokaler mittlerer Blutflussgeschwindigkeit (AMV) zu Spitzenflussgeschwindigkeit (APV) ist in einem schmaleren Gefäß (parabolisches Profil) niedriger als in einem weiten Gefäß (flaches Profil), wie eigene Messungen mit dem Dopplerdraht in etwas größeren Venenmodellen zeigten.

In den Simulationen mit Verzweigung (Abb. 12) wurde die Flussrate an jeder Verzweigung über eine empirisch in Koronargefäßen gefundene fraktale Korrelation zwischen Flussrate und Gefäßdurchmesser berechnet ($\dot{V} \sim d^{2.6}$) (272) .

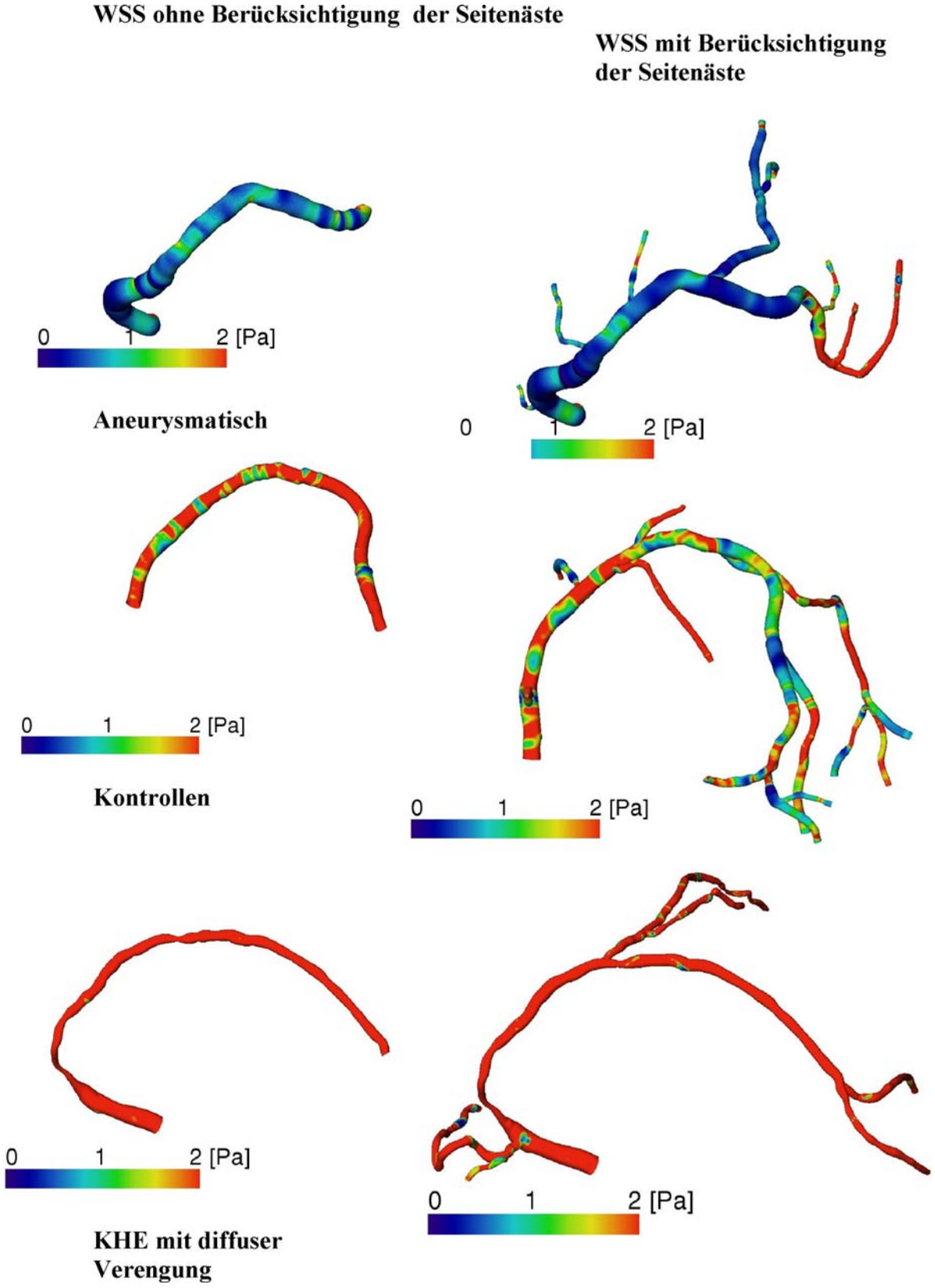

Abbildung 12: Vergleich Wandschubspannung mit und ohne Berücksichtigung der Seitenäste

Die Summe der Outlet-Flüsse muss unter Annahme vernachlässigbarer Flüssigkeitsverluste entsprechend dem Kontinuitätsprinzip gleich dem Inlet-Fluss sein. Daraus ergibt sich, dass bei Vernachlässigung von Verzweigungen zu hohe Flussgrößen für den distalen Gefäßstamm angenommen werden. Eine Auswirkung der Einbeziehung von Gefäßverzweigungen in die Simulation im Sinne einer niedrigeren WSS ist deshalb allein deshalb zu erwarten, weil sich durch den abzweigenden Fluss der Fluss in den Hauptgefäßen verringert.

In der Literatur wird allerdings vertreten, dass Verzweigungsflüsse im Bereich der RCA im Hauptgefäß untergeordnete Bedeutung für die WSS Feldstruktur besitzen (193). Aufgrund unserer derzeit durchgeführten Simulation in Gefäßen mit Verzweigungen (Abbildung 12) würden wir diese Meinung nicht mehr teilen, da die Strömungssimulation mit Verzweigungen nicht nur korrektere WSS-Bestimmungen sondern auch neue Informationen aus dem Vergleich des Leitungsgefäßes mit den Seitenästen liefert. Zur Modellierung der Verzweigungen für WSS Berechnungen wurde kürzlich vorgeschlagen, die Fusionsbildgebung aus IVUS und Angiographie durch 3-D Rekonstruktion aus der Angiographie in die Seitenäste zu erweitern (145).
Eine weitere wesentliche Randbedingung bei Strömungssimulation sind die Drücke. Der Druck im Ostium entspricht weitgehend dem Druck in der Aorta ascendens und wird mit dem Koronarkatheter über eine flüssigkeitsgefüllte Messkette registriert. Flüssigkeitsgefüllte Messketten weisen Resonanzen und Dämpfungen auf, die näherungsweise korrigiert werden können (273).

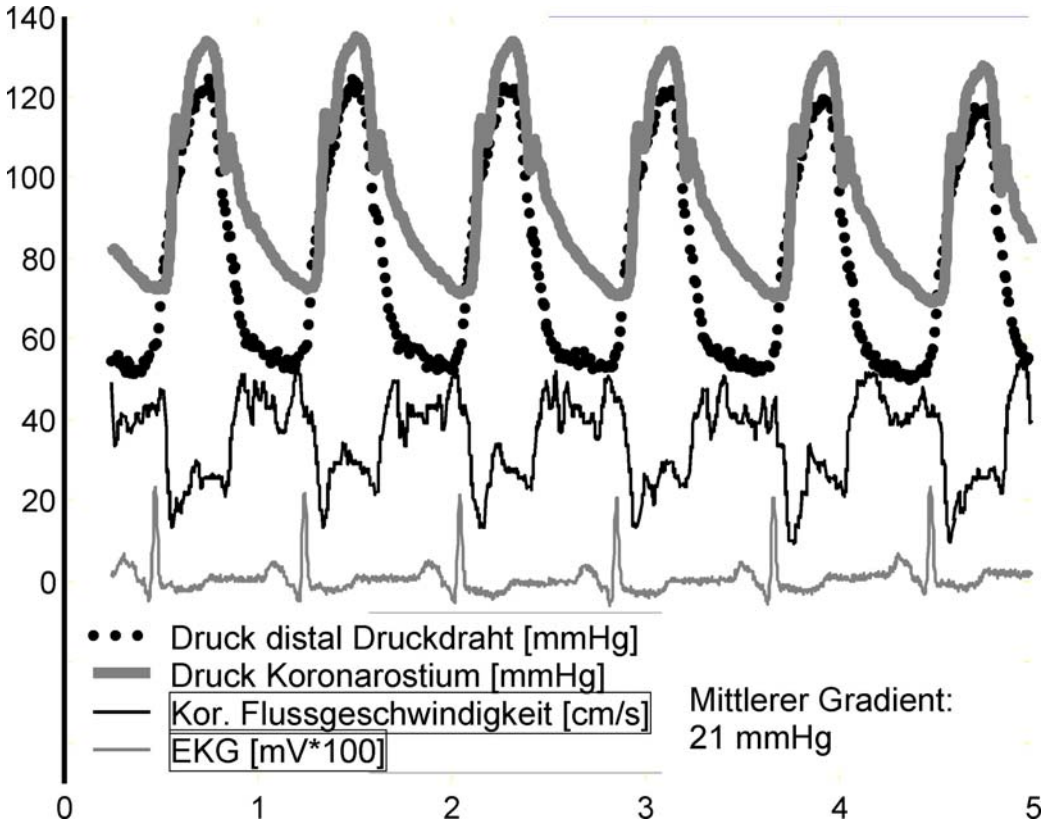

Abbildung 13: Beispiel hämodynamischer Eingangsparameter

Der Widerstand und damit der Druck am Ausgang der Endäste der sichtbaren Gefäße sind durch den intramyokardialen Druck bestimmt und variieren zwischen Systole und Diastole. Eine Messung mit einem Druckdraht distal einer hochgradigen Stenose demonstriert diesen gedämpften ventrikulären Druck (Abb. 13). Da dieser intramyokardiale dynamische Widerstand vor allem in der systolischen Phase auftritt, muss er bei instationären Simulationen wohl berücksichtigt werden. Bei unserer stationären Simulation über den Zyklus gemittelter Strömungen war es vertretbar ihn zu vernachlässigen.

Blut ist eine Nicht-Newton'sche Flüssigkeit, d.h. dass Zähigkeit (kinematische Viskosität) von der Scherrate abhängt. Diese Eigenschaft des Blutes wurde bisher nur in einer Modelluntersuchung (121) und in neuen noch nicht publizierten Simulationen (Abb. 14) berücksichtigt. Hier wurde das Blut als Nicht-Newton'sche Flüssigkeit mittels eines verallgemeinerten PotenzGesetzes simuliert (274) wobei Koeffizienten von Thurston et al. (275) verwendet wurden, die aus Datenanpassungen an rheologische Messungen im Blut unter pulsatilen Flussbedingungen stammen.

,

$$\mu = C \cdot \left(\mu_0 \cdot (1-H)^{-2.5} + \Delta\mu \cdot \exp\left(-\left(1 + \frac{\dot{\gamma}}{A} \right) \cdot \exp\left(-\frac{B}{\dot{\gamma}} \right) \right) \right)$$

wobei μ_0 = 0.0008585, $\Delta\mu$ = 0.00707, A = 67.916, B = 1.54, C = 1.056, $\dot{\gamma}$ = Scherrate und H = Hämatokrit ($0 < H < 1$). Die Parameter A, B und C sind berechnet für einen Hämatokrit von 40 % , eine Temperatur von 37°C und ein Gesamtprrotein minus Albumin (Fibrinogen und Globulin) von 27 g/l. Das Modell wurde modifiziert durch Einarbeitung der Abhängigkeit vom Hämatokrit nach Fung (276).

Die Viskoelastizität des Blutes wird dominiert durch die durch die Blutzellen gebildeten Mikrostrukturen. Die dynamische Deformierbarkeit der roten Blutzellen, ihr Aggregationsverhalten, die Zellkonzentration, die Gefäßgröße und die Flussrate sind die bestimmenden Einflussfaktoren. Viskoelastische Eigenschaften, Viskosität und Elastizität betreffen Speicherung und Verlust von Energie, wohingegen die Relaxationszeit und die Weissenbergzahl die relative Bedeutung der Elastizität bezogen auf die Viskosität beurteilen. Bei Simulationen in feinen Röhren und porösen Medien (Modell für kleine Gefäße mit vielen Seitenästen) tritt bei verminderter Viskosität möglicherweise ein Fåhraeus- Lindqvist Effekt auf, und bei hohen Scherraten entwickelt das Blut Dilatanz (277).

Für eine ausführliche aktuelle Diskussion unterschiedlicher Modelle der Modellierung der Blutviskosität darf auf die Literatur verwiesen werden (184;185;278).

Die geometrische Struktur ist der Haupteinflussfaktor auf die WSS (193). Lokale Information über die WSS wird durch unseren Ansatz etwas geglättet. Für das Studium der Korrelation zwischen WSS-Verteilung und der Entwicklung atherosklerotische Wandveränderungen wird der lokalen Genauigkeit große Bedeutung zugemessen. Strikt lokale "Point-to-Point" Korrelationen von WSS und Plaquedicke erwiesen sich jedoch als enttäuschend, während räumliche Mittelung bzw. Glättung der Daten in Strömungsrichtung überraschend gute Korrelationen aufwiesen. Dies

wird darauf zurückgeführt, dass es sich bei den Wandveränderungen um Prozesse mit Vorgeschichte handelt (55).

Wir konnten zeigen, dass einfache geometrische Vereinfachungen, wie die Annahme eines zirkulären Querschnitts und geringe Unterschiede der räumlichen Auflösung nur einen begrenzten Effekt auf die Strömungssimulation und die berechnete Wandschubspannung haben. Die Unterschiede der Wandschubsspannungswerte zwischen elliptischer und zirkulärer Querschnittsrekonstruktion waren 4.6% ±5.3% (maximal 14.3 %) (123). Dies ist zum Teil darauf zurückzuführen, dass die Lumina sogar in exzentrischen atherosklerotischen Läsionen im Rahmen des Remodelingprozesses dazu tendieren, zirkuläre oder elliptische Querschnitte mit nur geringem Unterschied der Halbachsen beizubehalten oder wiederauszubilden (279). Zudem wirkt die vena contracta als Folge der „no slip condition“ wie eine leichte Glättung. Der Rechenaufwand verringert sich durch diese Vereinfachungen aber erheblich. Das Verhältnis des erheblichen Zusatzaufwands für eine detailgenaue Querschnittsrekonstruktion in hoher Auflösung zum potentiellen klinischen Nutzen ist somit derzeit noch sehr groß. Weitere Verbesserungen im Bereich der Bildakquisition, der Rekonstruktionsalgorithmen und der Rechenleistung könnten allerdings dazu führen, dass sich dieser Aufwand erheblich reduziert und eine detailgenauere Rekonstruktion vorzuziehen wäre. Dies gilt insbesondere für die Untersuchung einzelner Läsionen im Verlauf.

Darüberhinaus verursacht die kontinuierliche und starke Bewegung der epikardialen Oberfläche eine permanente ortsabhängige Bewegung und Deformation der Gefäße. Unter den durch Bewegung der Herzoberfläche übertragenen Deformationen der Koronararterien gelten vor allem die Torsionen als Ursache von begrenzten Auswirkungen auf die lokale WSS. Krümmungen beeinflussen insbesondere im höheren Frequenzbereich Scherraten und WSS (189;190). Für über den Herzzyklus gemittelte Betrachtungen können diese Effekt vernachlässigt werden (191;191;193).

Die Annahme einer starren Wand liefert ausreichend genaue Ergebnisse für klinische Zwecke zum Studium der Athersoklerose (18;280). Die atherosklerotischen Wandveränderungen sind mit einer Erhöhung der Steifigkeit bzw. einer Annäherung an das „Starre Wand“ Model verbunden (183).

Die Pulsatilität hat nur geringe Auswirkung auf die WSS in Herzkranzarterien. Es wurden keine signifikanten Unterschiede zwischen “steady- state” und über den Herzzyklus gemittelten pulsatilen Simulationen gefunden (193;281). Die mittlere berechnete Womersleyzahl ist wegen der kleinen Gefäßradien der Koronargefäße sogar in den großen epikardialen Segmenten sehr niedrig (3.05±1.00, 117 eigene nicht publizierte Messungen). Da ein signifikanter Einfluss der Pulsatilität auf die WSS nur bei Womersleyzahlen wesentlich größer als 1 (cut-off : 5) zu erwarten ist (282), erscheint eine pulsatile Strömungssimulation im koronaren Gefäßbett nicht zwingend erforderlich. Das liegt daran, dass der Durchmesser der Gefäße sehr klein ist. Voll ausgebildete turbulente Strömung ist, trotz Diskussion in der Literatur (282), selbst in Koronargefäßen mit

hochgradigen Stenosen kaum zu erwarten, da die maximalen Reynoldszahlen wegen der kleinen Gefäßdurchmesser selbst in und hinter Stenosen sehr klein sind. Wir fanden mit intrakoronaren Flussgeschwindigkeitsmessungen und QCA Reynoldszahlen von 617±464 in stenosierten Koronarien (eigene nicht publizierte Messungen). Dies stimmt gut mit Werten aus der Literatur überein (283). Eine turbulente Strömung wäre mit erhöhter und isotroper WSS verbunden.

3.5. Limitationen und Anmerkungen

Ein möglicher Langzeiteffekt auch geringer in unserer Untersuchung nicht erfasster Abweichungen der lokalen WSS auf die Entwicklung atherosklerotischer Veränderungen über Jahre ist nicht auszuschließen, überschreiten aber den Horizont unserer Modelle. Neben der WSS, die unbestritten als das mechanische Signal gilt, das den Blutfluss mit adaptiven und pathologischen Gefäßwandveränderungen koppelt, werden weitere hier nicht näher untersuchte Parameter für wichtig gehalten. Das sind die zeitlichen und räumlichen WSS Gradienten (WSSG) (77;208) und der oszillatorische WSS Index (OSI) (23). Die Untersuchungen des OSI und des temporalen WSSG sind nur bei instationärer Modellierung der Koronarströmung im Herzzyklus möglich. Solche Untersuchungen sind sehr rechenaufwändig und sind derzeit deshalb nur in einer kleinen stratifizierten Stichprobe geplant. Der WSSG im Raum scheint die Zellproliferation nicht zu stimulieren (77;208) und korreliert im übrigen mit dem WSS, wie eigene unveröffentlichte Messungen zeigten.

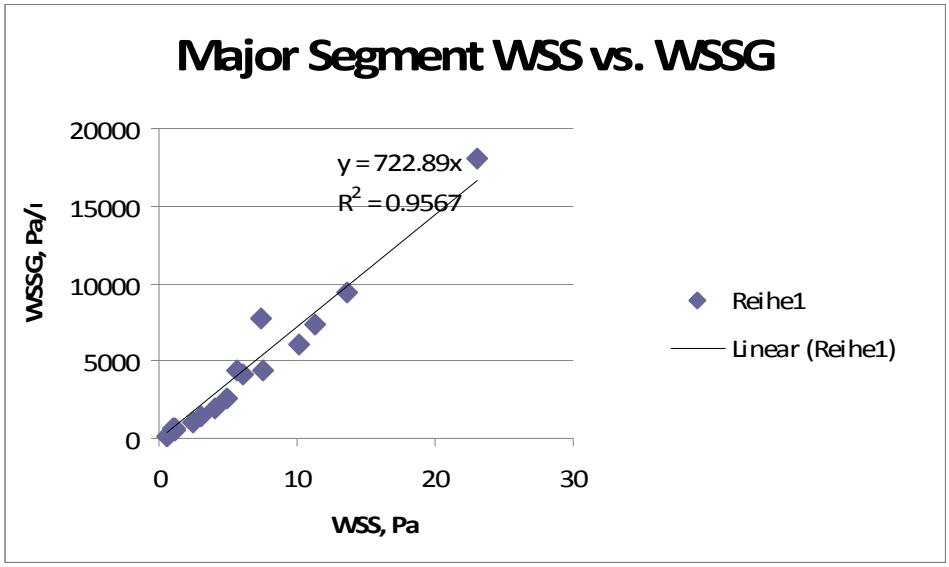

Abbildung 14: Korrelation zwischen WSS und WSSG

Allgemein sind die Limitationen unseres Ansatzes darin begründet,

- dass der immer noch erhebliche Aufwand dazu zwingt, 3-D Rekonstruktionen und Simulationen auf vereinfachte Modelle unter Berücksichtigung der wesentlichen Einflussgrößen zu beschränken,
- dass die Stichproben zwar stratifiziert aber immer noch sehr klein sind

- und weitere prospektive Evaluationen der entwickelten klinischen Charakteristika ausstehen.

3.6. Ausblick und Trends

Durch die rasante Entwicklung des CT (161;163;213), der Rotationsangiographie (171;172) und der kardialen Magnetresonanztomographie (164;213-215) hat sich die Entwicklung der 3-DRekonstruktion weitgehend in die F&E-Abteilungen der Großgerätehersteller und ihrer Softwarelieferanten verlagert. Kommerziell erhältliche Software, z. B. CAAS 5.2™ oder CardioOp-B™, erlaubt eine effiziente Konstruktion von koronaren 3-D Modellen aus Routinedaten und wird zu einer vermehrten klinischen Anwendung auf dem diagnostischen und interventionellen Sektor führen. Entwicklungen auf dem Sektor der nicht invasiven kardialen Bildgebung (Rotationsangiographie, CT and MRT) werden neue Geometriedatenquellen für Flusssimulationsstudien erschließen (10; 12; 13). Die zunehmende Leistung der Hardware und die Entwicklung auf dem Softwaresektor werden dazu führen, dass Flusssimulationen genauso wie virtuelle Endoskopie als professionelle Anwendertools unmittelbar für den Arzt zur Verfügung stehen werden (154;200).

4. Zusammenfassung

Die WSS ist ein zentraler Risikofaktor für Lokalisation und Entwicklung atherosklerotischer Veränderungen in den Herzkranzgefäßen. Dieser Risikofaktor ist in den Herzkranzgefäßen bis dato nicht direkt messbar, kann aber über Simulationsmodellstudien bewertet werden. Hierfür sind relativ aufwändige Strömungssimulationsstudien in 3-D Rekonstruktionen von Herzkranzgefäßen erforderlich. Entwicklungen der letzten Jahrzehnte in der 3-D Rekonstruktion und der Rechenleistung eröffnen die Perspektive eines Transfers der Beurteilung dieses Risikofaktors in die klinische Medizin (bench-to–bedside). Von besonderem Interesse ist hier der Blick auf ganze Koronarbäume und die Früherkennung und Verlaufsbeurteilung diffuser und früher Veränderungen der Geometrie und der Strömung.

Der Autor war an der Entwicklung der 3-D Rekonstruktion am DHZB beteiligt und hat die Methode klinisch validiert und in einer Verlaufsstudie das klinische Potential der 3 D- QCA zeigen können.

An unterschiedlichen Modellen und stratifizierten Stichproben hat der Autor Kriterien und Verfahren entwickelt, die zur Beurteilung der WSS im Hinblick auf klinische Fragestellungen bzgl. der Früherkennung und Verlaufsbeurteilung diffuser und früher Veränderungen der Geometrie und der Strömung geeignet sind.

Durch die rasante Entwicklung der Computertomographie, der Rotationsangiographie und der kardialen Magnetresonanztomographie hat sich die Entwicklung der 3-D Rekonstruktion weitgehend in die F&E -Abteilungen der Großgerätehersteller und ihrer Softwarelieferanten verlagert. Kommerziell erhältliche Software erlaubt eine effiziente Konstruktion von koronaren 3-D Modellen aus Routinedaten. Entwicklungen auf dem Sektor der nicht invasiven kardialen Bildgebung (Rotationsangiographie, CT und MRT) werden neue Geometriedatenquellen für Flusssimulationsstudien erschließen. Die zunehmende Rechenleistung der Hardware und die Entwicklung auf dem Softwaresektor werden dazu führen, dass Flusssimulationen genau wie virtuelle Endoskopie als professionelle Anwendertools unmittelbar dem Arzt zur Verfügung stehen und den Risikofaktor WSS für die klinische Medizin bereitstellen.

5. Literatur

(1) Charytan D, Kuntz RE, Mauri L, DeFilippi C. Distribution of coronary artery disease and relation to mortality in asymptomatic hemodialysis patients. Am J Kidney Dis 2007 March;49(3):409-16.

(2) el Fawal MA, Berg GA, Wheatley DJ, Harland WA. Sudden coronary death in Glasgow: the severity and distribution of chronic coronary atherosclerotic stenoses. Br Heart J 1987 May;57(5):420-6.

(3) Hochman JS, Phillips WJ, Ruggieri D, Ryan SF. The distribution of atherosclerotic lesions in the coronary arterial tree: relation to cardiac risk factors. Am Heart J 1988 November;116(5 Pt 1):1217-22.

(4) Jost S, Deckers JW, Nikutta P, Rafflenbeul W, Wiese B, Hecker H, Lippolt P, Lichtlen PR. Progression of coronary artery disease is dependent on anatomic location and diameter. The INTACT investigators. J Am Coll Cardiol 1993 May;21(6):1339-46.

(5) Spaan JAE. Basic coronary physiology. In: Spaan JAE, editor. Coronary Blood Flow - Mechanics, Distribution, and Control. 1 ed. Dordrecht: Kluwer Academic Publishers; 1991. p. 2.

(6) Spaan JAE. Water balance within the myocardium. In: Spaan JAE, editor. Coronary Blood Flow - Mechanics, Distribution, and Control. 1 ed. Dordrecht: Kluwer Academic Publishers; 1991. p. 276.

(7) Spaan JAE. Capillary density and volume. In: Spaan JAE, editor. Coronary Blood Flow - Mechanics, Distribution, and Control. 1 ed. Dordrecht: Kluwer Academic Publishers; 1991. p. 70.

(8) Chatzizisis YS, Coskun AU, Jonas M, Edelman ER, Feldman CL, Stone PH. Role of endothelial shear stress in the natural history of coronary atherosclerosis and vascular remodeling: molecular, cellular, and vascular behavior. J Am Coll Cardiol 2007 June 26;49(25):2379-93.

(9) Leung WH, Stadius ML, Alderman ED. Determinants of Normal Coronary Artery Dimensions in Humans. Circulation 1991;84:2294-306.

(10) Lewis BS, Gotsman MS. Relation between coronary artery size and left ventricular wall mass. Br Heart J 1973;35:1150-3.

(11) Seiler C, Kirkeeide RL, Gould KL. Basic structure-function relations of the epicardial coronary vascular tree. Basis of quantitative coronary arteriography for diffuse coronary artery disease. Circulation 1992 June;85(6):1987-2003.

(12) Ben Driss A, Benessiano J, Poitevin P, Levy BI, Michel JB. Arterial expansive remodeling induced by high flow rates. Am J Physiol 1997 February;272(2 Pt 2):H851-H858.

(13) Cines DB, Pollak ES, Buck CA, Loscalzo J, Zimmerman GA, McEver RP, Pober JS, Wick TM, Konkle BA, Schwartz BS, Barnathan ES, McCrae KR, Hug BA, Schmidt A-M, Stern DM. Endothelial Cells in Physiology and in the Pathophysiology of Vascular Disorders. Blood 1998;91:3527-61.

(14) Hayden MR, Tyagi SC. Arterial vascular remodeling: the endothelial cell's central role. Mo Med 1998 May;95(5):213-7.

(15) Kamiya A, Togawa T. Adaptive regulation of wall shear stress to flow change in the canine carotid artery. Am J Physiol 1980;239:H14-H21.

(16) Langille BL, O'Donnell F. Reductions in arterial Diameter Produced by Chronic Decreases in Blood Flow are Endothelium -Dependent. Science 1986;231:405-7.

(17) Langille BL. Arterial remodeling: relation to hemodynamics. Can J Physiol Pharmacol 1996 July;74(7):834-41.

(18) Katritsis D, Kaiktsis L, Chaniotis A, Pantos J, Efstathopoulos EP, Marmarelis V. Wall shear stress: theoretical considerations and methods of measurement. Prog Cardiovasc Dis 2007 March;49(5):307-29.

(19) Cheng C, Helderman F, Tempel D, Segers D, Hierck B, Poelmann R, van TA, Duncker DJ, Robbers-Visser D, Ursem NT, van HR, Wentzel JJ, Gijsen F, van der Steen AF, de CR, Krams R. Large variations in absolute wall shear stress levels within one species and between species. Atherosclerosis 2007 December;195(2):225-35.

(20) Malek AM, Alper SL, Izumo S. Hemodynamic shear stress and its role in atherosclerosis. JAMA 1999 December 1;282(21):2035-42.

(21) Stone PH, Coskun AU, Kinlay S, Clark ME, Sonka M, Wahle A, Ilegbusi OJ, Yeghiazarians Y, Popma JJ, Orav J, Kuntz RE, Feldman CL. Effect of endothelial shear stress on the progression of coronary artery disease, vascular remodeling, and in-stent restenosis in humans: in vivo 6-month follow-up study. Circulation 2003 July 29;108(4):438-44.

(22) Wentzel JJ, Krams R, Schuurbiers JC, Oomen JA, Kloet J, van der Giessen WJ, Serruys PW, Slager CJ. Relationship between neointimal thickness and shear stress after Wallstent implantation in human coronary arteries. Circulation 2001 April 3;103(13):1740-5.

(23) Ku DN, Giddens DP, Zarins CK, Glagov S. Pulsatile flow and atherosclerosis in the human carotid bifurcation. Positive correlation between plaque location and low oscillating shear stress. Arteriosclerosis 1985 May;5(3):293-302.

(24) Orr AW, Helmke BP, Blackman BR, Schwartz MA. Mechanisms of mechanotransduction. Dev Cell 2006 January;10(1):11-20.

(25) Barakat AI. Responsiveness of vascular endothelium to shear stress: potential role of ion channels and cellular cytoskeleton (review). Int J Mol Med 1999 October;4(4):323-32.

(26) Liu Y, Chen BP, Lu M, Zhu Y, Stemerman MB, Chien S, Shyy JY. Shear stress activation of SREBP1 in endothelial cells is mediated by integrins. Arterioscler Thromb Vasc Biol 2002 January;22(1):76-81.

(27) Liu Y, Sweet DT, Irani-Tehrani M, Maeda N, Tzima E. Shc coordinates signals from intercellular junctions and integrins to regulate flow-induced inflammation. J Cell Biol 2008 July 14;182(1):185-96.

(28) Tzima E, del Pozo MA, Shattil SJ, Chien S, Schwartz MA. Activation of integrins in endothelial cells by fluid shear stress mediates Rho-dependent cytoskeletal alignment. EMBO J 2001 September 3;20(17):4639-47.

(29) Tzima E, Irani-Tehrani M, Kiosses WB, Dejana E, Schultz DA, Engelhardt B, Cao G, DeLisser H, Schwartz MA. A mechanosensory complex that mediates the endothelial cell response to fluid shear stress. Nature 2005 September 15;437(7057):426-31.

(30) Katsumi A, Orr AW, Tzima E, Schwartz MA. Integrins in mechanotransduction. J Biol Chem 2004 March 26;279(13):12001-4.

(31) Puklin-Faucher E, Sheetz MP. The mechanical integrin cycle. J Cell Sci 2009 January 15;122(Pt 2):179-86.

(32) Schwartz MA, DeSimone DW. Cell adhesion receptors in mechanotransduction. Curr Opin Cell Biol 2008 October;20(5):551-6.

(33) Tarbell JM, Pahakis MY. Mechanotransduction and the glycocalyx. J Intern Med 2006 April;259(4):339-50.

(34) Chien S. Molecular basis of rheological modulation of endothelial functions: importance of stress direction. Biorheology 2006;43(2):95-116.

(35) del Alamo JC, Norwich GN, Li YS, Lasheras JC, Chien S. Anisotropic rheology and directional mechanotransduction in vascular endothelial cells. Proc Natl Acad Sci U S A 2008 October 7;105(40):15411-6.

(36) Castier Y, Brandes RP, Leseche G, Tedgui A, Lehoux S. p47phox-dependent NADPH oxidase regulates flow-induced vascular remodeling. Circ Res 2005 September 16;97(6):533-40.

(37) Li YS, Haga JH, Chien S. Molecular basis of the effects of shear stress on vascular endothelial cells. J Biomech 2005 October;38(10):1949-71.

(38) Tzima E. Role of small GTPases in endothelial cytoskeletal dynamics and the shear stress response. Circ Res 2006 February 3;98(2):176-85.

(39) Chiu JJ, Chen CN, Lee PL, Yang CT, Chuang HS, Chien S, Usami S. Analysis of the effect of disturbed flow on monocytic adhesion to endothelial cells. J Biomech 2003 December;36(12):1883-95.

(40) Longest PW, Kleinstreuer C, Truskey GA, Buchanan JR. Relation between near-wall residence times of monocytes and early lesion growth in the rabbit aorto-celiac junction. Ann Biomed Eng 2003 January;31(1):53-64.

(41) Asakura T, Karino T. Flow patterns and spatial distribution of atherosclerotic lesions in human coronary arteries. Circ Res 1990 April;66(4):1045-66.

(42) Buchanan JR, Kleinstreuer C, Hyun S, Truskey GA. Hemodynamics simulation and identification of susceptible sites of atherosclerotic lesion formation in a model abdominal aorta. J Biomech 2003 August;36(8):1185-96.

(43) Chatzizisis YS, Coskun AU, Jonas M, Edelman ER, Stone PH, Feldman CL. Risk stratification of individual coronary lesions using local endothelial shear stress: a new paradigm for managing coronary artery disease. Curr Opin Cardiol 2007 November;22(6):552-64.

(44) Chatzizisis YS, Jonas M, Coskun AU, Beigel R, Stone BV, Maynard C, Gerrity RG, Daley W, Rogers C, Edelman ER, Feldman CL, Stone PH. Prediction of the localization of high-risk coronary atherosclerotic plaques on the basis of low endothelial shear stress: an intravascular ultrasound and histopathology natural history study. Circulation 2008 February 26;117(8):993-1002.

(45) Cheng C, Tempel D, van HR, van der BA, Grosveld F, Daemen MJ, Krams R, de CR. Atherosclerotic lesion size and vulnerability are determined by patterns of fluid shear stress. Circulation 2006 June 13;113(23):2744-53.

(46) Cunningham KS, Gotlieb AI. The role of shear stress in the pathogenesis of atherosclerosis. Lab Invest 2005 January;85(1):9-23.

(47) Krams R, Wentzel JJ, Oomen JA, Vinke R, Schuurbiers JC, de Feyter PJ, Serruys PW, Slager CJ. Evaluation of endothelial shear stress and 3D geometry as factors determining the development of atherosclerosis and remodeling in human coronary arteries in vivo. Combining 3D reconstruction from angiography and IVUS (ANGUS) with computational fluid dynamics. Arterioscler Thromb Vasc Biol 1997 October;17(10):2061-5.

(48) Rybicki FJ, Melchionna S, Mitsouras D, Coskun AU, Whitmore AG, Steigner M, Nallamshetty L, Welt FG, Bernaschi M, Borkin M, Sircar J, Kaxiras E, Succi S, Stone PH, Feldman CL. Prediction of coronary artery plaque progression and potential rupture from 320-detector row prospectively ECG-gated single heart beat CT angiography: Lattice Boltzmann evaluation of endothelial shear stress. Int J Cardiovasc Imaging 2009 January 15;25:289-99.

(49) Slager CJ, Wentzel JJ, Gijsen FJ, Schuurbiers JC, van der Wal AC, van der Steen AF, Serruys PW. The role of shear stress in the generation of rupture-prone vulnerable plaques. Nat Clin Pract Cardiovasc Med 2005 August;2(8):401-7.

(50) Slager CJ, Wentzel JJ, Gijsen FJ, Thury A, van der Wal AC, Schaar JA, Serruys PW. The role of shear stress in the destabilization of vulnerable plaques and related therapeutic implications. Nat Clin Pract Cardiovasc Med 2005 September;2(9):456-64.

(51) Stone PH, Coskun AU, Kinlay S, Popma JJ, Sonka M, Wahle A, Yeghiazarians Y, Maynard C, Kuntz RE, Feldman CL. Regions of low endothelial shear stress are the sites where coronary plaque progresses and vascular remodelling occurs in humans: an in vivo serial study. Eur Heart J 2007 March;28(6):705-10.

(52) Suo J, Oshinski JN, Giddens DP. Blood flow patterns in the proximal human coronary arteries: relationship to atherosclerotic plaque occurrence. Mol Cell Biomech 2008 March;5(1):9-18.

(53) van der Giessen AG, Wentzel JJ, Meijboom WB, Mollet NR, van der Steen AF, van d, V, de Feyter PJ, Gijsen FJ. Plaque and shear stress distribution in human coronary bifurcations: a multislice computed tomography study. EuroIntervention 2009 March;4(5):654-61.

(54) Wellnhofer E, Goubergrits L, Kertzscher U, Affeld K, Fleck E. Novel non-dimensional approach to comparison of wall shear stress distributions in coronary arteries of different groups of patients. Atherosclerosis 2009 February;202(2):483-90.

(55) Wentzel JJ, Gijsen FJ, Schuurbiers JC, Krams R, Serruys PW, de Feyter PJ, Slager CJ. Geometry guided data averaging enables the interpretation of shear stress related plaque development in human coronary arteries. J Biomech 2005 July;38(7):1551-5.

(56) Brooks AR, Lelkes PI, Rubanyi GM. Gene expression profiling of vascular endothelial cells exposed to fluid mechanical forces: relevance for focal susceptibility to atherosclerosis. Endothelium 2004 January;11(1):45-57.

(57) Davies PF, Barbee KA, Volin MV, Robotewskyj A, Chen J, Joseph L, Griem ML, Wernick MN, Jacobs E, Polacek DC, dePaola N, Barakat AI. Spatial relationships in early signaling events of flow-mediated endothelial mechanotransduction. Annu Rev Physiol 1997;59:527-49.:527-49.

(58) Brooks AR, Lelkes PI, Rubanyi GM. Gene expression profiling of human aortic endothelial cells exposed to disturbed flow and steady laminar flow. Physiol Genomics 2002;9(1):27-41.

(59) Dai G, Kaazempur-Mofrad MR, Natarajan S, Zhang Y, Vaughn S, Blackman BR, Kamm RD, Garcia-Cardena G, Gimbrone MA, Jr. Distinct endothelial phenotypes evoked by arterial waveforms derived from atherosclerosis-susceptible and -resistant regions of human vasculature. Proc Natl Acad Sci U S A 2004 October 12;101(41):14871-6.

(60) Gimbrone MA, Jr., Topper JN, Nagel T, Anderson KR, Garcia-Cardena G. Endothelial dysfunction, hemodynamic forces, and atherogenesis. Ann N Y Acad Sci 2000 May;902:230-9; discussion 239-40.:230-9.

(61) Resnick N, Yahav H, Shay-Salit A, Shushy M, Schubert S, Zilberman LC, Wofovitz E. Fluid shear stress and the vascular endothelium: for better and for worse. Prog Biophys Mol Biol 2003 April;81(3):177-99.

(62) Resnick N, Einav S, Chen-Konak L, Zilberman M, Yahav H, Shay-Salit A. Hemodynamic forces as a stimulus for arteriogenesis. Endothelium 2003;10(4-5):197-206.

(63) Harrison DG, Widder J, Grumbach I, Chen W, Weber M, Searles C. Endothelial mechanotransduction, nitric oxide and vascular inflammation. J Intern Med 2006 April;259(4):351-63.

(64) Lam CF, Peterson TE, Richardson DM, Croatt AJ, d'Uscio LV, Nath KA, Katusic ZS. Increased blood flow causes coordinated upregulation of arterial eNOS and biosynthesis of tetrahydrobiopterin. Am J Physiol Heart Circ Physiol 2006 February;290(2):H786-H793.

(65) Go YM, Boo YC, Park H, Maland MC, Patel R, Pritchard KA, Jr., Fujio Y, Walsh K, rley-Usmar V, Jo H. Protein kinase B/Akt activates c-Jun NH(2)-terminal kinase by increasing NO production in response to shear stress. J Appl Physiol 2001 October;91(4):1574-81.

(66) Cheng C, van HR, de WM, van Damme LC, Tempel D, Hanemaaijer L, van Cappellen GW, Bos J, Slager CJ, Duncker DJ, van der Steen AF, de CR, Krams R. Shear stress affects the intracellular distribution of eNOS: direct demonstration by a novel in vivo technique. Blood 2005 December 1;106(12):3691-8.

(67) Gambillara V, Chambaz C, Montorzi G, Roy S, Stergiopulos N, Silacci P. Plaque-prone hemodynamics impair endothelial function in pig carotid arteries. Am J Physiol Heart Circ Physiol 2006 June;290(6):H2320-H2328.

(68) Qiu Y, Tarbell JM. Interaction between wall shear stress and circumferential strain affects endothelial cell biochemical production. J Vasc Res 2000 May;37(3):147-57.

(69) Ziegler T, Bouzourene K, Harrison VJ, Brunner HR, Hayoz D. Influence of oscillatory and unidirectional flow environments on the expression of endothelin and nitric oxide synthase in cultured endothelial cells. Arterioscler Thromb Vasc Biol 1998 May;18(5):686-92.

(70) Chien S. Molecular and mechanical bases of focal lipid accumulation in arterial wall. Prog Biophys Mol Biol 2003 October;83(2):131-51.

(71) Yeh M, Cole AL, Choi J, Liu Y, Tulchinsky D, Qiao JH, Fishbein MC, Dooley AN, Hovnanian T, Mouilleseaux K, Vora DK, Yang WP, Gargalovic P, Kirchgessner T, Shyy JY, Berliner JA. Role for sterol regulatory element-binding protein in activation of endothelial cells by phospholipid oxidation products. Circ Res 2004 October 15;95(8):780-8.

(72) Buchanan JR, Jr., Kleinstreuer C, Truskey GA, Lei M. Relation between non-uniform hemodynamics and sites of altered permeability and lesion growth at the rabbit aorto-celiac junction. Atherosclerosis 1999 March;143(1):27-40.

(73) Himburg HA, Grzybowski DM, Hazel AL, LaMack JA, Li XM, Friedman MH. Spatial comparison between wall shear stress measures and porcine arterial endothelial permeability. Am J Physiol Heart Circ Physiol 2004 May;286(5):H1916-H1922.

(74) Traub O, Berk BC. Laminar shear stress: mechanisms by which endothelial cells transduce an atheroprotective force. Arterioscler Thromb Vasc Biol 1998 May;18(5):677-85.

(75) Chen YL, Jan KM, Lin HS, Chien S. Ultrastructural studies on macromolecular permeability in relation to endothelial cell turnover. Atherosclerosis 1995 November;118(1):89-104.

(76) Tricot O, Mallat Z, Heymes C, Belmin J, Leseche G, Tedgui A. Relation between endothelial cell apoptosis and blood flow direction in human atherosclerotic plaques. Circulation 2000 May 30;101(21):2450-3.

(77) White CR, Haidekker M, Bao X, Frangos JA. Temporal gradients in shear, but not spatial gradients, stimulate endothelial cell proliferation. Circulation 2001 May 22;103(20):2508-13.

(78) Feldman CL, Ilegbusi OJ, Hu Z, Nesto R, Waxman S, Stone PH. Determination of in vivo velocity and endothelial shear stress patterns with phasic flow in human coronary arteries: a methodology to predict progression of coronary atherosclerosis. Am Heart J 2002 June;143(6):931-9.

(79) Hwang J, Ing MH, Salazar A, Lassegue B, Griendling K, Navab M, Sevanian A, Hsiai TK. Pulsatile versus oscillatory shear stress regulates NADPH oxidase subunit expression: implication for native LDL oxidation. Circ Res 2003 December 12;93(12):1225-32.

(80) Hwang J, Saha A, Boo YC, Sorescu GP, McNally JS, Holland SM, Dikalov S, Giddens DP, Griendling KK, Harrison DG, Jo H. Oscillatory shear stress stimulates endothelial production of O2- from p47phox-dependent NAD(P)H oxidases, leading to monocyte adhesion. J Biol Chem 2003 November 21;278(47):47291-8.

(81) McNally JS, Davis ME, Giddens DP, Saha A, Hwang J, Dikalov S, Jo H, Harrison DG. Role of xanthine oxidoreductase and NAD(P)H oxidase in endothelial superoxide production in response to oscillatory shear stress. Am J Physiol Heart Circ Physiol 2003 December;285(6):H2290-H2297.

(82) Mueller CF, Widder JD, McNally JS, McCann L, Jones DP, Harrison DG. The role of the multidrug resistance protein-1 in modulation of endothelial cell oxidative stress. Circ Res 2005 September 30;97(7):637-44.

(83) Collins T, Cybulsky MI. NF-kappaB: pivotal mediator or innocent bystander in atherogenesis? J Clin Invest 2001 February;107(3):255-64.

(84) Hsiai TK, Cho SK, Wong PK, Ing M, Salazar A, Sevanian A, Navab M, Demer LL, Ho CM. Monocyte recruitment to endothelial cells in response to oscillatory shear stress. FASEB J 2003 September;17(12):1648-57.

(85) Mohan S, Hamuro M, Sorescu GP, Koyoma K, Sprague EA, Jo H, Valente AJ, Prihoda TJ, Natarajan M. IkappaBalpha-dependent regulation of low-shear flow-induced NF-kappa B activity: role of nitric oxide. Am J Physiol Cell Physiol 2003 April;284(4):C1039-C1047.

(86) Nagel T, Resnick N, Dewey CF, Jr., Gimbrone MA, Jr. Vascular endothelial cells respond to spatial gradients in fluid shear stress by enhanced activation of transcription factors. Arterioscler Thromb Vasc Biol 1999 August;19(8):1825-34.

(87) Orr AW, Sanders JM, Bevard M, Coleman E, Sarembock IJ, Schwartz MA. The subendothelial extracellular matrix modulates NF-kappaB activation by flow: a potential role in atherosclerosis. J Cell Biol 2005 April 11;169(1):191-202.

(88) Conklin BS, Zhong DS, Zhao W, Lin PH, Chen C. Shear stress regulates occludin and VEGF expression in porcine arterial endothelial cells. J Surg Res 2002 January;102(1):13-21.

(89) Palumbo R, Gaetano C, Antonini A, Pompilio G, Bracco E, Ronnstrand L, Heldin CH, Capogrossi MC. Different effects of high and low shear stress on platelet-derived growth factor isoform release by endothelial cells: consequences for smooth muscle cell migration. Arterioscler Thromb Vasc Biol 2002 March 1;22(3):405-11.

(90) Ross R. Atherosclerosis--an inflammatory disease. N Engl J Med 1999 January 14;340(2):115-26.

(91) Gambillara V, Montorzi G, Haziza-Pigeon C, Stergiopulos N, Silacci P. Arterial wall response to ex vivo exposure to oscillatory shear stress. J Vasc Res 2005 November;42(6):535-44.

(92) Jones GT, Jiang F, McCormick SP, Dusting GJ. Elastic lamina defects are an early feature of aortic lesions in the apolipoprotein E knockout mouse. J Vasc Res 2005 May;42(3):237-46.

(93) Sukhova GK, Wang B, Libby P, Pan JH, Zhang Y, Grubb A, Fang K, Chapman HA, Shi GP. Cystatin C deficiency increases elastic lamina degradation and aortic dilatation in apolipoprotein E-null mice. Circ Res 2005 February 18;96(3):368-75.

(94) Bassiouny HS, Song RH, Hong XF, Singh A, Kocharyan H, Glagov S. Flow regulation of 72-kD collagenase IV (MMP-2) after experimental arterial injury. Circulation 1998 July 14;98(2):157-63.

(95) Magid R, Murphy TJ, Galis ZS. Expression of matrix metalloproteinase-9 in endothelial cells is differentially regulated by shear stress. Role of c-Myc. J Biol Chem 2003 August 29;278(35):32994-9.

(96) Choudhary S, Higgins CL, Chen IY, Reardon M, Lawrie G, Vick GW, III, Karmonik C, Via DP, Morrisett JD. Quantitation and localization of matrix metalloproteinases and their inhibitors in human carotid endarterectomy tissues. Arterioscler Thromb Vasc Biol 2006 October;26(10):2351-8.

(97) Galis ZS, Sukhova GK, Lark MW, Libby P. Increased expression of matrix metalloproteinases and matrix degrading activity in vulnerable regions of human atherosclerotic plaques. J Clin Invest 1994 December;94(6):2493-503.

(98) Galis ZS, Khatri JJ. Matrix metalloproteinases in vascular remodeling and atherogenesis: the good, the bad, and the ugly. Circ Res 2002 February 22;90(3):251-62.

(99) de Nooijer R, Verkleij CJ, von der Thusen JH, Jukema JW, van der Wall EE, van Berkel TJ, Baker AH, Biessen EA. Lesional overexpression of matrix metalloproteinase-9 promotes intraplaque hemorrhage in advanced lesions but not at earlier stages of atherogenesis. Arterioscler Thromb Vasc Biol 2006 February;26(2):340-6.

(100) Galis ZS. Vulnerable plaque: the devil is in the details. Circulation 2004 July;110(3):244-6.

(101) Tousoulis D, Antoniades C, Koumallos N, Stefanadis C. Pro-inflammatory cytokines in acute coronary syndromes: from bench to bedside. Cytokine Growth Factor Rev 2006 August;17(4):225-33.

(102) Xu Y, Wang L, Buttice G, Sengupta PK, Smith BD. Interferon gamma repression of collagen (COL1A2) transcription is mediated by the RFX5 complex. J Biol Chem 2003 December 5;278(49):49134-44.

(103) Rosner D, Stoneman V, Littlewood T, McCarthy N, Figg N, Wang Y, Tellides G, Bennett M. Interferon-gamma induces Fas trafficking and sensitization to apoptosis in vascular smooth muscle cells via a PI3K- and Akt-dependent mechanism. Am J Pathol 2006 June;168(6):2054-63.

(104) Um HD, Orenstein JM, Wahl SM. Fas mediates apoptosis in human monocytes by a reactive oxygen intermediate dependent pathway. J Immunol 1996 May 1;156(9):3469-77.

(105) Lutgens E, Gijbels M, Smook M, Heeringa P, Gotwals P, Koteliansky VE, Daemen MJ. Transforming growth factor-beta mediates balance between inflammation and fibrosis during plaque progression. Arterioscler Thromb Vasc Biol 2002 June 1;22(6):975-82.

(106) Shao JS, Cai J, Towler DA. Molecular mechanisms of vascular calcification: lessons learned from the aorta. Arterioscler Thromb Vasc Biol 2006 July;26(7):1423-30.

(107) Sorescu GP, Song H, Tressel SL, Hwang J, Dikalov S, Smith DA, Boyd NL, Platt MO, Lassegue B, Griendling KK, Jo H. Bone morphogenic protein 4 produced in endothelial cells by oscillatory shear stress induces monocyte adhesion by stimulating reactive oxygen species production from a nox1-based NADPH oxidase. Circ Res 2004 October 15;95(8):773-9.

(108) Waxman S, Ishibashi F, Muller JE. Detection and treatment of vulnerable plaques and vulnerable patients: novel approaches to prevention of coronary events. Circulation 2006 November 28;114(22):2390-411.

(109) Glagov S, Zarins C, Giddens DP, Ku DN. Hemodynamics and atherosclerosis. Insights and perspectives gained from studies of human arteries. Arch Pathol Lab Med 1988 October;112(10):1018-31.

(110) Feldman CL, Coskun AU, Yeghiazarians Y, Kinlay S, Wahle A, Olszewski ME, Rossen JD, Sonka M, Popma JJ, Orav J, Kuntz RE, Stone PH. Remodeling characteristics of minimally diseased coronary arteries are consistent along the length of the artery. Am J Cardiol 2006 January 1;97(1):13-6.

(111) Sipahi I, Tuzcu EM, Schoenhagen P, Nicholls SJ, Crowe T, Kapadia S, Nissen SE. Static and serial assessments of coronary arterial remodeling are discordant: an intravascular ultrasound analysis from the Reversal of Atherosclerosis with Aggressive Lipid Lowering (REVERSAL) trial. Am Heart J 2006 September;152(3):544-50.

(112) Wentzel JJ, Janssen E, Vos J, Schuurbiers JC, Krams R, Serruys PW, de Feyter PJ, Slager CJ. Extension of increased atherosclerotic wall thickness into high shear stress regions is associated with loss of compensatory remodeling. Circulation 2003 July 8;108(1):17-23.

(113) Virmani R, Kolodgie FD, Burke AP, Farb A, Schwartz SM. Lessons from sudden coronary death: a comprehensive morphological classification scheme for atherosclerotic lesions. Arterioscler Thromb Vasc Biol 2000 May;20(5):1262-75.

(114) Feldman CL, Stone PH. Intravascular hemodynamic factors responsible for progression of coronary atherosclerosis and development of vulnerable plaque. Curr Opin Cardiol 2000 November;15(6):430-40.

(115) Fukumoto Y, Hiro T, Fujii T, Hashimoto G, Fujimura T, Yamada J, Okamura T, Matsuzaki M. Localized elevation of shear stress is related to coronary plaque rupture: a 3-dimensional intravascular ultrasound study with in-vivo color mapping of shear stress distribution. J Am Coll Cardiol 2008 February 12;51(6):645-50.

(116) Groen HC, Gijsen FJ, van der LA, Ferguson MS, Hatsukami TS, Yuan C, van der Steen AF, Wentzel JJ. High shear stress influences plaque vulnerability Part of the data presented in this paper were published in Stroke 2007;38:2379-81. Neth Heart J 2008 August;16(7-8):280-3.

(117) Schoenhagen P, Ziada KM, Vince DG, Nissen SE, Tuzcu EM. Arterial remodeling and coronary artery disease: the concept of "dilated" versus "obstructive" coronary atherosclerosis. J Am Coll Cardiol 2001 August;38(2):297-306.

(118) Antoniadis AP, Chatzizisis YS, Giannoglou GD. Pathogenetic mechanisms of coronary ectasia. Int J Cardiol 2008 November 28;130(3):335-43.

(119) Hartnell GG, Parnell BM, Pridie RB. Coronary artery ectasia. Its prevalence and clinical significance in 4993 patients. Br Heart J 1985;54:392-5.

(120) Wellnhofer E, Mugaragu I, Wahle A, Oswald H, Fleck E. Diffuse Diease & Fractal Properties of Coronary Trees- A 3-dimensional Study. JACC 27 Suppl. A, 351 A. 1996. (Abstract)

(121) Wellnhofer E, Bocksch W, Hiemann N, Dandel M, Klimek W, Hetzer R, Fleck E. Shear stress and vascular remodeling: study of cardiac allograft coronary artery disease as a model of diffuse atherosclerosis. J Heart Lung Transplant 2002 April;21(4):405-16.

(122) Wellnhofer E, Wahle A, Fleck E. Progression of coronary atherosclerosis quantified by analysis of 3-D reconstruction of left coronary arteries. Atherosclerosis 2002 February;160(2):483-93.

(123) Wellnhofer E, Goubergrits L, Kertzscher U, Affeld K. In-vivo coronary flow profiling based on biplane angiograms: influence of geometric simplifications on the three-dimensional reconstruction and wall shear stress calculation. Biomed Eng Online 2006 June 14;5:39.:39.

(124) Zamir M. On fractal properties of arterial trees. J Theor Biol 1999 April 21;197(4):517-26.

(125) Wahle A, Wellnhofer E, Mugaragu I, Sauer HU, Oswald H, Fleck E. Assessment of Diffuse Coronary Artery by Quantitative Analysis of Coronary Morphology Based upon 3-D Reconstruction from Biplane Angiograms. IEEE Transactions on Medical Imaging 1995;14(No. 2):230-41.

(126) Weibel ER. Morphometry of the Human Lung. Academic Press; 1963.

(127) Strahler AN. Hypsometric (area altitude) analysis of erosional topology. Bull Geol Soc Amer 1952;63:1117-42.

(128) Kassab GS, Rider CA, Tang NT, Fung Y-C. Morphometry of pig coronary arterial trees. Am J Physiol 1993;265:H350-H365.

(129) Wahle A, Wellnhofer E, Mugaragu I, Sauer HU, Oswald H, Fleck E. Quantitative volume analysis of coronary vessel systems by 3-D recontruction from biplane angiograms. San Francisco, C.A. 1993 p. 1217-21.

(130) Molloi S, Wong JT. Regional blood flow analysis and its relationship with arterial branch lengths and lumen volume in the coronary arterial tree. Phys Med Biol 2007 March 7;52(5):1495-503.

(131) Kassab GS. Scaling Laws of Vascular Trees: Of Form and Function. Am J Physiol Heart Circ Physiol 2005 September 2;.

(132) Dietz U, Rupprecht HJ, Brennecke R, Fritsch HP, Woltmann J, Blankenberg S, Meyer J. Comparison of QCA systems. Int J Card Imaging 1997 August;13(4):271-80.

(133) Hausleiter J, Jost S, Nolte CW, Dirschinger J, Kastrati A, Stiel GM, Wunderlich W, Fischer F, Linderer T, Hausmann D, Schomig A. Comparative in-vitro validation of eight first- and second-generation quantitative coronary angiography systems. Coron Artery Dis 1997 February;8(2):83-90.

(134) Keane D, Haase J, Slager CJ, Montauban vS, Lehmann KG, Ozaki Y, Di MC, Kirkeeide R, Serruys PW. Comparative validation of quantitative coronary angiography systems. Results and implications from a multicenter study using a standardized approach. Circulation 1995 April 15;91(8):2174-83.

(135) Muhlestein JB, Zhang Q, Parker DJ, Horn SD, Parker DL, Anderson JL. A comparison of the accuracy and reproducibility of digital three-dimensional coronary artery reconstructions using edge detection or videodensitometry. Comput Biomed Res 1997 December;30(6):415-26.

(136) Sirnes PA, Myreng Y, Molstad P, Golf S. Reproducibility of quantitative coronary analysis, Assessment of variability due to frame selection, different observers, and different cinefilmless laboratories. Int J Card Imaging 1996 September;12(3):197-203.

(137) Wellnhofer E, Wahle A, Mugaragu I, Gross J, Oswald H, Fleck E. Validation of an accurate method for three-dimensional reconstruction and quantitative assessment of volumes, lengths and diameters of coronary vascular branches and segments from biplane angiographic projections. Int J Card Imaging 1999 October;15(5):339-53.

(138) de Feyter PJ, Serruys PW, Davies MJ, Richardson P, Lubsen J, Oliver MF. Quantitative coronary angiography to measure progression and regression of coronary atherosclerosis. Circulation 1991;84:412-23.

(139) Andriotis A, Zifan A, Gavaises M, Liatsis P, Pantos I, Theodorakakos A, Efstathopoulos EP, Katritsis D. A new method of three-dimensional coronary artery reconstruction from X-ray angiography: validation against a virtual phantom and multislice computed tomography. Catheter Cardiovasc Interv 2008 January 1;71(1):28-43.

(140) Pellot C, Bloch I, Herment A, Sureda F. An attempt to 3D reconstruct vessel morphology from X-ray projections and intravascular ultrasounds modeling and fusion. Comput Med Imaging Graph 1996 May;20(3):141-51.

(141) Prause GP, De Jong SC, McKay CR, Sonka M. Towards a geometrically correct 3-D reconstruction of tortuous coronary arteries based on biplane angiography and intravascular ultrasound. Int J Card Imaging 1997 December;13(6):451-62.

(142) Slager CJ, Wentzel JJ, Schuurbiers JC, Oomen JA, Kloet J, Krams R, Von Birgelen C, van der Giessen WJ, Serruys PW, de Feyter PJ. True 3-dimensional reconstruction of coronary arteries in patients by fusion of angiography and IVUS (ANGUS) and its quantitative validation. Circulation 2000 August 1;102(5):511-6.

(143) Wahle A, Prause GPM, Von Birgelen C, Erbel R. Fusion of angiography and intravascular ultrasound in vivo: establishing the absolute 3-D frame orientation. IEEE Transactions on Biomedical Engineering 1999 October;Volume 46, Issue 10:1176-80.

(144) Coskun AU, Yeghiazarians Y, Kinlay S, Clark ME, Ilegbusi OJ, Wahle A, Sonka M, Popma JJ, Kuntz RE, Feldman CL, Stone PH. Reproducibility of coronary lumen, plaque, and vessel wall reconstruction and of endothelial shear stress measurements in vivo in humans. Catheter Cardiovasc Interv 2003 September;60(1):67-78.

(145) Gijsen FJ, Wentzel JJ, Thury A, Lamers B, Schuurbiers JC, Serruys PW, van der Steen AF. A new imaging technique to study 3-D plaque and shear stress distribution in human coronary artery bifurcations in vivo. J Biomech 2007;40(11):2349-57.

(146) Gijsen FJ, Wentzel JJ, Thury A, Mastik F, Schaar JA, Schuurbiers JC, Slager CJ, van der Giessen WJ, de Feyter PJ, van der Steen AF, Serruys PW. Strain distribution over plaques in human coronary arteries relates to shear stress. Am J Physiol Heart Circ Physiol 2008 October;295(4):H1608-H1614.

(147) Goubergrits L, Affeld K, Wellnhofer E, ZurbruggR, Holmer T. Estimation of wall shear stress in bypass grafts with computational fluid dynamics method. Int J Artif Organs 2001 March;24(3):145-51.

(148) Goubergrits L, Kertzscher U, Schoneberg B, Wellnhofer E, Petz C, Hege HC. CFD analysis in an anatomically realistic coronary artery model based on non-invasive 3D imaging: comparison of magnetic resonance imaging with computed tomography. Int J Cardiovasc Imaging 2007 October 23;.

(149) Goubergrits L, Wellnhofer E, Kertzscher U, Affeld K, Petz C, Hege HC. Coronary Artery WSS Profiling Using a Geometry Reconstruction Based on Biplane Angiography. Ann Biomed Eng 2009 February.

(150) Ilegbusi OJ, Hu Z, Nesto R, Waxman S, Cyganski D, Kilian J, Stone PH, Feldman CL. Determination of blood flow and endothelial shear stress in human coronary artery in vivo. J Invasive Cardiol 1999 November;11(11):667-74.

(151) Krams R, Wentzel JJ, Oomen JA, Schuurbiers JC, Andhyiswara I, Kloet J, Post M, de Smet B, Borst C, Slager CJ, Serruys PW. Shear stress in atherosclerosis, and vascular remodelling. Semin Interv Cardiol 1998 March;3(1):39-44.

(152) Stone PH, Coskun AU, Yeghiazarians Y, Kinlay S, Popma JJ, Kuntz RE, Feldman CL. Prediction of sites of coronary atherosclerosis progression: In vivo profiling of endothelial shear stress, lumen, and outer vessel wall characteristics to predict vascular behavior. Curr Opin Cardiol 2003 November;18(6):458-70.

(153) Stone PH. Evaluating cardiovascular pathophysiology and anatomy in atherosclerosis. Am Heart Hosp J 2005;3(3):187-92.

(154) Wahle A, Olszewski E. Interactive Virtual Endoscopy in Coronary Arteries Based on Multimodality Fusion. IEEE Transactions on Medical Imaging 2004;Vol. 23, No. 11 (6):1391-403.

(155) Qingfen Lin. Enhancement, Extraction, and Visualisation of 3D Volume Data 2003.

(156) Zeiler S, Gloor F. Pfadbasierte Methode zur Bewegungsvektorschätzung. 2004 p. 182-3.

(157) CAAS QCA-3D. http://www piemedical com/ 2010;Available from: URL: http://www.piemedical.com/

(158) CardioOp-B. http://www paieon com/ 2010;Available from: URL: http://www.paieon.com/

(159) Gradaus R, Mathies K, Breithardt G, Bocker D. Clinical assessment of a new real time 3D quantitative coronary angiography system: evaluation in stented vessel segments. Catheter Cardiovasc Interv 2006 July;68(1):44-9.

(160) Ramcharitar S, Daeman J, Patterson M, van Guens RJ, Boersma E, Serruys PW, van der Giessen WJ. First direct in vivo comparison of two commercially available three-dimensional quantitative coronary angiography systems. Catheter Cardiovasc Interv 2008 January 1;71(1):44-50.

(161) Schuurbiers JC, Lopez NG, Ligthart J, Gijsen FJ, Dijkstra J, Serruys PW, van der Steen AF, Wentzel JJ. In vivo validation of CAAS QCA-3D coronary reconstruction using fusion of angiography and intravascular ultrasound (ANGUS). Catheter Cardiovasc Interv 2009 April 1;73(5):620-6.

(162) Tsuchida K, van der Giessen WJ, Patterson M, Tanimoto S, Garcia-Garcia HM, Regar E, Ligthart JM, Maugenest AM, Maatrijk G, Wentzel JJ, Serruys PW. In vivo validation of a novel three-dimensional quantitative coronary angiography system (CardiOp-B): comparison with a conventional two-dimensional system (CAAS II) and with special reference to optical coherence tomography. EuroIntervention 2007 May;3(1):100-8.

(163) Cademartiri F, Palumbo AA, Maffei E, La Grutta L, Casolo G, Aldrovandi A, Reverberi C, Brambilla V, Coruzzi P, Beghi C, Ardissino D, Crisi G, Zompatori M. Non invasive imaging of coronary arteries with 64-slice CT and 1.5T MRI: challenging invasive techniques. Acta Biomed 2007;78(1):6-15.

(164) Jahnke C, Paetsch I, Nehrke K, Schnackenburg B, Gebker R, Fleck E, Nagel E. Rapid and complete coronary arterial tree visualization with magnetic resonance imaging: feasibility and diagnostic performance. Eur Heart J 2005 June 29;.

(165) Sato Y, Kanmatsuse K, Inoue F, Horie T, Kato M, Kusama J, Yoshimura A, Imazeki T, Furuhashi S, Takahashi M. Noninvasive coronary artery imaging by multislice spiral computed tomography. Circ J 2003 February;67(2):107-11.

(166) Sun Z, Lin C, Davidson R, Dong C, Liao Y. Diagnostic value of 64-slice CT angiography in coronary artery disease: A systematic review. Eur J Radiol 2007 August 31;.

(167) Blondel C, Malandain G, Vaillant R, Ayache N. Reconstruction of coronary arteries from a single rotational X-ray projection sequence. IEEE Trans Med Imaging 2006 May;25(5):653-63.

(168) Bousse A, Zhou J, Yang G, Bellanger JJ, Toumoulin C. Motion Compensated Tomography Reconstruction of Coronary Arteries in rotational Angiography. IEEE Trans Biomed Eng 2008 October 14.

(169) Hansis E, Schafer D, Dossel O, Grass M. Evaluation of iterative sparse object reconstruction from few projections for 3-D rotational coronary angiography. IEEE Trans Med Imaging 2008 November;27(11):1548-55.

(170) Hansis E, Schafer D, Dossel O, Grass M. Projection-based motion compensation for gated coronary artery reconstruction from rotational x-ray angiograms. Phys Med Biol 2008 July 21;53(14):3807-20.

(171) Schafer D, Borgert J, Rasche V, Grass M. Motion-compensated and gated cone beam filtered back-projection for 3-D rotational X-ray angiography. IEEE Trans Med Imaging 2006 July;25(7):898-906.

(172) Schmitt H, Grass M, Suurmond R, Kohler T, Rasche V, Hahnel S, Heiland S. Reconstruction of blood propagation in three-dimensional rotational X-ray angiography (3D-RA). Comput Med Imaging Graph 2005 October;29(7):507-20.

(173) Wahle A. Präzise dreidimensionale Rekonstruktion von Gefäßsystemen aus biplanen angiographischen Projektionen und deren klinische Anwendung, Dissertation TU-Berlin; 1994, erschienen Fortschritt-Berichte, Reihe 17 (Biotechnik) VDI-Verlag, Bd 152 1997. ISBN3-18-315217-7.

(174) Chatzizisis YS, Giannoglou GD, Matakos A, Basdekidou C, Sianos G, Panagiotou A, Dimakis C, Parcharidis GE, Louridas GE. In-vivo accuracy of geometrically correct three-dimensional reconstruction of human coronary arteries: is it influenced by certain parameters? Coron Artery Dis 2006 September;17(6):545-51.

(175) Chatzizisis YS, Giannoglou GD, Sianos G, Ziakas A, Tsikaderis D, Dardas P, Matakos A, Basdekidou C, Misirli G, Zamboulis C, Louridas GE, Parcharidis GE. In vivo comparative study of linear versus geometrically correct three-dimensional reconstruction of coronary arteries. Am J Cardiol 2008 January 15;101(2):263-7.

(176) Giannoglou GD, Chatzizisis YS, Koutkias V, Kompatsiaris I, Papadogiorgaki M, Mezaris V, Parissi E, Diamantopoulos P, Strintzis MG, Maglaveras N, Parcharidis GE, Louridas GE. A novel active contour model for fully automated segmentation of intravascular ultrasound images: in vivo validation in human coronary arteries. Comput Biol Med 2007 September;37(9):1292-302.

(177) Slager CJ, Wentzel JJ, Oomen JA, Schuurbiers JC, Krams R, von BC, Tjon A, Serruys PW, de Feyter PJ. True reconstruction of vessel geometry from combined X-ray angiographic and intracoronary ultrasound data. Semin Interv Cardiol 1997 March;2(1):43-7.

(178) McInerney T, Hamarneh G, Shenton M, Terzopoulos D. Deformable organisms for automatic medical image analysis. Med Image Anal 2002 September;6(3):251-66.

(179) Messenger JC, Chen SY, Carroll JD, Burchenal JE, Kioussopoulos K, Groves BM. 3D coronary reconstruction from routine single-plane coronary angiograms: clinical validation and quantitative analysis of the right coronary artery in 100 patients. Int J Card Imaging 2000 December;16(6):413-27.

(180) Wahle A, Lopez JJ, Olszewski ME, Vigmostad SC, Chandran KB, Rossen JD, Sonka M. Plaque development, vessel curvature, and wall shear stress in coronary arteries assessed by X-ray angiography and intravascular ultrasound. Med Image Anal 2006 August;10(4):615-31.

(181) Wink O. Vessel Axis Determination for Diagnosis and Treatment. Dissertation Universität, Utrecht, 2004, ISBN 90-393-3698-9.

(182) Boutsianis E, Dave H, Frauenfelder T, Poulikakos D, Wildermuth S, Turina M, Ventikos Y, Zund G. Computational simulation of intracoronary flow based on real coronary geometry. Eur J Cardiothorac Surg 2004 August;26(2):248-56.

(183) Frobert O, Schionning J, Gregersen H, Baandrup U, Petersen JA, Bagger JP. Impaired human coronary artery distensibility by atherosclerotic lesions: a mechanical and histological investigation. Int J Exp Pathol 1997 December;78(6):421-8.

(184) Johnston BM, Johnston PR, Corney S, Kilpatrick D. Non-Newtonian blood flow in human right coronary arteries: steady state simulations. J Biomech 2004 May;37(5):709-20.

(185) Johnston BM, Johnston PR, Corney S, Kilpatrick D. Non-Newtonian blood flow in human right coronary arteries: transient simulations. J Biomech 2006;39(6):1116-28.

(186) Soulis JV, Giannoglou GD, Chatzizisis YS, Seralidou KV, Parcharidis GE, Louridas GE. Non-Newtonian models for molecular viscosity and wall shear stress in a 3D reconstructed human left coronary artery. Med Eng Phys 2008 January;30(1):9-19.

(187) Jung J, Lyczkowski RW, Panchal CB, Hassanein A. Multiphase hemodynamic simulation of pulsatile flow in a coronary artery. J Biomech 2006;39(11):2064-73.

(188) Moore JEJ, Guggenheim N, Delfino A, Doriot PA, Dorsaz PA, Rutishauser W, Meister JJ. Preliminary analysis of the effects of blood vessel movement on blood flow patterns in the coronary arteries. J Biomech Eng 1994 August;116(3):302-6.

(189) Moore JE, Jr., Weydahl ES, Santamarina A. Frequency dependence of dynamic curvature effects on flow through coronary arteries. J Biomech Eng 2001 April;123(2):129-33.

(190) Weydahl ES, Moore JE. Dynamic curvature strongly affects wall shear rates in a coronary artery bifurcation model. J Biomech 2001 September;34(9):1189-96.

(191) Zeng D, Ding Z, Friedman MH, Ethier CR. Effects of cardiac motion on right coronary artery hemodynamics. Ann Biomed Eng 2003 April;31(4):420-9.

(192) Prandtl L, Oswatitsch K, Wieghardt K. Bewegung zäher Flüssigkeiten, Turbulenz, Widerstände, Technische Anwendungen. In: Oswatitsch K, ieghardt K, editors. Führer duch die Strömungslehre. 8 ed. Braunschweig/Wiesbaden: Friedr. Vieweg & Sohn; 1984. p. 167.

(193) Myers JG, Moore JA, Ojha M, Johnston KW, Ethier CR. Factors influencing blood flow patterns in the human right coronary artery. Ann Biomed Eng 2001 February;29(2):109-20.

(194) Prakash S, Ethier CR. Requirements for mesh resolution in 3D computational hemodynamics. J Biomech Eng 2001 April;123(2):134-44.

(195) Gibson CM, Diaz L, Kandarpa K, Sacks FM, Pasternak RC, Sandor T, Feldman C, Stone PH. Relation of vessel wall shear stress to atherosclerosis progression in human coronary arteries. Arterioscler Thromb 1993 February;13(2):310-5.

(196) Oswald H, Wahle A, Wellnhofer E, Fleck E. 3-D coronary angiography for quantitative analysis of coronary morphology. In: Reiber JHC, Van Der Wall EE, editors. Cardiovascular Imaging. 1 ed. Dordrecht: Kluwer Academic Publishers; 1996. p. 57-78.

(197) Gensini GG. A more meaningful scoring system for determining the severity of coronary heart disease. Am J Cardiol 1983 February;51(3):606.

(198) Jukema JW, van Boven AJ, Zinderman AH, Bal ET, Reiber JH, Bruschke AV. The influence of angiographic endpoints on the outcome of lipid intervention studies. A proposal for standardization. REGRESS study group
12. Angiology 1996 July;47(7):633-42.

(199) Doucette JW, Corl PD, Payne HM, Flynn AE, Goto M, Nassi M, Segal J. Validation of a Doppler Guide Wire for Intravascular Measurement of Coronary Artery Flow Velocity
77. Circulation 1992;85:1899-911.

(200) Diekmann P. Using Simulations for Education, Training and Research. [3]. 2009. Lengerich, Pabst Science Publishers. Work Research Multidisciplinary. Wehner, T and Manser, T.
Ref Type: Serial (Book,Monograph)

(201) Ueba H, Kawakami M, Yaginuma T. Shear stress as an inhibitor of vascular smooth muscle cell proliferation. Role of transforming growth factor-beta 1 and tissue-type plasminogen activator. Arterioscler Thromb Vasc Biol 1997 August;17(8):1512-6.

(202) Berk BC, Abe JI, Min W, Surapisitchat J, Yan C. Endothelial atheroprotective and anti-inflammatory mechanisms. Ann N Y Acad Sci 2001 December;947:93-109; discussion 109-11.:93-109.

(203) Chien S. Effects of disturbed flow on endothelial cells. Ann Biomed Eng 2008 April;36(4):554-62.

(204) Chiu JJ, Lee PL, Chang SF, Chen LJ, Lee CI, Lin KM, Usami S, Chien S. Shear stress regulates gene expression in vascular endothelial cells in response to tumor necrosis factor-alpha: a study of the transcription profile with complementary DNA microarray. J Biomed Sci 2005;12(3):481-502.

(205) Davis ME, Grumbach IM, Fukai T, Cutchins A, Harrison DG. Shear stress regulates endothelial nitric-oxide synthase promoter activity through nuclear factor kappaB binding. J Biol Chem 2004 January 2;279(1):163-8.

(206) Lehoux S, Castier Y, Tedgui A. Molecular mechanisms of the vascular responses to haemodynamic forces. J Intern Med 2006 April;259(4):381-92.

(207) Siasos G, Tousoulis D, Siasou Z, Stefanadis C, Papavassiliou AG. Shear stress, protein kinases and atherosclerosis. Curr Med Chem 2007;14(14):1567-72.

(208) White CR, Stevens HY, Haidekker M, Frangos JA. Temporal gradients in shear, but not spatial gradients, stimulate ERK1/2 activation in human endothelial cells. Am J Physiol Heart Circ Physiol 2005 December;289(6):H2350-H2355.

(209) World CJ, Garin G, Berk B. Vascular shear stress and activation of inflammatory genes. Curr Atheroscler Rep 2006 May;8(3):240-4.

(210) Zou Y, Hu Y, Metzler B, Xu Q. Signal transduction in arteriosclerosis: mechanical stress-activated MAP kinases in vascular smooth muscle cells (review). Int J Mol Med 1998 May;1(5):827-34.

(211) Giannoglou GD, Chatzizisis YS, Sianos G, Tsikaderis D, Matakos A, Koutkias V, Diamantopoulos P, Maglaveras N, Parcharidis GE, Louridas GE. In-vivo validation of spatially correct three-dimensional reconstruction of human coronary arteries by integrating intravascular ultrasound and biplane angiography. Coron Artery Dis 2006 September;17(6):533-43.

(212) Collingwood R, Bermudez E, Fischell TA. Comparison between three-dimensional angiographic reconstruction and intravascular ultrasound imaging for the measurement of cross-sectional luminal dimensions in intermediate coronary lesions. J Interv Cardiol 2009 June;22(3):277-81.

(213) Goubergrits L, Kertzscher U, Schoneberg B, Wellnhofer E, Petz C, Hege HC. CFD analysis in an anatomically realistic coronary artery model based on non-invasive 3D imaging: comparison of magnetic resonance imaging with computed tomography. Int J Cardiovasc Imaging 2008 April;24(4):411-21.

(214) Wentzel JJ, Aguiar SH, Fayad ZA. Vascular MRI in the diagnosis and therapy of the high risk atherosclerotic plaque. J Interv Cardiol 2003 April;16(2):129-42.

(215) Wentzel JJ, Corti R, Fayad ZA, Wisdom P, Macaluso F, Winkelman MO, Fuster V, Badimon JJ. Does shear stress modulate both plaque progression and regression in the thoracic aorta? Human study using serial magnetic resonance imaging. J Am Coll Cardiol 2005 March 15;45(6):846-54.

(216) Swanton RH, Thomas ML, Coltart DJ, Jenkins BS, Webb-Peploe MM, Williams BT. Coronary artery ectasia-a variant of occlusive coronary atherosclerosis. Br Heart J 1978;40:393-400.

(217) Glagov S, Weisenberg E, Zarins CK, Stankunavicius R, Kolettis GJ. Compensatory Enlargement of Human Atherosclerotic Coronary Arteries. N Engl J Med 1987;316(22):1371-5.

(218) Lerman A, Cannan CR, Higano SH, Nishimura RA, Holmes DRJ. Coronary vascular remodeling in association with endothelial dysfunction. Am J Cardiol 1998 May 1;81(9):1105-9.

(219) Ivan E, Khatri JJ, Johnson C, Magid R, Godin D, Nandi S, Lessner S, Galis ZS. Expansive arterial remodeling is associated with increased neointimal macrophage foam cell content: the murine model of macrophage-rich carotid artery lesions. Circulation 2002 June 4;105(22):2686-91.

(220) Pasterkamp G, Galis ZS, de Kleijn DP. Expansive arterial remodeling: location, location, location. Arterioscler Thromb Vasc Biol 2004 April;24(4):650-7.

(221) Lessner SM, Martinson DE, Galis ZS. Compensatory vascular remodeling during atherosclerotic lesion growth depends on matrix metalloproteinase-9 activity. Arterioscler Thromb Vasc Biol 2004 November;24(11):2123-9.

(222) Korshunov VA, Berk BC. Strain-dependent vascular remodeling: the "Glagov phenomenon" is genetically determined. Circulation 2004 July 13;110(2):220-6.

(223) Wentzel JJ, Krams R, Slager CJ. Letter regarding article by Korshunov and Berk, "Strain-dependent vascular remodeling: the 'Glagov phenomenon' is genetically determined". Circulation 2005 March 8;111(9):e119.

(224) Mikawa T, Gourdie RG. Pericardial mesoderm generates a population of coronary smooth muscle cells migrating into the heart along with ingrowth of the epicardial organ. Dev Biol 1996 March 15;174(2):221-32.

(225) Canero C, Vilarino F, Mauri J, Radeva P. Predictive (un)distortion model and 3-D reconstruction by biplane snakes. IEEE Trans Med Imaging 2002 September;21(9):1188-201.

(226) Chen SJ, Carroll JD. 3-D reconstruction of coronary arterial tree to optimize angiographic visualization. IEEE Trans Med Imaging 2000 April;19(4):318-36.

(227) Chen SY, Carroll JD, Messenger JC. Quantitative analysis of reconstructed 3-D coronary arterial tree and intracoronary devices. IEEE Trans Med Imaging 2002 July;21(7):724-40.

(228) Cronemeyer J. Untersuchungen zur automatischen 3-D-Rekonstruktion des koronaren Gefäßbaums aus biplanen Angiogrammen. Dissertation TU Berlin,1997.

(229) Garreau M, Coatrieux JL, Collorec R. A knowledge-based approach for 3-D reconstruction and labeling of vascular networks from biplane angiographic projections. IEEE Transactions on Medical Imaging 1991 June;Volume 10, Issue 2:122-31.

(230) Kitamura K, Tobis JM. Estimating the 3D skeletons and transverse areas of coronary arteries from biplane angiograms. IEEE Transactions on Medical Imaging 1988 September;Volume 7, Issue 3:173-87.

(231) Klein JL, Hoff JG, Peifer JW, Folks R, Cooke CD, King SB, Garcia EV. A quantitative evaluation of the three dimensional reconstruction of patients' coronary arteries. Int J Card Imaging 1998 April;14(2):75-87.

(232) Movassaghi B, Rasche V, Grass M, Viergever MA, Niessen WJ. A quantitative analysis of 3-D coronary modeling from two or more projection images. IEEE Trans Med Imaging 2004 December;23(12):1517-31.

(233) Puentes J, Garreau M, Lebreton H, Roux C. Understanding coronary artery movement: a knowledge-based approach. Artif Intell Med 1998 July;13(3):207-37.

(234) Rougee A, Picard C, Saint-Felix D, Trousset Y, Moll T, Amiel M. Three-dimensional coronary arteriography. Int J Card Imaging 1994 March;10(1):67-70.

(235) Sarry L, Boire JY. Three-dimensional tracking of coronary arteries from biplane angiographic sequences using parametrically deformable models. IEEE Trans Med Imaging 2001 December;20(12):1341-51.

(236) Sarwal A, Dhawan AP. Three dimensional reconstruction of coronary arteries from two views. Comput Methods Programs Biomed 2001 April;65(1):25-43.

(237) Shechter G, Devernay F, Coste-Maniere E, Quyyumi A. Three-dimensional motion tracking of coronary arteries in biplane cineangiograms. IEEE Transactions on Medical Imaging 2003 April;Volume 22, Issue 4:493-503.

(238) Terzopoulos D, McInerney T. Deformable models and the analysis of medical images. Stud Health Technol Inform 1997;39:369-78.:369-78.

(239) van Tran L, Bahn RC. Reconstructing the cross sections of coronary arteries from biplane angiograms. IEEE Transactions on Medical Imaging 1992 December;Volume 11, Issue 4:517-29.

(240) Wang R. Multiresolution method for reconstructing the cross sections of coronary arteries from biplane angiograms. Conference C: Image, Speech and Signal Analysis, Proceedings , 11th IAPR International Conference on Pattern Recognition 1992;Vol.III.:667-70.

(241) Zeiler S, Kirchner D, Orglmeister R. Three Dimensional Reconstruction from Biplane Angiograms with Uncertain Geometric Parameters. Biomedizinische Technik 50/1. Schiele & Schön, Berlin, 2005 p. 66-7

(242) Dvir D, Marom H, Guetta V, Kornowski R. Three-dimensional coronary reconstruction from routine single-plane coronary angiograms: in vivo quantitative validation. Int J Cardiovasc Intervent 2005;7(3):141-5.

(243) Bullitt E, Liu A, Pizer SM. Three-dimensional reconstruction of curves from pairs of projection views in the presence of error. I. Algorithms. Med Phys 1997 November;24(11):1671-8.

(244) Bullitt E, Liu A, Pizer SM. Three-dimensional reconstruction of curves from pairs of projection views in the presence of error. II. Analysis of error. Med Phys 1997 November;24(11):1679-87.

(245) Jähne B. Digitale Bildverarbeitung, 5. überarb. u. erw. Aufl. 5 ed. Springer; 2002. p.14.

(246) Lehmann GC, Holdsworth DW, Drangova M. Angle-independent measure of motion for image-based gating in 3D coronary angiography. Med Phys 2006 May;33(5):1311-20.

(247) Liang J, McInerney T, Terzopoulos D. United snakes. Med Image Anal 2006 April;10(2):215-33.

(248) McInerney T, Terzopoulos D. Topology adaptive deformable surfaces for medical image volume segmentation. IEEE Trans Med Imaging 1999 October;18(10):840-50.

(249) Gollapudi RR, Valencia R, Lee SS, Wong GB, Teirstein PS, Price MJ. Utility of three-dimensional reconstruction of coronary angiography to guide percutaneous coronary intervention. Catheter Cardiovasc Interv 2007 March 1;69(4):479-82.

(250) Dvir D, Marom H, Assali A, Kornowski R. Bifurcation lesions in the coronary arteries: early experience with a novel 3-dimensional imaging and quantitative analysis before and after stenting. EuroIntervention 2007 May;3(1):95-9.

(251) Ramcharitar S, Onuma Y, Aben JP, Consten C, Weijers B, Morel MA, Serruys PW. A novel dedicated quantitative coronary analysis methodology for bifurcation lesions. EuroIntervention 2008 March;3(5):553-7.

(252) Dvir D, Assali A, Kornowski R. Percutaneous coronary intervention for chronic total occlusion: novel 3-dimensional imaging and quantitative analysis. Catheter Cardiovasc Interv 2008 May 1;71(6):784-9.

(253) Green NE, Chen SY, Hansgen AR, Messenger JC, Groves BM, Carroll JD. Angiographic views used for percutaneous coronary interventions: a three-dimensional analysis of physician-determined vs. computer-generated views. Catheter Cardiovasc Interv 2005 April;64(4):451-9.

(254) Florin C, Paragios N, Williams J. Particle filters, a quasi-Monte-Carlo-solution for segmentation of coronaries. Med Image Comput Comput Assist Interv Int Conf Med Image Comput Comput Assist Interv 2005;8(Pt 1):246-53.

(255) Shechter G, Ozturk C, Resar JR. Respiratory Motion of the Heart From Free Breathing Coronary Angiograms. IEEE Transactions on Medical Imaging 2004 August;Vol. 23, No. 8:1046-56.

(256) Solzbach U, Wollschlager H, Zeiher A. Optical distortion due to geomagnetism in quantitative angiography. Proceedings Computers in Cardiology 1988 September 25;355-7.

(257) Herrington DM, Siebes M, Walford GD. Sources of error in quantitative coronary angiography. Cathet Cardiovasc Diagn 1993 August;29(4):314-21.

(258) Beier J. Automatische Quantifizierung von Koronarstenosen aus angiograpischen Röntgenbildern. Dissertation TU Berlin, erschienen Fortschritt- Berichte, Reihe 17 (Biotechnik) VDI-Verlag, Bd 95 1993.

(259) Chen SY, Metz CE. Improved determination of biplane imaging geometry from two projection images and its application to three-dimensional reconstruction of coronary arterial trees. Med Phys 1997 May;24(5):633-54.

(260) Cheriet F, Meunier J. Self-calibration of a biplane X-ray imaging system for an optimal three dimensional reconstruction. Comput Med Imaging Graph 1999 May;23(3):133-41.

(261) Lotjonen J, Magnin IE, Nenonen J, Katila T. Reconstruction of 3-D geometry using 2-D profiles and a geometric prior model. IEEE Trans Med Imaging 1999 October;18(10):992-1002.

(262) Metz CE, Fencil LE. Determination of three-dimensional structure in biplane radiography without prior knowledge of the relationship between the two views: theory. Med Phys 1989 January;16(1):45-51.

(263) Wahle A, Wellnhofer E, Oswald H, Fleck E. Biplane coronary angiography: accurate quantitative 3-D reconstruction without isocenter. Computers in Cardiology 1993, London UK, IEEE press, p. 97-100. (Conference Proceeding)1993 p. 97-100.

(264) Jähne B. Digitale Bildverarbeitung, 5. überarb. u. erw. Aufl. 5 ed. Springer; 2002. p. 317. ISBN 3-540-67754-2.

(265) Jähne B. Digitale Bildverarbeitung, 5. überarb. u. erw. Aufl. 5 ed. Springer; 2002. p. 39. ISBN 3-540-67754-2.

(266) Qingfen Lin. Enhancement, Extraction, and Visualisation of 3D Volume Data. Thesis. Linköping, erschienen Linköping Studys in Science and Technology, Vol. 824, 2003. p.11 ISBN 917373-657-0.

(267) Wahle A, Oswald O. A New 3-D Attributed Data Model for Achiving and Interchanging of Coronary Vessel Systems. Computers in Cardiology, London UK, IEEE press, 1993. p. 603-6.(Conference Proceeding)

(268) Brutzman D. The Virtual Reality Modeling Language and Java. Communications of the ACM 1998;41:57-68.

(269) Kim S, Choi B. High Dynamic Range Image Texture Mapping Based on VRML. Computational Science and Its Applications-ICCSA 2003.Berlin/Heidelberg: Springer-Verlag; 2003. p. 488-97.

(270) Qingfen Lin. Enhancement, Extraction, and Visualisation of 3D Volume Data Thesis. Linköping, erschienen Linköping Studys in Science and Technology, Vol. 824, 2003. p.153 ISBN 917373-657-0.2003.

(271) Chatzizisis YS, Jonas M, Beigel R, Coskun AU, Baker AB, Stone BV, Maynard C, Gerrity RG, Daley W, Edelman ER, Feldman CL, Stone PH. Attenuation of inflammation and expansive remodeling by Valsartan alone or in combination with Simvastatin in high-risk coronary atherosclerotic plaques. Atherosclerosis 2009 April;203(2):387-94.

(272) Changizi MA, Cherniak C. Modeling the large-scale geometry of human coronary arteries. Can J Physiol Pharmacol 2000 August;78(8):603-11.

(273) Wellnhofer E, Combe V, Oswald H, Fleck E. High fidelity correction of pressure signals from fluid-filled systems by harmonic analysis. J Clin Monit Comput 1999 July;15(5):307-15.

(274) Ballyk PD, Steinman DA, Ethier CR. Simulation of non-Newtonian blood flow in an end-to-side anastomosis. Biorheology 1994 September;31(5):565-86.

(275) Thurston GB. Rheological parameters for the viscosity viscoelasticity and thixotropy of blood. Biorheology 1979;16(3):149-62.

(276) Fung Y. Biomechanics. Mechanical properties of living tissues. Berlin: Springer; 1993.

(277) Thurston GB, Henderson NM. Effects of flow geometry on blood viscoelasticity. Biorheology 2006;43(6):729-46.

(278) Soulis JV, Giannoglou GD, Chatzizisis YS, Seralidou KV, Parcharidis GE, Louridas GE. Non-Newtonian models for molecular viscosity and wall shear stress in a 3D reconstructed human left coronary artery. Med Eng Phys 2008 January;30(1):9-19.

(279) Berglund H, Luo H, Nishioka T, Fishbein MC, Eigler NL, Tabak SW, Siegel RJ. Highly localized arterial remodeling in patients with coronary atherosclerosis: an intravascular ultrasound study. Circulation 1997 September 2;96(5):1470-6.

(280) Perktold K, Hofer M, Rappitsch G, Loew M, Kuban BD, Friedman MH. Validated computation of physiologic flow in a realistic coronary artery branch. J Biomech 1998 March;31(3):217-28.

(281) LaDisa JF, Jr., Olson LE, Douglas HA, Warltier DC, Kersten JR, Pagel PS. Alterations in regional vascular geometry produced by theoretical stent implantation influence distributions of wall shear stress: analysis of a curved coronary artery using 3D computational fluid dynamics modeling. Biomed Eng Online 2006 June 16;5:40.

(282) Samet MM, Lelkes PI. The hemodynamic environment of the endothelium. In: Mechanical forces and the endothelium. Lelkes PI, ed. in: The endothelial cell research series. Rubanyi GM ed., Harwood academic publishers. Amsterdam. 1999. p. 15

(283) Nosovitsky VA, Ilegbusi OJ, Jiang J, Stone PH, Feldman CL. Effects of curvature and stenosis-like narrowing on wall shear stress in a coronary artery model with phasic flow. Comput Biomed Res 1997 February;30(1):61-82.

Credits for permissions:

Danksagung

Bei Prof. Fleck bedanke ich mich für die Überlassung des Themas und seine Aufgeschlossenheit gegenüber technisch anspruchsvollen Ideen. Mein besonderer Dank gilt auch den vielen interessanten Menschen, mit denen ich in meiner Forschung zusammenarbeiten durfte. Insbesondere bedanke ich mich bei Herrn Prof. Affeld und Herrn Dr. Leonid Goubergrits für die Zusammenarbeit bei der Flusssimulation, bei Herrn Steffen Zeiler für tiefe Einblicke in die Mathematik der 3-D-Rekonstruktion und die Überlassung von Bildern. Weiter gilt mein Dank meinen langjährigen Kollegen, Dr. Michael Gräfe und Dr. Stephan Götze, die mich moralisch unterstützt haben, und meiner Frau Agnes Sauter- Wellnhofer, die viel Verständnis für mein wissenschaftliches Chaos aufgebracht hat. Bei Frau Inge Artmann bedanke ich mich herzlich für das Korrekturlesen der Endfassung der Arbeit.

Erklärung

§4 Abs 3 (k) der HabOMed der Charité

Hiermit erkläre ich,

- dass weder früher noch gleichzeitig ein Habilitationsverfahren durchgeführt oder angemeldet wurde,

- die vorgelegte Habiltationsschrift ohne fremde Hilfe verfasst, die beschriebenen Ergebnisse selbst gewonnen sowie die verwendeten Hilfsmittel, die Zusammenarbeit mit anderen Wissenschaftlern/Wissenschaftlerinnen und mit technischen Hilfskräften sowie die verwendete Literatur vollständig in der Habilitationsschrift angegeben wurden,

- mir die geltende Habilitationsordnung bekannt ist.

Berlin, den 13. 1. 2010